ANGLIA RUSKIN UNIVERSITY

FACULTY OF MEDICAL SCIENCES

OPTIMISING RV-PA VENTRICULOARTERIAL-COUPLING TO IMPROVE RV DIASTOLIC FUNCTION IN PATIENTS WITH CARDIOPULMONARY DISORDERS

RICHARD G. AXELL BENG, MSC, CSCI, CENG, MIPEM.

A THESIS IN PARTIAL FULFILMENT OF THE

REQUIREMENTS OF ANGLIA RUSKIN UNIVERSITY

FOR THE DEGREE OF DOCTORATE OF PHILOSOPHY

THIS RESEARCH PROGRAMME WAS CARRIED OUT

IN COLLABORATION WITH

CAMBRIDGE UNIVERSITY HOSPITALS NHS FOUNDATION TRUST

AND

PAPWORTH HOSPITALS NHS FOUNDATION TRUST

SUBMITTED: FEBRUARY 2017

This thesis is independent research arising from a Chief Scientific Officer Healthcare Scientist Doctoral Fellowship awarded to Dr Richard Axell (NIHR-HCS-D12-14) supported by the National Institute for Health Research. The views expressed in this publication are those of the author and not necessarily those of the NHS, the National Institute of Health Research, Health Education England, or the Department of Health.

Acknowledgements

The author would like to acknowledge and thank the following people who have made significant contributions to this thesis:

Dr Stephen Hoole, DM FRCP, Consultant Interventional Cardiologist

Dr Hoole clinically supervised all of the work contained in this thesis. In particular he contributed to the design and planning of all the research studies, performed the interventional procedures and assisted with the clinical interpretation of the results.

Professor James Hampton-Till, PhD PGCDME, Dean

Professor Hampton-Till supervised all of the work contained in this thesis. He also proofread this manuscript before submission.

Professor Paul White, PhD FIPEM, Consultant Clinical Scientist

Professor White supervised all of the work contained in this thesis. He also assisted with the acquisition of the conductance catheter data and proofread this manuscript before submission.

Dr Simon Messer, MBChB MRCS, Cardiothoracic Surgical Fellow

Dr Messer performed the surgical procedures for the animal studies. He also assisted with the design and acquisition of the ex-vivo working heart perfusion.

Dr Hatim Alibhai, PhD FHEA, Consultant Veterinary Anaesthetist

Dr Alibhai performed the anaesthetic care for the animal studies.

Dr Joel Giblett, MB BS MRCP, Interventional Cardiology Fellow

Dr Giblett assisted the interventional procedures.

Dr Cameron Densem, MD MRCP, Consultant Interventional Cardiologist

Dr Densem performed the interventional procedures.

Dr Stephen Large, MA, FRCS, Consultant Cardiothoracic Surgeon

Dr Large performed the surgical procedures for the animal studies.

Dr Lynne Williams, MD MRCP, Consultant Cardiologist

Dr Williams performed the echocardiographic assessments for the interventional procedures.

Dr Bushra Rana, MD MRCP, Consultant Cardiologist

Dr Rana performed the echocardiographic assessments for the interventional procedures.

Dr Andrew Klein, MD FRCA, Consultant Anaesthetist

Dr Klein performed the anaesthetic care for the interventional procedures.

Dr Leonard Shapiro, MD FRCP, Consultant Interventional Cardiologist

Dr Shapiro performed the interventional procedures.

Dr Michael O'Sullivan, PhD FRCP, Consultant Interventional Cardiologist

Dr O'Sullivan performed the interventional procedures.

The author would like to thank the staff of the Catheter Laboratories at Papworth Hospital NHS Foundation Trust for their help in the interventional studies. The author would also like to thank the staff of the Royal Veterinary College for their help in the animal studies. I would also like to thank to the patients who participated in the studies without whom this research would not have been possible.

I feel very fortunate to have been awarded a National Institute of Healthcare Research Chief Scientific Officer Healthcare Scientist Doctoral Fellowship. I thank the NIHR for this privilege. The Fellowship allowed me to dedicate three years of my life solely to research. I gave it my all – I'm not sure there was much left to give. This was a life changing, challenging, and rewarding experience for me. The collaborative nature of our research programmes gifted me the opportunity to work on a number of other projects beyond the scope of the work presented in this PhD. Being part of the first Donation after Circulatory Determined Death heart transplantation in Europe was an amazing but at times difficult and heart breaking experience. I'm humbled by the generosity of the organ donor and their family. There is no greater gift than the gift of life to another human being when one's own body is ready to leave this world. Life is so fragile. Friends, family, time must be cherished.

Finally, I thank my friends and family, with a special thank you to Liz, for her patience, and faith in me. The thanks I give you can hardly be expressed on paper. You have all taken it in turns to be there for me during the highs and lows of this long and humbling journey. Your continued support and encouragement got me to the end. I dedicate this work to you.

ANGLIA RUSKIN UNIVERSITY

ABSTRACT

FACULTY OF MEDICAL SCIENCES

OPTIMISING RV-PA VENTRICULOARTERIAL-COUPLING TO IMPROVE RV DIASTOLIC FUNCTION IN PATIENTS WITH CARDIOPULMONARY DISORDERS

RICHARD G. AXELL

FEBRUARY 2017

In recent years, an increasing body of evidence has emerged postulating that right ventricular (RV) - pulmonary artery (PA) ventriculoarterial coupling may offer insight into the transition from RV adaptation to RV maladaptation in different cardiopulmonary disorders and heart failure. RV-PA ventriculoarterial coupling is a matching between RV contractility (Ees – End-Systolic Elastance) and afterload (Ea – Effective Arterial Elastance). While ventriculoarterial coupling has been extensively described in the LV and used to determine optimal conditions for the efficient transfer to blood from the ventricle into the aorta, it remains unclear whether this relationship can be translated to the thinner walled RV that pumps at lower pressures against a more compliant pulmonary vascular system. Therefore, the pressure-volume (PV)-loop studies in this thesis were undertaken to assess whether ventriculoarterial uncoupling due to pressure overload or sub-optimal contractility contributed to further RV diastolic dysfunction.

An in-vivo porcine model of RV-PA ventriculoarterial coupling was developed to define optimal conditions. This animal model was used to provide insights into two clinical patient groups that have RV dysfunction due to: i) long-term RV pressure overload in patients with a clinical diagnosis of chronic thromboembolic disease (CTED) / pulmonary hypertension (CTEPH); and ii) aortic valve stenosis transmitted by ventricular interdependence and septal wall reconfiguration in patients treated with transcatheter aortic valve implantation (TAVI).

The animal model determined an ventriculoarterial coupling ratio at maximal stroke work ($Ees/Ea_{max\ sw}$ = 0.68±0.23) threshold, below which cardiac output and RV stroke work fell. In the first clinical study this threshold was used to reclassify 25% of a cohort of patients with CTED or CTEPH. Two patients with CTED were identified with an EesEa below 0.68 suggesting occult RV dysfunction whilst three patients with CTEPH demonstrated Ees/Ea≥0.68 suggesting residual RV energetic reserve. In the second clinical study ventricular interdependence phenomena caused septal reconfiguration and increased RV volumes after valve deployment, due to the reduction in LV afterload. However, the rapid pacing (RP) protocol used to stabilise the aortic valve during deployment also caused RP-induced ischemia and stunning. This resulted in the reduction of Ees and led to Ees/Ea uncoupling and further diastolic dysfunction.

This work has demonstrated that: Low Ees/Ea aligns with features of RV maladaptation in CTED. Characterization of Ees/Ea in CTED may allow for better identification of occult RV dysfunction in patients with otherwise normal pulmonary hemodynamics; and a reduction in Ees following TAVI correlates with increased RV diastolic dysfunction, due to RP-induced ischemia and stunning.

Key words: Right Ventricle; Diastolic Dysfunction; Ventriculoarterial Coupling; RV Energetic Reserve; Maximal Stroke Work

Table of Contents

List of Figures

List of Tables

Notation

CI	Cardiac Index
CO	Cardiac Output
CTEPH	Chronic Thromboembolic Pulmonary Hypertension
CTED	Chronic Thromboembolic Disease
dP/dt max	Maximal Rate of Isovolumic Contraction
dP/dt min	Maximal Rate of Isovolumic Relaxation
Ea	Effective Arterial Elastance
Echo	Echocardiography
EDP	End-Diastolic Pressure
EDPVR	End-Diastolic Pressure Volume Relationship
ESPVR	End-Systolic Pressure Volume Relationship
EDV	End-Diastolic Volume
Ees	End-Systolic Elastance
ESV	End-Systolic Volume
LV	Left Ventricle
MAP	Mean Arterial Pressure
mPAP	Mean Pulmonary Artery Pressure
PCWP	Pulmonary Capillary Wedge Pressure
PH	Pulmonary Hypertension
PRSW	Preload Recruitable Stroke Work
PV-loop	Pressure-Volume Loop
PVR	Pulmonary Vascular Resistance
RA	Right Atrium
RHC	Right Heart Catheterisation
RV	Right Ventricle
TAPSE	Tricuspid Annular Plane Systolic Excursion
TAVI	Transcatheter Aortic Valve Implantation
TDIs	Tissue Doppler Imaging

List of Appendices

Aims of Thesis

The aims of this thesis were to determine whether:

- A ventriculoarterial coupling mismatch causes right ventricular diastolic dysfunction
- A porcine model of right ventricular – pulmonary artery ventriculoarterial coupling can determine the optimal coupling ratio at maximal stroke work
- A ventriculoarterial coupling mismatch causes right ventricular diastolic dysfunction in patients with pulmonary hypertension
- Patients with aortic stenosis undergoing transcatheter aortic valve implantation have improved right ventricular diastolic function after left ventricular afterload reduction following valve implantation; due to ventricular interdependence phenomena leading to changes in left ventricular – right ventricular interaction through septal wall reconfiguration

1 A Theory of RV-PA Ventriculoarterial Coupling and RV Diastolic Dysfunction

1.1 Introduction

William Harvey is considered the father of modern cardiac physiology after he first deduced the existence of blood recirculation and experimentally demonstrated pulmonary blood flow (Comtor, 1982) in his monograph titled “Du Motu Cordis” published in 1628. While the importance of the left ventricle (LV) has long been accepted; the importance of the right ventricle (RV) in cardiac function has been debated greatly over the last 400 years. Starr et al. (1943) reported as late as the mid-twentieth century that the RV had no greater purpose other than to provide a capacitive reservoir to the pulmonary circulation. In more recent times RV function, or more specifically diastolic RV function, has been accepted as an important indicator in the assessment of ventricular dysfunction in heart failure (Riggs, 1993).

The phenomenon of RV diastolic dysfunction was first described in 1993 by Riggs (1993) and abnormalities in RV diastolic function underlie many pathologies (Cicala et al., 2002; Dourvas et al., 2004; Florea et al., 2000; Chakko et al., 1990; Habib and Zoghbi, 1992). However, the underlying mechanisms and precise role of RV diastolic dysfunction in heart failure remain poorly described and are compounded by imprecise definitions of diastolic dysfunction; with the term being used to describe many variants in diastolic pathophysiology and function, such as changes in myocardial relaxation time (Caso et al., 2001), ventricular wall structure (Schwarz and Dashti, 2010), myocardial stiffening (Schwarz and Dashti, 2010), ventricular wall thickening (Schwarz and Dashti, 2010), and abnormal ventricular chamber geometry (Schwarz and Dashti, 2010).

Diastolic dysfunction is a mechanical irregularity in the intrinsic properties of the ventricular muscle function during diastole (Van Herck et al., 2005). However, this

could be directly or indirectly related to changes in arterial distensibility; attributable to changes in coronary flow; a passive change in ventricular compliance; or a dynamic change in ventricular relaxation. RV diastolic dysfunction can be caused by any combination of abnormalities in RV distensibility (Chin and Coghlan, 2012), RV relaxation (Chin and Coghlan, 2012), pericardial constraint (Chin and Coghlan, 2012), and LV distension (Chin and Coghlan, 2012). RV compliance is dependent on myocardial elasticity (Wauthy et al., 2004), end-diastolic volume (Moon et al., 1997) and right coronary artery pressure (Moon et al., 1997). An increase in RV pressure causes increased RV wall stress and dilatation of the ventricle which flattens the inter-ventricular septum (Guazzi et al., 2012). This shift in septal wall position causes the RV to become more spherical in structure and impairs LV function. Abnormalities in LV pressure and end-diastolic volume affect RV diastolic function by limiting RV volume (Chin et al., 2008; Zeng et al., 2011).

Recent work has postulated that RV- pulmonary artery (PA) ventriculoarterial coupling may offer insight into the transition from RV adaptation to RV maladaptation (Kuehne et al., 2004). Simplistically, RV-PA ventriculoarterial coupling is a matching between RV contractility and afterload (Sunagawa et al., 1984). This can be used to interpreted RV function and RV adaptation to afterload.

The work set out in this thesis aims to address whether ventriculoarterial coupling derived from the conductance technique can be used to unlock the mechanisms of RV diastolic function and give clinical insight into the role of RV diastolic dysfunction in different cardiopulmonary disorders and heart failure.

1.2 The Circulatory System

The heart is a pump that propels blood around the body in conduit vessels (Figure 1-1). The heart is made up of four chambers: the upper chambers, or atria, receive the blood returning to the heart and transfer it to the lower chambers, ventricles, which then pump the blood from the heart. The two chambers on the right side send deoxygenated blood to the lungs (pulmonary circulation). The two chambers on the left side supply oxygenated blood through arteries to the rest of the body (systemic circulation). The ventricles contract during systole and relax during diastole. During early diastole isovolumic relaxation occurs, the pressure within the RV diminishes below pulmonary pressure, closing the pulmonary valve and opening the tricuspid valve. Rapid RV filling occurs at the end of isovolumic relaxation during the continued decline in RA pressure that began during isovolumic relaxation due to the suction mechanism caused by the pressure gradient across the RV-RA. The RA then actively contracts during the slow ventricular filling phase to contribute the final 20% of ventricular filling. At the start of isovolumic RV contraction ventricular pressure increases, exceeding RA pressure and causing the tricuspid valve to close. The pressure within the RV continues to increase until it exceeds the pulmonary pressure, forcing the pulmonary valve to reopen and blood to flow into the pulmonary artery. The blood continues to flow into the PA until the pressure in the RV falls below pulmonary pressure again and the cycle is repeated (Figure 1-2).

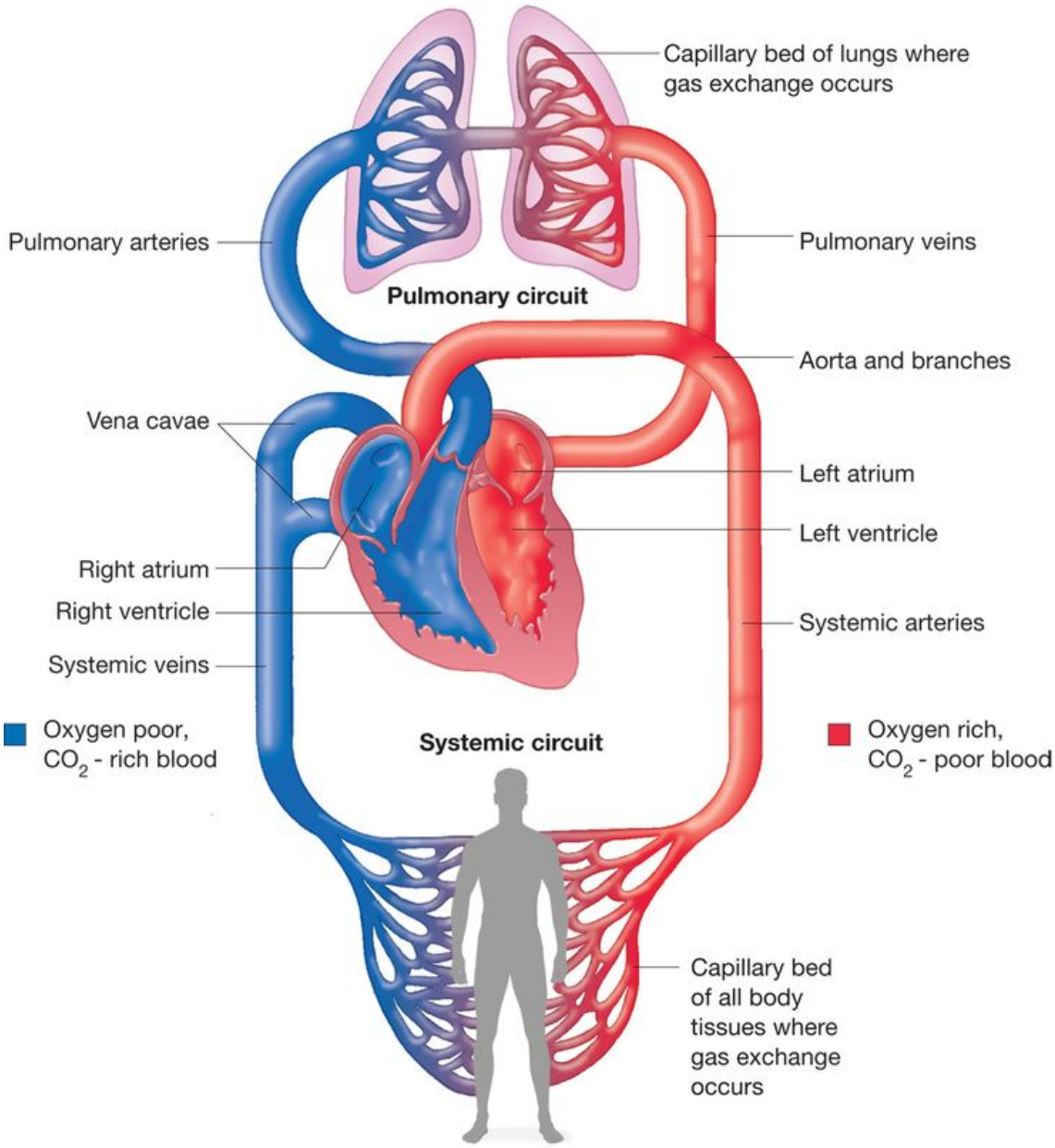

Figure 1-1 The circulatory system, taken from http://www.freerider.ro/wp-content/uploads/2015/12/heart-rate.jpg

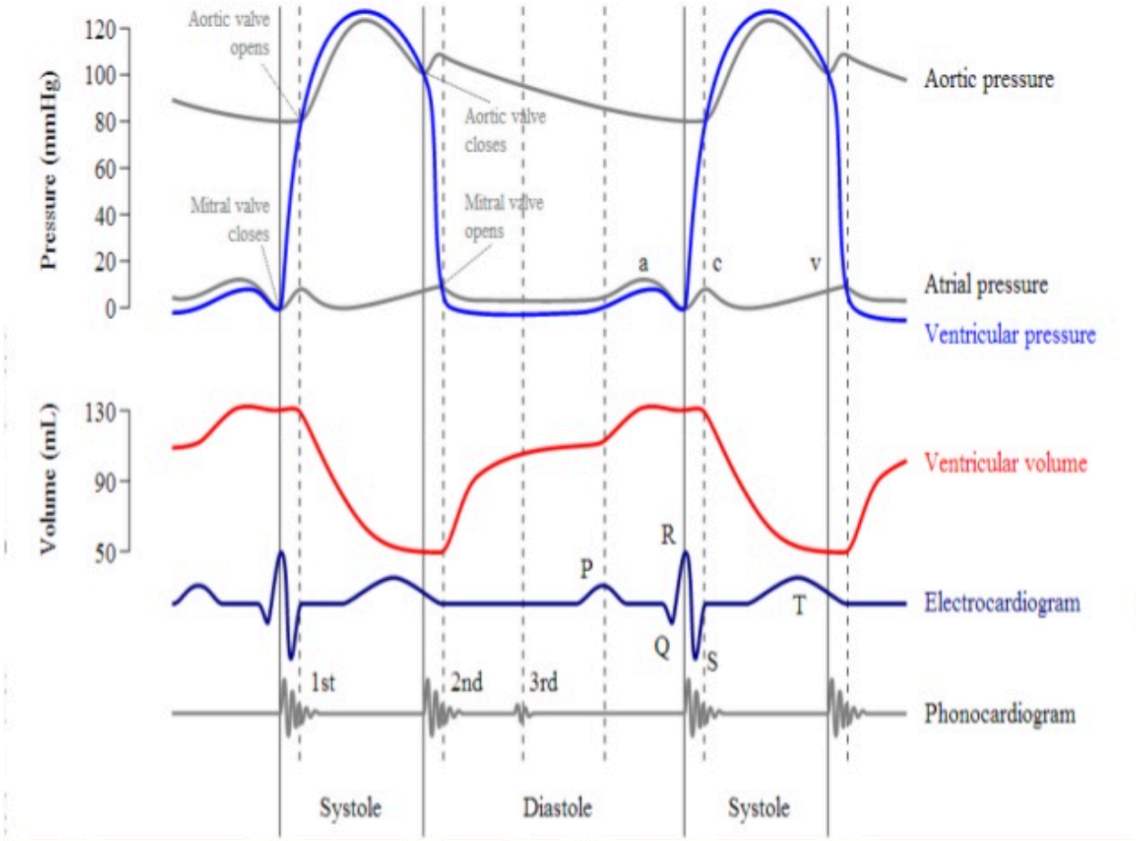

Figure 1-2 The cardiac cycle, taken from http://www.slideshare.net/PraveenNagula/cardiac-cycle-29216898

The primary purpose of the RV and pulmonary circulation is to deliver blood to the lungs for gaseous exchange. The pulmonary artery (PA) is a thin elastic vessel that branches out to support numerous lobar pulmonary arteries, pulmonary arterioles and alveolar capillaries. Since the gaseous exchange happens within thin, permeable alveolar membranes, pulmonary pressures must remain low to prevent pulmonary oedema (abnormal build-up of fluid in the lungs) (Homik et al., 1988). Since the pulmonary circulatory system is in series with the systemic circulatory system, the entire cardiac output (CO) has to pass through the lungs. Therefore, the demand on the RV is considerably different to that in the LV. Not only must the RV deliver a low pressure, high volume pulmonary circulatory system, it has to be able to buffer energetic changes in pressure, volume and flow rates due to changes in cardiac output, respiration and LV haemodynamics.

In routine clinical care, pulmonary vascular resistance (PVR) is used to determine the afterload experienced by the RV. PVR is defined as the resistance in the pulmonary vascular bed against which the RV must eject blood. However, PVR is predominately determined from the small vessel resistance or physical obstruction of the larger pulmonary vessels and ignores the pulsatile nature of both pressure and flow. PVR can be determined using the equation:

Equation 1-1

$$PVR = \frac{(mPAP - LAP) \times 80}{CO}$$

Where $mPAP$ is the mean PA pressure, LAP is the left atrial pressure and CO is the cardiac output. While the pulsatile nature of PA load is low in health, the pulsatile load may be amplified in different disease states such as pulmonary embolism (Castelain et al., 2001) and septic shock (Lambermont et al., 1999). In this way, full characterization of the resistance to blood flow in the pulmonary circulation can only be determined from combined parameter models such as the windkessel model (Grant and

Paradowski, 1987), which encompass all three major components: PVR; pulmonary artery compliance; and dynamic inductance. Compliance describes the elastic properties of the vessel, defined as the ratio of volume to pressure change. These elastic vessel properties buffer blood flow during RV ejection, which helps to reduce the overall pulmonary artery pressure exposed to the distal vasculature. Inductance describes the dynamic response of the vessel as it adapts to changes in the blood flow through the vessel due to the relative mass and inertia of the blood.

In this thesis, the conductance technique will be used to confirm effective arterial elastance (Ea), defined as the ratio of end-systolic pressure to stroke volume, as a combined parameter model of pulmonary afterload. This has been well characterised in experimental models of the systemic (Sunagawa et al., 1983) and pulmonary (Morimont et al., 2008) circulation.

1.3 The Right Ventricle

The normal RV is a complex geometrical shape (Dell'Italia, 1991). The RV is described in terms of three anatomical components (Figure 1-3A): an inlet made up of the tricuspid valve, chordae tendineae and papillary muscles; a coarse trabeculae myocardium; and an outflow tract or conus extending from the pulmonary valve (Goor and Lillehei, 1975; Ho and Nihoyannopoulos, 2006). The normal RV free wall contracts in a peristaltic movement, starting at the base and apex and finishing at the outflow tract (Dell'Italia, 1991). There is a delay of approximately 25 – 50 ms between the start of the contraction at the inflow to outflow tract regions (Dell'Italia, 1991) and the outflow tract remains contracted longer. The RV muscle fibres predominantly shorten in the long axis during contraction, a small inward motion of the free wall ejects the same stroke volume as the LV.

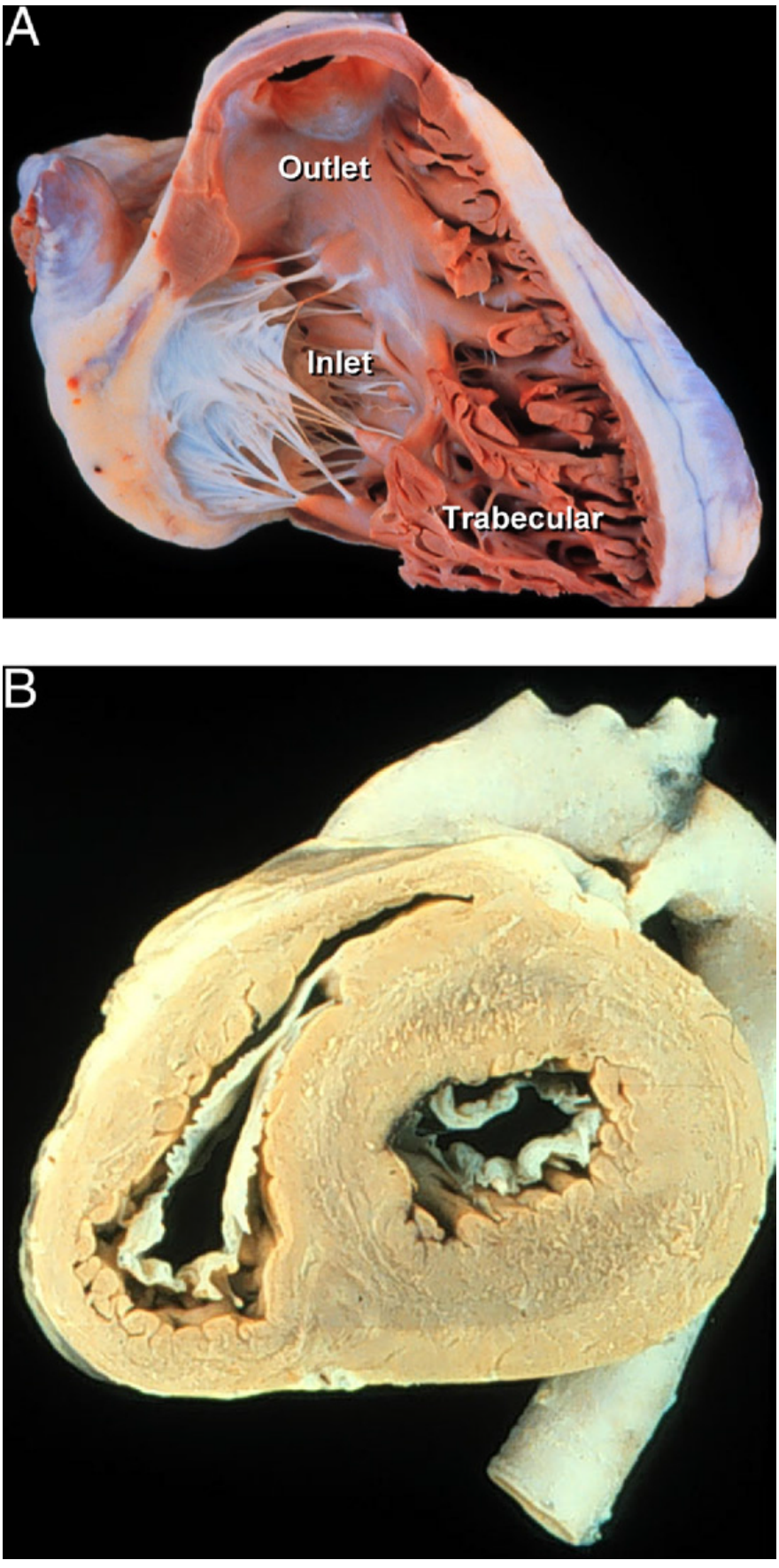

Figure 1-3 (A) Pathological specimen of the RV with the free-wall removed to show the three anatomical regions. (B) Pathological specimen of the heart cut transversely to show the crescent shape of the RV. Taken from Warnes (2009)

In contrast to the LV that couples with the systemic circulation, the RV is coupled to the pulmonary circulation, which under normal loading conditions has a lower vascular resistance and higher arterial distensibility (Dell'Italia, 1991). Therefore, in health the RV pressures are much lower than LV pressures (Zipes and Braunwald, 2005); the RV chamber remains concave towards the LV during both systole and diastole (Figure 1-3B); and the RV has a thin ventricular free wall that has a muscle mass approximately one-sixth of the LV (Dell'Italia, 1991). Connections between the muscle fibres of the RV and LV tether the ventricles together through the inter-ventricular septum. Septal wall reconfiguration, along with the effect of the pericardium causing pericardial constraint (which in health contributes 70% of RV diastolic function), has an impact on the diastolic phenomenon known as ventricular independence (Dell'Italia, 1991; Brookes et al., 1998). The size, shape and compliance of one ventricle can directly affect the size, shape and haemodynamic function of the contralateral ventricle (Santamore and Dell'Italia, 1998a), caused by ventricular-ventricular interactions, through septal wall motion reconfiguration assuming minimal free wall motion caused by pericardial constraint. The muscle fibres of the RV free wall are orientated transversely and squeeze the blood within the ventricle in a circumferential compression motion (Saleh et al., 2006). The inter-ventricular septum is formed of an ascending and descending apical loop of obliquely orientated muscle fibres (Torrent-Guasp et al., 2001), which continue to form the LV free wall. Therefore, the higher LV pressures and oblique orientation of the septal muscle fibres means the septal twist and shortening during contraction accounts for a significant proportion of the RV ejection force during systole.

1.4 The Assessment of RV Diastolic Dysfunction

The detailed assessment of the RV contractile performance is challenging due to the complex geometric shape of the RV structure. Since the pulmonary circulation is fundamentally different to the systemic circulation, the contractile performance of the better characterised LV is not transferrable to the RV (Bellofiore and Chesler, 2013).

Clinical RV diastolic dysfunction can be assessed non-invasively using imaging techniques such as Echocardiography (Chakko et al., 1990; Zimbarra Cabrita et al., 2013) and Cardiac Magnetic Resonance (CMR) (Kilner, 2011; Kilner et al., 2010); and invasively using Radionuclide Angiography (Davlouros et al., 2006), Right Heart Catheterisation (RHC) (Kolb and Hassoun, 2012) and Conductance Catheterisation (McKay et al., 1984; McCabe et al., 2014).

1.4.1 Non-Invasive Assessment of RV Diastolic Dysfunction

1.4.1.1 Echocardiography

Echocardiography is a non-invasive ultrasound assessment technique that can be used to assess RV function (Davlouros et al., 2006). Typically RV volume is assessed in comparison to the LV, described as either normal, mildly, moderately or severely enlarged (Warnes, 2009). The complex geometrical shape and trabeculated internal structure of the RV, combined with the long- and short-axis measurement techniques (Lai et al., 2008), mean the mathematical modelling assumptions that are needed to quantify LV volume and function from 2D echocardiography are based on geometric assumptions that do not translate to the RV (Warnes, 2009). The continued improvement of real-time 3D echocardiography allows volumes to be calculated which are comparable with the gold standard MRI-derived volumes (Leibundgut et al., 2010). However, limitations with defining the endocardial border of the thin walled RV means those volumes are typically smaller than those derived by MRI (Danton et al., 2003).

2D echocardiography can be used to measure septal wall motion, with the LV eccentricity index (LVEI) being a measure of ventricular interdependence (Ryan et al., 1985). The LVEI describes the geometrical relationship between the LV and RV (Ryan et al., 1985). The LVEI is calculated by dividing the distance between the inferior to the anterior free wall, by the distance between the septum to the lateral free wall (Ryan et al., 1985; Wilkins et al., 2005). An EI > 1 is considered abnormal and geometrically describes a D-Shaped LV (Wilkins et al., 2005). Spectral Doppler echocardiography

can be used to diagnose RV diastolic dysfunction by performing measurements on the flow across the tricuspid valve (Chakko et al., 1990). Characteristically two waves are seen on the spectral Doppler trace; the passive pre-load filling of the ventricle (E-wave); and the active filling with atrial systole (A-wave). In the normal RV, the E-wave velocity is greater than the A-wave velocity. An E/A ratio < 1 is abnormal indicating slow filling and RV diastolic dysfunction. The E/A ratio can be termed pseudo-normalized where the E/A ratio appears to be normal, however, by performing a Valsalva manoeuvre and repeating the measurements the irregular relaxation pattern can be unmasked. Tissue Doppler Imaging (TDI) can be used to measure the RV Isovolumic Relaxation Time (IVRT), a measure of diastolic function. The RV IVRT is the time interval between the closure of the pulmonary valve and the opening of the tricuspid valve. An RV IVRT >75ms is considered abnormal (Zimbarra Cabrita et al., 2013). RV IVRT has been shown to correlate well with pulmonary arterial systolic pressure (Zimbarra Cabrita et al., 2013). Tricuspid annular plane systolic excursion (TAPSE) represents the distance of systolic excursion of the RV annular plane to the RV apex. It is obtained using M-Mode aligned through the triscupid lateral annulus in a four-chamber view and measuring the longitudinal displacement at systole. In the normal RV TAPSE should be greater than 15-20 mm (Jurcut et al., 2010), and has been shown to correlate well with isotopic RV ejection fraction (Kaul et al., 1984). RV fractional area change (FAC) expresses the percentage change in RV area between end-diastole and end-systole. It has been shown to have a good correlation with MRI-derived RV ejection fraction (Morcos et al., 2009). The main limitation when calculating RV FAC is the need for good endocardial boarder delineation, which can be challenging in the trabeculated RV. All echocardiographic measures of RV function are load-dependant. Therefore, measurements made on different occasions can be difficult to correlate and interpret correctly.

1.4.1.2 Cardiac Magnetic Resonance Imaging

Cardiac Magnetic Resonance (CMR) is considered the gold standard technique for non-invasively assessing RV mass, volume and ejection fraction (Kilner, 2011; Kilner et al., 2010); and has been shown to correlate well with disease severity (van Wolferen et al., 2007). However, coarse trabeculations and difficulties in defining the endocardial border can make this difficult (Niemann et al., 2007; Winter et al., 2008), leading to considerable inter- and intra-operator variability in the precision of the measurement of RV function (Sheehan et al., 2008). CMR also excludes patients with metallic implantable devices and has a relatively high cost when compared with other functional imaging assessment techniques (Babu-Narayan et al., 2005). Limits on the spatial resolution of the CMR image acquisition process means the images have to be processed offline and do not provide a beat-to-beat real-time assessment of RV size and function. Currently, novel applications only extend as far as calculating mean pressures (Reiter et al., 2008).

1.4.2 Invasive Assessment of RV Diastolic Dysfunction

1.4.2.1 Radionuclide Angiography

Radionuclide Angiography was first developed over 50 years ago (Folse and Braunwald, 1962) and once considered as the gold standard technique for assessing RV function (Davlouros et al., 2006). Radionuclide Angiography has all but been replaced by newer non-invasive methods like echocardiography and CMR (Vogel et al., 1997; Pignatelli et al., 2003; Samyn, 2004). This replacement of Radionuclide Angiography is mainly due to the invasive nature of the technique, the requirement of a potentially significant dose of ionising radiation and contrast agents (Davlouros et al., 2006); and the fact it is not as accurate as the other non-invasive methods (Davlouros et al., 2006).

1.4.2.2 Right Heart Catheterisation

Right Heart Catheterisation (RHC) remains the gold standard assessment technique for pulmonary and RV pressures (Kolb and Hassoun, 2012). An increased pressure in the RV is often associated with RV dilatation that causes the septum to shift towards the LV causing LV diastolic dysfunction. The RHC can measure load-dependent indices of RV function such as the time constant of diastolic relaxation (tau) (Weiss et al., 1976; Raff and Glantz, 1981; Matsubara et al., 1995) and the first derivative of RV Pressure (dP/dt min) (Bachman et al., 2013). Both are load-dependent, and cannot assess how the ventricle is coupled with the pulmonary vasculature.

1.4.2.3 Conductance Catheterisation

The Pressure-Volume (PV)-loop derived by a conductance catheter is a sensitive invasive measure of LV (Baan et al., 1984) and RV function (McKay et al., 1984). However, due to the cost of the equipment, invasive nature of the procedure and technical complexities in the measurement technique it is currently limited to a research setting. The significant clinical contribution of the conductance catheter to RV function is the real-time beat-to-beat assessment of simultaneous ventricular pressures and volumes. The RV PV-loop (Figure 1-4) can be interrogated to determine systolic and diastolic properties of myocardial performance. Typically the RV PV-loop is triangular in loop morphology as the ejection of blood from the ventricle continues during pressure decline within the ventricle due to the increased compliance of the pulmonary vasculature structure. The PV-loop can also offer a load-independent measure of RV contractility and compliance, currently unobtainable by other invasive and non-invasive methods (Kass et al., 1986; Kass et al., 1988). This load-independent measure is obtained by collecting a family of PV-loops while altering the pre-load on the ventricle, typically achieved by an Inferior Vena Cava (IVC) balloon occlusion (Kass et al., 1986; Kass et al., 1988). Conductance theory is described in detail in Section 2.3.

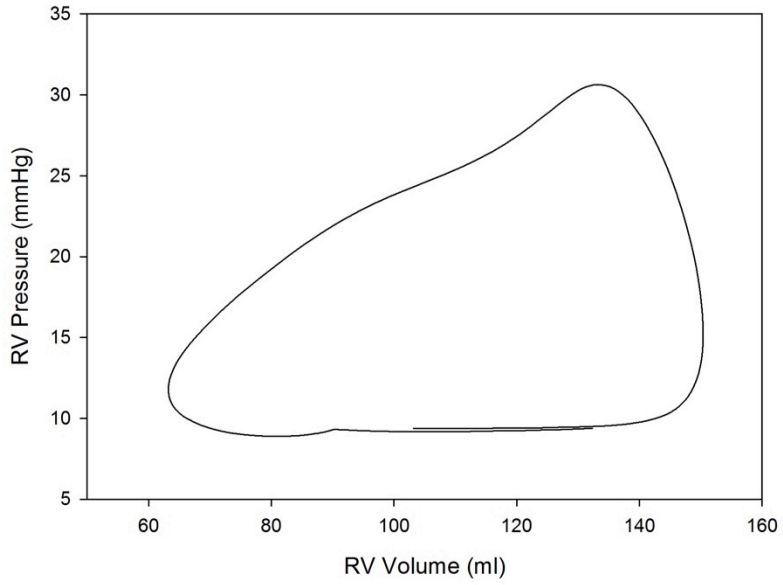

Figure 1-4 The normal RV PV-loop derived from the conductance catheter technique.

1.5 Factors Affecting RV Diastolic Dysfunction

Three main factors that have been independently described which could have an effect on RV diastolic dysfunction: Coronary Flow Reserve, Ventricular Interdependence and Ventriculoarterial Coupling.

1.5.1 Coronary Flow Reserve

Coffman and Gregg first described the concept of Coronary Flow Reserve (CFR) 1960, where the coronary circulation was described to have a maximal hyperaemic blood flow capacity (Coffman and Gregg, 1960). At rest, coronary flow depends on myocardial oxygen demand which is affected by heart rate (Ramanathan and Skinner, 2005), ventricular contractility (Ramanathan and Skinner, 2005) and ventricular load (Ramanathan and Skinner, 2005). Coronary flow at rest when the myocardial oxygen demand is constant is within the limits of autoregulation and can be considered independent of perfusion pressure (Rigo, 2005). During hyperemia there is an increase in microvascular volume and myocytes adjacent to these vessels are stretched, opening stretch-activated calcium channels, causing calcium influx and augmentation of calcium-dependent myofibrillar contractility, known as the Gregg effect (Gregg, 1963). Reactive hyperaemia is an augmentation of coronary flow due to coronary vasodilatation to repay the oxygen debt (Heyndrickx et al., 1975). In a model of LV supply ischemia (Hoole et al., 2010) this hyperemic response masks stunning in the early phase of reperfusion (Stahl et al., 1986). Interestingly, diastolic dysfunction remains depressed during this period and this may be due to a scaffold effect from distended coronary and collateral vessels during hyperemia that stiffens the ventricular cavity (Hoole et al., 2010). At maximal microvascular dilation, coronary flow can no longer be considered autoregulated, and coronary flow varies linearly with perfusion pressure (Rigo, 2005). CFR is the difference between the basal coronary flow during the autoregulation plateau and the hyperaemic coronary flow during maximal microvascular dilation (Rigo, 2005). Therefore, CFR is expressed by the ratio between basal and hyperaemic coronary flow. Since the hyperaemic coronary flow is linearly

related to perfusion pressure, CFR can also be expressed as the relationship between instantaneous maximal coronary diastolic flow and pressure (Mancini et al., 1989; de Bruyne et al., 1996), measured using invasive Doppler and pressure wires. The normal range for CFR, when measured with Doppler catheters, is 3.5 to 4.5 (Marcus et al., 1987), and is clinically considered abnormal < 2.0 (Westerhof et al., 2006).

Clinically, CFR is a useful tool for understanding basic physiological function (De Rosa et al., 2011); interpreting the effects of structural (De Rosa et al., 2011) and pharmacological (Galderisi and D'Errico, 2008) interventions on coronary flow. CFR has been demonstrated as a sensitive marker for patient outcome, with echocardiographic studies showing that preserved CFR in the Right Coronary Artery (RCA) predict a favourable patient outcome (Cortigiani et al., 2009), whereas an impaired or reduced CFR is a predictor of dysfunction and worse patient outcome (Cortigiani et al., 2009; Rigo et al., 2011). Although little work has been completed to look at the effect of CFR on the RV function, studies have demonstrated links between impaired CFR and LV diastolic dysfunction (Galderisi et al., 2001; Galderisi et al., 2002; Teragaki et al., 2003). Galderisi et al. (2008) demonstrated that decreased CFR is associated with impaired relaxation and increased filling pressures; thus, reduced CFR is independent of LV geometry and pre-load. Patients with diabetes mellitus have a reduced CFR, which may cause myocardial ischemia due to a disturbance of coronary microcirculation and lead to LV diastolic dysfunction (Strauer et al., 1997; Kalkan et al., 2013). However, this is further complicated as the coronary flow velocity waveforms differ between the RCA and LCA (Hadjiloizou et al., 2008), so the studies on CFR and LV diastolic dysfunction may or may not be transferable to the RCA and RV diastolic dysfunction.

1.5.2 Ventricular Interdependence

Bernheim (1910) first demonstrated the concept of ventricular interdependence in 1910, where RV function was shown to be compromised by compression of the RV

through dilation of the LV. Subsequently, Henderson and Prince demonstrated that RV filling was influenced by LV function in 1914 (Henderson, 1914). There is not a functional left- and right-sided septum, hence abnormalities in LV or RV function directly affects the contralateral ventricle and vice versa. Ventricular interdependence means that the dysfunction of one ventricle will lead to the dysfunction of the contralateral ventricle and eventual heart failure. An increase in ventricular dysfunction will result in an increase in the end-diastolic pressure and cause the septum to bow towards the contralateral ventricle in the presence of an intact pericardium (Saleh et al., 2006). This geometrical change in chamber orientation directly affects the orientation of the septal muscle fibres and will reduce the contribution of septal contraction to the overall contraction of both ventricles (Saleh et al., 2006). LV dysfunction can alter the geometry of the two ventricles and the position of the septal wall and may cause RV contraction to be predominantly provided by weaker contraction of the RV free wall. Clinical echocardiographic studies of patients with aortic stenosis (Efthimiadis et al., 1999) and those with systemic hypertension (Chakko et al., 1990; Cicala et al., 2002), have shown that the subsequent increase in LV pressures can lead to RV diastolic dysfunction. Similarly, clinical echocardiographic studies in patients with hypertrophic cardiomyopathy (Efthimiadis et al., 2002) and those with RV hypertrophy (Kitahori et al., 2009) have shown elevated RV pressures have been reported to cause LV diastolic dysfunction.

The ability to use the conductance catheter simultaneously to derive PV-loops in the LV and RV could feasibly allow for the critical analysis of LV-RV interaction in many clinical pathologies (Faber et al., 2006). Therefore, this may offer new therapeutic approaches for the treatment of RV dysfunction, e.g. by treating and improving LV function ventricular interdependence should reduce the inter-ventricular load on the RV and subsequently improve RV function.

1.5.3 Ventriculoarterial Coupling

Sunagawa et al. (1983) first described the concept of ventriculoarterial coupling in 1983 using an isolated canine heart model and is fundamental to the correct interpretation of RV function. To understand ventriculoarterial coupling in the RV, we must first consider the normal healthy LV, coupled to the aorta. During systole, the aorta acts as an energy reservoir and delivers energy back to the LV during diastole. Effectively, all the energy expended during the pulsatile contraction of the LV is converted into flow energy due to the elastic recoil of the aorta (Yaginuma et al., 1985; Sasayama and Asanoi, 1991) hence, the LV can be considered to be well coupled with the aorta. The normal healthy RV is coupled with the pulmonary vascular structure, but the coupling is more complex than with the aorta. The pulmonary artery is a relatively short elastic proximal vessel that branch early into the pulmonary trunk. This relatively short elastic proximal portion of the pulmonary vessels means that 25-40% of the energy expended during the pulsatile contraction of the RV is not converted in to flow energy due to the restricted elastic recoil of the pulmonary vessels (Grignola et al., 2007; Saouti et al., 2010). Further stiffening of the pulmonary vessels will increase the afterload on the ventricle, increasing the systolic pressure (Chen et al., 1998) and will cause abnormalities in diastolic relaxation times and pressures (Leite-Moreira et al., 1999).

Although non-invasive Echocardiography and CMR are widely accepted as the clinical standard for the assessment of RV function they cannot provide a load-independent beat-to-beat assessment of RV contractility. An assessment of ventriculoarterial coupling cannot be performed using non-invasive methods without making assumptions about pressures and volumes. Load-independent assessment can be provided from interrogating the PV-loop measured using a conductance catheter. This was first performed in the RV by McKay et al. (1984), where they successfully used the Valsalva manoeuvre to collect a family of loops from which the load independent parameters could be calculated. The ventriculoarterial coupling ratio is defined by the

relationship between the End-Systolic Elastance (E_{es}) and the Effective Arterial Elastance (E_a):

Equation 1-2

$$Ventriculoarterial - Coupling\ Ratio = \frac{E_a}{E_{es}}$$

The E_{es} of the RV is defined by as the slope of the end-systolic pressure volume relationship (ESPVR). The ESPVR can be measured by obtaining a family of loops from a preload reduction, routinely performed by an inferior vena cava (IVC) balloon occlusion. E_a is a steady state parameter which offers an assessment of RV afterload that incorporates the principal elements of the windkessel model of the pulmonary vascular bed (Sunagawa et al., 1983; Sunagawa et al., 1985). The PV-loop derived from a conductance catheter allows E_a to be calculated from the ratio of End-Systolic Pressure (P_{es}) to Stroke Volume (SV):

Equation 1-3

$$E_a = \frac{P_{es}}{SV}$$

The ratio between E_{es} and E_a describes the energetic efficiency of the energy transfer between the RV and pulmonary vasculature. Typically a normal coupling ratio is close to 1.0; the RV and pulmonary vessels would be considered uncoupled if the E_{es}/E_a ratio was anything less than or greater than 1.0 (Kawaguchi et al., 2003).

1.6 Translating Sunagawa's Theory of Ventriculoarterial Coupling to the RV

Sunagawa et al. (1987) deconstructed the circulatory system into four major components (left heart - systemic vascular bed; right heart - pulmonary vascular bed) in a bilaterally coupled system (Figure 1-5) (Sunagawa et al., 1984). The cardiac output (CO) through each of the functional blocks (systemic and pulmonary) were calculated from the pressure across the inflow and outflow. The CO of the left heart - systemic vascular bed, CO_s, was defined by:

Equation 1-4

$$CO_s = F_s\,(P_{ra}, P_{la})$$

Where F_s is the systemic flow, P_{ra} is the mean right atrial pressure and P_{la} is the mean left atrial pressure. In the same way, the CO of the right heart - pulmonary vascular bed, CO_p, was defined by:

Equation 1-5

$$CO_p = F_p\,(P_{ra}, P_{la})$$

Where F_p is the pulmonary flow. Since the CO through both the systems must be identical, the closed-loop CO was determined from the equilibrium flow when $F_s = F_p$.

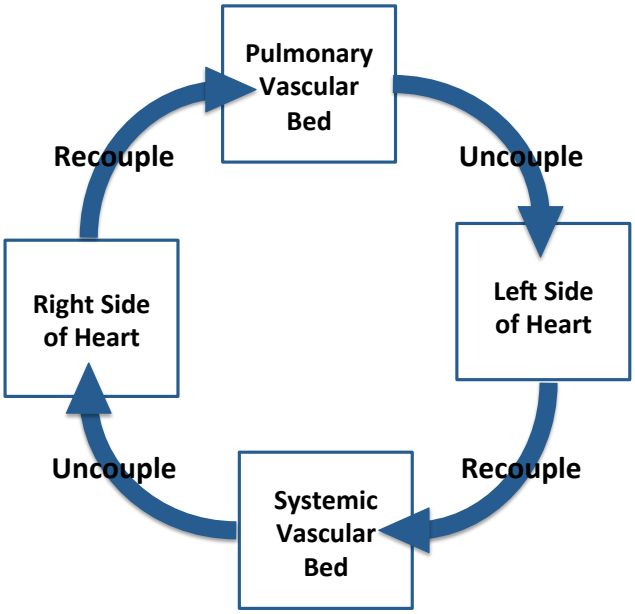

Figure 1-5 The four major components of the circulatory system in a bilaterally coupled system, taken from Sunagawa et al. (1984)

The coupling between the ventricular and arterial systems was then characterised using the ESPVR. Since ESPVR is a sensitive load-independent marker of contractility, the relationship between left ventricular end-systolic pressure (P_{es}) and stroke volume was defined by:

Equation 1-6

$$P_{es} = E_{es} (V_{ed} - SV - V_0)$$

Where E_{es} is the slope of the ESPVR, V_{ed} is end-diastolic volume, and V_0 is the volume axis intercept of the ESPVR slope. Therefore, for a given V_{ed}, P_{es} varies linearly and inversely with SV (Figure 1-6), so the ventricular system could be characterised in terms of a P_{es}- SV relationship.

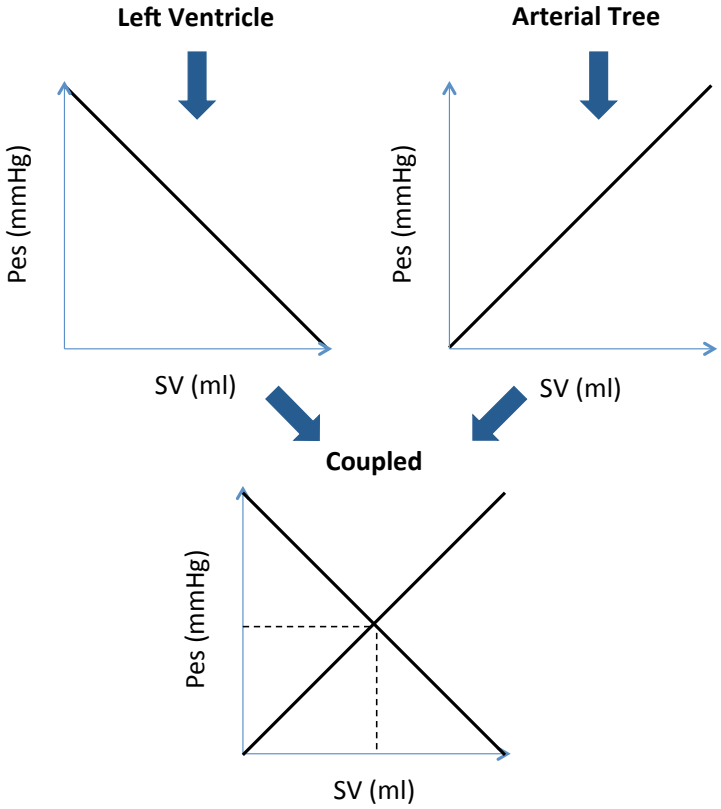

Figure 1-6 Characterising the left ventricular and arterial system in terms of end-systolic pressure to stroke volume, the intersecting stroke volume represents the point where the ventricle is coupled to the arterial system, taken from Sunagawa et al. (1983)

The arterial system was also characterised in terms of a P_{es} - SV relationship. Graphically both systems are coupled at the intersection between the two lines (Figure 1-6). The relationship between the mean arterial pressure (MAP) and mean arterial flow (F_a) was defined by:

Equation 1-7

$$MAP = R_T F_a$$

Where R_T is the total arterial resistance. From the assumption that P_{es} equals MAP and F_a can be estimated with SV divided by the cycle length of cardiac contraction (T), the P_{es} was defined by:

Equation 1-8

$$P_{es} = \frac{R_T}{T} SV$$

Therefore the slope of the P_{es}- SV relationship, more commonly termed the effective arterial Elastance (E_a), could be approximated by:

Equation 1-9

$$E_a = \frac{R_T}{T}$$

Expermentally, Sunagawa et al. (1984) used a working heart perfusion model to isolate LV ejection against fixed arterial resistances (afterload) and demonstrated a high correlation (r = 0.999; P < 0.001) between R_T / T and the PV-loop derived E_a. Therefore, E_a can be estimated using the P_{es}- SV relationship with a high level of accuracy by dividing the total arterial resistance by the duration of one cardiac cycle. The slopes of the P_{es}- SV relationships have the units of volume elastance (mmHg / ml). The arterial system is treated as an elastic chamber with effective arterial elastance (E_a) and the ventricle is treated as an elastic chamber with end-systolic elastance (E_{es}).

The arterial elastance is not a direct measure of the physical elastance or compliance of the arterial system. Rather it is termed the effective arterial elastance as it changes more in terms with physical arterial resistance then arterial compliance. Characterising the arterial and ventricular systems in terms of the P_{es}- SV relationship allows the determination of the intersecting SV that would result in a coupled ventricular-arterial system, derived from Equation 1-6 and Equation 1-8:

Equation 1-10

$$SV = \frac{E_{es}\,(V_{ed} - V_0)}{(E_{es} + E_a)}$$

After predicting the equilibrium SV when the ventricle is coupled to the arterial system, it is possible to determine how much blood volume will be transferred from the first elastic chamber (left ventricle – with a known volume elastance and initial volume) to the second elastic chamber (arterial system - with a known volume elastance). The distribution of blood volume between the two chambers is determined by the ratio of the volume elastance values or more commonly termed the ventriculoarterial coupling ratio (E_{es}/E_a).

Sunagawa et al. (1987) developed a simplified graphical approach of using the pressure-volume relationship to describe the ventriculoarterial coupling ratio in terms of changes in arterial resistance (afterload), end-diastolic volume (preload) and contractility on stroke volume. His work demonstrated that the fundamental concept of ventriculoarterial coupling could be graphically represented using the end-systolic pressure and ventricular volume plane (Figure 1-7) rather than needing to measure the arterial system directly (Figure 1-6). In this graphical representation, Line A is the slope of the arterial ESPVR, E_a, and is determined by connecting a straight line between the end-systolic pressure point on the PV-loop with the volume axis intercept, the end-diastolic volume. Line B is the slope of the ventricular ESPVR, E_{es}, which can be determined by plotting a family of PV-loops during a change in preload, typically

determined from a preload reduction. Line B has a volume intercept V_0. Graphically, the intersecting point between the arterial and ventricular ESPVR lines, A and B respectively, determines how the ventricle is coupled with the arterial system. The stroke volume is the difference between the end-diastolic volume and end-systolic volume.

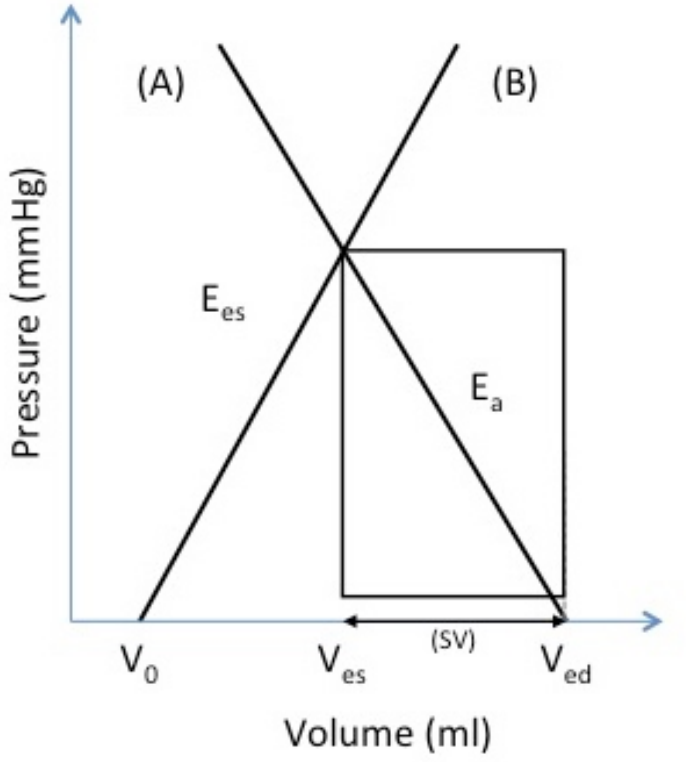

Figure 1-7 The graphical representation of LV ventriculoarterial coupling taken from Sunagawa et al. (1987)

Sunagawa et al. (1987) then demonstrated how this graphical approach could be used to observe how changes in arterial resistance (afterload), end-diastolic volume (preload) and contractility affect stroke volume and subsequently influence the ventriculoarterial coupling parameters. Figure 1-8A shows the effect of varying afterload (arterial resistance) while maintaining a constant preload and contractility. Since E_a can be estimated from R_T/T, increasing the arterial resistance (Red) increases the slope of the arterial ESPVR (E_a). Hence, the SV decreases as the intersection between the arterial and ventricular ESPVR moves to the right. Conversely, a decrease in arterial resistance (Blue) will cause the SV to increase as the intersection between the arterial and ventricular ESPVR moves to the left. Figure 1-8B shows the effect of varying LV preload (end-diastolic volume) while maintaining a constant afterload and contractility. An increase in the end-diastolic volume (Red) will cause the arterial ESPVR (E_a) to shift to the right, hence, SV increases. Conversely, a decrease in the end-diastolic volume (Blue) will cause the arterial ESPVR (E_a) to shift to the left, hence, SV decreases. Figure 1-8C shows the effect of varying LV contractility while maintaining a constant afterload and preload. An increase in the LV contractility (Red) will increase the slope of the ventricular ESPVR while maintaining the same volume intercept (V_0). Since the slope of the arterial ESPVR (E_a) remains constant, SV increases. Conversely, a decrease in the LV contractility (Blue) will decrease the slope of the ventricular ESPVR and subsequently decrease the SV.

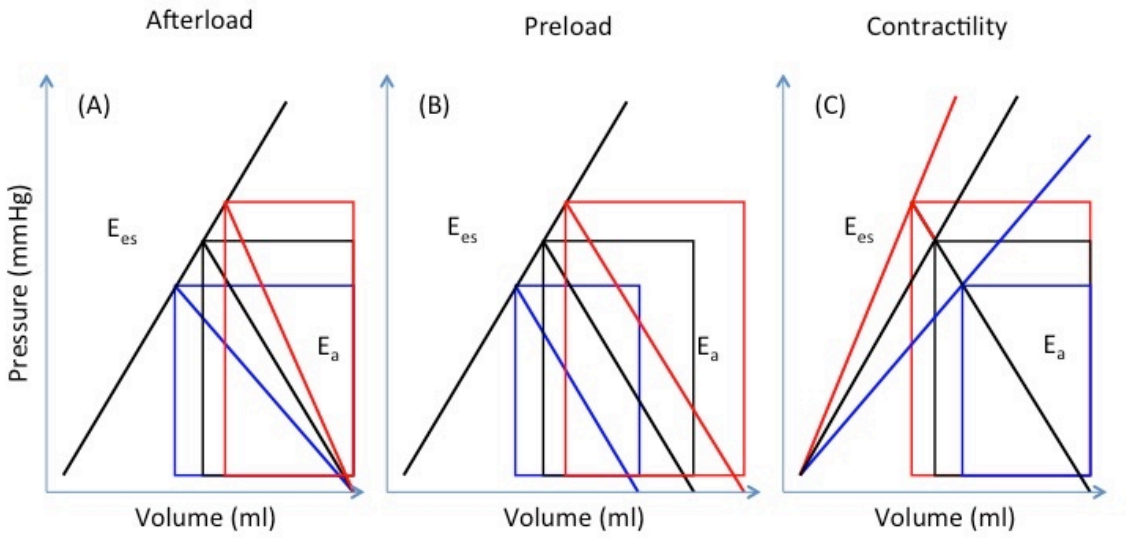

Figure 1-8 The effects of changing (A) afterload; (B) preload; and (C) contractility on the LV ventriculoarterial coupling pressure volume relationship at (Black) baseline; (Blue) reduced; and (Red) increased, taken from Sunagawa et al. (1987)

The PV-loop can be used to determine the mechanical efficiency of the ventricle as it pumps blood around the body. The efficiency of the heart to pump blood against the vascular system can be defined by the ratio of mechanical work done by the heart and the energy consumed by the heart to perform this work. In normal aerobic conditions, the source of the heart muscles energy can be considered proportional to the oxygen consumed by the myocardium from coronary blood flow. The total mechanical work performed by the LV is the sum of the external stroke work (SW) that propels the blood from the ventricle and mechanical potential energy (PE) stored in the ventricle at the end of each contraction (Suga, 1979). However, the theory of ventriculoarterial interaction only incorporates the mechanical work required to propel blood from the ventricle in to the aorta, the LV SW (Burkhoff and Sagawa, 1986). Therefore, from the theory of ventriculoarterial interaction, LV efficiency can be defined by the ratio between LV SW and oxygen consumption (Burkhoff and Sagawa, 1986).

The pressure volume relationship can be used to determine Pressure-Volume Area (PVA), a linear surrogate for the oxygen consumed by the myocardium from coronary blood flow (Suga et al., 1980; Suga et al., 1983; Suga et al., 1984). PVA is defined as the sum of the SW (area bound within the PV-loop) and PE (triangular portion defined by the ESPVR and EDPVR) shown in Figure 1-9. Therefore, ventricular efficiency can be calculated from the equation:

Equation 1-11

$$Ventricular\ Efficiency = \frac{SW}{PVA}$$

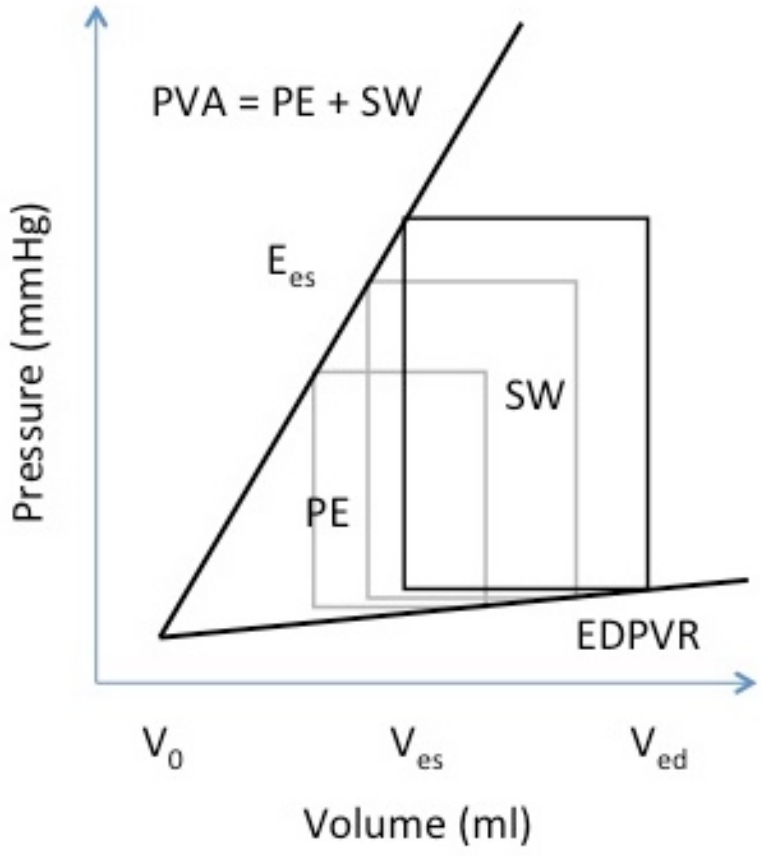

Figure 1-9 LV pressure-volume relationship. The end-systolic pressure volume relationship is characterised by slope Ees and volume axis intercept V_0. The pressure-volume area (PVA) is the sum of external stroke work (SW) and potential energy (PE) taken from Burkhoff and Sagawa (1986)

In health, the SW-Ea relationship is ideally coupled to maintain optimal cardiac output but it is possible to determine the maximal achievable efficiency (SW/PVA) and maximal SW in response to an acute artificial increase in afterload (Ea). This has been demonstrated in both theoretical (Burkhoff and Sagawa, 1986) and experimental (De Tombe et al., 1993) relationships between LV function and increasing aortic afterload. Figure 1-10 shows that Burkhoff and Sagawa (1986) used a theoretical model for predicting that maximal efficiency occurs at a lower afterload than maximal SW. This finding was supported by the experimental canine isolated heart model developed by De Tombe et al. (1993). The Ea at which maximal SW is reached is termed $Ea_{max\ sw}$ (Figure 1-11B). Below the $Ea_{max\ sw}$ threshold there is LV energetic reserve, however, if exceeded there is no energetic reserve and LV dysfunction will ensue (Burkhoff and Sagawa, 1986).

Since auto-regulation takes between 30 to 60 seconds for ventricular contractility to adapt in response to increasing afterloads (von Anrep, 1912), it is possible to use an acute variation in afterload change to determine the SW-Ees/Ea relationship. In the isolated canine heart De Tombe et al. (1993) determined maximal SW occurred at the inverse ventriculoarterial coupling ratio (Ea/Ees) of 0.80 ± 0.16 (Figure 1-11B). The inverse Ea/Ees coupling ratio at which maximal SW is reached is termed $Ea/Ees_{max\ sw}$. Below this inverse $Ea/Ees_{max\ sw}$ coupling threshold there is LV energetic reserve, however, if exceeded there is no energetic reserve and LV dysfunction will ensue.

However, the ventriculoarterial coupling ratio is normally presented as LV contractility over LV afterload (Ees/Ea). Therefore, the Ees/Ea coupling ratio at which maximal SW is reached is termed $Ees/Ea_{\ max\ sw}$. If this $Ees/Ea_{\ max\ sw}$ coupling threshold is exceeded there is LV energetic reserve, however, below this threshold there is no energetic reserve and LV dysfunction will ensue.

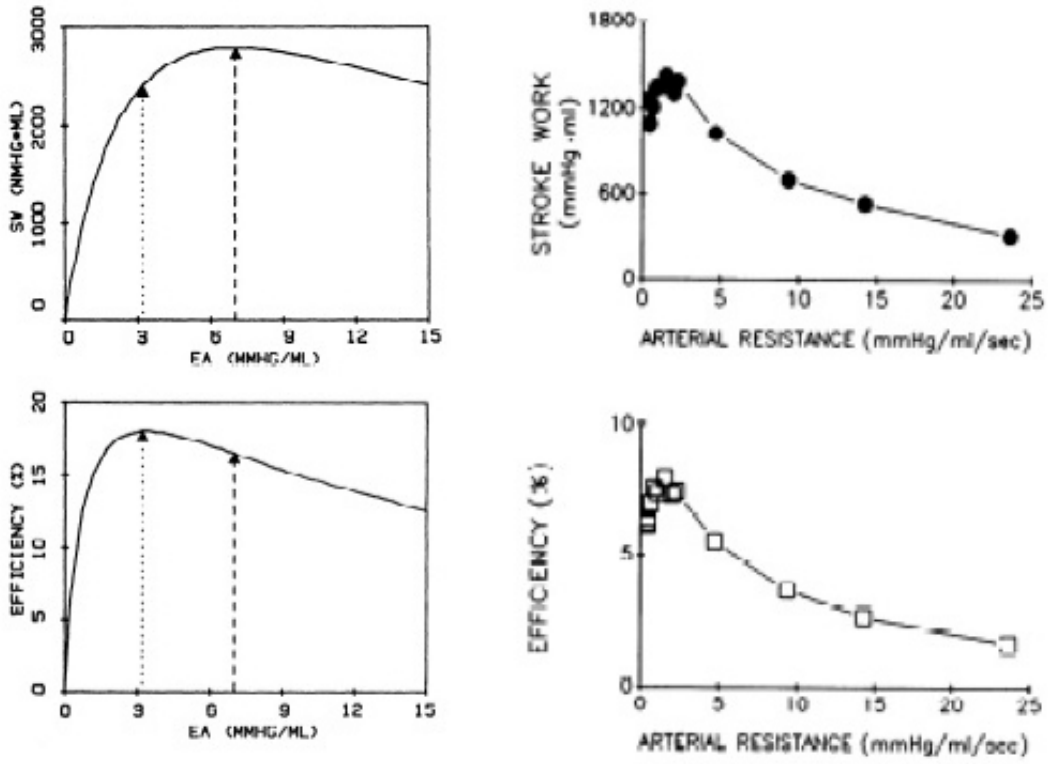

Figure 1-10 (Top Left) Theoretical relation between afterload quantified by effective arterial elastance (Ea) and stroke work; (Bottom Left) and efficiency taken from Burkhoff and Sagawa (1986); (Top Right) Experimental Relation between afterload quantified by effective arterial elastance (Ea) and stroke work; (Bottom Right) and efficiency taken from De Tombe et al. (1993)

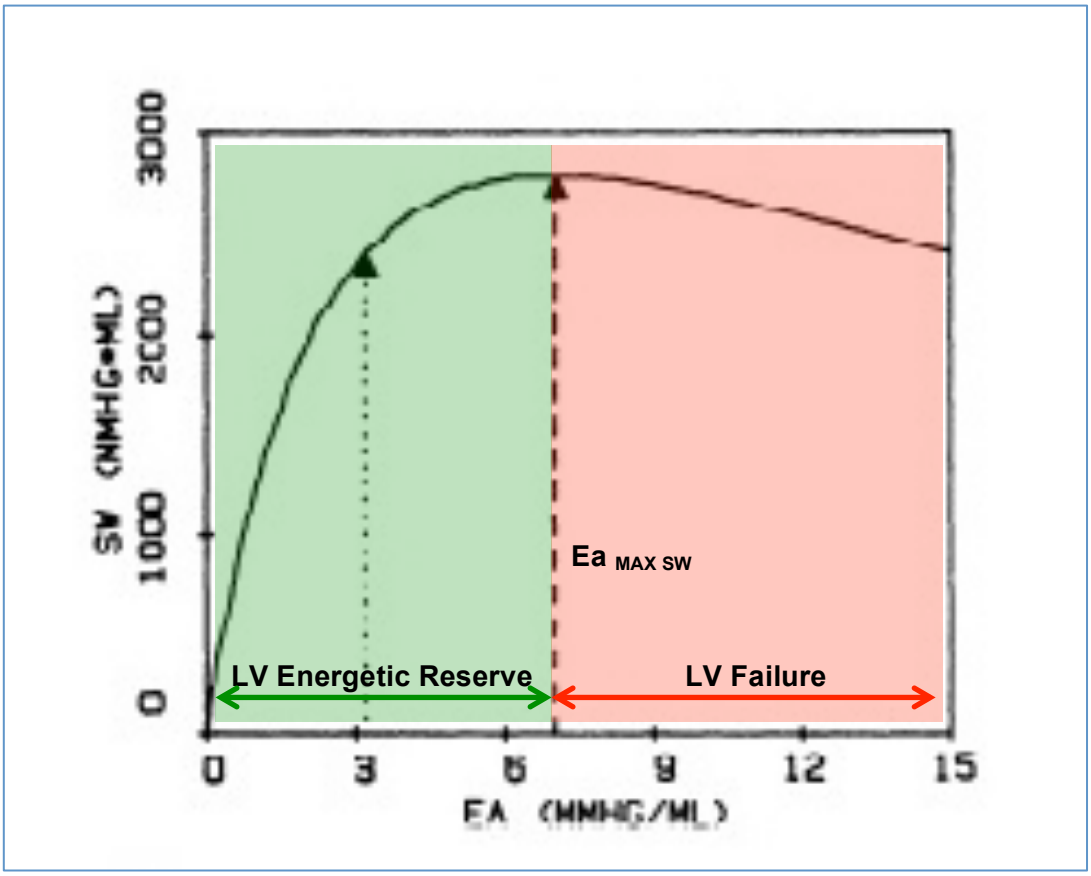

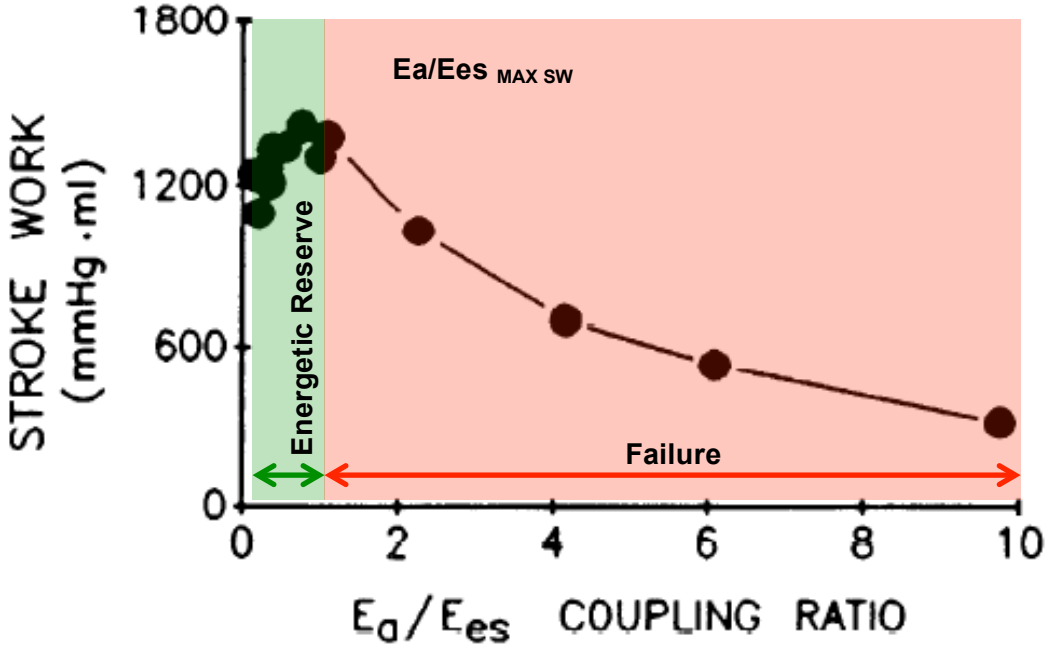

Figure 1-11 (Top) Theoretical relation between afterload quantified by effective arterial elastance (Ea) and stroke work taken from Burkhoff and Sagawa (1986). LV energetic reserve (green) below the threshold for Ea at maximal stroke work (Ea $_{MAX\ SW}$) and LV failure beyond this afterload threshold. (Bottom) Experimental relation between the inverse LV ventriculoarterial (Ea/Ees) coupling ratio and stroke work taken from De Tombe et al. (1993). LV energetic reserve (green) below the threshold for Ea/Ees at maximal stroke work (Ea/Ees $_{MAX\ SW}$) and LV failure beyond this inverse ventriculoarterial coupling threshold.

1.7 Summary

This chapter has described a number of physiological and structural differences between the LV and RV; and why the pulmonary circulation is fundamentally different to the systemic circulation (Dell'Italia, 1991). In contrast to the LV, the RV is coupled to the compliant pulmonary circulation and operates at lower pressure. The RV chamber remains concave towards the LV during both systole and diastole. The RV has a thin ventricular free wall that has a muscle mass approximately one-sixth of the LV (Dell'Italia, 1991). Therefore, the contractile performance of the better characterised LV may not be directly transferrable to the RV (Bellofiore and Chesler, 2013).

The normal healthy RV is coupled with the pulmonary vascular structure, but the coupling is more complex than with the aorta. The pulmonary artery is a relatively short elastic proximal vessel that branch early into the pulmonary trunk. This relatively short elastic proximal portion of the pulmonary vessels means that 25-40% of the energy expended during the pulsatile contraction of the RV is not converted into flow energy due to the restricted elastic recoil of the pulmonary vessels (Grignola et al., 2007; Saouti et al., 2010). Further stiffening of the pulmonary vascular vessels will increase in the afterload on the ventricle, increasing the systolic pressure (Chen et al., 1998) and will cause abnormalities in diastolic relaxation times and pressures (Leite-Moreira et al., 1999).

The aim of this work is to determine if the theory described for LV maximal efficiency and maximal SW from the pressure volume relationship could be translated to the lower pressure RV and less compliant pulmonary circulation. Chapter 3 describes the methodological development of a new large animal model for the assessment of RV-PA ventriculoarterial coupling. Using a PA snare to partially occlude the PA while keeping RV contractility and heart rate constant in a healthy swine heart to record RV PV-loops during preload reduction. This new model was used in Chapter 4 to assess how RV efficiency and RV SW varied in response to changes in the PA loading

conditions (Ea), RV contractility (Ees) and RV ventriculoarterial coupling (Ees/Ea). Relations for RV afterload (quantified by Ea) and RV ventriculoarterial coupling (quantified by Ees/Ea) defined maximal efficiency and maximal SW values within a physiologically normal porcine RV.

These data were then applied in two clinical cohorts with pathological RV loading: symptomatic patients with Chronic Thromboembolic Pulmonary Hypertension – CTEPH and Chronic Thromboembolic Disease without pulmonary hypertension - CTED (Chapter 5 – elevated Ea). In a complimentary clinical study, the affects of ventricular interdependence on RV contractility and the RV-PA ventriculoarterial coupling ratio following Transcatheter Aortic Valve Implantation (TAVI) was assessed (Chapter 6 – changing Ees).

2 Materials and Methods

2.1 Introduction

This chapter describes the materials and methods for the development of an animal model:

1. The effect of right ventricular (RV) – pulmonary artery (PA) ventriculoarterial coupling ratio on the maximal efficiency and maximal stroke work as RV function adjusts to maintain ejection of blood against increasing afterload

and the translation of this animal model into two clinical studies:

1. The effect of different pulmonary hypertension (PH) etiologies (chronic thromboembolic disease (CTED) and chronic thromboembolic pulmonary hypertension (CTEPH)) on RV function and RV-PA ventriculoarterial coupling
2. The effect of left ventricular (LV) afterload reduction on RV function and RV-PA ventriculoarterial coupling following transcatheter aortic valve implantation (TAVI)

All the studies in this thesis use the conductance technique to determine the real-time beat-to-beat measurement of right ventricular pressures and volumes in animals and humans. Principles of conductance theory to assess RV function are discussed, followed by the protocol used for data acquisition and analysis. Principles of the thermodilution technique and Fick are discussed, as the Pressure-volume (PV)-loops were calibrated from cardiac output determined by thermodilution technique or Fick. In the TAVI study, an echocardiographic assessment was performed to assess aortic valve, left ventricular (LV) and RV function. Principles of echocardiographic assessment are discussed.

2.2 Research Governance

2.2.1 Statistical Power

The studies were powered to the primary outcome measure of Tau between treatment groups. The number of subjects had been calculated from previous work (Read et al., 2011). To detect a change in Tau of 10 ± 8 ms between groups, we estimated 11 subjects would be required ($\alpha = 0.05$, $\beta = 0.2$). Therefore, the aim was to recruit 15 subjects into each treatment group or study arm to allow for any withdrawal of consent or incomplete datasets.

2.2.2 Statistical Analysis

The specific statistical tests used to describe the data analysed in each clinical study are described in greater detail in each chapter. All statistical analysis was performed using SigmaPlot 12.5 (Systat Software Inc, San Jose California, USA) statistical analysis package. In summary, continuous data was expressed as mean ± 1.S.D. Paired Student t-tests were used as a parametric statistical test to compare a change that occurred before or after an intervention, or between patient groups when the observed effects were normally distributed. The null hypothesis was rejected when $p<0.05$. Linear regression analysis was used as a parametric statistical test to find the straight line that most closely predicted the value of the dependent variable, given the observed value of the independent variable. The Pearson correlation coefficient (R) was used as a parametric statistical test to measure the linear correlation between two independent variables. Linear regression and the Pearson correlation coefficient were used extensively throughout this thesis to determine PRSW, ESPVR, EDPVR and the parallel conductance volume (Vc). The Bland-Altman method (Bland and Altman, 1986) was used to compare a new measurement technique with an established one to determine whether the two data sets agree sufficiently.

2.2.3 Governance for Animal Studies

All the animal studies were performed at a specialist facility at the Royal Veterinary College in Hatfield, London. All the studies were performed using Large White pigs under terminal anaesthesia and was approved by the Home Office (Project Licence 70/7967). All animals received humane care under the Code of practice for the housing and care of animals bred, supplied or used for scientific purposes. The code of practice sets out the standards of care and accommodation of animals required by the Animals (Scientific) Procedures Act 1986 and provides advice about the way in which those responsible under ASPA may comply with those requirements, published 2014.

2.2.4 Governance for Human Studies

All patient studies were performed at Papworth Hospital NHS Foundation Trust, Cambridgeshire. The Trust Research & Development Department sponsored all studies, and the National Research Ethics Service (NRES) Local Research Ethics Committee granted ethics approval. Individual informed consent was obtained before the study. All studies complied with the principles outlined in the Declaration of Helsinki in 1964 (Rickham, 1964; World Medical, 2013). These were as follows for the clinical studies:

1. Study Title: Analysis of exercise responses in chronic thromboembolic disease. Approved by Cambridge South local research ethics committee (REC number 12/EE/0085). Approved by Papworth Hospital NHS Foundation Trust, Research & Development Department.
2. Study Title: Diastolic RV EvAluation with Millar catheter in patients undergoing transfemoral Transcatheter Aortic Valve Implantation – DREAM TAVI study. Approved by Cambridge South local research ethics committee (REC number 12/EE/0473). Approved by Papworth Hospital NHS Foundation Trust, Research & Development Department. The study trial number was UKCRN ID 14028.

2.2.5 Conduct of Work

2.2.5.1 Location of Work

The animal studies were conducted in the Biological Services Unit at the Royal Veterinary College, Hatfield, London. The conductance data was recorded on a Papworth Hospital NHS Foundation Trust laptop and then backed up onto a secure server at Cambridge University Hospital NHS Foundation Trust for analysis.

The interventional studies were conducted in the Cardiac Catheterisation Laboratories at Papworth Hospital NHS Foundation Trust. The conductance data was recorded on a Papworth Hospital NHS Foundation Trust laptop and then backed up onto a secure server at Cambridge University Hospital NHS Foundation Trust for analysis. The echocardiographic data was downloaded off the machine onto a secure server at Cambridge University Hospital NHS Foundation Trust. The fluoroscopic images were downloaded and stored on a secure server at Cambridge University Hospital NHS Foundation Trust.

2.2.5.2 Work Conducted by the Author

The author was involved in all aspects of the work presented from the first inception. For the animal studies, the author wrote the protocols and developed the ex-vivo perfusion rig. Dr Simon Messer (Cardiothoracic Transplant Fellow and PhD student) wrote the application for approval from the Home Office. For the interventional studies, the author wrote the protocols, the applications for approval from ethics committees and Papworth Research and Development Department under the supervision of Dr Stephen Hoole (Consultant Interventional Cardiologist and Chief Investigator).

For the animal studies, Dr Hatim Alibhai (Consultant Veterinary Anaesthetist) was responsible for the humane care of the animals. The animal studies were performed under Dr Simon Messer's Project Licence. Dr Hatim Alibhai performed the anaesthetic preparation of the animals, and Dr Simon Messer performed the surgical preparation.

The author acquired and analysed the in-vivo conductance catheter data. The author developed the ex-vivo perfusion rig. The author took the explanted heart and perfused the heart on the ex-vivo perfusion rig. The author modified the rig from Langendorff perfusion into a working heart mode and acquired and analysed the ex-vivo conductance catheter data.

For the interventional studies, Dr Stephen Hoole (Consultant Interventional Cardiologist) recruited the patients into the studies. The author oversaw all the interventional procedures to ensure compliance with the protocol. The Consultant Interventional Cardiologist responsible for the care of the patient performed the interventional procedures. The author acquired and analysed the conductance catheter data. The Consultant Cardiologist responsible for the echocardiographic assessment during the interventional procedure performed the additional measurements required for the research protocol. The author transferred the echocardiographic data to a secure server at Cambridge University Hospital NHS Foundation Trust and performed all analysis.

In all the studies, the author performed all data analysis, statistical analysis and presentation of the data.

2.3 Conductance Theory

The modern-day conductance catheter has stood the test of time and remains identical to the one first used by Baan et al. (1984). A measure of intra-ventricular volume is obtained based on the electrical conductance of the blood within the ventricular cavity. Since blood is a relatively good conductor of electricity (Blood Resistivity ≈160 Ω cm) (Geddes and Baker, 1967) and the ventricular wall is a relatively poor one (ventricular wall resistivity ≈ 400 Ω cm) (Geddes and Baker, 1967); at end-diastole a full ventricle will have a high conductance whereas at end-systole a partially filled or empty ventricle will have low conductance (Baan et al., 1984; Baan et al., 1981).

The conductance catheter has a series of equally spaced platinum electrodes (between 8 to 12) mounted on an angiographic pigtail catheter that can be positioned in a ventricle under fluoroscopic guidance. A single field excitation conductance catheter will have eight equally spaced electrodes. The outermost electrodes are used to generate an intracavity electric field, typically 20-kHz and 30μA. The remaining sensing electrode pairs are used to measure the cylindrical volume defined by the endocardial surface of the ventricular wall and the equipotential surface of the electrodes (Baan et al., 1981). Total ventricular volume can be approximated by considering the paired volumes as a column of cylindrical volumes stacked on top of each other. Dual field excitation catheters use additional pairs of electrodes (up to 12 electrodes in total) to provide a second electric field of opposite polarity (Steendijk et al., 1992) to increase electric field homogeneity. During the cardiac cycle, changes in the cross-sectional area of the ventricular cavity cause variations in the resistance between the two sensing electrodes and lead to changes in the electrical conductance measured. The relationship between resistance and cross-sectional area of the ventricle is given by:

Equation 2-1

$$R = \frac{\rho L}{A}$$

Where R = resistance (ohms), ρ = blood resistivity (ohms / cm), L = distance between the sensing electrodes or inter-electrode distance (cm) and A = cross-sectional area of the ventricle (cm^2). Since the blood conductivity (G) is the reciprocal of resistance it can be calculated from the formula:

Equation 2-2

$$G = \frac{1}{R} = \frac{A}{\rho L}$$

As an alternating current is applied to the outermost electrodes, the remaining sensing electrode pairs measure the potential difference across the electrodes to derive the time-varying conductance ($G_{(t)}$) for the ventricular segment. The relationship between the time-varying ventricular volume and the time-varying conductance ($G_{(t)}$) is given by:

Equation 2-3

$$V_{(t)} = \left(\frac{1}{\alpha}\right)\left(\frac{L^2}{\sigma}\right)\left(G_{(t)} - G_{(p)}\right)$$

Where α = dimensionless slope factor, L = inter-electrode length (cm), σ = blood conductivity (cm / ohm) and $G_{(p)}$ = parallel conductance of structures extrinsic to the volume of blood in the ventricular cavity (1 / ohm). Although the formulae was developed by Baan et al. (1984) for use within the Left Ventricle (LV), which can be considered as a single ellipsoid chamber, and the equation assumes the region at the apex of the LV (not interrogated by the conductance catheter) to have a volume equal to one-third of the most distal segment. This technique has been used successfully by many researchers (McKay et al., 1984; Bishop et al., 1997; Tabima et al., 2010) in the Right Ventricle (RV), which can be considered as crescentic in cross-section and triangular when viewed from the side. White et al. (1995) demonstrated a good correlation between known volumes and conductance derived volumes using human post-mortem ventricular casts.

2.3.1 The Millar Conductance Catheter

The Millar (Houston, Texas, USA) conductance catheter used throughout these studies is shown in Figure 2-1**Error! Reference source not found.** The catheter is a 7F 8 electrode over 5 or 6 centimetres. Typically a 5 cm catheter would be used with 6 cm catheters only used with larger patients. The 5 cm catheter has 8 electrodes spaced 7.1 mm apart. The 6 cm catheter has 8 electrodes spaced 8.6 mm apart. Electrodes 1 and 8 are used to generate the 20kHz electric field. The remaining electrode pairs (2-3, 3-4, 4-5, 5-6, 6-7) are used to measure the potential difference generated across each catheter segment. A pressure transducer is located between electrodes 4 and 5 to measure ventricular pressure simultaneously. The catheter has a pigtail at the end to prevent it from damaging the ventricular wall. The catheter is 120 cm long and has two connection ports at the distal end of the catheter that are used to transmit the volume and pressure signals to the Millar MPVS Ultra box (Section 2.4). The conductance catheter was inserted into the patient via a 7F sheath using either a femoral or jugular approach. The catheter was then advanced into the RV under fluoroscopic guidance and was used to visually check the catheter was correctly positioned in the ventricle (Figure 2-1).

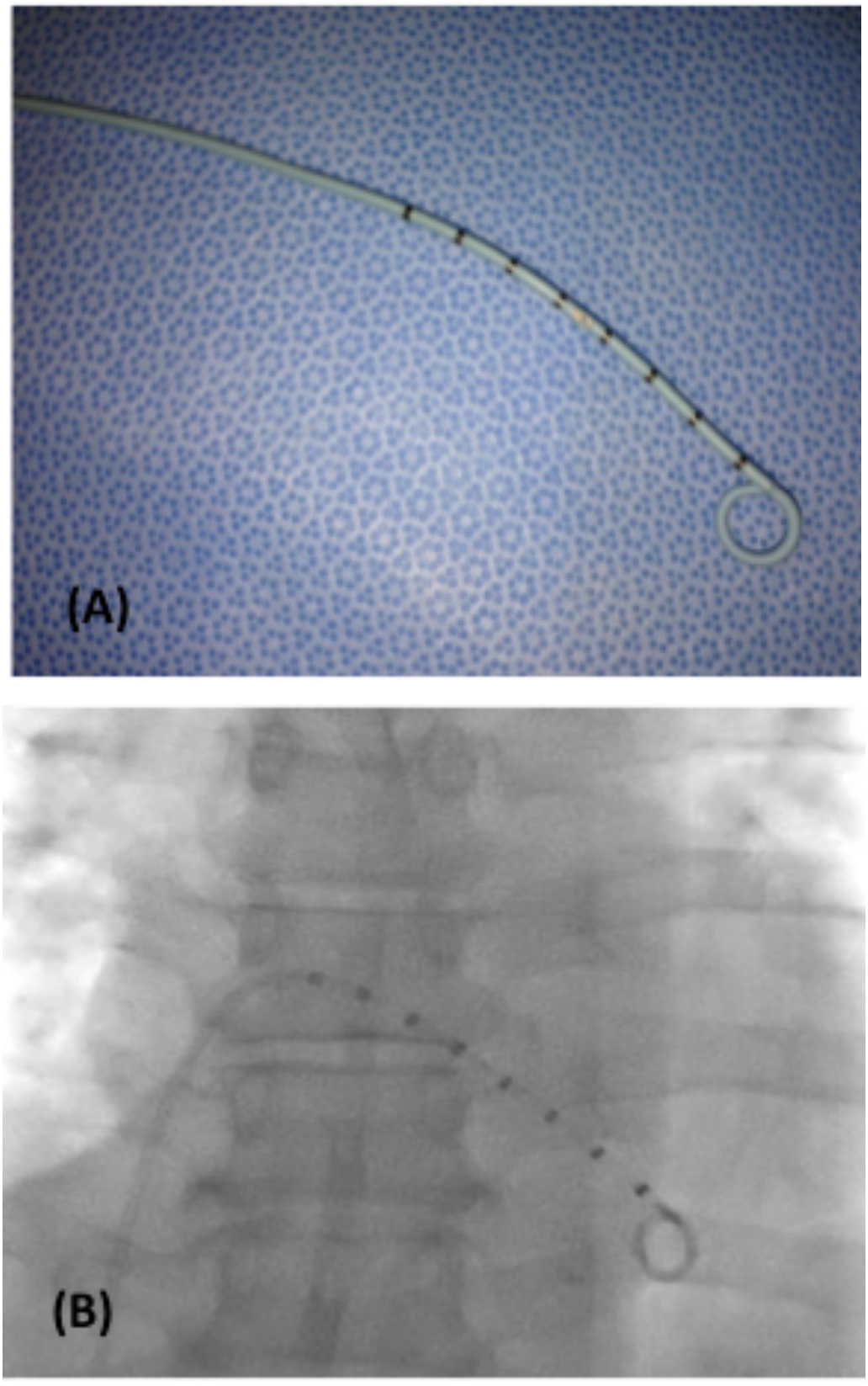

Figure 2-1 (A) Millar (Houston, Texas, USA) conductance catheter; (B) positioned in the right ventricle under fluoroscopic guidance

2.3.2 Calibration Factors

The theory of the conductance technique volume measurements is based on a number of contested assumptions (Salo et al., 1986):

1. The ventricle has a uniform cross section;
2. The resistivity of blood is homogeneous and isotropic (the blood has the same properties in all directions);
3. The ventricle is surrounded by an electrical insulator (no current can transmit beyond the ventricular wall); and
4. The electric field produced by the catheter is homogeneous throughout the blood volume and parallel to the long axis of the ventricle.

Assumption two is considered to be correct (Salo et al., 1986). However, assumptions three and four can introduce significant errors in ventricular volume estimation if not taken into consideration. Two calibration factors are used to determine the absolute ventricular volume from conductance measurements. To help reduce the errors associated with assumption three an estimation of the volume offset, known as parallel conductance (Vc) is used to account for the current that is transmitted beyond the ventricular cavity. To help reduce the errors associated with assumption four an estimation of the dimensionless slope factor known as alpha (α) to correct for the inhomogeneity of the electric field and correcting the difference between the absolute blood volume and that determined by the conductance technique.

2.3.2.1 Parallel Conductance

One of the main limitations and sources of error with the conductance technique is that the current created by the excitation electrodes on the catheter extends beyond the ventricular cavity, contradicting the third assumption. It extends beyond the ventricle and measures the conductivity of the structures extrinsic to the blood within the ventricle. For the RV this is predominantly from the contralateral LV, myocardium and lungs. Therefore, the conductance measured by the conductance catheter

overestimates the blood conductance due to parallel conductance $G_{(p)}$. This overestimation of blood conductance creates a volume offset (Vc), which in turn overestimates the absolute ventricular volume (Kornet et al., 2000).

Parallel conductance is determined using the saline dilution technique. The technique is based on the analysis of temporary changes in blood resistivity which occur during an injection of a small bolus of hypertonic saline (Baan et al., 1984). A controlled injection of approximately 5ml of 10% hypertonic saline is injected into the blood upstream of the ventricle. This upstream injection allows for the hypertonic saline to mix with the blood by the time it reaches the ventricle. The blood / hypertonic saline mixture will enter the ventricle and increases the blood conductivity in the RV and is subsequently displayed as an increase in the blood volume detected within the RV.

The bolus of hypertonic saline increases the measured blood conductivity without altering the actual volume of blood within the ventricle. The blood conductivity of the surrounding structures remains constant. Since the absolute stroke volume remains constant, the changes in the conductance values observed are due to the alterations in blood conductivity. Figure 2-2A shows the RV PV-loops recorded during an injection of hypertonic saline. The conductance catheter senses an increase in blood conductivity during the saline injection, which is subsequently displayed as an increase in the blood volume detected within the ventricle. The End-Diastolic Volume (Ved) and End-Systolic Volume (Ves) points are identified for each beat during the hypertonic saline injection. The Ves point is plotted against the Ved point for each beat. A linear regression of these points are performed and the point where the regression line intercepts the line of identity (ESV = EDV) is equal to G(p), the volume of blood measured by the conductance catheter due to the current conducted through the ventricular wall and into the surrounding structures (Figure 2-2B).

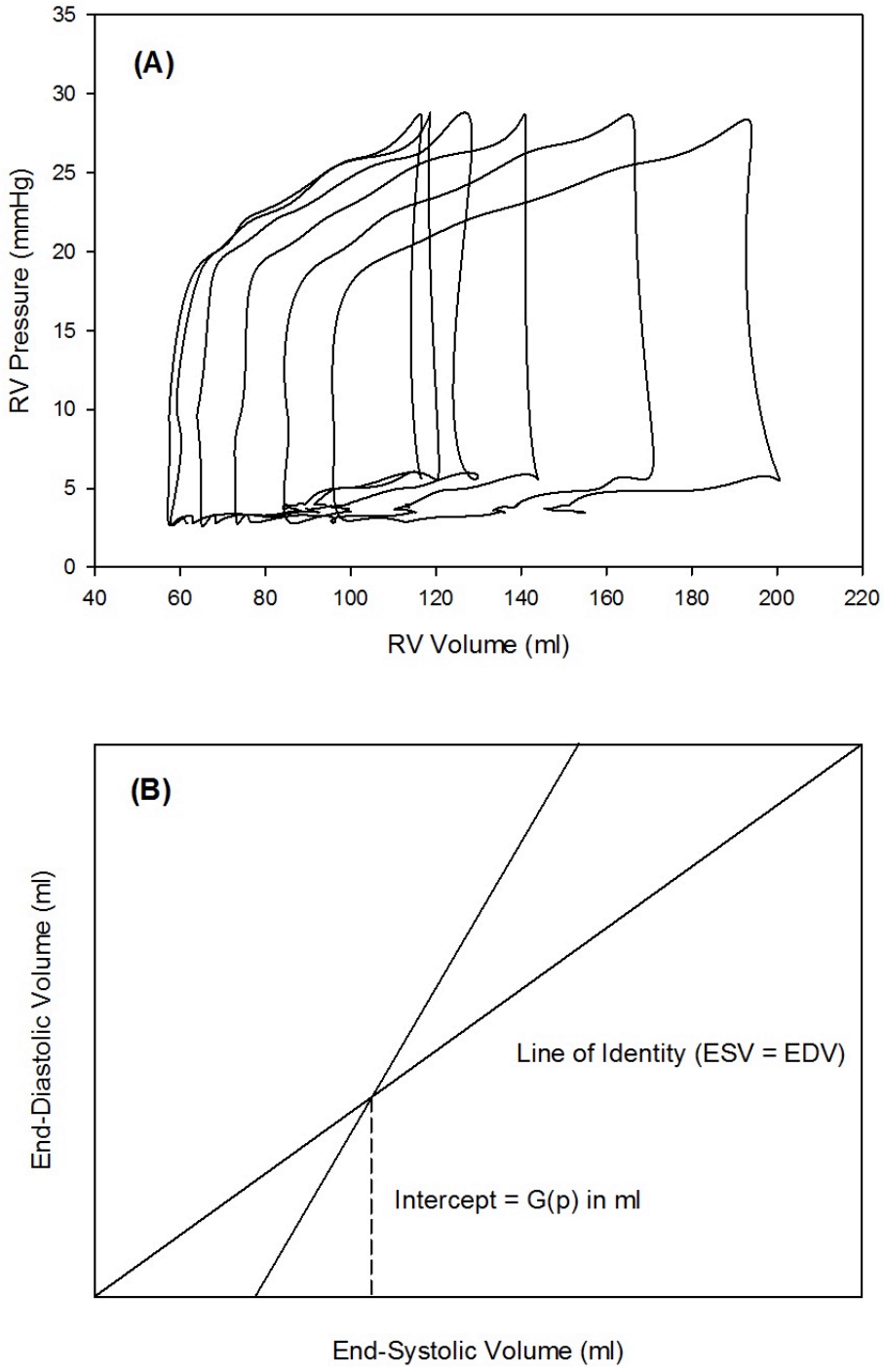

Figure 2-2 Increase in RV volume during a hypertonic saline injection

2.3.2.2 Dimensionless Slope Factor Alpha

The second limitation and potential source of error with the conductance technique is the accuracy of the conductance-derived absolute blood volume and must be considered when interpreting the conductance-derived assessment of RV function. The dimensionless slope factor alpha (α) is a result of the inhomogeneity of the excitation field and is an estimate of the slope between the conductance derived stroke volume and the actual stroke volume. This is further complicated by the fact that the dimensionless slope factor alpha varies with ventricular size. Alpha is estimated from the relationship of cardiac output derived from conductance as a ratio of that calculated from the Fick Principle or thermodilution method described in Section 2.6.

The variability of alpha with ventricular size can be explained by considering that the non-uniformity of the electric field is caused by the excitation electrodes acting like point sources rather than flat plates (Salo, 1989). A point source electrode placed in a ventricle of a non-uniform cross section will generate an inhomogeneous electric field within the ventricular cavity, contradicting the fourth assumption. Therefore, as the density of the electric field decreases exponentially with the distance from the axis of the catheter, field inhomogeneity increases with ventricular volume. Therefore, the electric field strength is greatest closest to the longitudinal axis of the catheter. Hence, the electrodes measure the larger electric fields proximal to the longitudinal axis of the catheter with a higher sensitivity than the weaker distal fields. This electric field inhomogeneity means the conductance-derived volumes will always underestimate the true ventricular volume.

The proportion of the ventricle interrogated by the conductance catheter further affects the value of the dimensionless slope factor alpha. Considering an ideal homogeneous electric field, an alpha value of 0.65 would indicate that the catheter is interrogating only 65% of the ventricle. Therefore, a catheter should be selected to match the length

of the long axis of the ventricle to minimise the effect of the ventricular length to catheter length ratio on alpha.

2.3.2.3 Blood Resistivity

An accurate measurement of blood resistivity (Rho = 1 / Conductivity) is fundamental to the conductance catheter method. Blood resistivity is known to vary with temperature (Geddes, 1973) and haematocrit (Gollan, 1970). The Millar (Houston, Texas, USA) MPVS Ultra system used throughout this thesis (Described in Chapter 2), measures the temperature of the blood sample while taking a measurement of blood resistivity. This prevents changes in the temperature of the patient's circulating blood affecting the measured resistivity.

Blood is a suspension of red blood cells, white blood cells and platelets in plasma. The percentage of cells within the blood sample is called the packed cell volume. Red blood cells (haematocrit) form the majority of the blood. Therefore, the percentage of haematocrit is nearly equal to the packed cell volume. Blood is an electrolytic solution containing a variety of suspended and dissolved substances. Hence, the resistivity of the blood sample is dependent on the packed cell volume (Hill 1975); with a reduction in the packed cell volume, causing the blood resistivity to lower.

The studies were performed in a Catheter Laboratory where the patients' temperature is monitored and kept constant. However, since fluids may have been given during the procedure, a blood resistivity measurement would be taken at the start and end of the procedure to ensure there were not any changes in blood resistivity caused by changes in blood haematocrit. Care must also be taken to ensure that the time from collecting the sample to performing the measurement is kept to a minimum to ensure that the measurement of blood resistivity is performed with the sample at the same temperature as the patients' circulating blood.

2.3.3 The PV-Loop

The PV-loop recorded using the conductance catheter provides an accurate, beat-to-beat assessment of the ventricular function. A steady state PV-loop can be used to calculate a wide variety of load-dependant parameters of ventricular function. However, load-independent parameters of the ventricular function are determined by obtaining a family of PV-loops recorded during a pre-load reduction. All measurement recordings were repeated to ensure consistent and accurate data were recorded.

2.3.3.1 Load-Dependant Parameters

A steady state PV-loop can be used to calculate a wide variety of load-dependant parameters of ventricular function including; heart rate, cardiac output, stroke volume, end-systolic volume, end-diastolic volume, end-systolic pressure, end-diastolic pressure, ejection fraction, maximum and minimum rates of pressure decay and the time constant of diastolic relaxation. After selecting a steady state PV-loop in LabChart, these parameters are automatically calculated and displayed in the haemodynamics table as described in section 2.5. However, these parameters remain load-dependant, which means they are affected by the preload and afterload conditions on the ventricle. Most parameters can also be derived from standard techniques of assessing ventricular function.

There are two important load-dependant measures of diastolic function. The minimum rate of pressure decay (dP/dt min) is a measure of ventricular compliance or “stiffness”. A larger value would indicate a stiffer, less compliant ventricle with increased diastolic dysfunction. The time constant of isovolumic relaxation (Tau) (Weiss et al., 1976; Raff and Glantz, 1981; Matsubara et al., 1995) represents the exponential decay of the RV pressure during isovolumic relaxation. Although it is an index of diastolic function that is considered load dependent, it is predominantly only affected by heart rate, with an increased heart rate reducing the time for the diastolic filling. Typically Tau is

approximately 52-56ms in a healthy ventricle and would increase as diastolic dysfunction increases (Read et al., 2011; McCabe et al., 2014).

2.3.3.2 Load-Independent Parameters

The load-independent assessment of RV function can be measured by obtaining a family of PV-loops during a preload reduction (Figure 2-3). Typically a preload reduction is achieved by inflating a balloon in the Inferior Vena Cava (IVC). The End Systolic Pressure Volume Relationship (ESPVR) is a measure of ventricular contractility and describes the maximal pressure that can be generated by the RV for a given volume. ESPVR is calculated from the gradient of the linear regression of the end-systolic point on the PV-loop for each beat. The gradient of the ESPVR linear regression is known as the End Systolic Elastance (Ees). This line becomes steeper and shifts to the left as contractility increases. The ESPVR is insensitive to changes in preload, afterload and heart rate.

The End Diastolic Pressure Volume Relationship (EDPVR) is a measure of ventricular compliance and describes the passive filling properties of the RV. EDPVR is calculated from the gradient of the regression of the end-diastolic point on the PV-loop for each beat. The ESPVR is insensitive to changes in preload, afterload and heart rate. The slope of the EDPVR regression is the reciprocal of the ventricular compliance. Bishop et al. (1997) demonstrated that the occlusion of the right coronary artery caused an upward and leftwards shift of the EDPVR, which then returned to normal on reperfusion. Therefore, impaired ventricular filling or diastolic dysfunction will result in a smaller End-Diastolic Volume for a given End-Diastolic Pressure.

The Preload Recruitable Stroke Work (PRSW) is a measure of myocardial contractility. PRSW is calculated from the gradient of the linear regression of the stroke work with end-diastolic volume. The PRSW is insensitive to changes in afterload and heart rate. The slope of the PRSW linear regression line becomes steeper, and shifts to the left as contractility increases (Figure 2-3).

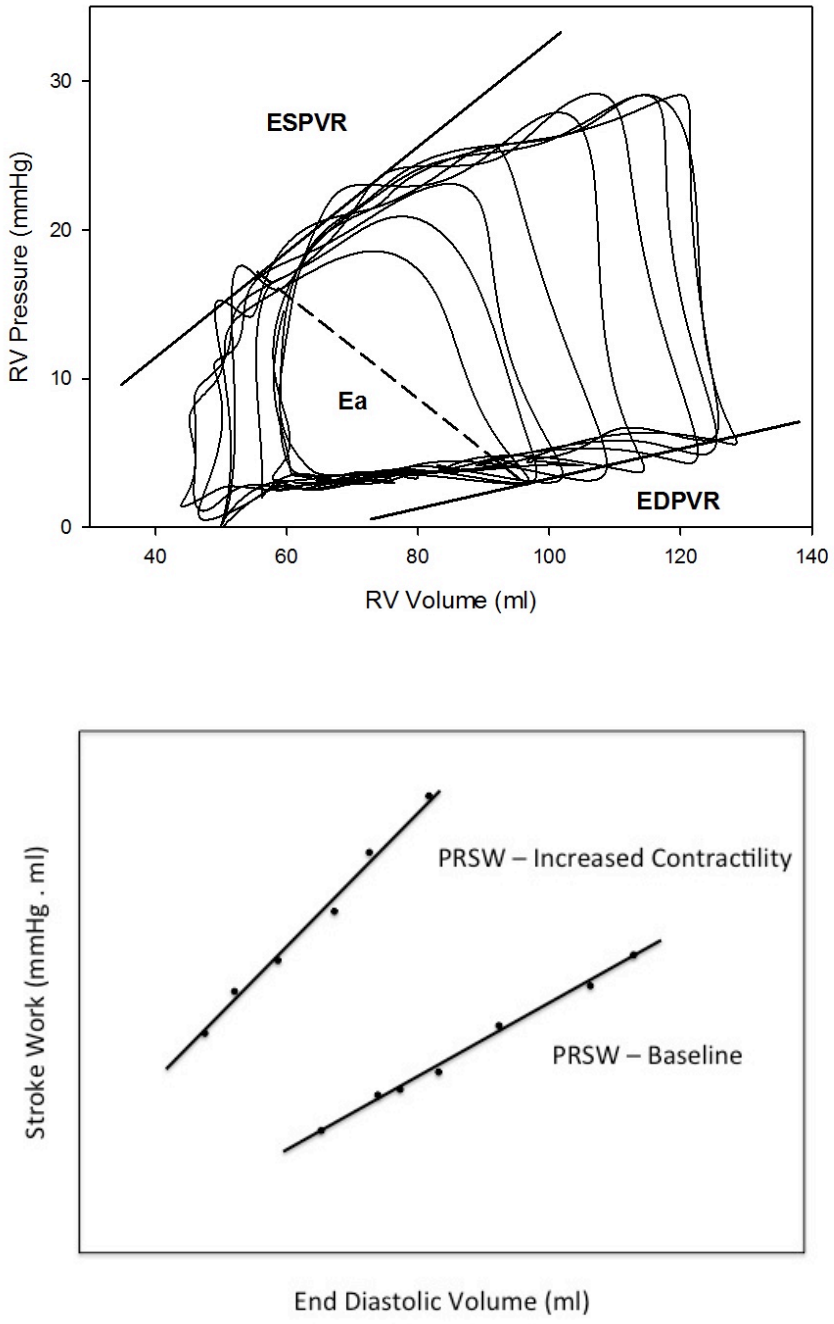

Figure 2-3 (Top) Load-independent family of RV PV-loops showing ESPVR, EDPVR and Ea; (Bottom) PRSW example

2.3.3.3 Single-Beat Determination of the Ventriculoarterial Coupling Ratio

In patients where it is not possible to insert an additional venous sheath and position a balloon in the IVC to create a preload reduction, computer-modeling techniques were used to predict Ees from a steady-state single-beat PV-loop. The relationship between maximal isovolumic pressure (Pmax) and EDV is a marker of ventricular contractility (Sunagawa et al., 1980). The single-beat method has been validated in the LV (Sunagawa et al., 1980) and RV (Brimioulle et al., 2003). The method assumes that the ESPVR is the same in ejecting and isovolumic beats, and the maximal pressure of an isovolumic beat (Pmax) can be extrapolated from a single normal ejecting beat (Brimioulle et al., 2003). The RV PV-loop pressure and volume data was exported from LabChart into a Matlab (MathWorks, MA, USA) file format. Pmax was determined by fitting the equation:

Equation 2-4

$$P = a + bsin(ct + d)$$

where P is the instantaneous pressure and t is time, to the RV pressure values before the maximal rate of isovolumic contraction (dP/dt max) and just after the maximal rate of isovolumic relaxation (dP/dt min) (Figure 2-4). Coefficients a-d were computed by a least squares nonlinear fitting equation in Matlab using the Levenberg-Marquardt method (Marquardt, 1963). Pmax was then obtained from the equation:

Equation 2-5

$$Pmax = a + 2b$$

The ESPVR line was drawn as the tangential line from the Pmax point at EDV, to the end-systolic point on the steady-state PV-loop (Figure 2-4). Ees was calculated as the slope of the Pmax-ESP divided by the SV. As previously described, Ea was calculated as the slope of the ESP divided by the SV.

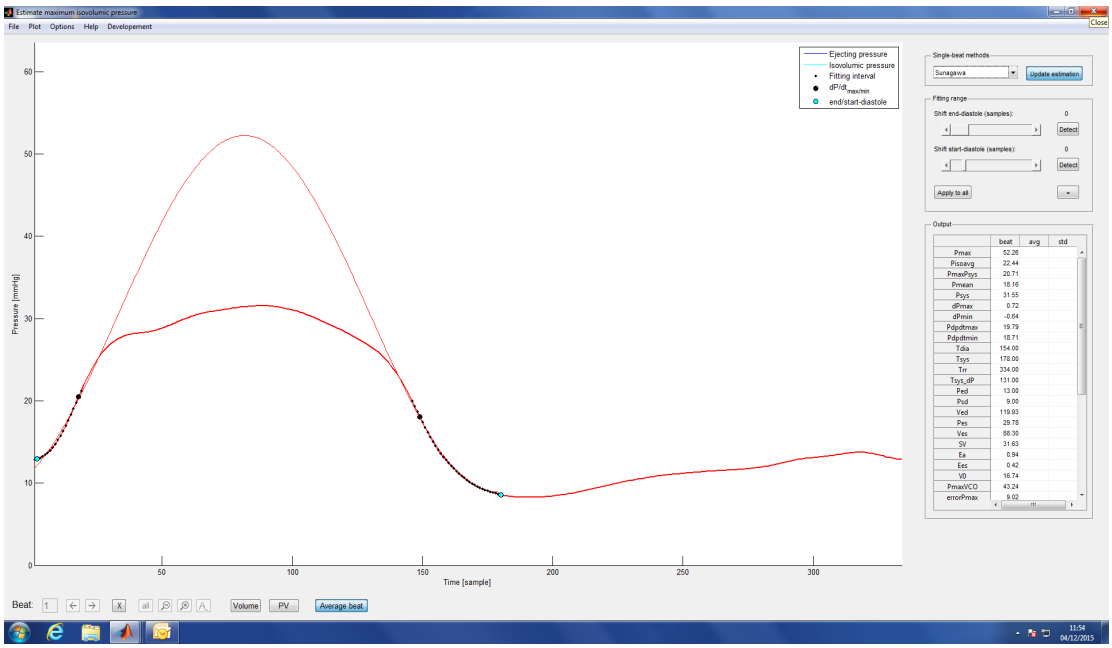

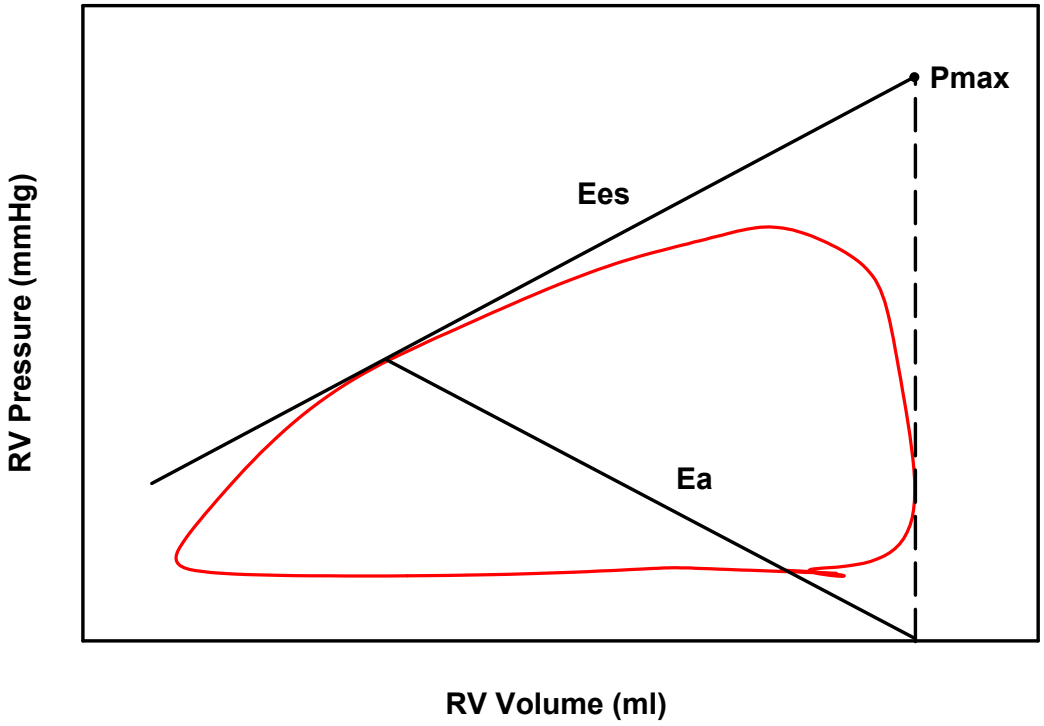

Figure 2-4 (Top) Single beat estimation of the maximal isovolumic pressure (Pmax). This is a screen capture of a patient with CTED from Chapter 5. (Bottom) Single beat estimation of Ees using Pmax (This is not to scale).

2.4 PV-Loop Data Acquisition

The Millar MPVS Ultra (Millar, Houston, Texas, USA) PV-loop system was used to simultaneously measure high-fidelity ventricular pressure and volume in-vivo in a human heart and in-vivo and ex-vivo in a mammalian heart. This was connected to an ADInstruments PowerLab 16/30 Series (ADInstruments, New South Wales, Australia) sixteen-channel amplifier. The output from the PowerLab was then displayed and data recorded using the ADInstruments LabChart Pro 8.0 (ADInstruments, New South Wales, Australia) software.

2.4.1 Millar MPVS Ultra

The Millar MPVS Ultra front panel connections are shown in Figure 2-5. The power indicator will illuminate green when the system is turned on and receiving power. There are four custom input connectors. The *Cuvette* input is colour-coded light grey and can be used to connect the cuvette (Figure 2-9) to the system and measure blood resistivity for volume calibration. The *ECG* input is colour coded green and can be used to connect a slaved ECG in to the system. The *PV-loop* input is colour coded black and can be used to connect the Millar multi-segment conductance catheter to the system. A specialist interface cable is required that connect directly to the white low profile and grey circular connectors on the Millar conductance catheter and the other end plugs into the *PV-loop* input. The cable transmits a signal to-and-from the volume sensing electrodes to the MPVS Ultra, and to-and-from the pressure sensor bridge to the MPVS Ultra. The cable can also be used to measure an internal ECG waveform. The *Pressure-Only* input is colour coded blue and can be used to connect a pressure catheter to the system. There are two analogue *Pressure Output* channels (CH 1 and CH 2) that can be used to output the pressure signals via a BNC connector to an input on the ADInstruments PowerLab 16/30. The pressure output signals are scaled to 1V / 100 mmHg. There are eight analogue *Volume Output* Channels (Composite, S1 – S7); the *Composite Volume* output channel outputs the analogue sum of the individual volume segments; the seven-volume segments (*V1-V7*) output the analogue signal for

each of the separate volume segments. The outputs are connected to the ADInstruments PowerLab 16/30 with a BNC connector. The analogue ECG Output channel can be used to output the signal measured from the internal conductance catheter ECG.

The rear panel on the Millar MPVS Ultra has a mini-USB connector, which can be used with a mini-USB to USB (v1.1 or later) cable to connect the Millar MPVS Ultra system to the Windows PC running the Millar MPVS Ultra Control Interface (See Section 2.4.2). On initial set-up with the PC software drivers had to be installed and the unique serial number for each Millar MPVS Ultra box had to be registered on the PC before the Control Interface can communicate with the box. At the start of each research study, the USB cable between the Millar MPVS Ultra system and the PC must be connected before the entire system is switched on. An IEC power cable connector can be used to connect the Millar MPVS Ultra System to the mains power supply. The Millar MPVS Ultra system is a Class I Type CF medical device. Therefore, the Millar MPVS Ultra system metal casing is connected directly to the earth pin on the power socket.

Figure 2-5 Millar (Houston, Texas, USA) MPVS Ultra front panel hardware connections

2.4.2 Millar MPVS Ultra Control Interface

The Millar MPVS Ultra *Control Interface* is an intuitive graphical interface that can be used to select and configure the catheter, calibrate the system and measure blood resistivity. The multi-segment mode must be activated to perform PV-loop measurements on a larger animal or human subject.

2.4.2.1 Catheter Configuration Tab

The *Catheter Configuration* tab (Figure 2-6) can be used to configure the hardware to operate with a specific model of Millar catheter, by setting the electrode configuration, field configuration, excitation current and gain. The *Catheter Configuration Locked* button must be activated (so that the button reads *Catheter Configuration Unlocked)* to make changes can be made to the *Catheter Configuration* tab This locking mechanism prevents any inadvertent changes to the catheter configuration and system settings while the system is in use. The Millar MPVS Ultra *Control Interface* will default to the catheter configuration that was used last. The *Catheter Configuration* button automatically locks after a period of 60 seconds inactivity. The *Millar Catheter Selection* field is set up with the custom catheters used for the human research studies. Typically we would use a 7F 8 Electrode over 5 cm (electrode spacing 7.1 mm) catheter with an x100 gain setting or a 7F 8 Electrode over 6 cm (electrode spacing 8.6 mm) catheter with an x100 gain setting. The *Blood Resistivity* field can then be used to enter the value of the measured blood resistivity. At the start of the research study, this would be set to 180-ohm/cm to calibrate the system.

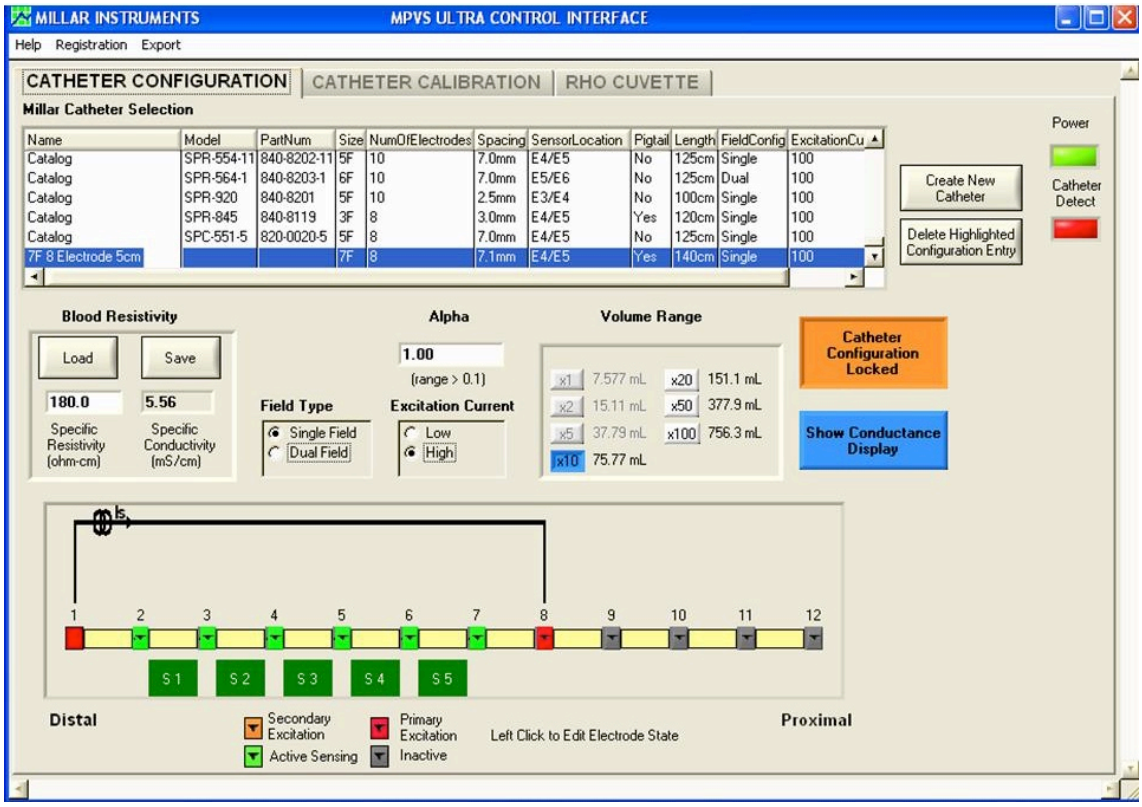

Figure 2-6 Millar MPVS Ultra control interface catheter configuration tab screen capture

2.4.2.2 Catheter Calibration Tab

The *Catheter Calibration* tab (Figure 2-7) can be used to calibrate the pressure and volume signals electronically. The pressure reading is numerically displayed on the *Catheter Calibration* tab, with a measurement range from -25 mmHg to 200 mmHg and scale 1.0 V / 100 mmHg. The MPVS Ultra provides 5.0 V excitation to the transducers that have an assumed sensitivity of 5.0 µV / V / mmHg. The MPVS is designed to work with Millar catheters with 1000 ohm input impedance and 1000 ohm output impedance. The active button on the *Pressure* tab is highlighted in green. To calibrate the pressure signal the *0-mmHg* button should be activated, so that the MPVS Ultra will output a 0.0-volt signal. The *100-mmHg* button should then be activated so that the MPVS Ultra will output a 1.0-volt signal. The LabChart software can then be used to perform a two-point calibration on the pressure channel, setting point one to 0 mmHg and point two to 100 mmHg. The *Transducer* button should then be activated so that the MPVS Ultra will read the pressure measured by the pressure sensor on the Millar catheter. The pressure offset can then be manually adjusted to set the zero point. After confirming the *Transducer* button is activated on the *Catheter Calibration* tab, the pressure sensor on the Millar catheter should be submerged in body temperature water. The *Balance Locked* button should then be activated so that the button now reads *Balance Unlocked*. Then by activating the *AUTO ZERO* button the desired pressure channel is set to zero mmHg. The *Balance Unlocked* button should then be activated to lock the pressure controls. However, the button automatically locks after a period of 60 seconds inactivity.

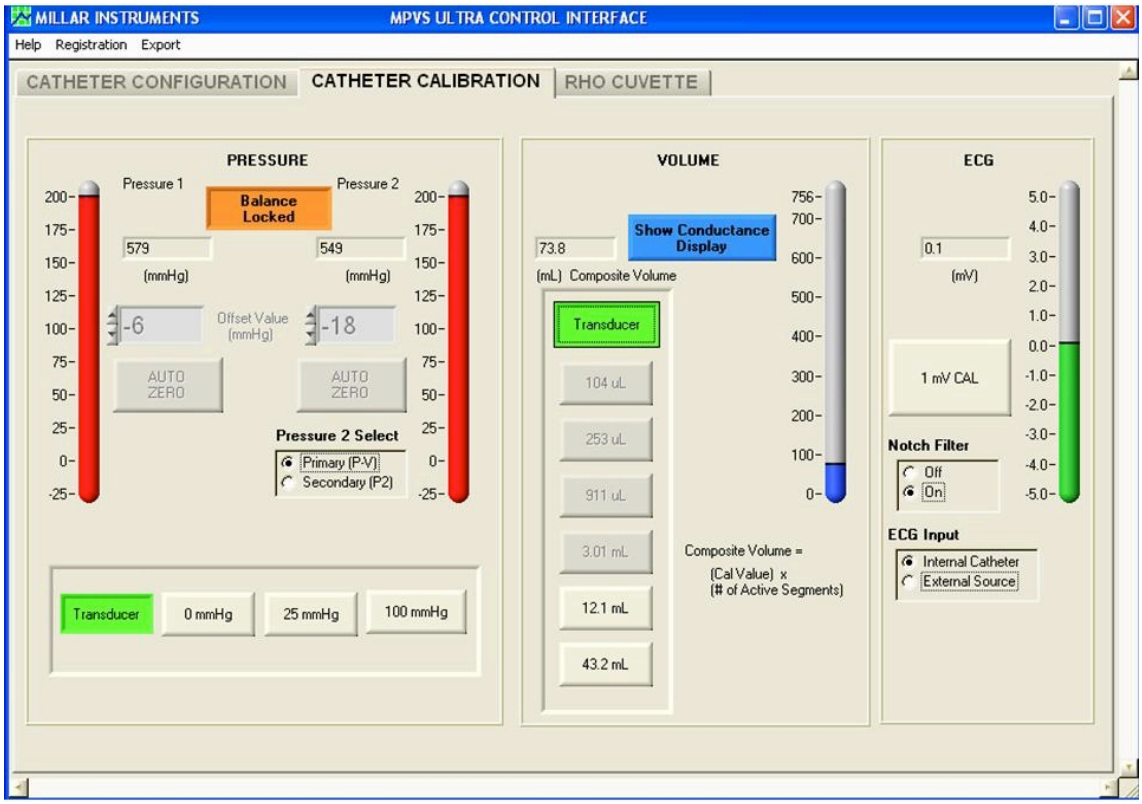

Figure 2-7 Millar MPVS Ultra control interface catheter calibration tab screen capture

The *Composite Volume* reading is numerically displayed on the *Catheter Calibration* tab. The values displayed on the calibration buttons change according to the current catheter configuration and are derived from Bann's equation. Therefore, the segment volumes are derived from the current set values for alpha, rho and segment length. The values displayed on the calibration button represent the per-segment conductance / volume. When the button is activated, the corresponding composite volume is displayed on the right-hand side of the button. A measurement of blood resistivity is performed during the clinical procedure as described in Section 2.4. At the start of a case, the correct size catheter is selected along with setting the blood resistivity to 180 ohms / cm on the *Catheter Configuration* tab, as described in Section 2.4. The data acquisition system incorporates six internal resistors of known conductance that are used to convert the voltage signal into a volume. Only two buttons will be selectable at any given range; the available button will be beige and the unavailable buttons will be greyed out (Figure 2-7). The MPVS *Control Interface* automatically determines the available buttons from the catheter segment length and gain setting selected on the *Catheter Configuration* tab, as described in Section 2.4. Figure 2-7 shows the volume options available for a 7F 5cm over 8 electrode catheter when the blood resistivity is set to 180 ohms / cm. To calibrate the lower range of the volume segments the *12.1-ml button* should be activated (highlighted green), so that the MPVS Ultra will output a 12.1 ml volume signal on the five volume segment volume channels and a 60.34 ml volume signal is outputted on the composite volume channel. To calibrate the upper range of the volume segments the *43.2-ml button* should then be activated (highlighted green), so that the MPVS Ultra will output a 43.2 ml volume signal on the five volume segment volume channels and a 216.0 ml volume signal is outputted on the composite volume channel. The *Transducer* button should then be activated so that the MPVS Ultra will read the volumes measured on the five volume segments and the composite volume on the Millar catheter. At the end of the procedure, the volume calibration is repeated after correcting the blood resistivity value displayed on the *Catheter Calibration* tab to the measured blood resistivity.

2.4.2.3 Rho Cuvette Tab

The *Rho Cuvette* tab (Figure 2-8) was used to measure the subjects' blood resistivity. The *Millar Cuvette Selection* field was used to identify the Millar MPVS Ultra cuvette used to perform the measurement (Figure 2-9). The K Factor is a calibration value supplied by Miller for the specific Millar MPVS Ultra Cuvette supplied with the system. The K Factor is used to reduce the error in resistivity reading caused by slight variations that are inherent in the design of the cuvette. Three different cuvettes are used with the system, so care must be taken to ensure the correct Cuvette with the correct K-Factor was selected in the *Rho Cuvette* tab when performing a measurement of blood resistivity. The Millar MPVS Ultra is set up to allow for seven different gain settings which can be used to optimise the accuracy of the resistivity reading depending on the fluid to be measured. When performing measurements on human and animal blood, the blood resistivity measurements should be carried out with the gain set to x 2.

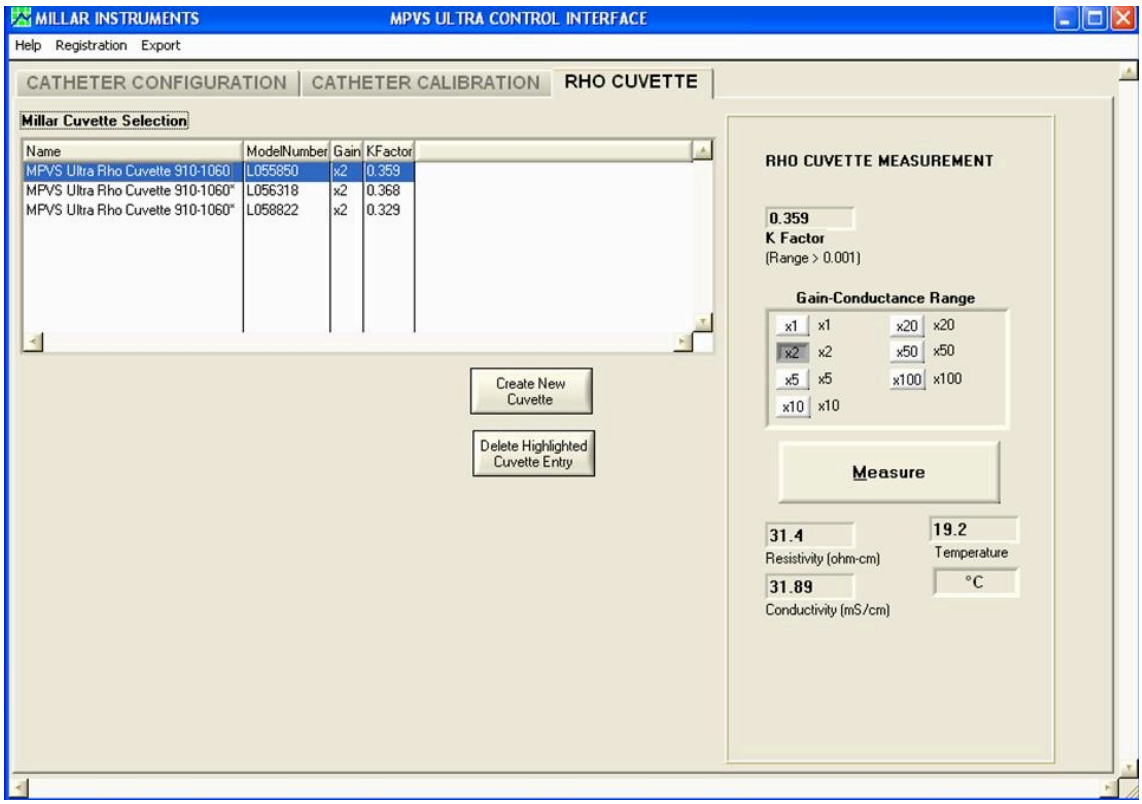

Figure 2-8 Millar MPVS Ultra control interface Rho cuvette tab screen capture

The cuvette must be connected to the *Cuvette* input to perform a measurement of blood resistivity from a sample of the subjects' blood, as shown in Figure 2-5. The appropriate cuvette must be selected in the *Cuvette Selection* field. The cuvette should be placed on a flat dry surface. Using a heparinised syringe the operator will draw up 3 to 5 ml of blood from the subject. While wearing protective gloves, the syringe of blood is then taken from the operator and injected into the well on the cuvette. The blood should be level with the top surface of the cuvette. Click on the *Measure* button in the *Rho Cuvette* tab and the *Measured Snapshot* will then display the measured resistivity, temperature and conductivity of the blood sample. The blood sample is disposed of using the correct Catheter Laboratory procedures. The cuvette is rinsed with warm water and then air-dried.

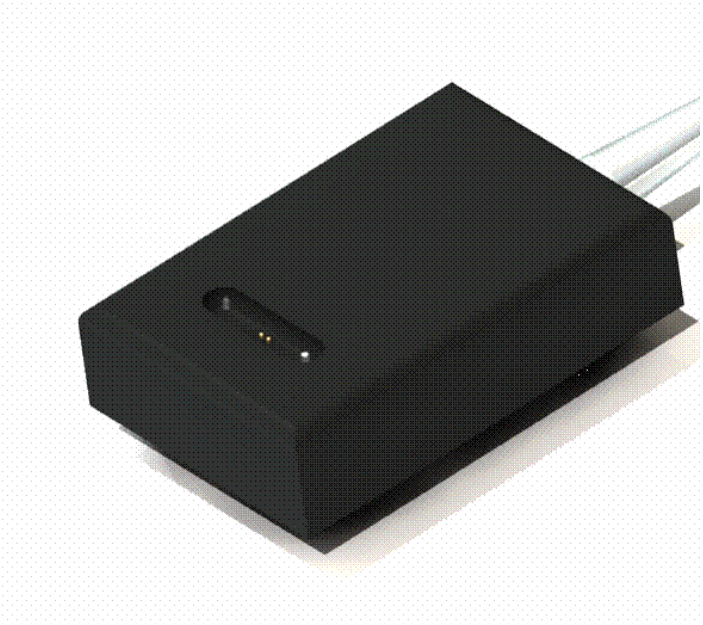

Figure 2-9 Millar (Houston, Texas, USA) MPVS Ultra cuvette

2.4.3 ADInstruments PowerLab 16/30 Series

The ADInstruments PowerLab 16/30 Series front panel connections are shown Figure 2-10. The PowerLab has three indicators at the left-hand side of the panel. All three indicators turn on briefly when the PowerLab is switched on. The *Power* indicator will illuminate blue when the system is turned on and receiving power. The *Status* indicator will flash yellow and then illuminate green when the system is turned on and receiving power. The *Trigger* indicator will flash yellow and turn off when a trigger signal is received the indicator will illuminate yellow. The *Status* indicator is used to communicate what is happening between the PowerLab and PC. The *Status* indicator will: illuminate green when the system is receiving power and is idle; illuminate yellow when it is sampling or communicating with the PC; illuminate red and flash if the system has detected a communication fault. The PowerLab has sixteen independent BNC connector inputs (1 – 16). The analogue inputs can receive external signals in the ±2 mV to ±10 V range with a maximum input voltage of ±15 V. A fixed 25 kHz analogue low pass filter is attached to each analogue input. Digital signal processing can be performed on each analogue input using the LabChart software (See Section 2.4) to set the gain, filtering, AC/DC coupling and to calibrate the input signals. The input impedance between the analogue inputs and earth pin on the rear panel is 100 Ohms. The analogue inputs are connected to the pressure output (*P1*), volume outputs (*Composite*, *V1 – V5*) and *ECG* Output on the Millar MPVS Ultra system using BNC connectors. The rear panel on the PowerLab has a USB port (v1.1 or later), which can be used with a USB cable to connect the PowerLab to the Windows PC running the LabChart software (See Section 2.4). At the start of each case, the USB cable between the PowerLab and the PC must be connected before the entire system is switched on. An IEC power cable connector can be used to connect the PowerLab to the mains power supply. The PowerLab is a Class I Type CF medical device, and an earth pin is provided which provides a direct connection to the earth pin on the power socket and the PowerLab metal casing.

Figure 2-10 ADInstruments (New South Wales, Australia) PowerLab 16/30 front panel hardware connections

2.4.4 ADInstruments LabChart Pro Software

2.4.4.1 ADInstruments LabChart Pro Settings File

A settings file was created to specify the different recording and display setting for each channel. To create a settings file (Figure 2-11) the *Channel Settings Dialogue* was opened when the Laptop was connected to the ADInstruments PowerLab and Millar MPVS Ultra boxes. In the bottom left-hand corner of the *Channel Settings Dialogue,* the number of channels was increased to 26. Channels 1 -16 correspond to the 16 BNC input connected to the front panel of the PowerLab. The remaining channels 17 – 26 are used for arithmetic data processing. The channel descriptions for a single RV setup are shown in Table 2-1. A number of the channels are switched off during RV measurement since the ADInstruments PowerLab, and Millar MPVS Ultra boxes remain permanently connected up to perform simultaneous LV and RV measurements.

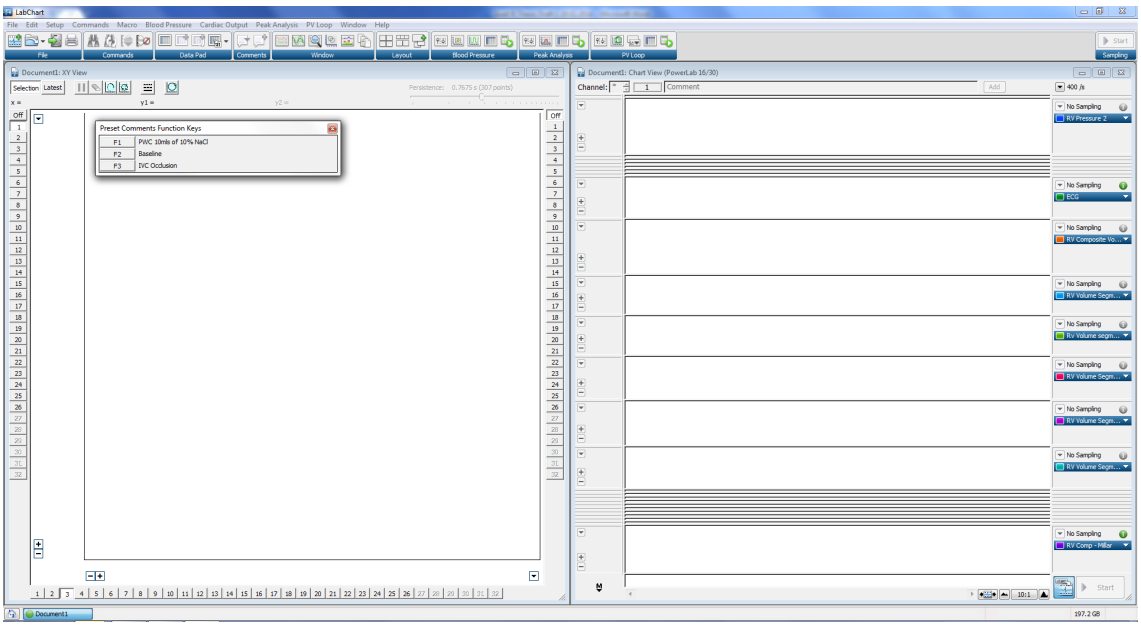

Figure 2-11 ADInstruments LabChart RV measurement setup screen capture

Table 2-1 ADInstruments LabChart RV channel description

Channel	Channel Description	Channel Source
1	OFF	N/A
2	RV Pressure	Millar MPVS Ultra Pressure Output P1
3	OFF	N/A
4	OFF	N/A
5	OFF	N/A
6	OFF	N/A
7	OFF	N/A
8	OFF	N/A
9	ECG	Millar MPVS Ultra ECG Output
10	RV Composite Volume	Millar MPVS Ultra Volume Output Composite
11	RV Volume Segment 1	Millar MPVS Ultra Volume Output S1
12	RV Volume Segment 2	Millar MPVS Ultra Volume Output S2
13	RV Volume Segment 3	Millar MPVS Ultra Volume Output S3
14	RV Volume Segment 4	Millar MPVS Ultra Volume Output S4
15	RV Volume Segment 5	Millar MPVS Ultra Volume Output S5
16	Slaved ECG	BNC ECG Output from Catheter Laboratory
17	OFF	N/A
18	dp/dt(RV)	Derivative of Channel 2
19	OFF	N/A
20	HR (RV)	Cyclic Measurement Channel 2
21	OFF	N/A
22	SV (RV)	Cyclic Measurement Channel 26
23	OFF	N/A
24	CO (RV)	Arithmetic - (Channel 20*Channel 22)/1000
25	OFF	N/A
26	RV Comp Millar	Arithmetic - (1/alpha)*Ch10-Vc

2.4.4.2 LabChart Pro Data Collection

At the start of the research study the Millar MPVS Ultra, ADInstruments PowerLab and Laptop were connected as described above. The RV LabChart settings file was loaded, and Millar MPVS Ultra *Control Interface* was opened on the laptop. In the LabChart file, the *Start* button was activated on the bottom right-hand corner of the *Chart View*. The MPVS Ultra *Control Interface* was then used to input the 2-point calibration signal for both the pressure and volume channels as described in Section 2.4. The calibration signal was highlighted on Channel 2 (RV Pressure). The *Channel Function* popup menu was selected on Channel 2 (RV Pressure), and the *Units Conversion* button was selected to open the *Units Conversion* dialogue. The pressure trace was selected for the 0.0-mmHg input signal, and the mean voltage was then calibrated to corresponded to 0.0-mmHg pressure (Figure 2-12). The pressure trace was selected for the 100.0-mmHg input signal, and the mean voltage was then calibrated to corresponded to 100-mmHg pressure.

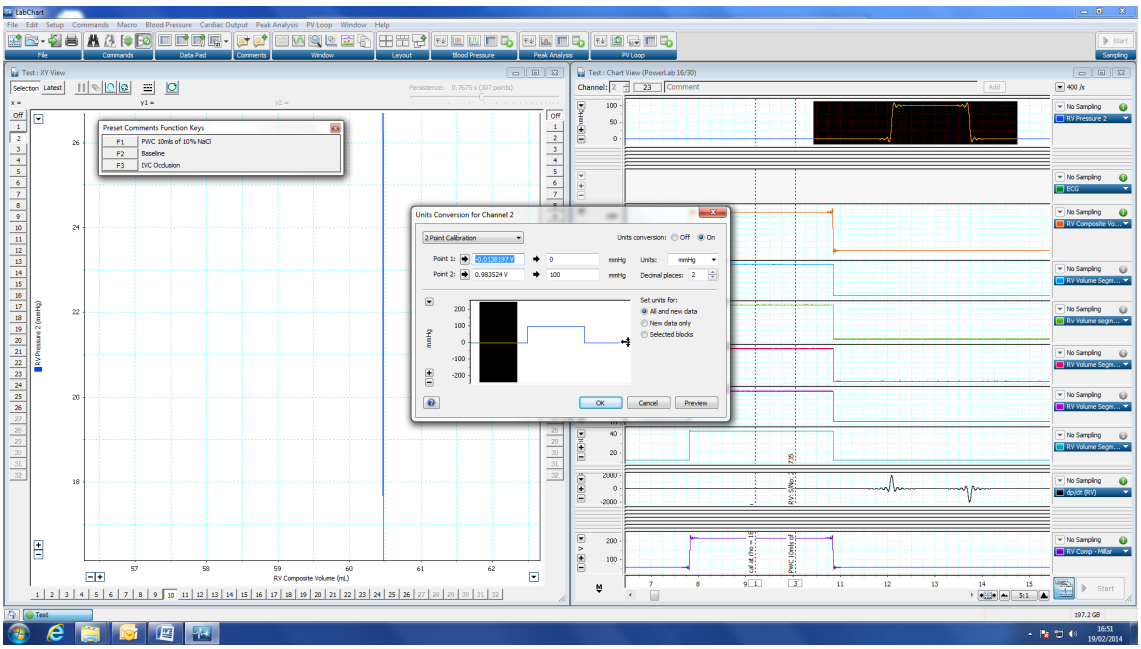

Figure 2-12 Pressure channel calibration screen capture

The calibration signal was highlighted on Channel 10 (RV Composite Volume) to calibrate the composite volume channel. The *Channel Function* popup menu was selected on Channel 10 (RV Composite Volume), and the *Units Conversion* button was selected to open the *Units Conversion* dialogue. As previously described in Section 2.4, for a 5cm catheter an 180 ohm/cm calibration signal would be used to calibrate the volume channels at the start of the study. The volume trace was selected for the 216.0 ml input signal and the Point 1 mean voltage was then calibrated to corresponded to a 216-ml volume (Figure 2-13). The volume trace was selected for the 60.34 ml input signal, and the Point 2 mean voltage was then calibrated to corresponded to a 60.34-ml volume. To calibrate the composite volume channel, the calibration signal was highlighted on Channel 11 (RV Volume Segment 1). The *Channel Function* popup menu was selected on Channel 11 (RV Volume Segment 1), and the *Units Conversion* button was selected to open the *Units Conversion* dialogue. The volume trace was selected for the 43.2 ml input signal and the Point 1 mean voltage was then calibrated to corresponded to a 43.2-ml volume. The volume trace was selected for the 12.1 ml input signal, and the Point 2 mean voltage was then calibrated to corresponded to a 12.1-ml volume. This process was repeated for the remaining four segment volume channels 12 (RV Volume Segment 2) – 15 (RV Volume Segment 5).

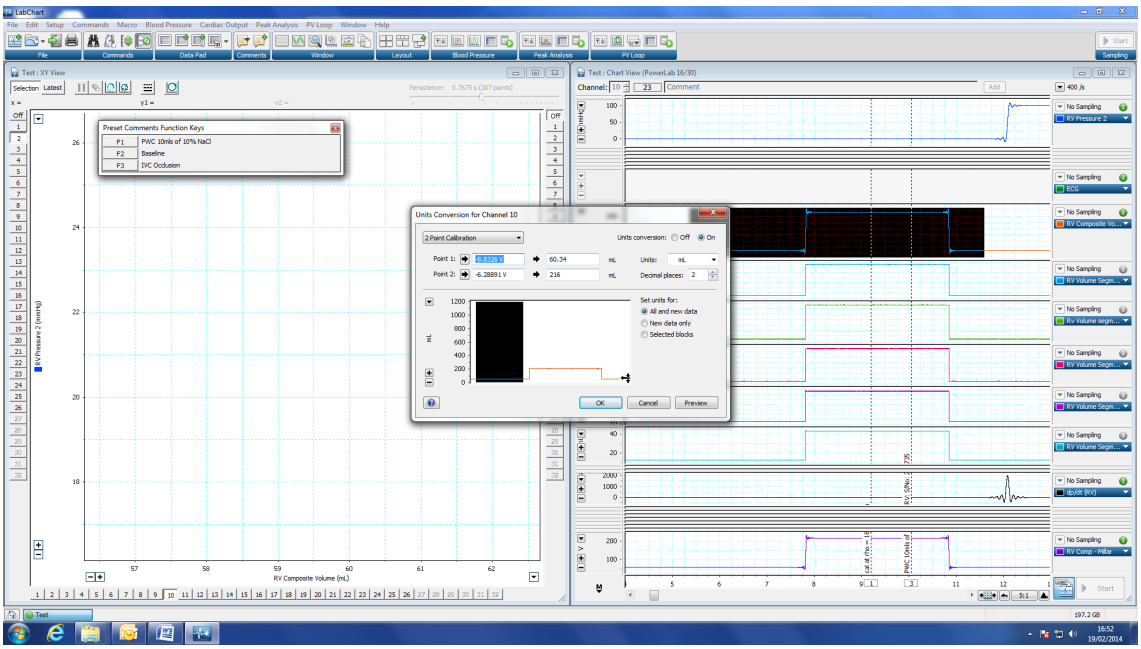

Figure 2-13 Volume channel calibration screen capture

The sterile Millar conductance catheter was connected to the Millar MPVS Ultra, and pressure channel zeroed to atmospheric pressure as described in Section 2.4. Via a femoral or jugular approach, the operator positioned the catheter in the RV. After activating the sampling button, the position of the catheter in the RV was confirmed using the *XY View* and that pressure and volume signals were received on all channels on the *Chart View*. The *Toggle Data Recording / Monitoring* button could then be used to change between data monitoring mode (used to observe the PV-loop without recording data) and data recording mode. A saline calibration was then performed to correct for parallel conductance. The *Toggle Data Recording / Monitoring* button was used to start the file recording. The ventilator was stopped at end-expiration, or the patient was asked to perform a breath hold by the operator. The preset file marker *PWC 10mls of 10% NaCl* was used to mark a saline injection on the LabChart file. The operator injected 5mls of hypertonic saline followed by a 5ml saline flush into the port on the venous sheath. The *XY View* was monitored to ensure an increase in the stroke volume was recorded. The *Toggle Data Recording / Monitoring* button was used to switch back to monitoring mode. The ventilator was started, or the patient was told that they could start breathing. The saline injection was repeated to ensure an accurate volume offset could be calculated.

Steady state PV-loops were recorded by using the *Toggle Data Recording / Monitoring* button to start the file recording. The ventilator was stopped at end-expiration, or the patient was asked to perform a breath hold by the Operator. The preset file marker *Baseline* was used to mark a steady state PV-loop recording on the LabChart file. Approximately 10 to 15 steady state PV-loops were recorded before the ventilator was started or the patient was told that they could start breathing. All recordings were repeated to ensure consistent and accurate data was collected.

Load independent PV-loops were recorded using an IVC balloon occlusion to alter the preload on the heart. The operator used a further femoral venous sheath to position a

34ml-sizing balloon in the mouth of the right atrium. The *Toggle Data Recording / Monitoring* button was used to start the file recording. The ventilator was stopped at end-expiration or the patient was asked to perform a breath hold by the consultant cardiologist. The preset file marker *IVC Occlusion* was used to mark an IVC Occlusion PV-loop recording on the LabChart file. The balloon was inflated with a contrast agent by the operator to occlude the IVC. Approximately 15 to 20 seconds of PV-loops were recorded before the balloon was deflated. The ventilator was started, or the patient was told that they could start breathing. All recordings were repeated to ensure consistent and accurate data was collected.

2.5 PV-Loop Data Analysis

2.5.1 Steady State PV-Loop Analysis

PV-loop data was analysed offline using LabChart Pro 8.0 software package. The files were link anonymised on the laptop and transferred to a desktop PC for analysis. The *Analysis Manager* function was used to mark and record a selection of six steady state PV-loops that were recorded at end-expiration during a breath hold or suspended ventilation (Figure 2-14). The correct data points are located using the comments (Baseline) that were marked on the file during the clinical procedure. The PV-loops were recorded on the analysis manager using the following coding:

RV Description (comment number): Alpha (Conductance CO / Actual CO) – Vc

Description - Baseline or Post Intervention

Comment Number – cross-reference to the comment number that the PV-loops correspond to on the LabChart file

Conductance CO – CO derived from the conductance catheter

Actual CO – CO derived from Fick or Thermodilution technique

Vc – Volume correction derived by the saline injection technique

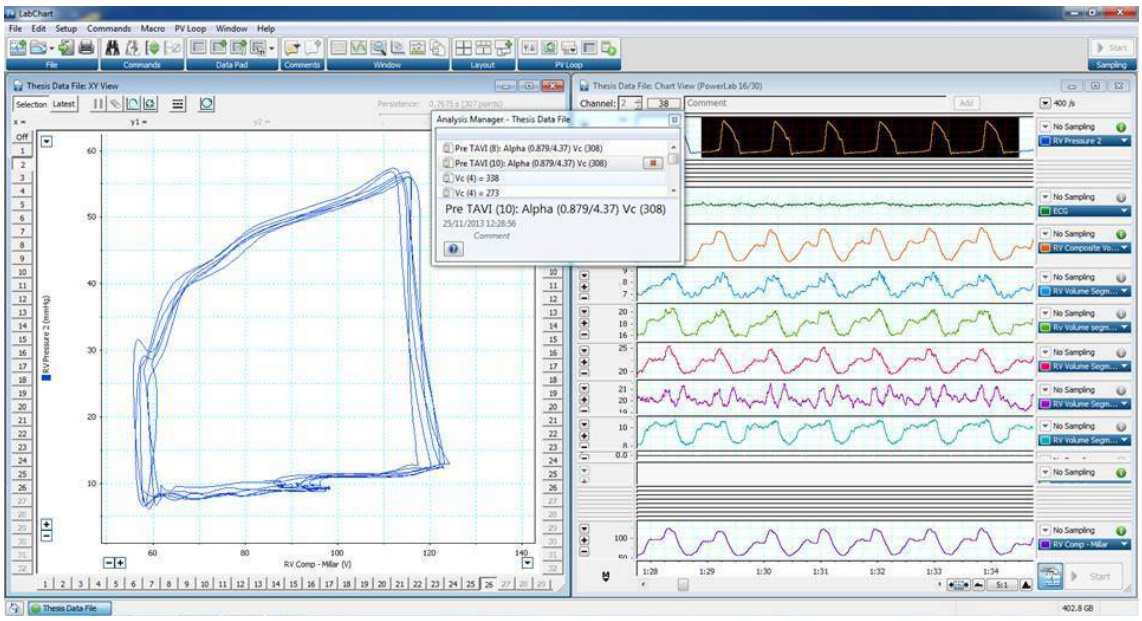

Figure 2-14 LabChart RV data selection screen capture

The conductance derived CO was then calculated for the steady state PV-loops. This was performed to correct for the dimensionless slope factor Alpha described in section2.3. On the *PV-loop* taskbar, the *Settings* button was selected to open the *PV-loop Setting* dialogue (Figure 2-15). The pressure signal was then set to Channel 2 (RV Pressure), and the volume signal was set to Channel 10 (RV Composite Volume). The analysis region was set to the *selection only*. The *OK* button was then selected to run the analysis and close the PV-loop Setting dialogue. On the *PV-loop* taskbar, the *Hemodynamics Table* button was selected to open the hemodynamics table and the conductance derived CO was recorded. The *Arithmetic* channel calculation was then opened on Channel 26 (RV Comp – Millar) so that the following equation could be entered to correct for the dimensionless slope factor Alpha:

(1/(Conductance CO / Actual CO)) * Ch10 – 1

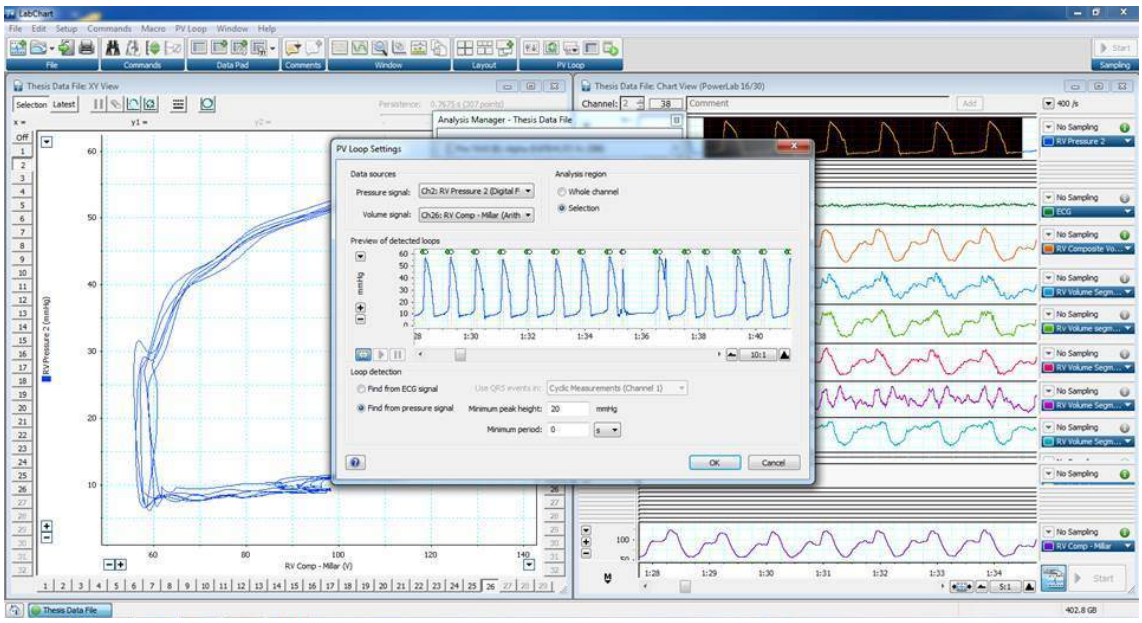

Figure 2-15 LabChart CO correction screen capture

The saline calibration was then analysed to correct for the volume offset described in section 2.3. The correct data points were located using the comment (saline calibration) that was marked on the file during the clinical procedure. The *Analysis Manager* was used to mark and record a selection of PV-loops collected during the injection of 10% hypertonic saline. The PV-loops were recorded in the *analysis manager* using the following coding:

Vc (comment number) = Volume Offset

Vc = Saline injection derived volume correction

Comment number – cross-reference to the comment number the PV-loops correspond to on the LabChart file

Volume offset – volume of blood to be subtracted

On the *PV-loop* taskbar, the *Settings* button was selected to open the *PV Loop Setting* dialogue. The pressure signal was then set to Channel 2 (RV Pressure), and the volume signal was set to Channel 26 (RV Comp – Millar). The analysis region was set to the *selection only*. The *OK* button was then selected to run the analysis and close the *PV-loop Setting* dialogue. On the *PV Loop* taskbar the *PV-loop Plots* button was selected, and then the *Saline Calibration* button was selected on the drop down tab to open the *Saline Calibration* plot (Figure 2-16). The analysed Vc is then displayed in the top left-hand corner. This value was recorded. The arithmetic channel calculation was then opened on Channel 26 (RV Comp – Millar) so that the following equation could be entered to correct for the parallel conductance Vc:

(1/(Conductance CO / Actual CO)) * Ch10 – Vc

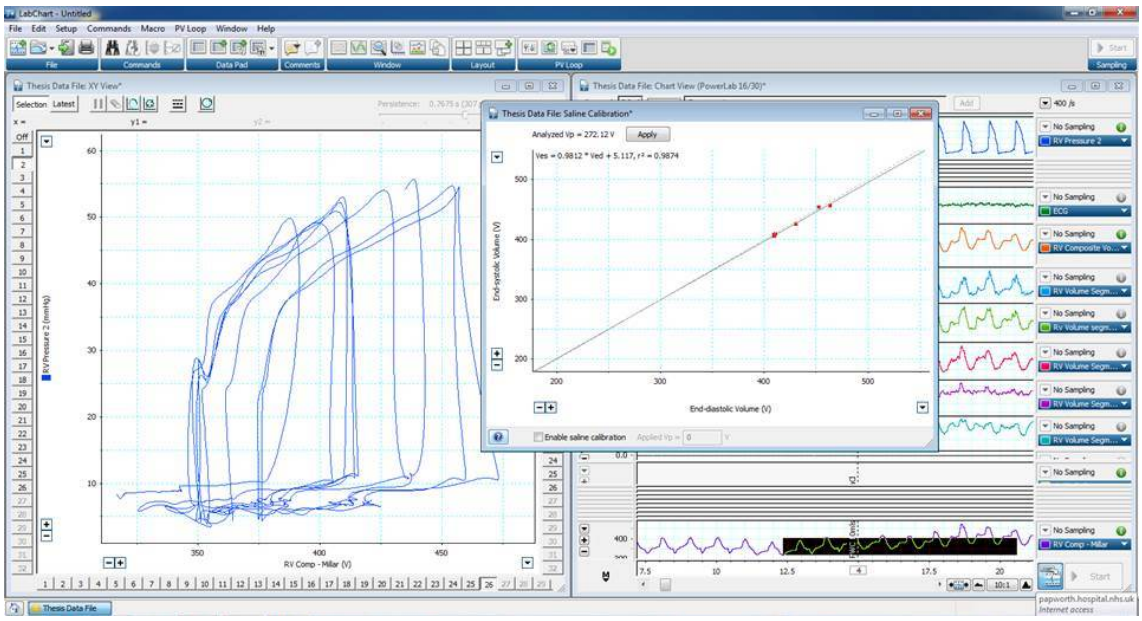

Figure 2-16 LabChart saline calibration screen s capture

The steady state PV-loops were then selected in the *Analysis Manager*. On the *PV-loop* taskbar, the *Settings* button was selected to open the *PV-loop Setting* dialogue. The pressure signal was then set to Channel 2 (RV Pressure), and the volume signal was set to Channel 26 (RV Comp – Millar). The analysis region was set to the *selection only*. The *OK* button was then selected to run the analysis and close the *PV-loop Setting* dialogue. On the *PV-loop* taskbar, the *Hemodynamics Table* button was selected to open the hemodynamics table detailing all the hemodynamic parameters for the analysed PV-loops. This data was then transferred to an excel file for further statistical analysis.

2.5.2 Load Independent PV Loop Analysis

The *Analysis Manager* was used to mark and record a selection of PV-loops that were recorded during an IVC balloon occlusion as described in section 2.3. The correct data points were located using the comment (IVC Occlusion) that was marked on the file during the clinical procedure. The PV-loops are recorded on the *analysis manager* using the following coding:

RV Description IVC Occlusion (comment number): ESPVR; EDPVR; PRSW

Description - Baseline or Post Intervention

Comment Number – cross-reference to the comment number the PV-loops correspond to on the LabChart file

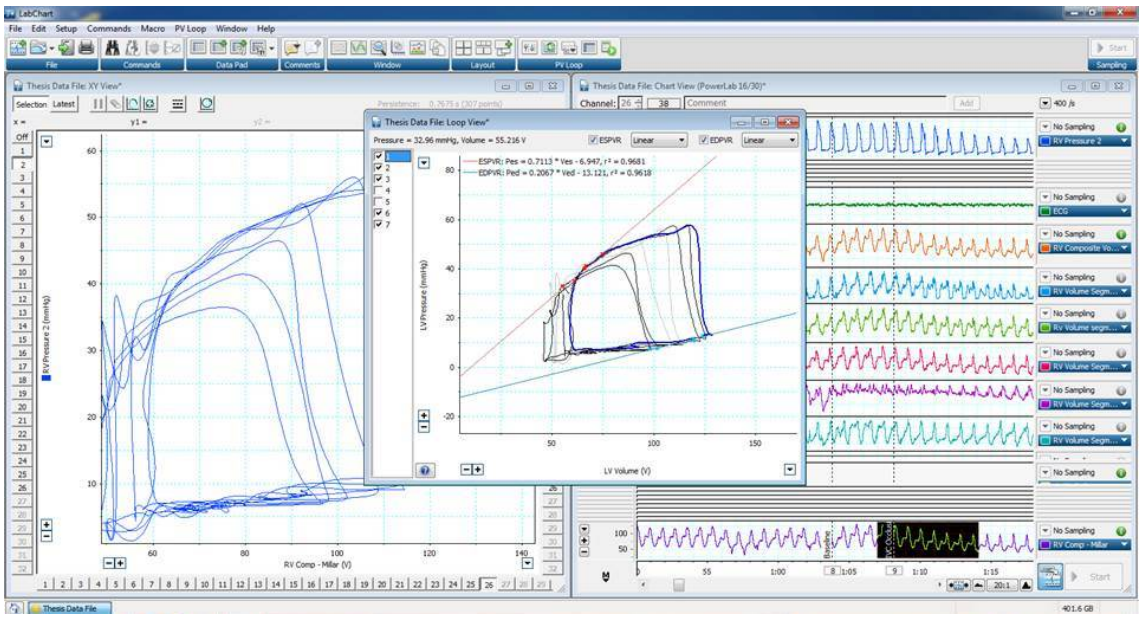

Figure 2-17 LabChart PV-loop view screen capture

On the *PV-loop* taskbar, the *Settings* button was selected to open the *PV-loop Setting* dialogue. The pressure signal was then set to Channel 2 (RV Pressure), and the volume signal was set to Channel 26 (RV Comp – Millar). The analysis region was set to *selection only*. The *OK* button was then selected to run the analysis and close the *PV-loop Setting* dialogue. To determine ESPVR and EDPVR, on the *PV-loop* taskbar, the *PV-loop View* button was selected to open the *PV-loop View* plot (Figure 2-17). Individual PV-loops were selected by clicking on the loop number at the left-hand side of the PV-*loop View* plot. Only PV-loops with a checked box next to the respective PV-loop number are included in the analysis. If an ectopic beat was included in the analysis, that beat was removed by un-checking the box. The ESPVR and EDPVR best-fit regressions values for the selected PV-loops are displayed in the top right-hand corner of the *PV-loop View* plot. To determine PRSW, on the *PV-loop* task bar, the *PV-loop Plots* button was selected. The *PRSW Plot* button was selected on the drop down tab to open the PRSW plot. The PRSW best-fit regression value for the selected PV-loops was displayed in the top right-hand corner of the *PRSW* plot. The values for ESPVR, EDPVR and PRSW were recorded on the record in the analysis manager. The data was transferred to an Excel file for statistical analysis.

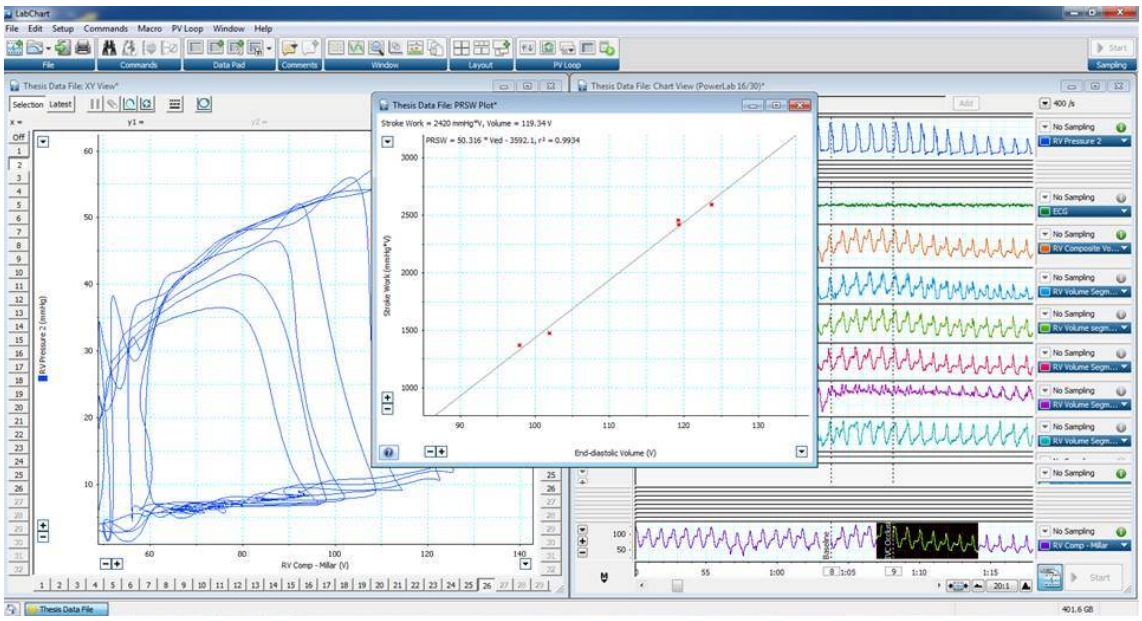

Figure 2-18 LabChart PRSW plot screen capture

2.6 Determination of Cardiac Output

Cardiac output (CO) is the effective volume of blood expelled by the ventricles per unit time and is used as a measure of the performance and health of the heart. A maintained CO is essential to deliver all the metabolic agents to the body and remove the unwanted waste products. CO is given by the following equation:

Equation 2-6

$$CO = HR \times SV$$

Where the heart rate (HR) is in beats per minute and the stroke volume (SV) is the volume of blood pumped from a ventricle in a single heartbeat (l). The CO is directly correlated to the size of the patient, by way of standardising to the body surface area (BSA) (m2). Cardiac index (CI) is given by the following equation:

Equation 2-7

$$CI = \frac{CO}{BSA}$$

The ejection fraction (EF) is the volumetric fraction of blood ejected in a single heartbeat, and is given by the following equation:

Equation 2-8

$$EF = \frac{SV}{EDV}$$

Where the end-diastolic volume (EDV) is the volume of blood left in the ventricle at the end of diastole. The end-systolic volume would be the volume of blood left in the ventricle at the end of systole. Throughout the research completed during the clinical studies CO was calculated invasively using the thermodilution method and the Fick principle; and non-invasively using echocardiography techniques.

2.6.1 Thermodilution

The pulmonary artery catheter, known as the Swan-Ganz catheter, allows the direct measurement of right atrial, right ventricular, and pulmonary artery pressures and blood saturations. It also allows the indirect measurement left atrial or wedge pressure by inflating the balloon when positioned in a pulmonary artery. By inserting a venous sheath into the internal jugular or femoral vein, the catheter can be passed along the vein and positioned within the right atrium, passed into the right ventricle, then out into the pulmonary artery. After inflating the balloon when the catheter is in the pulmonary capillary, a wedge pressure (PCWP) can be recorded as a measure of the left atrial pressure transmitted back through pulmonary veins to pulmonary capillaries and recorded when catheter wedged in a peripheral branch.

The catheter is also used to perform the thermodilution method of determining CO. The catheter is advanced into the pulmonary artery, and the balloon is inflated to float the catheter tip into the pulmonary artery. When in-situ the balloon is deflated. The tip of the catheter contains a temperature-sensitive thermistor that is used to measure the transient temperature change after injection of a small bolus (10 ml) of cold saline (0.9% NaCl). By measuring the blood temperature a known distance from the tip of the catheter, CO can be calculated by measuring the resistance change of the thermistor as a function of time as it responds to the pulmonary artery blood temperature change due to the injected bolus of saline. A greater temperature change will correspond to a lower cardiac output. Thermodilution derived CO measurement would normally be repeated 3 to 5 times and a mean measurement would then be taken as the true CO.

2.6.2 Fick Principle

The Fick principle states that if the oxygen concentration in arterial blood supplying an organ, the oxygen concentration in venous blood leaving an organ, and the rate of oxygen uptake by an organ per unit time is known, then the cardiac output can be calculated by the following equation:

Equation 2-9

$$CO = \frac{VO_2}{C_a - C_v}$$

Where VO_2 is the oxygen consumption (l/min), C_a is the oxygen concentration of the blood sample taken from the artery (l/l), and C_v is the oxygen concentration of the blood sample taken from the pulmonary artery (l/l). The blood samples are analyzed in a blood-gas analyzer to determine the oxygen concentration, and the oxygen consumption is measured by using spirometry. By assuming a value for oxygen consumption, cardiac output can be closely approximated to the actual value without the need for the spirometry equipment. The assumed oxygen consumption is typically calculated from the LaFarge equation:

Equation 2-10

$$VO_{2\sim males} = 138.1 - (11.49 \log_e age) + (0.378HR)$$

and

Equation 2-11

$$VO_{2\sim females} = 138.1 - (17.04 \log_e age) + (0.378HR)$$

Where $VO_{2\sim males}$ is the assumed oxygen consumption in males and $VO_{2\sim females}$ is the assumed oxygen consumption in females (ml / min / m^2).

2.7 Echocardiographic Assessment

Echocardiography was used in the second clinical study to assess RV function and aortic valve stenosis (AS) severity to determine if aortic valve replacement was needed. These measurements are performed as part of the routine care pathway for patients undergoing transcatheter aortic valve implantation (TAVI) at Papworth Hospital NHS Foundation Trust.

2.7.1 Ultrasound Machines

A Philips iE33 ultrasound scanner (Philips Healthcare, MA, USA) was used to perform transthoracic echocardiographic (TTE) and transesophageal echocardiographic (TEE) assessment of the patients' aortic valve stenosis and right ventricular function during the transcatheter aortic valve implantation (TAVI) study. TEE was performed using an X7-2t transducer (Philips Healthcare, MA, USA). TTE was performed using either an X3-1 or S5-1 transducer (Philips Healthcare, MA, USA).

2.7.2 Aortic Valve Assessment

Initial aortic valve assessment was performed with a TEE ultrasound probe in an outpatients' clinic to determine that the patients were suitable for undergoing a TAVI procedure. The difference in pressure between the LV and aorta in systole, the transvalvular gradient, is a standard measure of AS severity (Currie et al., 1985). A stenosis of the aortic valve creates an obstacle to aortic ejection, increasing the gradients between the LV and aorta. Doppler was used to measure the maximum velocity across the aortic valve and then the pressure gradient was determined using Bernoulli law. An apical 5 chamber view was used to align the Doppler beam with the jet through the aortic valve. The peak gradient was determined from the peak velocity of the jet. The mean gradient was determined by averaging the instantaneous gradient by the ejection period. Although there is a good correlation between peak and mean gradients, the relationship depends on the shape of the velocity curve which varies with the severity of AS, therefore, mean gradients are normally reported. Mean

transvalvular gradients greater than 40-mmHg are defined as severe AS (Baumgartner et al., 2009).

Aortic valve area (AVA) is calculated based on the continuity-equation concept that the stroke volume (SV) ejected through the LV outflow tract (LVOT) all passes through the stenotic aortic valve. Because volume flow rate through any cross sectional area (CSA) is equal to the CSA times flow velocity over the ejection period (the velocity time integral (VTI) of the systolic velocity curve), the aortic valve area can be determined:

Equation 2-12

$$AVA = \frac{CSA_{LVOT} \times VTI_{LVOT}}{VTI_{AV}}$$

Where CSA_{LVOT} is the CSA of the LVOT, VTI_{LVOT} is the VTI of the LVOT and VTI_{AV} is the VTI of the aortic valve. A parasternal long-axis view was used to measure the diameter of the LVOT. The LVOT diameter was measured at the start of diastole. In adults the LVOT diameter is approximately 18-25 mm. An apical five-chamber view was used to measure the VTI of the LVOT and across the aortic valve. In adults the AVA is approximately 3-4 cm^2, severe AS is defined as an AVA <1.0 cm^2 (Baumgartner et al., 2009). The effective orifice area index (EOAI) is used to correct an AVA measurement in small or large patients. The EOAI was calculated by dividing the AVA by the patients' body surface area, severe AS is defined as an EOAI <0.6 cm^2/m^2 (Baumgartner et al., 2009).

The final step in evaluating the severity of AS is to determine the LV EF. The LV EF is calculated from the difference between the EDV – ESV divided by the EDV. An apical four-chamber view was used take a 2D measurement of the LV volume at end-systole and end-diastole. The LV EF function on the ultrasound scanner was used to trace the endocardial boarder at end-systole and again at end-diastole to compute the LV EF.

An LV EF greater than 50% is good, between 30-49% is moderate and below 30% is poor (Baumgartner et al., 2009).

2.7.3 RV Functional Assessment

Tricuspid annular plane systolic excursion (TAPSE) represents the distance of systolic excursion of the RV annular plane to the RV apex. It was obtained using M-Mode aligned through the triscupid lateral annulus in a four-chamber view and measuring the longitudinal displacement at systole. In the normal RV, TAPSE should be greater than 15-20 mm (Jurcut et al., 2010), and has been shown to correlate well with isotopic RV ejection fraction (Kaul et al., 1984).

RV fractional area change (FAC) expresses the percentage change in RV area between end-diastole and end-systole. An apical four-chamber view was used take a 2D measurement of the RV volume at end-systole and end-diastole. The RV FAC function on the ultrasound scanner was used to trace the endocardial boarder at end-systole and again at end-diastole to compute the RV FAC. RV FAC has been shown to have a good correlation with MRI-derived RV ejection fraction (Morcos et al., 2009). The main limitation when calculating RV FAC is the need for good endocardial boarded delineation, which can be challenging in the trabeculated RV.

2.8 Electrical Safety

The electrical medical devices used in this study were electrically safety tested by the Clinical Engineering Department at Papworth Hospital NHS Foundation Trust. The devices are tested to the IEC 60061-1 standard. The devices are tested annually and this is recorded on the medical device asset register and the devices will be labelled with a next test due label.

The Millar MPVS Ultra, ADInstruments PowerLab's 16/30 and Windows Laptop running the Millar MPVS Ultra Control Unit and ADInstruments LabChart software are operated in a medical electrical system to perform conductance derived PV-loop measurements. The IEC power sockets on the Millar MPVS Ultra, ADInstruments PowerLab's and power transformer on the Windows Laptop are powered through an ONEAC (Chloride Power, Columbus, OH, USA) PCM1000I medical grade isolation transformer. The isolation transformer provides 1000 VA at a maximum of 4.2 A, which allows the system to be operated with a single earth point and limits the earth leakage current to levels acceptable in the IEC 60061-1 standard.

2.9 Summary

This chapter has described the materials and methods common to the experimental and clinical research completed for the remainder of this thesis.

3 The Development of an Porcine Model of Right Ventriculoarterial Coupling

This chapter describes the methodological development of the porcine model of right ventriculoarterial coupling used in Chapter 4. The aim of this chapter is to develop a porcine model which can be used to determine if the theory of LV ventriculoarterial coupling and the Pressure-Volume relationship described by Sunagawa et al. (1987) can be translated to the thinner-walled RV that pumps at lower pressures. Section 1.6 describes a mathematical theory of using the pressure-volume relationship to assess LV ventriculoarterial coupling. This theory can be assessed in the RV to confirm if it is consistent between ventricular chambers. To test the theory of ventriculoarterial coupling of the RV, the technique of a working heart perfusion rig to assess LV ventriculoarterial interaction and coupling must be validated. Once confirmation of the work described by Sunagawa et al. (1987) has been achieved, the RV working heart perfusion rig can be developed to determine if similar pressure-volume relationships of the RV and pulmonary artery exist.

Section 3.1 describes the validation of an ex-vivo model of LV ventriculoarterial coupling and the Pressure-Volume relationship described by Sunagawa et al. (1987). This was performed to ensure that the working heart apparatus used in this study could successfully validate the findings previously described by Sunagawa. After demonstrating this work was repeatable, Section 3.2 describes the translation of this work into an ex-vivo model of RV ventriculoarterial coupling and the Pressure-Volume relationship. Due to complexities in RV physiology and limitations with the RV working heart apparatus it was not possible to develop a physiologically accurate ex-vivo model of RV ventriculoarterial coupling. Therefore, Section 3.3 describes the development of an in-vivo model of RV ventriculoarterial coupling. The model developed in Section 3.3 is then used in Chapter 4 to define the optimal ventriculoarterial coupling ratio of the porcine RV – PA.

As this work was not funded from the grant awarded to me by the NIHR some methodological compromises had to be accepted. This work was carried out under Dr Simon Messer's Project License 70/7967 - Is the circulatory determined death (DCD) donor heart suitable for transplantation. Their experimental protocol required that baseline PV-Loop assessments were performed following sternomoty, pericardectomy and with the hearts paced atrial. The operating theatre at the Royal Veterinary College does not have access to a mobile fluoroscopy unit. Therefore, the conductance catheters were placed in the ventricle via an apical puncher rather than percutaneously under fluoroscopic guidance.

3.1 An Ex-Vivo Model of Left Ventriculoarterial Interaction: Validation of Sunagawa's Model

3.1.1 Introduction

This section describes the validation of an ex-vivo model of LV ventriculoarterial coupling and the Pressure-Volume relationship described by Sunagawa et al. (1987). This was performed to ensure that the working heart apparatus used in this study could successfully validate the findings previously described by Sunagawa. The design and development of an LV working heart model perfusion rig for the ex-vivo assessment in a porcine model of LV ventriculoarterial interaction and coupling will be described.

3.1.2 Methods

This work was carried out at the Royal Veterinary College (Hatfield, London) under the Project Licence 70/7967 as previously described in Section 2.2.3. As previously described in Section 2.2.5, Dr Hatim Alibhai (Consultant Veterinary Anaesthetist) was responsible for the humane care of the animals and performed the anaesthetic preparation of the animals. Dr Simon Messer performed the surgical preparation.

3.1.2.1 Development of an LV Working Heart Perfusion Rig

3.1.2.1.1 Concept Design Requirements

The basic concept design requirements for an LV working heart perfusion rig is shown in Figure 3-1. An isolated heart needs to be perfused by Langendorff (Langendorff, 1895) retrograde perfusion of the coronary arteries within a system that can be modified into an LV working heart for functional assessment. The heart is perfused in a reverse fashion via the aorta; this backwards flow causes the aortic valve to close forcing the blood into the coronary arteries to perfuse the myocardium. The isolated heart is suspended in a chamber so that the perfused blood can drain into the reservoir. A centrifugal pump pumps the perfused blood from the reservoir through a blood filter and oxygenator. A heating mechanism warms the blood to 37°C. Typically this is achieved by circulating heated water through the oxygenator. The warm, oxygenated blood is then pumped along the circuit and into the aorta to perfuse the coronary arteries retrograde. Compliance chambers are placed in series with the inflow and outflow of the heart. Compliance chambers help to regulate the cyclic pressure by correcting for any intrinsic cyclic instability from perfusion pump pressure. The flow circuitry is designed so that the same pump can be used in a modified working heart configuration to fill the heart via the left atrium and pump blood out through the aorta into the aortic afterload chamber and then drain into the blood reservoir. A monitoring device is required to measure LA and aortic flows and pressures.

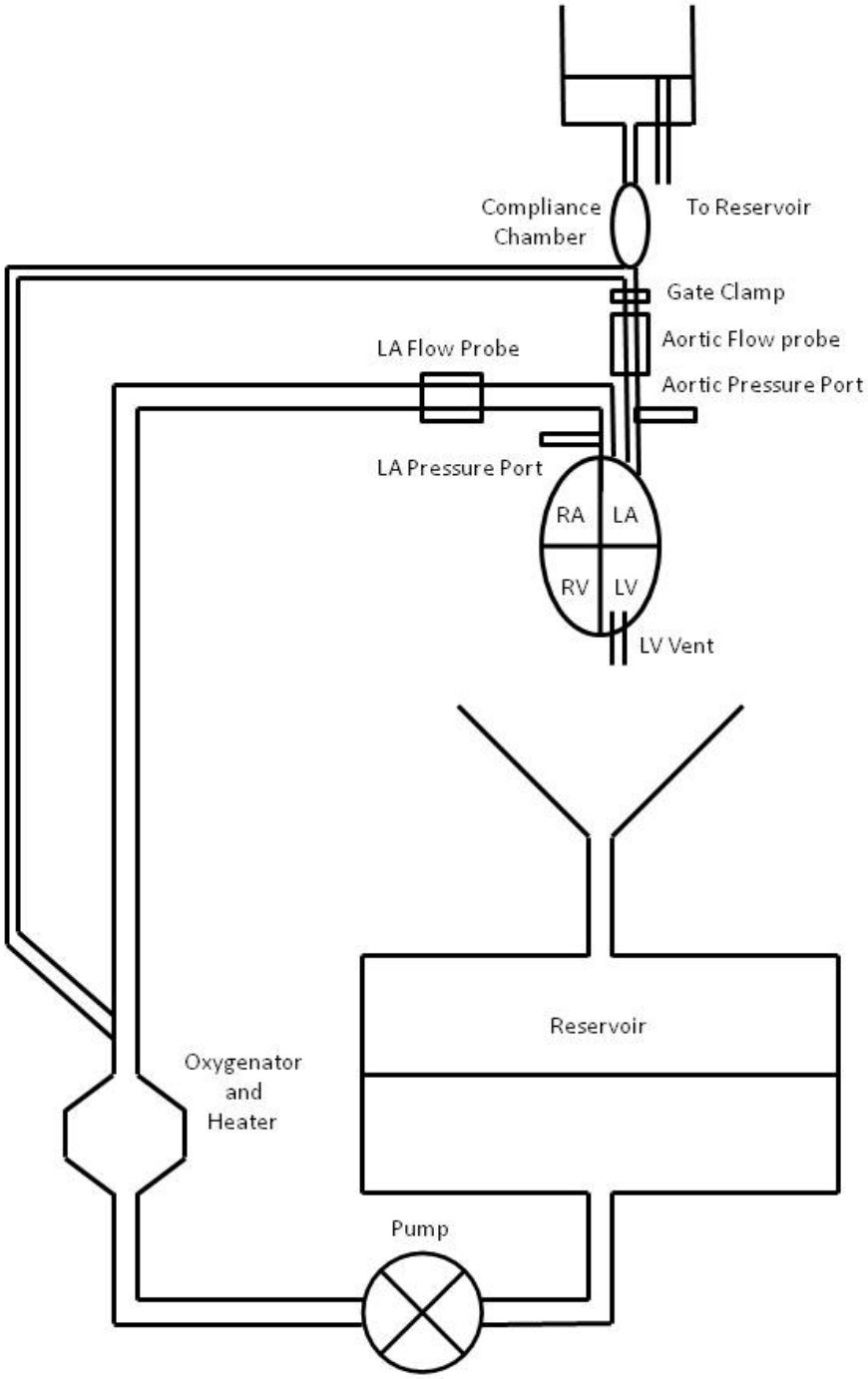

Figure 3-1 Concept design for the LV working heart perfusion rig

3.1.2.1.2 LV Working Heart Perfusion Rig

The TransMedics Organ Care System (OCS) (Andover, MA, USA) provides a Langendorff heart perfusion system with all the necessary connectors, tubing, compliance chambers, oxygenators, heaters, infusion pumps, flow sensors and pressure monitors contained in a single mobile unit (Figure 3-2). TransMedics have proprietary priming and maintenance solutions (this is used to replenish nutrients and substrates into the blood). The priming solution is mixed with 20 mEq of 8.4% sodium bicarbonate and 250 mg methylprednisolone, before emptying into the blood reservoir with approximately 1.5 litres is blood from the sacrificed animal. 30 units of insulin are added to the maintenance solution before priming the line and attaching to the built-in Alaris pump (30 ml / hr). A 500 ml bag of 5% glucose had 0.25 ml adrenaline and 50 units of insulin added to it, before priming a line and attaching it to a second built-in Alaris pump (10 ml / hr).

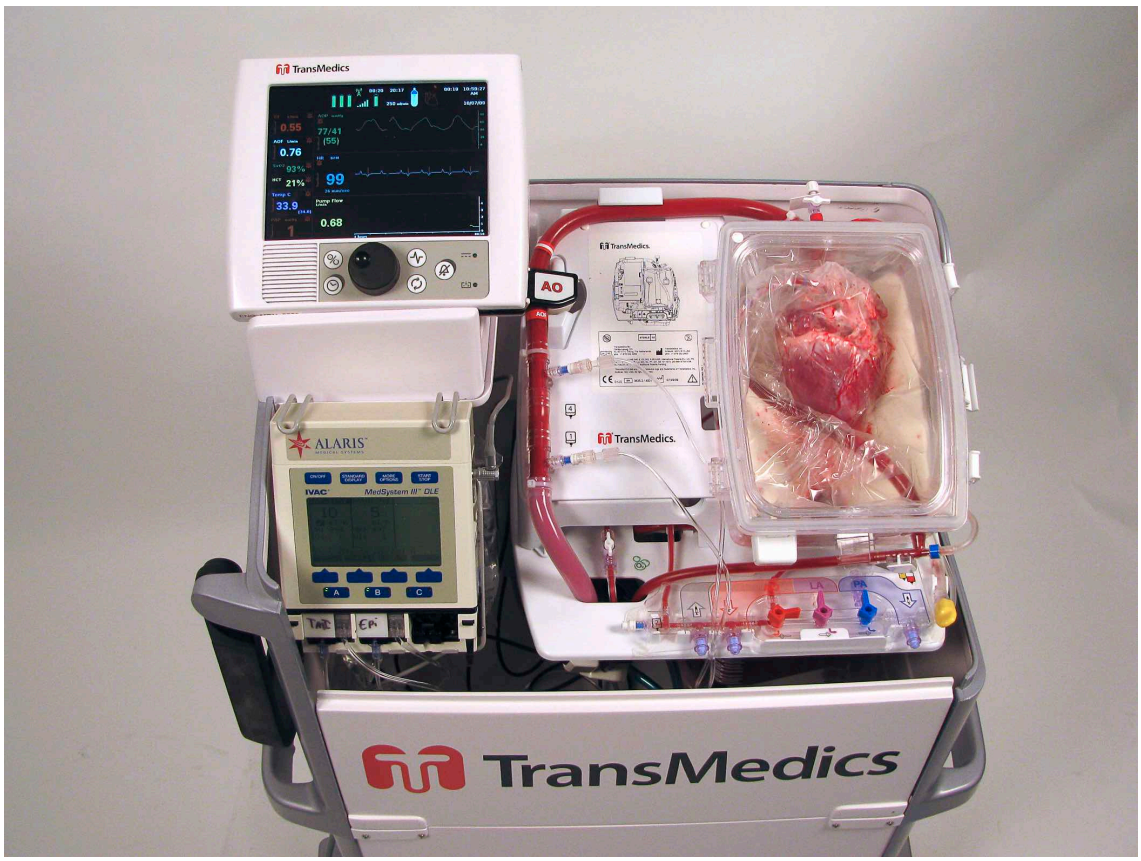

Figure 3-2 TransMedics (Andover, MA, USA) Organ Care System (OCS)

The TransMedics OCS was modified to provide an LV working heart perfusion (Figure 3-3). A Biomedicus centrifugal pump (BPX-80 BIO Pump Plus, Medtronic, USA) was connected to the system so that the propriety TransMedics OCS pump could be bypassed in the circuitry. The Biomedicus pump was then used to pump the perfused blood from the reservoir through the oxygenator and heater. The pump was replaced to provide a constant pulsatile flow so that functional assessment could be performed using the conductance technique. This tube was then split into two; one to act as the flow controlled Langendorff, and the second to act as the LA inflow port. The compliance chamber was then moved to the inflow of the aorta, for flow controlled Langendorff. The inflow to the aorta was then split a second time, to act as the 60-mmHg afterload, set by the height of the afterload chamber. Again a compliance chamber was added to this circuitry. This combination of modifications to the propriety TransMedics OCS circuitry would allow us to clamp off the Langendorff perfusion and put the isolated heart into an LV working heart perfusion.

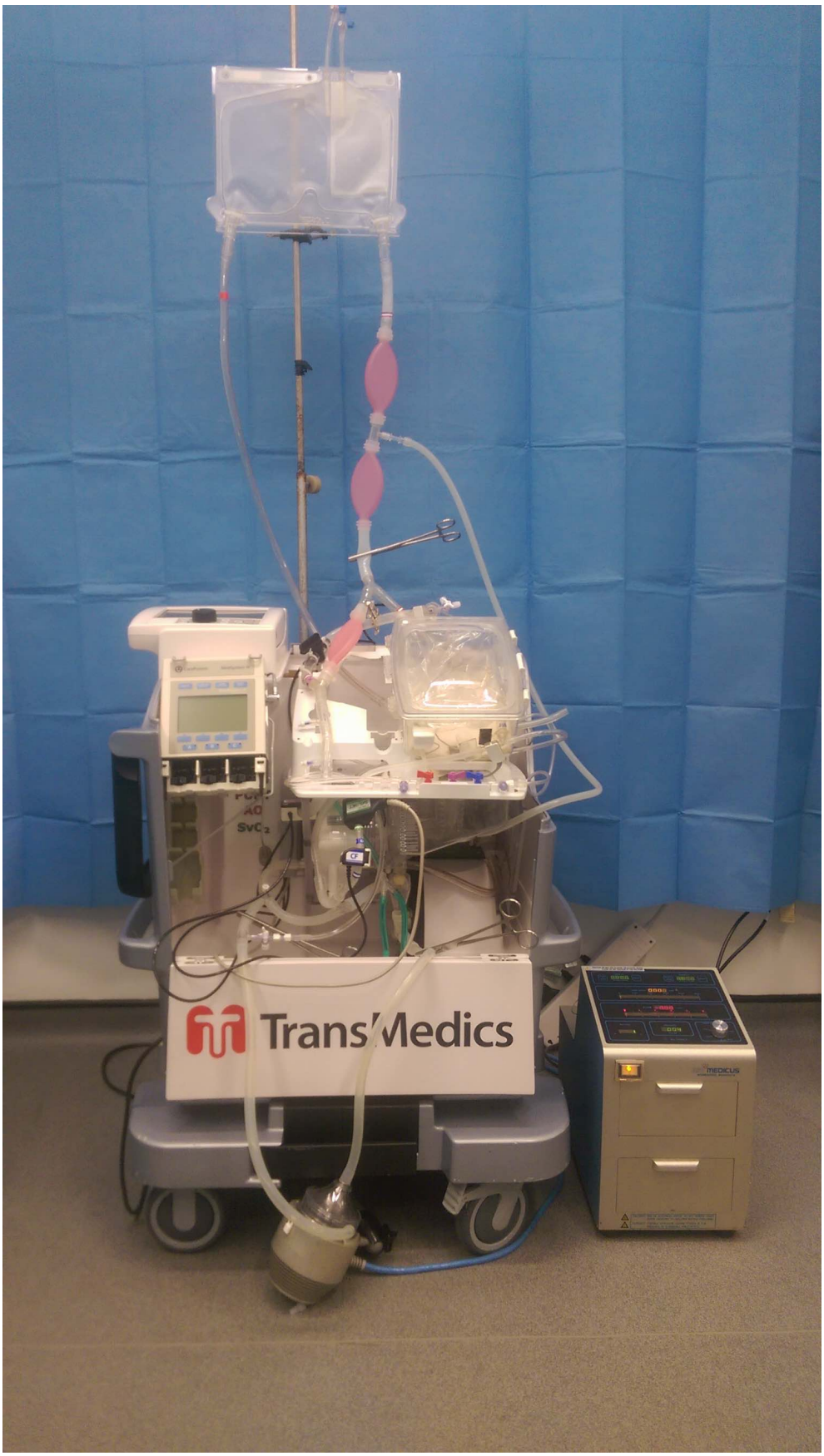

Figure 3-3 Modified TransMedics (Andover, MA, USA) OCS in LV working heart mode

3.1.2.2 Surgical Preparation

The pigs were fasted for 12 hours leading up to the procedure. Water was allowed until one hour before premedication. Premedication was undertaken with intramuscular injection of midazolam (0.5 mg/kg), ketamine (15 mg/kg) and atropine (0.02 mg/kg). Induction of anaesthesia was performed using an intravenous (IV) injection of fentanyl (5.0 mcg/kg) over 5 min and propofol (2.0-4.0 mg/kg) administered to effect. Oral endotracheal intubation was established for institution of mechanical ventilation (Aestiva 5, GE Healthcare, Hatfield, UK) with a respiratory rate of 12-15 breaths per min and tidal volume 10 ml/kg. The ventilator was set with volume control with peak pressure was always lower than 12 cmH_2O and positive end-expiratory pressure (PEEP) of 5 cmH_2O. Paralysis was induced with an IV injection of pancuronium (0.15 mg/kg). Maintenance of anaesthesia was performed using syringe drivers (Asena CC, CareFusion, Hatfield, UK) with a constant rate infusion of fentanyl (0.2 mcg/kg/min) and propofol (0.2 mg/kg/min). Arterial and venous cannulas were located for measurement of arterial blood pressure and central venous pressure respectively using multi-parameter anaesthesia monitor (GE Healthcare S5, Hatfield, UK). Before to placing the conductance catheter into the RV an IV injection of lidocaine (100mg, total dose) was administered.

The chest was prepared with a surgical scrub and draped to create a sterile operating environment. A midline sternotomy was performed, and the pericardium was removed. A small incision into the wall at the apex of the LV and sewing a purse string around the opening allowed a Millar conductance catheter to be securely located in the LV for functional assessment using the conductance catheter. A 7-F, 8 electrode conductance catheter (Millar Instruments, Houston, Texas, USA) was inserted through a puncher in the LV apex and placed along the long axis of the ventricle (Section 2.4). PV-loop morphology was used to confirm the correct placement of the catheter within the LV. Routine Swan-Gantz catheterization was performed via a 7-F sheath placed in the right

jugular vein, and the thermodilution technique was used to calculate cardiac output (Section 2.6.1).

3.1.2.3 Surgical Preparation of the Isolated Heart

After performing an initial assessment of hemodynamic function within the native physiological system to ensure that the hearts were healthy, a small incision was then made in the wall of the right atrium and a cannula was inserted into the heart. This cannula was used to collect 1.5L of blood to prime the TransMedics OCS in addition to 500mls of propriety priming solution (Figure 3-4). The TransMedics OCS pump flow was set to approximately 0.5 l/min so the blood was circulated and allowed to warm to 34°C. Retrieval of the heart was undertaken by cross clamping the ascending aorta, venting the heart and delivering 500mls of pressurised cold crystalloid cardioplegia at 4°C directly into the aorta. Cardioplegia is delivered to intentionally cause the cessation of cardiac activity, lowering the metabolic activity of the heart and prevent cell death during the period of prolonged ischemia. The heart was then explanted in a standard fashion using surgical scissors to cut the pulmonary vessels, aorta and pulmonary artery; and submerged in a bowl of iced water. The aorta and pulmonary artery were then dissected and trimmed. A ¾ inch cannula was secured in the aorta using a sterile cable tie. The outflow tubing was then secured in the pulmonary artery using surgical silk.

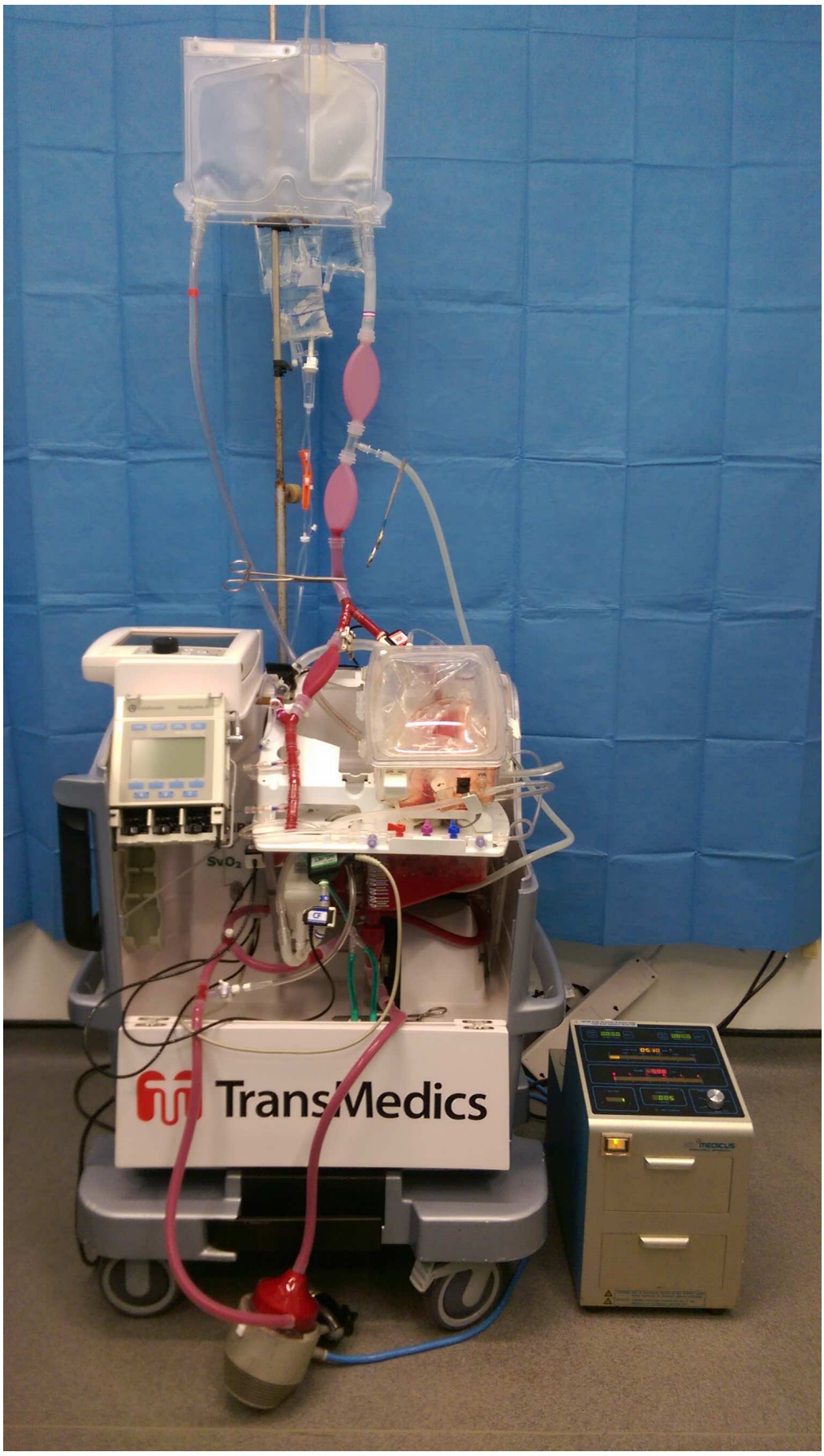

Figure 3-4 Modified TransMedics (Andover, MA, USA) OCS primed with blood

The cannulised heart was then instrumented upon the TransMedics OCS, to provide retrograde Langendorff perfusion of the coronary arteries. The pump flow was then increased (approx. 0.75 - 1lt / min) to maintain a mean arterial pressure of 65 mmHg. The volumetric pumps (Alaris GP, CareFusion, San Diego, USA) containing the TransMedics propriety maintenance solution (30 ml / hr) and adrenaline solution (10 ml / hr) were started (Section 3.1.2.1.2). Atrial and ventricular pacing wires were then sutured into the RV, connected to a Reocor external pacing box (Biotronik, Oregan, USA) and the heart was paced at 100 beats per minute (BPM). A small incision was then made in the apex of the LV, and a purse string was sutured in to allow the LV vent to be secured in place. The vent would later be replaced (when the heart was put into a working mode perfusion) by the conductance catheter for data collection. The inferior vena cava (IVC) and pulmonary veins were located and tied-off using surgical silk. A purse string was then sutured around a pulmonary vein to secure the LA cannula to allow the heart to be put into working mode perfusion.

3.1.2.4 Functional Assessment of the Isolated LV Working Heart

After 2 hours retrograde Langendorff reperfusion, the temperature of the circulating blood was increased to 37°C. The heart was allowed to reperfuse for this period to allow the myocardium to recover from the ischemic injury of cardioplegia and explanation. The Millar MPVS Ultra, ADInstruments PowerLab hardware and ADInstruments LabChart software was set up and calibrated as described in Chapter 2. The LV vent was then removed, and the conductance catheter was positioned in the LV for data collection. The propriety TransMedic OCS pump was then switched over to the Biomedicus centrifugal pump (BPX-80 BIO Pump Plus, Medtronic, USA). The left side of the heart was put into working mode with an afterload set by height to 60 mmHg and a left atrial filling pressure of 20 mmHg. The CO; mean, systolic and diastolic LA pressures; mean, systolic and diastolic aortic pressures were recorded. Five steady-state PV-loops were recorded to generate load-dependant parameters of the systolic and diastolic function. A family of PV-loops were recorded while partially clamping the

inflow to the LA to generate load-independent parameters of systolic and diastolic function during a preload reduction. This family of PV-loops was used to determine Ees. A second family of PV-loops were recorded while partially clamping the outflow to the aorta to generate load-independent parameters of systolic and diastolic function during an afterload increase (Figure 3-5). This was family of PV-loops was acquired to determine how the LV functions adapted to changes in Ea.

A bolus of inotrope dopamine equivalent to a 20-minute infusion at 5 μg/kg/min was then given directly to the blood reservoir to increase contractility. This was perfused for 15 minutes before repeating the measurement protocol. The CO; mean, systolic and diastolic LA pressures; mean, systolic and diastolic aortic pressures were recorded. Five steady-state PV-loops were recorded and families of PV-loops were recorded during a preload reduction and an afterload increase. This was performed to determine the effect of increasing Ees on LV function.

This controlled variation of Ea while keeping Ees and heart rate constant, and then the independent variation of Ees while keeping Ea and heart rate constant, would allow us to describe ventriculoarterial coupling (Ees/Ea) for an isolated LV working heart.

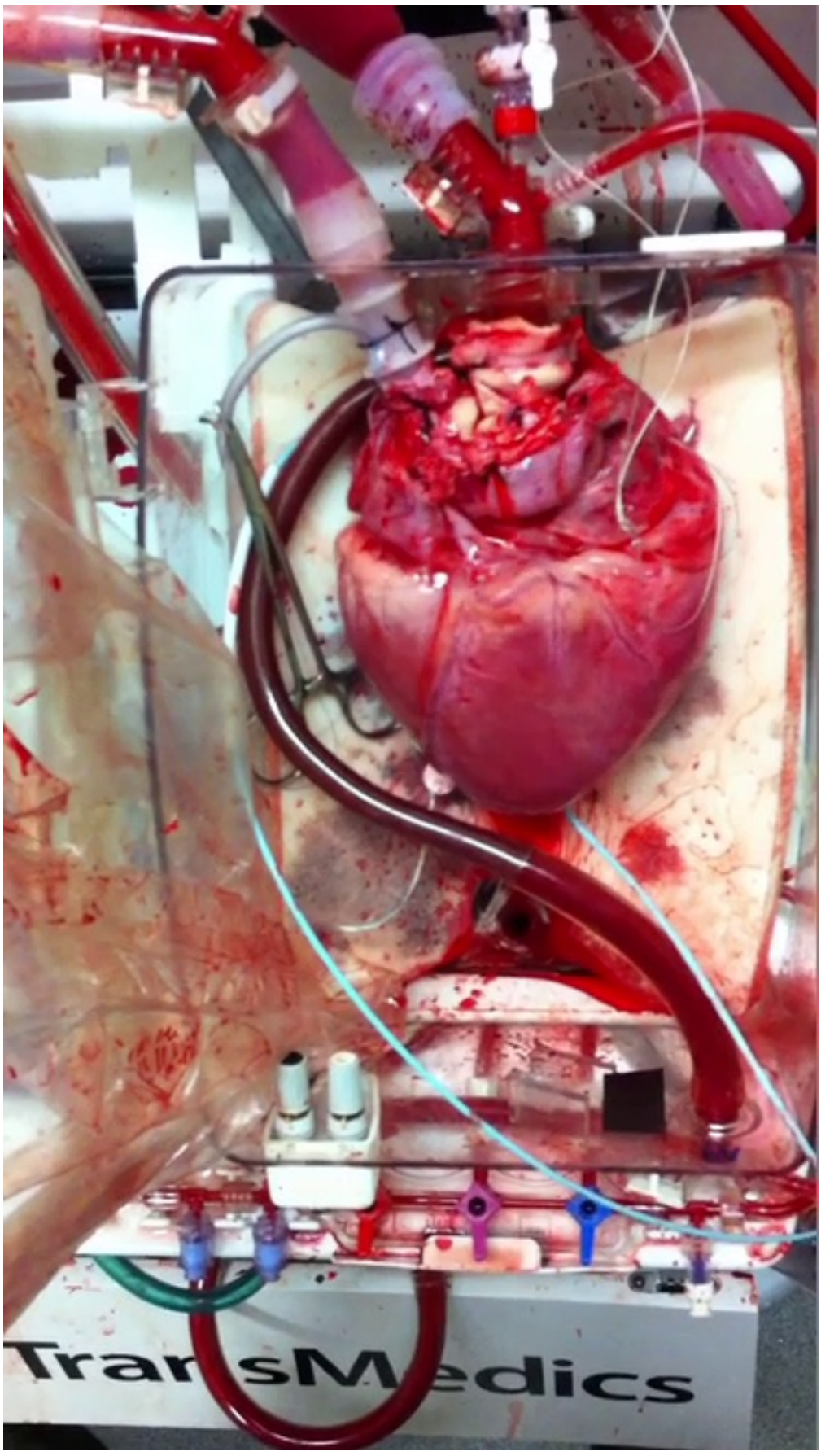

Figure 3-5 Modified TransMedics (Andover, MA, USA) OCS in working heart mode and functional assessment with PV-loops

3.1.3 Results

3.1.3.1 Demographics

The demographic data is shown in Table 3-1. This demonstrated that this work was carried out on a porcine heart with normal baseline haemodynamics (CO and mPAP).

Table 3-1 Demographic data

	Heart
Demographics	
Weight, kg	86.5
Height, cm	136.0
Baseline Haemodynamics Prior to Explanation	
Heart Rate, BPM	100
MAP, mmHg	50.0
MPAP, mmHg	22.0
Mixed Venous Sats,%	61.9
CO, L	6.4
CI, L/m^2	3.8
LV Working Mode Haemodynamics	
MAP, mmHg	52.0
CO, L	3.0

MAP = mean aortic pressure; MPAP = mean pulmonary arterial pressure; CO = Cardiac Output; CI = Cardiac Index.

3.1.3.2 Preload and the Pressure-Volume Relationship

Figure 3-6 shows the effect of a preload reduction on LV function. The slope of the ESPVR determined that the load-independent marker of contractility, Ees = 1.63 mmHg/ml. Table 3-2 shows the beat-to-beat analysis starting at baseline (PV-loop = 1) and then sequentially as the PV-loop morphology adapted due to the preload reduction (PV-loop = 6). This demonstrated that there was a gradual reduction in SW, ESP, EDP, EDV, ESV, dP/dt max and dP/dt min with decreasing preload. However, CO, SV and Ea remained constant. Therefore, the ventriculoarterial coupling ratio remained fairly constant increasing from Ees/Ea = 0.31 mmHg/ml at baseline to Ees/Ea = 0.32 mmHg/ml at the greatest preload reduction.

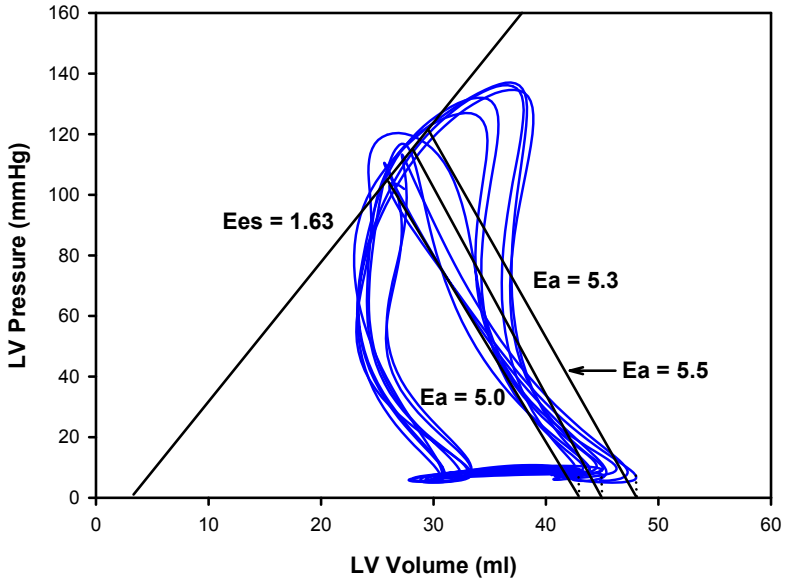

Figure 3-6 A family of PV-loops recorded during a preload reduction

Table 3-2 LV haemodynamic data for each PV-loop during a preload reduction

PV-loop Number	SW	CO	SV	ESP	EDP	EF	Ea	dp/dt max	dp/dt min
1	1530	3.3	20.9	121.6	10.1	56.5	5.3	2284	-1519
2	1283	3.3	20.5	118.5	9.4	59.9	5.8	2206	-1473
3	1149	3.4	21.1	115.8	8.7	62.7	5.5	2081	-1417
4	800	3.6	22.2	115.8	7.2	71.4	5.2	1809	-1270
5	810	3.4	21.4	113.4	6.4	64.6	5.3	1714	-1217
6	698	3.5	21.9	110.6	6.2	66.1	5.1	1644	-1196

SW = stroke work, mmHg.ml; CO = cardiac output, L; SV = stroke volume, ml; ESP = end-systolic pressure, mmHg; EDP = end-diastolic pressure, mmHg; EF = ejection fraction, %; Ea = Effective arterial Elastance, mmHg / ml; dP/dt max = maximum rate of isovolumic contraction, mmHg/s; dP/dt min = maximum rate of isovolumic relaxation, mmHg/s.

3.1.3.3 Afterload and the Pressure-Volume Relationship

Figure 3-7 shows the effect of an increase in afterload on LV function. Table 3-3 shows the beat-to-beat analysis starting at baseline (PV-loop = 1) and then sequentially as the PV-loop morphology adapted due to the increase in afterload (PV-loop = 10). This change in PV-loop morphology confirmed that Ea increased with increasing afterload. Since Ees was calculated from the preload reduction as 1.63 mmHg/ml, the ventriculoarterial coupling ratio reduced from Ees/Ea = 0.31 at baseline to Ees/Ea = 0.16 as the LV struggled to maintain ejection of blood against the increasing afterload. The reduction in SV and CO combined with the increases to SW, ESP, EDP, dP/dt max and dP/dt min, would indicate that the RV was struggling to maintain output with increasing afterload.

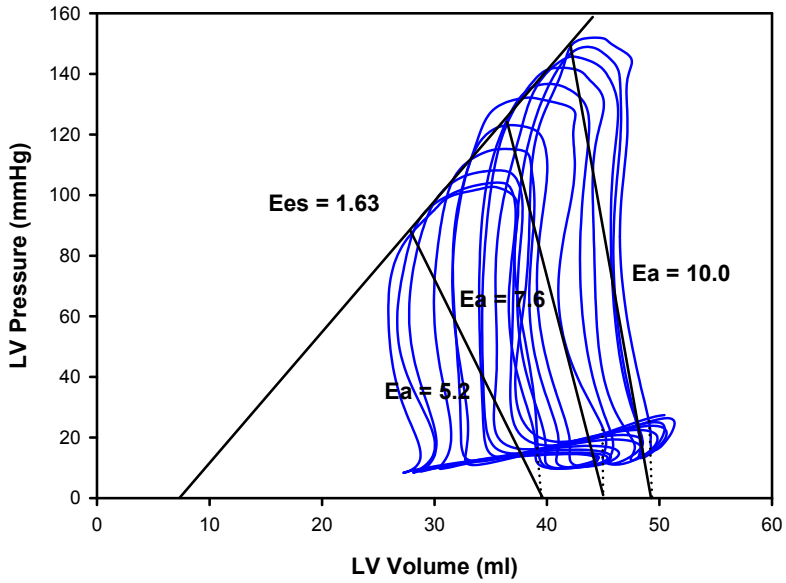

Figure 3-7 A family of PV-loops recorded during an increasing afterload

Table 3-3 LV haemodynamic data for each PV-loop during an afterload increase

PV-loop	SW	CO	SV	ESP	EDP	EF	Ea	dp/dt max	dp/dt min
1	936	3.0	18.6	98.3	9.9	49.7	5.3	1048	-844
2	809	3.0	18.7	95.9	9.9	51.2	5.1	1072	-857
3	833	2.9	18.0	102.9	10.0	48.0	5.7	1109	-900
4	813	2.6	16.5	109.9	10.2	42.8	6.7	1156	-975
5	777	2.7	16.9	119.7	10.5	43.2	7.1	1186	-1027
6	1113	2.7	16.9	128.1	11.1	41.2	7.6	1265	-1130
7	1027	2.5	15.9	133.8	11.5	36.9	8.4	1283	-1155
8	1153	2.6	16.4	139.3	12.7	37.0	8.5	1332	-1202
9	1216	2.4	15.2	141.5	13.2	33.1	9.3	1349	-1210
10	1083	2.3	14.6	146.5	14.7	31.7	10.0	1365	-1226

SW = stroke work, mmHg.ml; CO = cardiac output, L; SV = stroke volume, ml; ESP = end-systolic pressure, mmHg; EDP = end-diastolic pressure, mmHg; EF = ejection fraction, %; Ea = Effective arterial Elastance, mmHg / ml; dP/dt max = maximum rate of isovolumic contraction, mmHg/s; dP/dt min = maximum rate of isovolumic relaxation, mmHg/s.

3.1.3.4 Contractility and the Pressure-Volume Relationship

Figure 3-8 shows the effect of an increase in contractility on LV function. While Ea remained fairly constant after using the inotrope dopamine to increase contractility, after performing a further preload reduction the slope of the ESPVR determined that the load-independent marker of contractility, Ees had increased to 3.22 mmHg/ml. This change confirmed that increasing LV contractility increased Ees while Ea remained constant, causing a two-fold increase in the ventriculoarterial coupling ratio (0.31 to 0.64). The other indices of LV hemodynamic function are shown in Table 3-4.

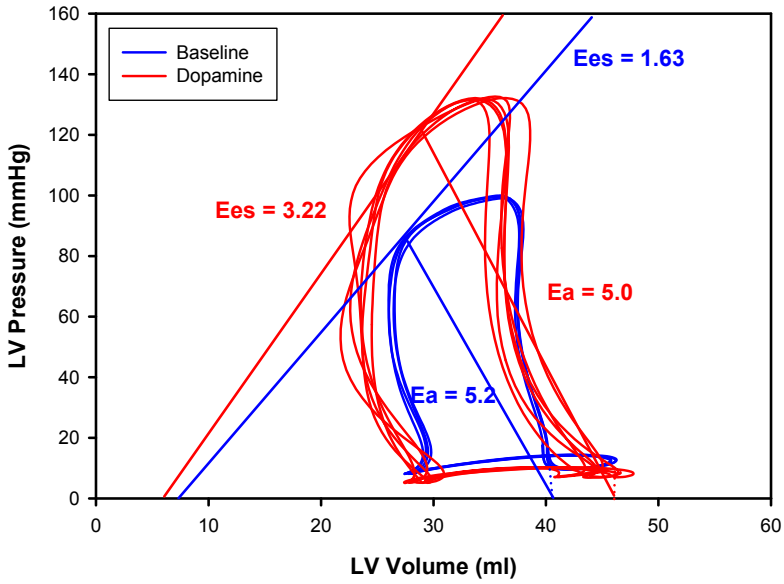

Figure 3-8 Steady-state LV PV-loops at baseline (Blue) and after 5 µg/kg/min dopamine (Red)

Table 3-4 LV haemodynamic data at baseline and after a dopamine Infusion to Increase contractility

	Baseline	Dopamine
CO, L	3.0	3.8
SV, ml	19.5	23.1
EF, %	45.0	64.0
ESV, ml	27.3	27.5
EDV, ml	40.0	44.5
ESP, mmHg	89.0	116.3
EDP, mmHg	9.8	9.4
dp/dt max, mmHg/s	1029	2173
dp/dt min, mmHg/s	-812	-1388

CO = cardiac output; SV = stroke volume; EF = ejection fraction; ESV = end-systolic volume; EDV = end-diastolic volume; ESP = end-systolic pressure; EDP = end-diastolic pressure; dP/dt max = maximum rate of isovolumic contraction; dP/dt min = maximum rate of isovolumic relaxation.

3.1.4 Discussion

This work has shown that the isolated LV working heart perfusion rig could be used to confirm Sunagawa's theory on the relationship between LV ventriculoarterial coupling and the PV-loop. Firstly, this work has confirmed that an acute reduction in preload could be used to determine the Ees, and this reduction in preload caused the leftwards shift of the EDV point on the PV-loop while Ea remained constant. Although the SV did not decrease as would be expected from Sunagawa's statement that "a decrease to the end-diastolic volume will cause the arterial ESPVR Ea to shift to the left. Hence, SV decreases" (Sunagawa et al., 1987); this work has confirmed that variations in preload have no effect on contractility (Ees) or afterload (Ea). Hence, the LV ventriculoarterial coupling ratio (Ees/Ea) remained constant.

Secondly, this work has confirmed that an acute increase in afterload caused the rightwards shift of ESV point on the PV-loop and increased Ea. Although it was not possible to prevent the LV from dilating and filling with blood, which subsequently prevented the EDV from remaining constant. These experimental findings support Sunagawa's statement that "increasing the arterial resistance increases the slope of the arterial ESPVR (Ea), hence the SV decreases as the intersection between the arterial and ventricular ESPVR moves to the right" (Sunagawa et al., 1987). Although the perceived increases in dP/dt max and dP/dt min suggest an immediate increase in contractility in response to the acute increases in afterload, this in fact just highlights the load-dependency of the measurement. The acute load variations used to determine Ees and the relationship between different RV hemodynamic parameters with Ees/Ea and Ea can be considered valid due to auto-regulation, termed the "Anrep Effect" - increasing afterload increases contractility and maintains CO, but it takes between 30 to 60 seconds for contractility to adapt in response to acute loading variations (von Anrep, 1912). Data were acquired during partial occlusions over approximately 10 seconds. Therefore, the perceived increases to dP/dt max and dP/dt min were due to the increase in ESP amplifying the measurement. Therefore, this work has confirmed

that while variations in afterload have no effect on contractility (Ees), Ea is increased; hence, the LV ventriculoarterial coupling ratio (Ees/Ea) reduces with increasing afterload.

Finally, this work has confirmed that an increase in contractility increases the slope of the Ees and increases the SV. These experimental findings support Sunagawa's statement that "An increase to the LV contractility will increase the slope of the ventricular ESPVR (Ees) while maintaining the same volume intercept V_0. Since the slope of the arterial ESPVR (Ea) remains constant, SV increases" (Sunagawa et al., 1987). Therefore, this work has confirmed that while variations in contractility have no effect on Ea, Ees is increased; hence, the LV ventriculoarterial coupling ratio (Ees/Ea) increases. These measurements have successfully replicated and validated Sunagawa's work on the relationship between the PV-loop and ventriculoarterial coupling in the LV.

3.2 An Ex-Vivo Model of Right Ventriculoarterial Interaction

3.2.1 Introduction

The aim of this section was to translate the working heart apparatus developed in Section 3.1 for the ex-vivo model of LV ventriculoarterial coupling and develop a RV working heart perfusion rig to model RV ventriculoarterial coupling.

3.2.2 Methods

This work was carried out at the Royal Veterinary College (Hatfield, London) under the Project Licence 70/7967 as previously described in Section 2.2.3. As previously described in Section 2.2.5, Dr Hatim Alibhai (Consultant Veterinary Anaesthetist) was responsible for the humane care of the animals and performed the anaesthetic preparation of the animals. Dr Simon Messer performed the surgical preparation.

3.2.2.1 RV Working Heart Perfusion Rig

3.2.2.1.1 Concept Design Requirements

The basic concept design requirements for an isolated RV working heart rig (Figure 3-9) are the same as those described for the isolated LV working heart rig in Section 3.1.2.1.1. However, the circuitry was designed so that the same pump can be used in a modified configuration to fill the heart via the right atrium and pump blood out through the pulmonary artery into the pulmonary afterload chamber and then drain into the blood reservoir, while maintaining perfusion of the coronary arteries. The monitoring device is now required to measure RA, PA and aortic flows and pressures.

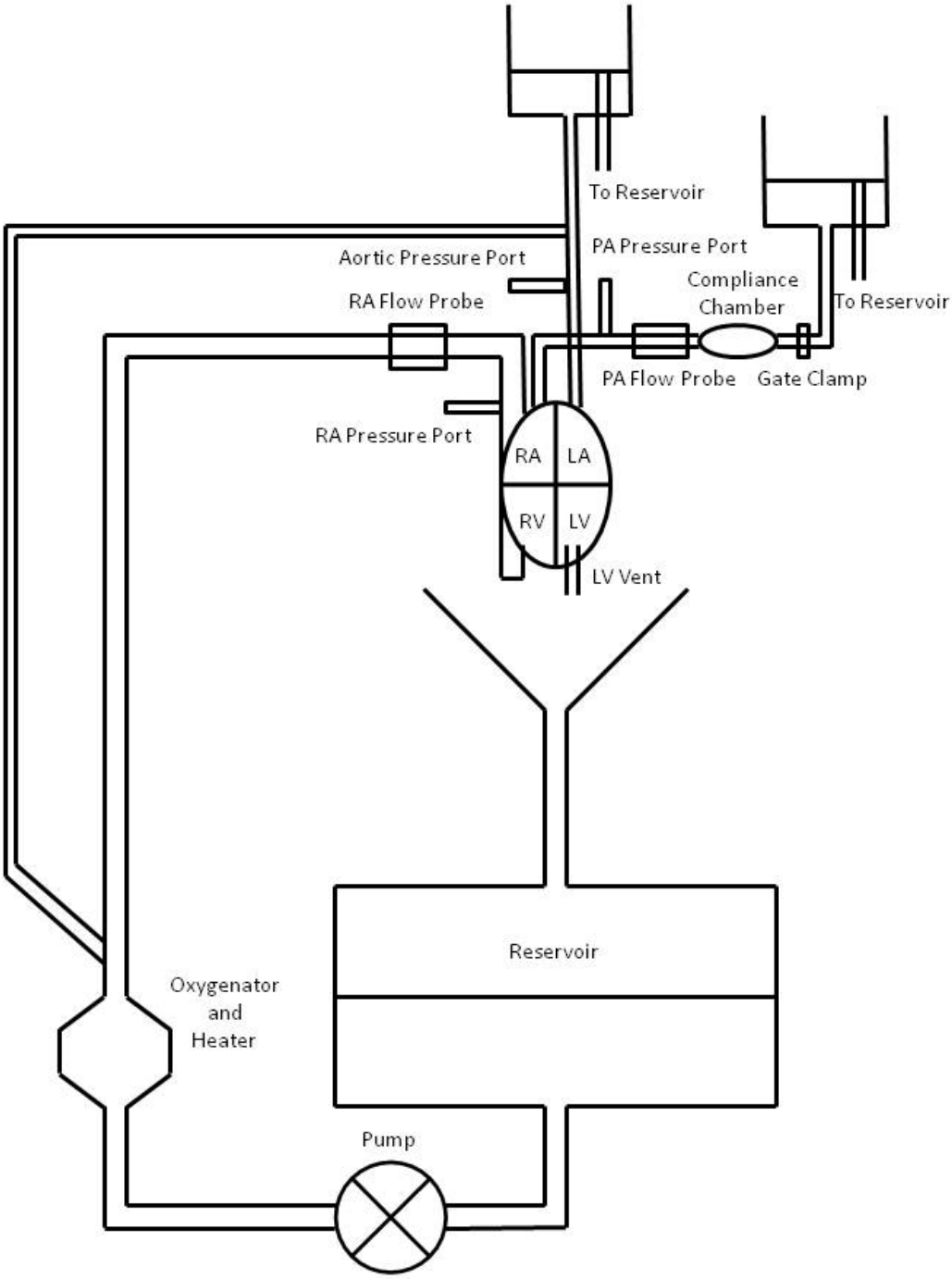

Figure 3-9 Schematic of the RV working heart perfusion rig

3.2.2.1.2 RV Working Heart Perfusion

The isolated RV working heart perfusion rig was manufactured in-house (Figure 3-10) from Perspex sheet, off-the-shelf oxygenators (QUADROX-i, Maquet, Rasstat, Germany), venous blood reservoirs (VHK 2000/2001, Maquet, Rasstat, Germany), silicon tubing and connectors, syringe pumps (Alaris CC CareFusion, San Diego, USA), water heaters (BioCal 370 BIOMEDICUS Cardiopulmonary Bypass Temperature Controller, Medtronic, Minneapolis, USA), centrifugal pumps (BPX-80 BIO-Medicus Pump Plus, Medtronic, Minneapolis, USA) and monitors (Datex Ohmeda S5, GE Healthcare, Buckinghamshire, UK). A cradle was made in-house using Perspex sheet to rest the isolated heart on and allow the perfused blood to drain into the reservoir.

The centrifugal pump was used to circulate the blood from the reservoir through the oxygenator and heat exchanger. This tube was then split into two, one to act as the flow controlled Langendorff and the second to act as the RA inflow port. A compliance chamber was put at the inflow to the aorta and the RA. A second afterload chamber was manufactured and would be connected to the PA so that the system could be put into an RV working heart mode, with an afterload of 20-mmHg and RA preload of 5-mmHg. The isolated heart can be perfused in Langendorff, and then modify the blood flow through the heart for an RV working mode perfusion that could be assessed with a conductance catheter. The syringe pump was used to deliver a 5μg/kg/min infusion of the inotrope Dopamine; this was used to improve the contractility of the stunned isolated heart.

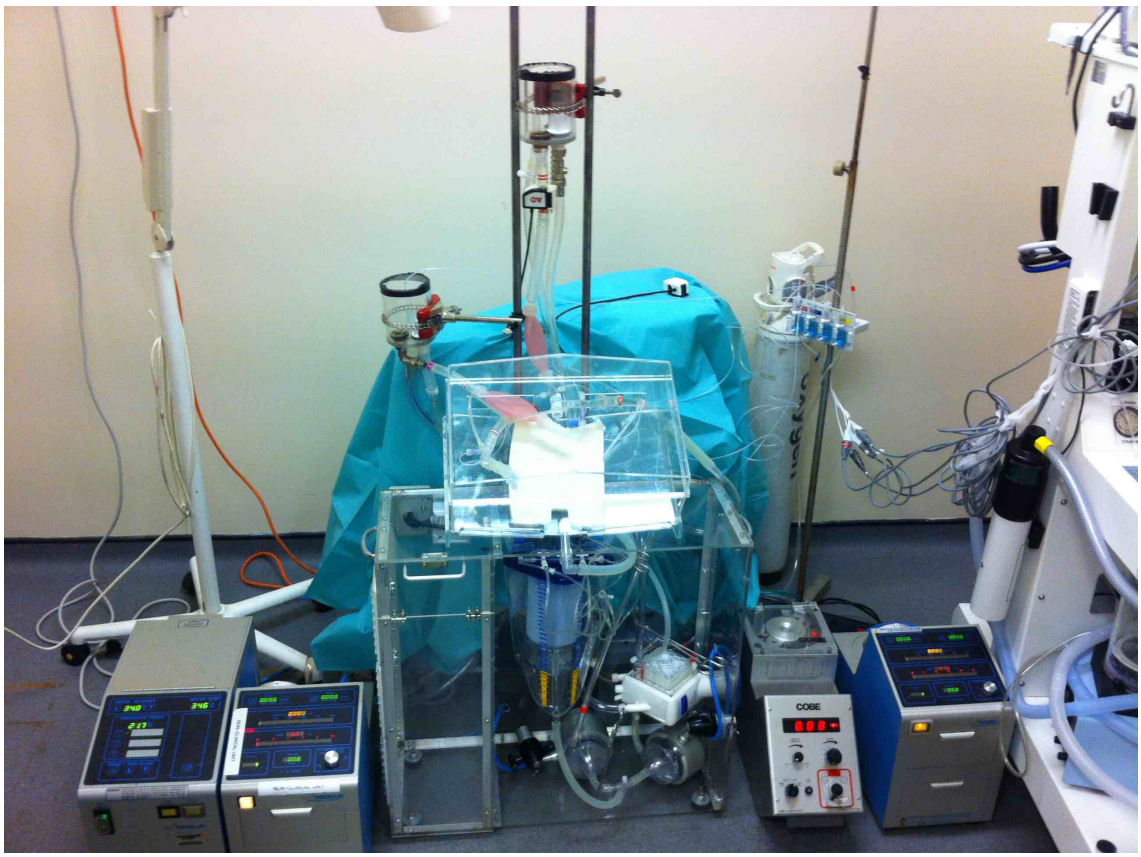

Figure 3-10 In-house isolated RV working heart perfusion rig

3.2.2.2 Surgical Preparation

The large white pig was surgically prepared as previously described in Section 3.1.2.2. However, a small incision into the wall at the apex of the RV and sewing a purse string around the opening allowed a Millar conductance catheter to now be securely located in the RV for functional assessment using the conductance catheter. A 7-F, 8 electrode conductance catheter (Millar Instruments, Houston, Texas, USA) was inserted through a puncher in the RV apex and placed along the long axis of the ventricle. PV-loop morphology was used to confirm the correct placement of the catheter within the RV.

3.2.2.3 Surgical Preparation of the Isolated Heart

The heart was surgically prepared as previously described in Section 3.1.2.3. However, the heart was instrumented in the in-house isolated RV working heart perfusion rig (Figure 3-11). A purse string was then sutured around the superior vena cava and the PA to secure the RA and PA cannulas respectively to allow the heart to be put into an isolated RV working heart perfusion.

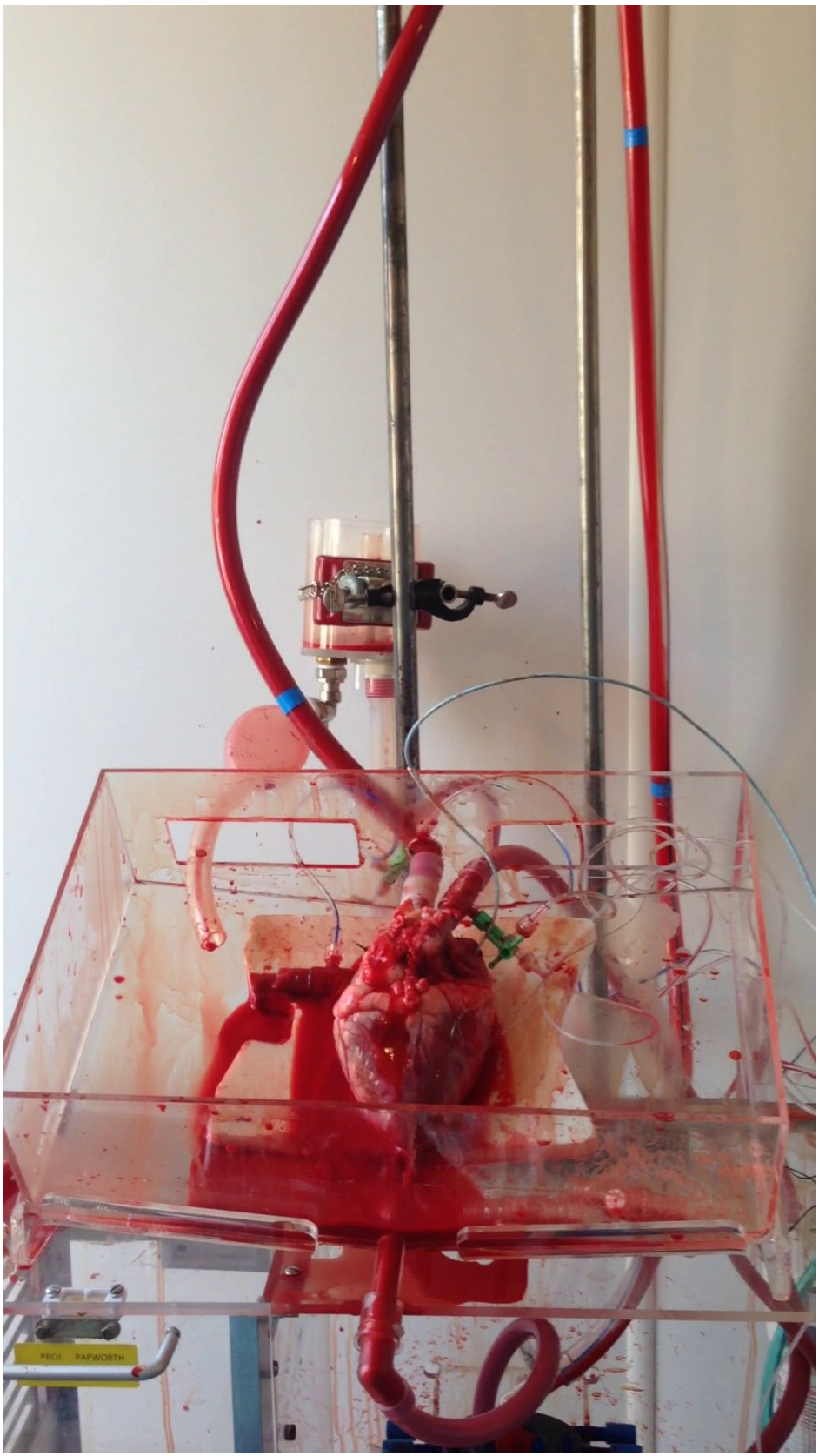

Figure 3-11 Porcine heart instrumented on the RV working heart rig in Langendorff perfusion

3.2.2.4 Functional Assessment of the Isolated RV Working Heart

Functional assessment was performed as described in Section 3.1.2.4. However, the conductance catheter was located in the RV for data collection. The right-sided heart was put into working mode with an afterload set by height to 20-mmHg and a left atrial filling pressure of 5-mmHg. The CO; mean, systolic and diastolic RA pressures; mean, systolic and diastolic PA pressures were recorded. A family of PV-loops were recorded while partially clamping the inflow to the RA to generate load-independent parameters of systolic and diastolic function during a preload reduction. This family of PV-loops was used to determine Ees. A second family of PV-loops were recorded while partially clamping the outflow to the PA to generate load-independent parameters of systolic and diastolic function during an afterload increase. This was performed to determine how the RV function adapted to changes in Ea (Figure 3-12).

A bolus of inotrope dopamine equivalent to a 20-minute infusion at 5 μg/kg/min was then given directly to the blood reservoir to increase contractility. This was perfused for 15 minutes before repeating the measurement protocol. This was performed to determine the effect of increasing Ees on RV function.

This controlled variation of Ea while keeping Ees and heart rate constant, and then the independent variation of Ees while keeping Ea and heart rate constant, would allow us to describe ventriculoarterial coupling (Ees/Ea) for an isolated RV working heart.

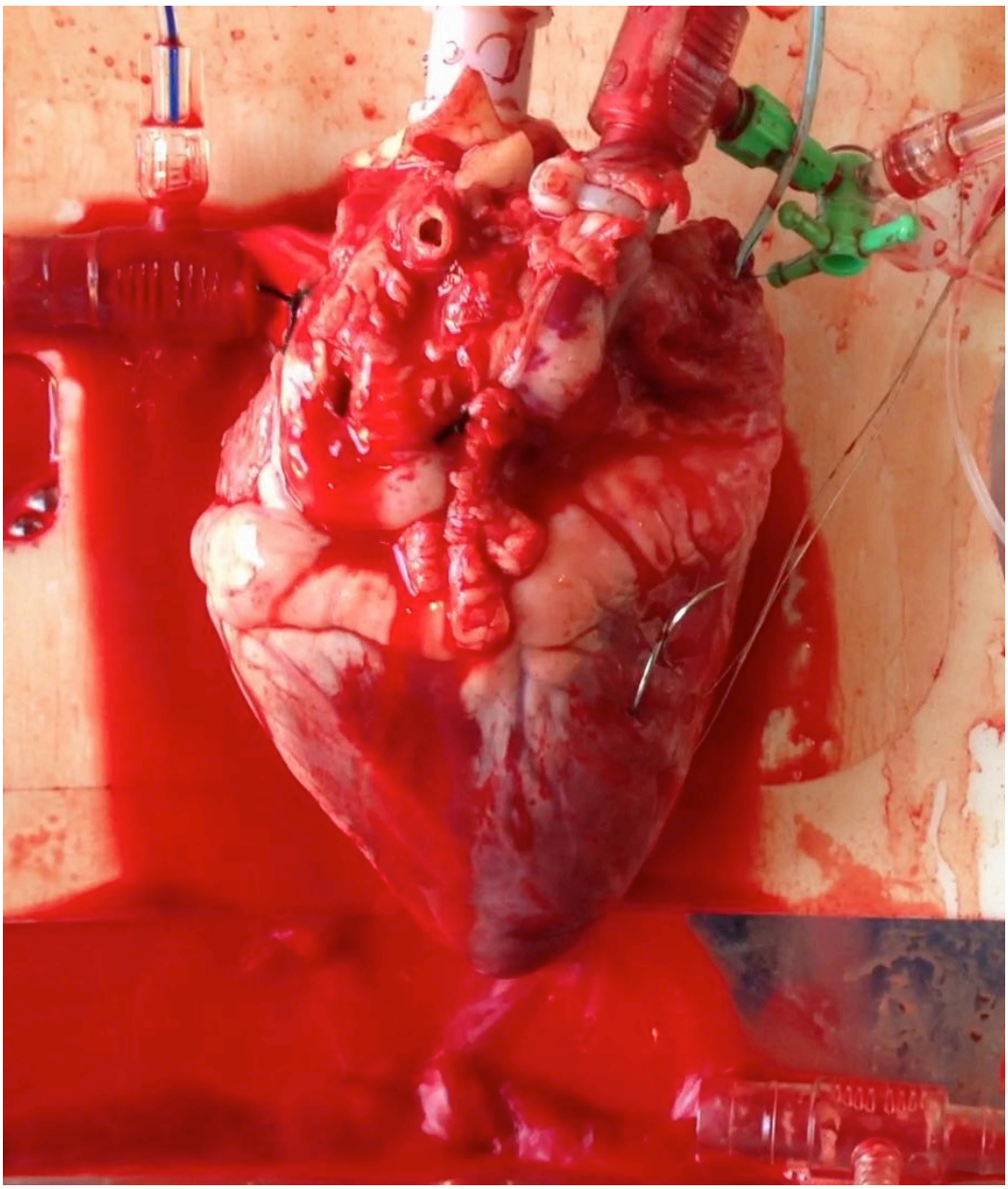

Figure 3-12 RV working heart mode with functional assessment with PV-loops

3.2.3 Results

3.2.3.1 Demographics

Demographic data is shown in Table 3-5. This demonstrated that this work was carried out on a porcine heart with normal baseline haemodynamics (CO and mPAP).

Table 3-5 Demographic data

	Pig (n=1)
Demographics	
Weight, kg	89.5
Height, cm	139.0
Baseline Haemodynamics	
Heart Rate, BPM	100
MAP, mmHg	86.0
MPAP, mmHg	15.0
Mixed Venous Sats,%	53.3
CO, L	7.1
CI,	4.1

MAP = mean aortic pressure; MPAP = mean pulmonary arterial pressure; CO = Cardiac Output; CI = Cardiac Index.

3.2.3.2 RV Functional Assessment

After modifying the rig into an RV working heart mode, the isolated heart did not have the contractile function to eject blood against the 20-mmHg PA afterload chamber. After altering the height of the afterload chamber to reduce the pressure the RV had to pump against, it soon became apparent that the heart would not be able to eject blood without greater contractile support. Increasing the inotropic support to an infusion of 10 µg/kg/min allowed the heart to ejected against the 20-mmHg afterload (Table 3-6). However, the PV-loop morphology was physiologically abnormal and suggested a high degree of pulmonary regurgitation (Figure 3-13). Therefore, it was not possible to test if the theory described Sunagawa for LV ventriculoarterial coupling could be translated to the RV-PA using this ex-vivo working heart perfusion rig.

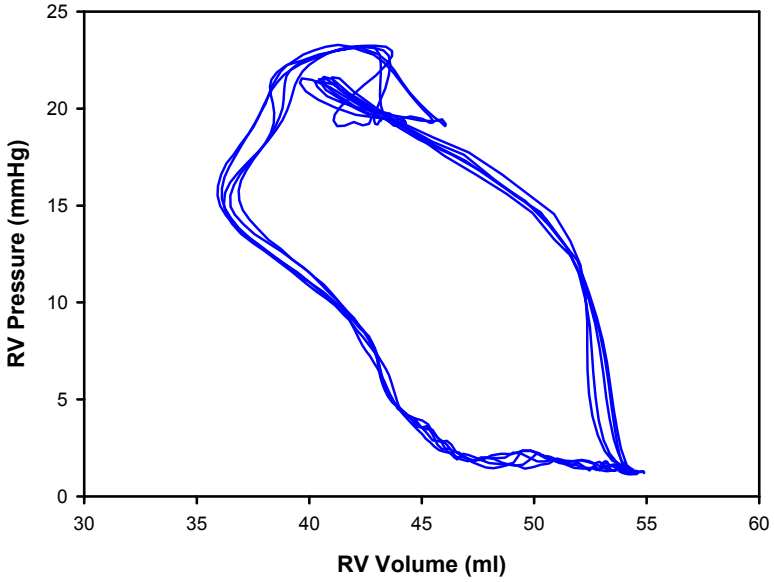

Figure 3-13 Steady-state RV PV-loops at during a 10 µg/kg/min dopamine infusion

Table 3-6 RV PV-loop data

	10µg/kg/min Dopamine
CO, L	2.2
SV, ml	18
EF, %	35.0
ESV, ml	39.8
EDV, ml	54.1
ESP, mmHg	22.5
EDP, mmHg	1.4
dp/dt max, mmHg/s	603
dp/dt min, mmHg/s	-229

CO = cardiac output; SV = stroke volume; EF = ejection fraction; ESV = end-systolic volume; EDV = end-diastolic volume; ESP = end-systolic pressure; EDP = end-diastolic pressure; dP/dt max = maximum rate of isovolumic contraction; dP/dt min = maximum rate of isovolumic relaxation.

3.2.4 Discussion

This work has shown that the isolated RV working heart perfusion rig could not be used to translate Sunagawa's theory on the relationship between LV ventriculoarterial coupling and the PV-loop to the RV. Although with increased inotropic support it was possible to get the isolated RV to eject blood against the PA afterload chamber, the PV-loop morphology would indicate that as the pressure was increased within the RV during systole, there was significant pulmonary regurgitation. It is now understood that there was a fundamental flaw with the design of our RV working heart perfusion rig. The basic RV physiology described in Chapter 1 established the normal RV to be a complex geometrical shape (Dell'Italia, 1991). The higher systemic pressures in the LV (Zipes and Braunwald, 2005) mean the inter-ventricular septum remains concave towards the RV throughout the cardiac cycle (Dell'Italia, 1991). Tethering between the RV and LV muscle fibres through the septum cause ventricular interdependence phenomena (Dell'Italia, 1991; Brookes et al., 1998); which means the size, shape and compliance of one ventricle can directly affect the size, shape and haemodynamic function of the contralateral ventricle (Santamore and Dell'Italia, 1998a). Since the muscle fibres of the RV free-wall predominantly shorten in the long axis during systole, it is the LV oblique orientation of the septal muscle fibres that generates the septal twist and shortening during a contraction that accounts for the majority of the RV ejection force during systole.

The perfusion rig isolated the RV to put the heart into a right-sided working heart mode. Although this model works well for the isolated heart in an LV working heart mode, with our work described earlier in this Chapter validating the results of Sunagawa et al. (1987). LV ejection is provided by the oblique contraction of the LV muscle fibres. Therefore, an isolated LV working heart model remains physiologically appropriate with an empty RV. However, the same cannot be said for an isolated RV working heart model when the LV remains unfilled. The septum will only remain concave to the RV when the pressure within the LV is greater. Since the LV does not fill with blood in an

isolated RV working heart perfusion rig, the system now becomes non-physiological as the pressure within the LV becomes less than the pressure in the RV. Consequently, this causes the increasing pressure within the RV to dilate the ventricle, overfilling it with blood, so that the septum now becomes concave to the LV wall. Outwith the abnormal RV geometry, this has a knock-on effect to the RV ejection force during systole. Since the LV wall is now contracting against an empty ventricular chamber, it is not able to transmit any ejection force across the septum to the RV. Therefore, the RV is relying on the peristaltic movement of the RV wall to eject blood. This abnormal physiology to the RV PV-loop means the RV working heart perfusion rig is not suitable for evaluating a model of RV-PA ventriculoarterial coupling.

While biventricular working heart perfusion rigs are possible to manufacture, two separate sub-circulations are required to independently pump the blood through the left and right sides of the heart. This necessitates the use of two centrifugal perfusion pumps. While this seems relatively straightforward to create, ventricular interdependence phenomena mean it is virtually impossible to manually control and maintain the flows and pressures in both the LV and RV without causing pressure or volume overload to one or both sides of the heart. After attempting to use a biventricular working mode perfusion rig, the LV could be switched from a Langendorff perfusion to an LV working heart with constant pressures and flows maintained. However, when the second pump was used to put the RV into a working heart mode, as the RV filled with blood, ventricular interdependence cause the pressures and flows to alter within the LV. It was not possible to manually control the pump flows through both the left and right sides of the heart, without causing significant problems to the contralateral ventricle. Although a group in Canada have reported the use of biventricular porcine working heart models, they used a computer-controlled closed-loop algorithm to simultaneously control the pump flows to maintain the desired constant preload and afterload pressures on both sides of the heart (Colah et al., 2012). While this should have been able to work to allow the assessment of RV

ventriculoarterial coupling, on a working heart perfusion rig that provided a physiologically normal RV PV-loop. The complexities of designing the closed-loop control algorithm software and hardware modifications that would need to be made to the centrifugal pumps to allow them to be controlled by the software were not feasible to develop during these studies.

3.3 An In-Vivo Model of Right Ventriculoarterial Interaction

3.3.1 Introduction

The aim of this section was to describe the development of an in-vivo model of RV ventriculoarterial coupling that would be used in Chapter 4 to define the optimal ventriculoarterial coupling ratio of the porcine RV-PA. After establishing that it was not possible to develop an isolated right-sided working heart perfusion rig that can provide physiological normal RV function; with the development of a closed-loop computer controlled biventricular perfusion right that could provide physiological normal RV function being the resources of this PhD; the decision was made to investigate the possibility of performing this assessment of RV ventriculoarterial coupling in-vivo, in a surgically prepared open-chested porcine model.

An anaesthetised surgically prepared open-chested porcine heart should provide a model that has physiologically normal RV function. Although the pericardial constraint has to be removed, this is no different to the isolated working heart perfusion rig model, where the heart is suspended in a chamber to collect the ejected blood and return it to the blood reservoir. The main advantage of utilising an in-vivo model is that both the LV and RV remain physiologically normal, in a normal circulatory system. Therefore, ventricular interdependence phenomena allow the LV to support and maintain RV contraction. By using surgical silk ties to loop around the IVC and PA, these loops can be snared to partially occlude the IVC and PA causing a preload reduction and afterload increase respectively. Therefore, families of PV-loops could be recorded, and the relationship between the RV-PA ventriculoarterial coupling could be explored in an RV system that had a functional LV.

3.3.2 Methods

This work was carried out at the Royal Veterinary College (Hatfield, London) under the Project Licence 70/7967 as previously described in Section 2.2.3. As previously described in Section 2.2.5, Dr Hatim Alibhai (Consultant Veterinary Anaesthetist) was

responsible for the humane care of the animals and performed the anaesthetic preparation of the animals. Dr Simon Messer performed the surgical preparation.

3.3.2.1 Surgical Preparation

The large white pigs were surgically prepared as previously described in Section 3.1.2.2. However, a small incision into the wall at the apex of the RV and sewing a purse string around the opening allowed a Millar conductance catheter to now be securely located in the RV for functional assessment using the conductance catheter. A 7-F, 8 electrode conductance catheter (Millar Instruments, Houston, Texas, USA) was inserted through a puncher in the RV apex and placed along the long axis of the ventricle. PV-loop morphology was used to confirm the correct placement of the catheter within the RV.

3.3.2.2 RV Functional Assessment of the Open-Chested Porcine Heart

After surgically preparing the open-chested porcine heart (Figure 3-14A) the Millar MPVS Ultra, ADInstruments PowerLab hardware and ADInstruments LabChart software was set up and calibrated as described in Chapter 2. The conductance catheter was positioned in the RV for data collection. Five steady-state PV-loops were recorded to generate load-dependant parameters of the systolic and diastolic function. Two families of PV-loops were recorded during ventilation suspension. A snare was looped around the inferior vena cava (IVC) and partially occluded to record a family of PV-loops during a preload reduction. This family of PV-loops was used to determine Ees. A separate snare was looped around the PA and partially occluded over a 10 to 15 second period so that multiple data points could be recorded to determine how RV hemodynamic parameters varied with acute changes in PA afterload (Figure 3-14B). This was used to determine how the RV function adapted to changes in Ea.

A 20-minute infusion of dopamine at 5 μg/kg/min was then given directly in a central intravenous line to increase contractility. The measurement protocol was repeated. This was performed to determine the effect of increasing Ees on RV function.

This controlled variation of Ea while keeping Ees and heart rate constant, and then the independent variation of Ees while keeping Ea and heart rate constant, would allow us to describe ventriculoarterial coupling (Ees/Ea) for the RV - PA.

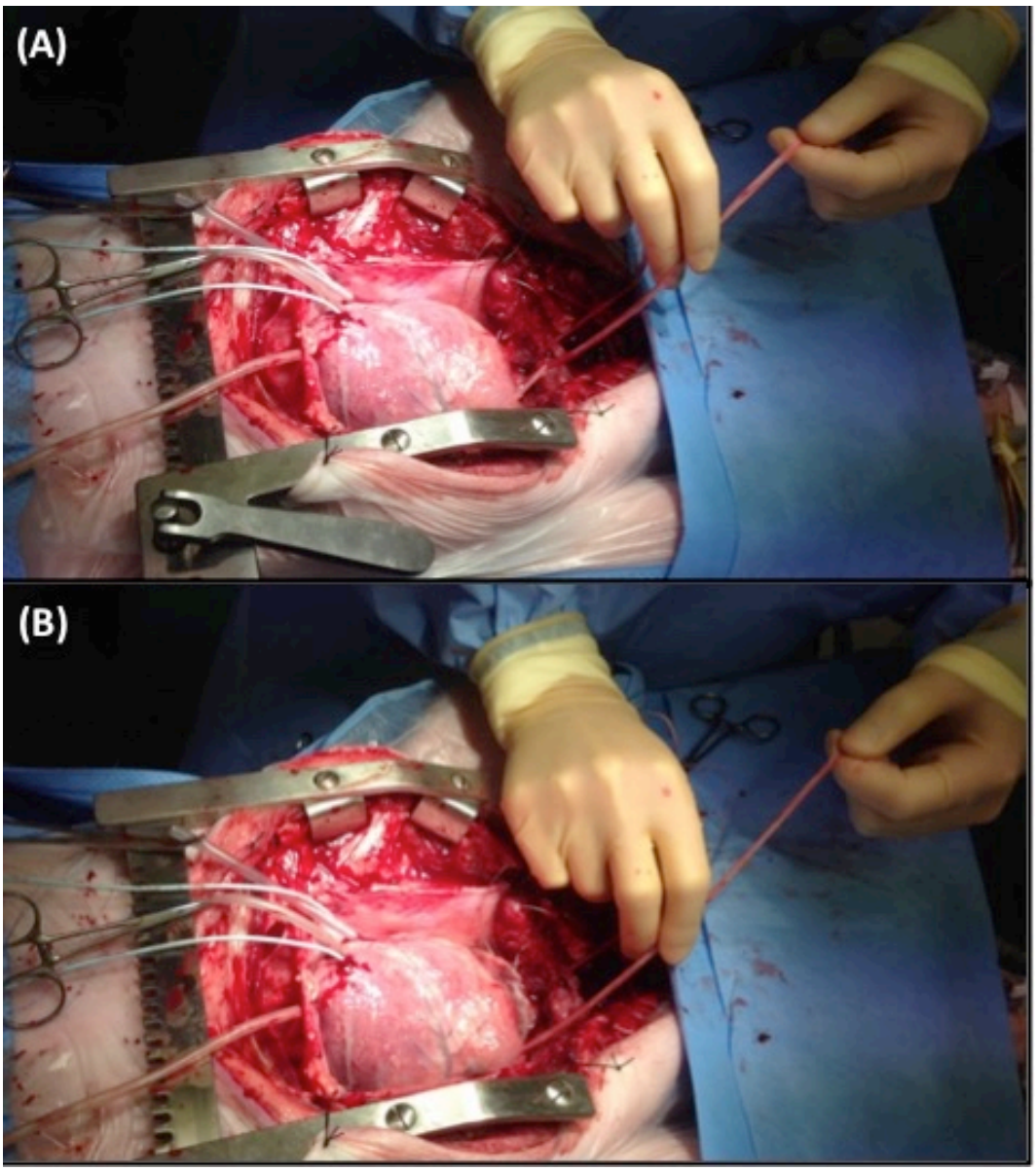

Figure 3-14 In-vivo open-chested porcine heart instrumented with the conductance catheter (A) with PA snare released (b) with PA snare partially occluded to increase the afterload on the RV

3.3.3 Results

3.3.3.1 Demographics

Two pigs were studied and the demographic data is shown in Table 3-7. A typical steady-state RV PV-loop is shown in Figure 3-15. The graphical pressure-volume relationship was described for pig 1 (Contractility) and pig 2 (Preload and Afterload).

Table 3-7 In-vivo porcine demographic data

	Pig 1	Pig 2
Demographics		
Weight, kg	89.5	80
Height, cm	135	118
Heart Rate, BPM	100	102
MAP, mmHg	86	95
MPAP, mmHg	15	17
Mixed Venous Sats, %	55.3	73.1
CO, L	7.1	6.6
CI,	4.1	4.5

Values are mean ± S.D. or n (%)

MAP = mean aortic pressure; MPAP = mean pulmonary arterial pressure; CO = Cardiac Output; CI = Cardiac Index.

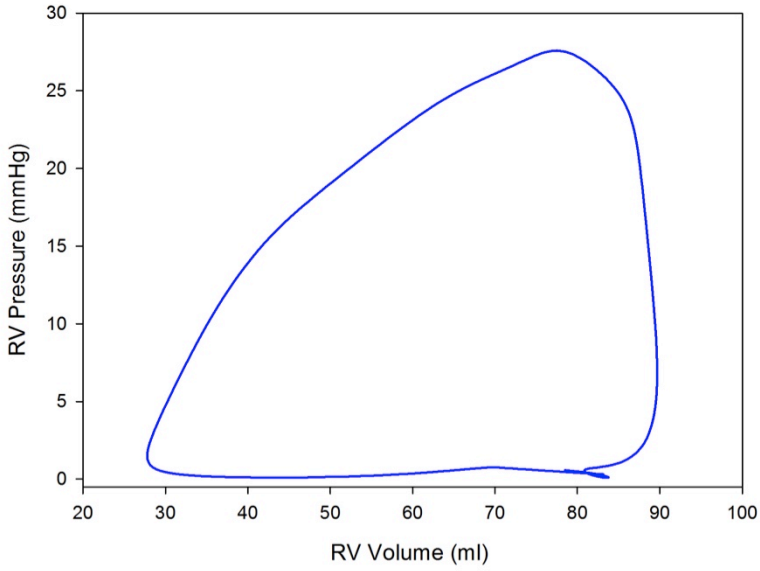

Figure 3-15 In-vivo porcine steady-state RV PV-loop

3.3.3.2 Preload and the Pressure-Volume Relationship

Figure 3-16 shows the effect of a preload reduction on RV function. The slope of the ESPVR determined that the load-independent marker of contractility, Ees = 0.31 mmHg/ml. Table 3-8 shows the beat-to-beat analysis starting at baseline (PV-loop = 1) and then sequentially as the PV-loop morphology adapted due to the preload reduction (PV-loop = 13). This demonstrated that there was a gradual reduction in SW, CO, SV, ESP, EDP, dP/dt max and dP/dt min with decreasing preload. However, Ea remained fairly constant. Therefore, the ventriculoarterial coupling ratio remained fairly constant increasing from Ees/Ea = 0.89 mmHg/ml at baseline to Ees/Ea = 1.03 mmHg/ml at the greatest preload reduction.

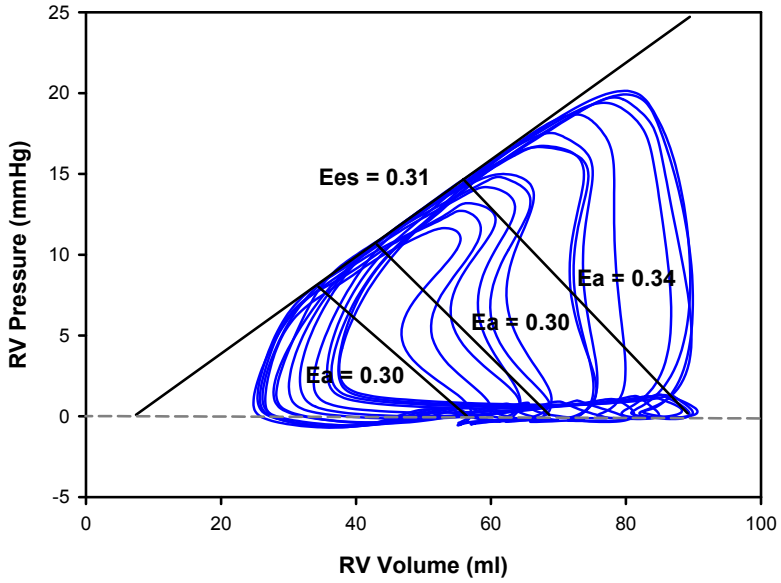

Figure 3-16 A family of PV-loops recorded during an IVC snare

Table 3-8 RV haemodynamic data for each PV-loop during an IVC snare

PV-loop	SW	CO	SV	ESP	EDP	EF	Ea	dp/dt max	dp/dt min
1	711	5.3	52.4	18.3	0.4	58.6	0.35	261	-167
2	716	5.3	52.5	18.0	0.5	58.5	0.34	249	-167
3	708	5.4	53.3	18.3	0.4	60.3	0.34	253	-164
4	686	5.1	51.0	16.8	0.4	59.3	0.33	240	-162
5	592	4.8	47.5	17.7	0.2	60.3	0.37	236	-164
6	543	4.8	48.1	15.8	0.0	65.2	0.33	218	-154
7	535	4.8	47.1	13.9	-0.2	65.2	0.30	207	-147
8	546	4.8	47.9	14.1	-0.1	66.7	0.29	210	-144
9	382	4.2	41.8	11.4	-0.3	69.7	0.27	187	-136
10	428	4.3	42.8	13.0	-0.2	68.6	0.30	183	-132
11	367	4.1	40.8	11.8	-0.3	70.2	0.29	170	-125
12	319	3.9	39.5	10.2	-0.2	73.0	0.26	162	-118
13	270	3.6	35.7	10.8	-0.5	68.5	0.30	154	-115

SW = stroke work, mmHg.ml; CO = cardiac output, L; SV = stroke volume, ml; ESP = end-systolic pressure, mmHg; EDP = end-diastolic pressure, mmHg; EF = ejection fraction, %; Ea = Effective arterial Elastance, mmHg / ml; dP/dt max = maximum rate of isovolumic contraction, mmHg/s; dP/dt min = maximum rate of isovolumic relaxation, mmHg/s.

3.3.3.3 Afterload and the Pressure-Volume Relationship

Figure 3-17 shows the effect of an increase in afterload on RV function. Table 3-9 shows the beat-to-beat analysis starting at baseline (PV-loop = 1) and then sequentially as the PV-loop morphology adapted due to the increase in afterload (PV-loop = 11). This confirmed that Ea increased with increasing afterload. Since Ees was calculated from the preload reduction as 0.31 mmHg/ml, the ventriculoarterial coupling ratio reduced from Ees/Ea = 0.92 at baseline to Ees/Ea = 0.24 as the RV struggled to maintain ejection of blood against the increasing afterload. The reduction in SW, SV and CO combined with the increases to ESP, dP/dt max and dP/dt min, would indicate that the RV was struggling to maintain sufficient output with increasing afterload.

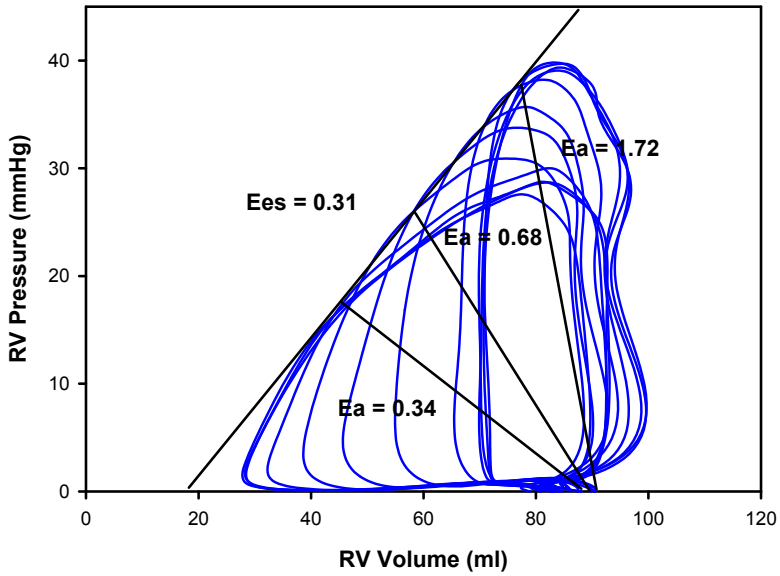

Figure 3-17 A family of PV-loops recorded during an PA snare

Table 3-9 RV haemodynamic data for each PV-loop during an PA snare

PV-loop	SW	CO	SV	ESP	EDP	EF	Ea	dp/dt max	dp/dt min
1	1292	6.5	64.6	21.8	1.0	69.5	0.34	375	-253
2	1192	6.3	61.9	22.9	0.9	69.7	0.37	366	-253
3	1308	6.5	64.5	24.8	1.1	69.7	0.38	379	-260
4	1296	6.0	60.4	24.5	1.1	65.5	0.41	377	-284
5	1158	5.0	49.9	26.4	0.8	57.0	0.53	366	-323
6	1114	4.5	44.5	30.3	0.8	50.2	0.68	359	-354
7	1018	3.8	37.8	33.4	0.9	41.9	0.88	348	-360
8	862	2.9	29.1	36.7	0.6	31.1	1.26	336	-376
9	799	2.6	25.7	38.9	1.2	27.2	1.52	354	-370
10	860	2.8	28.0	38.0	1.1	28.8	1.36	347	-366
11	897	3.0	29.8	37.9	1.2	30.6	1.27	346	-361

SW = stroke work, mmHg.ml; CO = cardiac output, L; SV = stroke volume, ml; ESP = end-systolic pressure, mmHg; EDP = end-diastolic pressure, mmHg; EF = ejection fraction, %; Ea = Effective arterial Elastance, mmHg / ml; dP/dt max = maximum rate of isovolumic contraction, mmHg/s; dP/dt min = maximum rate of isovolumic relaxation, mmHg/s.

3.3.3.4 Contractility and the Pressure-Volume Relationship

Figure 3-18 shows the effect of an increase in contractility on RV function. Ea remained relatively constant after using the inotrope dopamine to increase contractility. However, after performing a further preload reduction, the slope of the ESPVR determined that the load-independent marker of contractility Ees had increased to 0.34 mmHg/ml. This confirmed that increasing RV contractility increased Ees while Ea remained constant, causing an increase in the ventriculoarterial coupling ratio (1.00 to 1.26). The other indices of RV hemodynamic function are shown in Table 3-10.

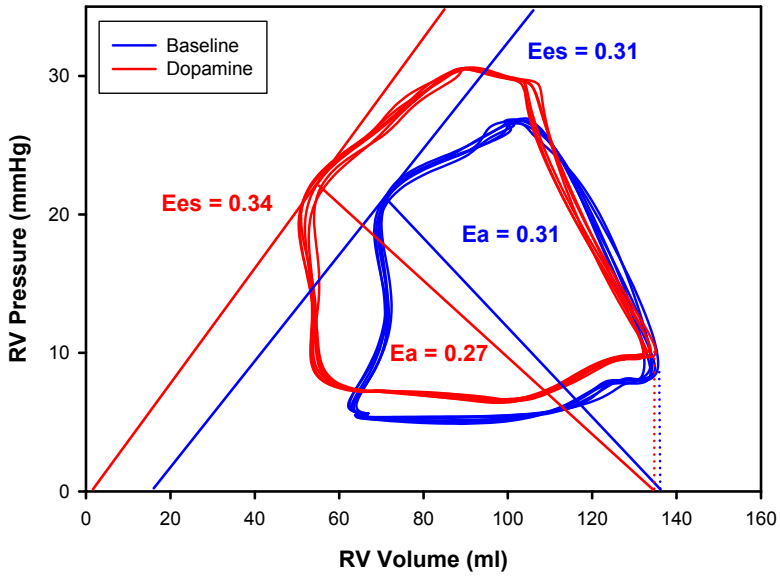

Figure 3-18 Steady-state RV PV-loops at baseline (Blue) and after 5 µg/kg /min dopamine (Red)

Table 3-10 RV PV-loop data

	Baseline	Dopamine (5ug/kg/min)
CO, L	7.1	8.4
SW, mmHg.ml	1047	1350
SV, ml	70.8	81.9
HR, BPM	100.2	100.9
EF, %	56.4	70.1
ESV, ml	73.2	55.1
EDV, ml	128.8	132.9
ESP, mmHg	21.9	22.3
EDP, mmHg	8.0	9.8
dp/dt max, mmHg/s	278	366
dp/dt min, mmHg/s	-228	-194

CO = cardiac output; SW = stroke work; SV = stroke volume; EF = ejection fraction; HR = Heart Rate; ESV = end-systolic volume; EDV = end-diastolic volume; ESP = end-systolic pressure; EDP = end-diastolic pressure; dP/dt max = maximum rate of isovolumic contraction; dP/dt min = maximum rate of isovolumic relaxation.

3.3.4 Discussion

This work has shown that a surgically anesthetised open-chested porcine heart could be used to translate Sunagawa's theory on the relationship between LV ventriculoarterial coupling and the PV-loop to the RV and PA. Firstly, this work has confirmed that an acute reduction in preload could be used to determine the Ees, and this reduction in preload caused the leftwards shift of the EDV point on the PV-loop; reducing SV while Ea remained constant. This validated Sunagawa's statement that "a decrease to the end-diastolic volume will cause the arterial ESPVR Ea to shift to the left. Hence, SV decreases" (Sunagawa et al., 1987) could be directly translated into the RV; this work has confirmed that variations in preload have no effect on contractility (Ees) or afterload (Ea). Hence, the RV ventriculoarterial coupling ratio (Ees/Ea) remained constant.

Secondly, this work has confirmed that an acute increase in afterload caused the rightwards shift of ESV point on the PV-loop, while EDV remained constant and increased Ea. This validated Sunagawa's statement that "increasing the arterial resistance increases the slope of the arterial ESPVR (Ea). Hence the SV decreases as the intersection between the arterial and ventricular ESPVR moves to the right" (Sunagawa et al., 1987) could be directly translated into the RV. Therefore, this work has confirmed that while variations in afterload have no effect on contractility (Ees), Ea is increased; hence, the RV ventriculoarterial coupling ratio (Ees/Ea) reduces with increasing afterload.

Finally, this work has confirmed that an increase in contractility increases the slope of the Ees and increases the SV. These experimental findings support Sunagawa's statement that "An increase to the LV contractility will increase the slope of the ventricular ESPVR (Ees) while maintaining the same volume intercept V_0. Since the slope of the arterial ESPVR (Ea) remains constant, SV increases" (Sunagawa et al., 1987) could be directly translated into the RV. Therefore, this work has confirmed that

while variations in contractility have no effect on Ea, Ees is increased; hence, the RV ventriculoarterial coupling ratio (Ees/Ea) increases. These measurements have successfully translated Sunagawa's work on the relationship between the PV-loop and ventriculoarterial coupling in the LV to the RV and PA.

Some limitations of our study must be recognized. Firstly, the open-chested porcine model of RV-PA ventriculoarterial interaction has an open pericardium that reduces RV contractility. However, this remains the best physiological model of assessing the response of normal RV function to changes in afterload, as LV-RV interdependence is retained and others have used this model (Nicolosi et al., 1996; Kuehne et al., 2003; Missant et al., 2007; Ghuysen et al., 2008; Guihaire et al., 2015). Second, the acute load variations used to determine Ees and the relationship between different RV hemodynamic parameters with Ees/Ea and Ea can be considered valid due to auto-regulation, termed the "Anrep Effect"; increasing afterload increases contractility and maintains CO, but it takes between 30 to 60 seconds for contractility to adapt in response to acute loading variations (von Anrep, 1912). Data were acquired for an adequate duration to detect these changes within the animal model. Thirdly, while the conductance catheter is designed for orientation along the long-axis of the ventricle with the pigtail positioned in the apex of the heart, many researchers have presented work with the conductance catheter inserted through the LV and RV apex (Chaturvedi et al., 1998; Messer et al., 2016).

3.4 Summary

The purpose of this chapter was to describe the development of an in-vivo model of RV ventriculoarterial coupling that could be used in Chapter 4 to define the optimal ventriculoarterial coupling ratio of the porcine RV-PA. Firstly, this chapter demonstrated that it was possible to develop an LV working heart apparatus to validate ex-vivo model of LV ventriculoarterial coupling and the Pressure-Volume relationship described by Sunagawa et al. (1987). Secondly, this chapter described the translation of this work into an ex-vivo model of RV ventriculoarterial coupling and the Pressure-Volume relationship. Due to complexities in RV physiology and limitations with the RV working heart apparatus it was not possible to develop a physiologically accurate ex-vivo model of RV ventriculoarterial coupling. Specifically, the absence of a functional LV in the isolated RV working heart perfusion rig impaired RV function to the extent that it was not possible to replicate Sunagawa's work for the RV. Finally, this chapter demonstrated it was possible to replicate Sunagawa's work in an in-vivo RV model. This in-vivo porcine model appeared suitable to further study RV – PA ventriculoarterial coupling that was most efficient… i.e. to determine the optimal relationship between the RV and PA. The in-vivo model will now be used in Chapter 4 to define the optimal ventriculoarterial coupling ratio of the porcine RV-PA.

4 The Determination of Maximal Efficiency and SW from an In-Vivo Porcine Model of Right Ventriculoarterial Coupling

4.1 Introduction

The in-vivo porcine model of RV ventriculoarterial interaction developed in Chapter 3 was used to determine the maximal efficiency and maximal SW, and define the optimal ventriculoarterial coupling ratio of the porcine RV – PA.

4.2 Methods

Eighteen open-chested large white pigs with a median weight of 77 kg (range 67 to 92) were studied. This work was carried out at the Royal Veterinary College (Hatfield, London) under the Project Licence 70/7967 as previously described in Section 2.2.3. As previously described in Section 2.2.5, Dr Hatim Alibhai (Consultant Veterinary Anaesthetist) was responsible for the humane care of the animals and performed the anaesthetic preparation of the animals. Dr Simon Messer performed the surgical preparation.

4.2.1 Surgical Preparation

The large white pigs were surgically prepared as previously described in Section 3.3.2.1.

4.2.2 RV Functional Assessment of the Open-Chested Porcine Heart

The RV functional assessment in the open-chested porcine heart was performed as previously described in Section 3.3.2.2. The beat-to-beat PV-loop data recorded during the PA snare were used to determine parameters of RV hemodynamic function at maximal SW (Figure 4-1), maximal efficiency (SW/PVA) and at maximal PA occlusion. This data was then pooled from each of the 18 subjects to give 324 data points. Regression lines with 95% prediction intervals were fitted to the data to determine how different parameters of RV hemodynamic function varied with the afterload loading condition (Ea) and ventriculoarterial coupling (Ees/Ea).

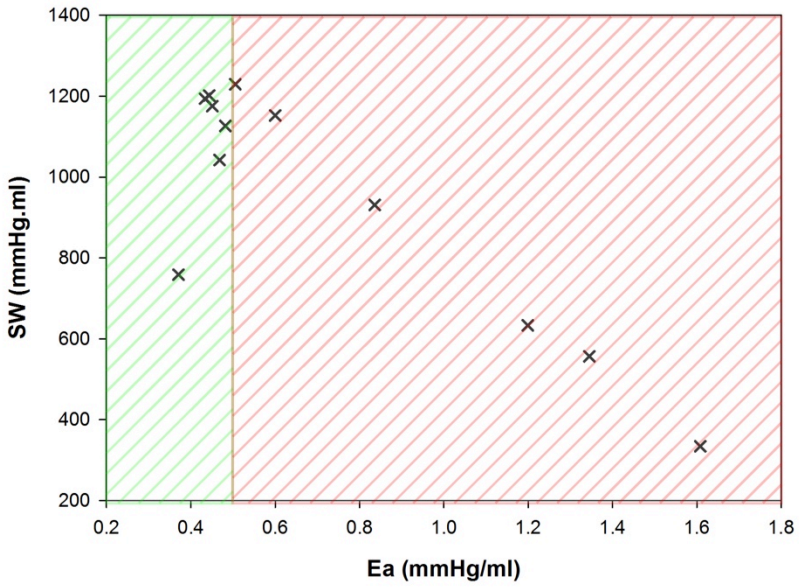

Figure 4-1 SW-Ea RV PV-loop relationship recorded during the PA snare in a single subject. RV energetic reserve is highlighted in the green-hatched box (Ea ≤ 0.5); RV failure is highlighted in the red-hatched box (Ea < 0.5).

4.2.3 Statistical Analysis

Statistical significance was determined as described in Section 2.2.2.

4.3 Results

4.3.1 Demographics

The demographic data is shown in Table 4-1. At baseline, none of the pigs had pulmonary hypertension or evidence of RV dysfunction. A typical steady-state RV PV-loop was previously shown in Figure 3-15. The data was used to determine maximal RV efficiency from the SW/PVA-Ea pressure-volume relationship and maximal SW from the SW-Ea pressure-volume relationship, as previously described for the LV in Chapter 1.

Table 4-1 In-vivo porcine demographic data

	Group (n=18)
Demographics	
Weight, kg	78.8 ± 6.7
Height, cm	128.2 ± 5.2
Heart Rate, BPM	101.3 ± 02.0
MAP, mmHg	78.5 ± 12.6
MPAP, mmHg	20.3 ± 3.4
Mixed Venous Sats, %	65.5 ± 8.7
CO, L/min	6.6 ± 1.1
CI, L/min/m^2	4.2 ± 0.6

Values are mean ± S.D.

MAP = mean aortic pressure; MPAP = mean pulmonary arterial pressure; CO = Cardiac Output; CI = Cardiac Index.

4.3.2 Stroke Work, Efficiency and the Pressure-Volume Relationship

Figure 4-2 shows a family of RV PV-loops recorded during a PA occlusion to increase afterload. The first highlighted PV-loop (Blue) was recorded at baseline and shows a typical triangular shape RV PV-loop. As the afterload on the RV increased, the ESP and ESV increased, while EDP and EDV remained relatively constant, which resulted in a reduced SV and increased developed pressure. The PV-loops at maximal efficiency and maximal SW were determined from the theory described in Chapter 1. As the afterload increased from baseline, the PV-loops at maximal efficiency and maximal SW were determined from the beat-to-beat analysis starting at baseline (PV-loop 1) and then sequentially reviewing each PV-loop as the morphology adapted due to the increasing afterload until maximal occlusion (PV-loop 13). The PV-loop highlighted in green was recorded at maximal efficiency and the PV-loop highlighted in Red was recorded at maximal SW. Beyond this point of maximal SW, as the afterload continued to increase, the SW that could be provided by the failing RV reduced.

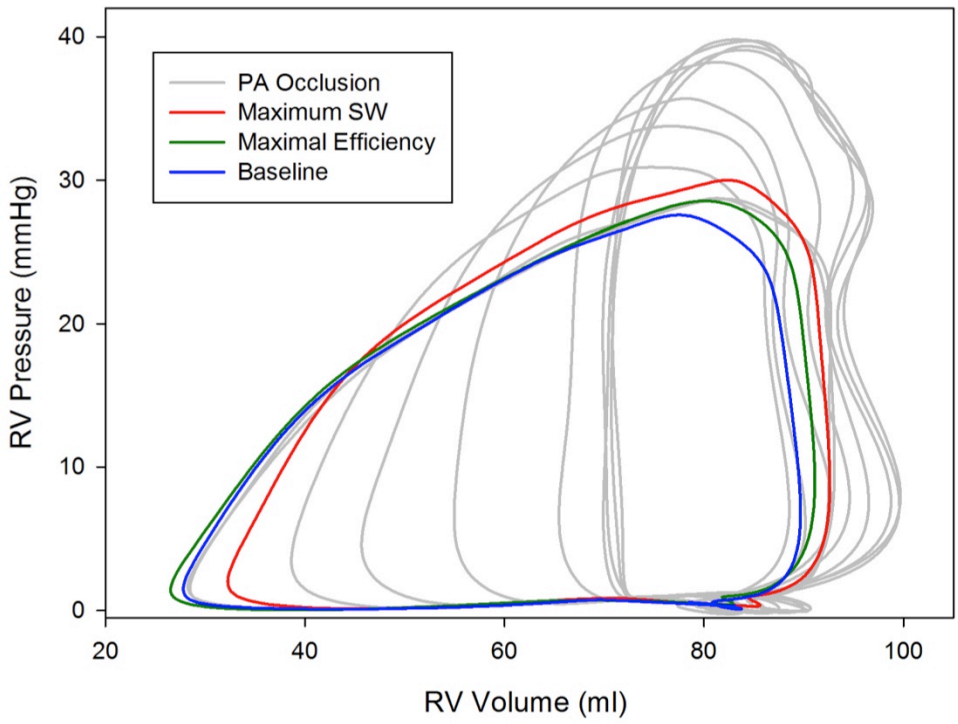

Figure 4-2 RV PV-loops recorded during a PA Snare to Increase afterload. PV-loops are highlighted at baseline (Blue); maximal efficiency (Green) and maximal SW (Red)

Load-independent indices of RV hemodynamic function derived from the conductance catheter at baseline demonstrated the systolic contractility Ees = 0.32 ± 0.07 mmHg/ml, preload recruitable stroke work (PRSW) = 16.8 ± 4.8 mmHg.ml^3 and diastolic function End-diastolic pressure volume relationship (EDPVR) = 0.05 ± 0.02 mmHg/ml. Conductance catheter data at baseline and during the PA snare are described in Table 4-2 and Figure 4-3. This shows the RV was slightly uncoupled at baseline (0.94 ± 0.18) and maximal efficiency occurred at a higher Ees/Ea than maximal SW: Ees/Ea 0.84 ± 0.23 vs. 0.68 ± 0.23 respectively. In terms of RV afterload, maximal efficiency occurred at a lower Ea than maximal SW: Ea (mmHg/ml) 0.39 ± 0.05 vs. 0.50 ± 0.14 respectively. While HR ($p=0.829$) and Tau ($p=0.930$) remained constant there was a significant increase in dP/dtmin ($p<0.001$). This can be explained by the load-dependency of dP/dtmin and the significant rise in ESP ($p<0.001$) with EDP ($p=0.626$) remaining constant. Beyond a threshold Ea = 0.50 mmHg/ml, an increase in Ea resulted in reductions in RV SW and efficiency and CO declined. All other parameters of RV hemodynamic function are shown in Table 4-2.

Table 4-2 Animal model RV hemodynamic data at baseline, maximal efficiency, maximal SW and during the maximal occlusion

	Baseline	Maximal Efficiency	Maximal SW	Maximal Occlusion	P-Value
CO, L/min	6.6 ± 0.9	6.7 ± 0.9	6.4 ± 1.1	4.2 ± 1.2	<0.001
ESV, ml	66.1 ± 18.8	65.9 ± 18.9	70.0 ± 18.9	96.7 ± 21.3	<0.001
EDV, ml	107.7 ±18.5	105.6 ±18.5	106 ± 19.4	120.5 ±22.3	0.103
SV, ml	65.2 ± 8.9	66.1 ± 8.9	63.1 ± 9.8	40.7 ± 11.6	<0.001
EF, %	64.0 ± 6.6	65.5 ± 9.0	61.3 ± 8.8	35.4 ± 9.9	<0.001
ESP, mmHg	22.0 ± 3.7	25.7 ± 4.3	30.6 ± 6.9	43.9 ± 7.0	<0.001
EDP, mmHg	5.2 ± 3.0	5.8 ± 3.2	5.7 ± 3.0	6.6 ± 3.2	0.626
HR, BPM	101.7 ± 1.8	101.8 ± 1.8	101.4 ± 1.8	103.2 ± 6.1	0.829
dp/dt max, mmHg/s	307 ± 61	352 ± 77	350 ± 71	344 ± 55	0.176
dp/dt min, mmHg/s	-217 ± 36	-248 ± 50	-299 ± 56	-360 ± 54	<0.001
Tau, ms	61.5 ± 27.0	58.7 ± 27.4	56.6 ± 25.0	61.5 ± 23.6	0.930
Ea, mmHg/ml	0.34 ± 0.06	0.39 ± 0.05	0.50 ± 0.14	1.18 ± 0.43	<0.001
SW, mmHg.ml	899 ± 205	1138 ± 263	1246 ± 285	844 ± 393	0.002
PVA, mmHg.ml	1616 ± 709	1327 ± 424	1614 ± 483	2152 ± 621	0.002
SW/PVA	0.63 ± 0.22	0.90 ± 0.21	0.80 ± 0.20	0.42 ± 0.23	<0.001
Ees/Ea	0.94 ± 0.18	0.84 ± 0.23	0.68 ± 0.23	0.32 ± 0.15	<0.001

Values are mean ± S.D.

CO = cardiac output; ESV = end-systolic volume; EDV = end-diastolic volume; SV = stroke volume; EF = ejection fraction; ESP = end-systolic pressure; EDP = end-diastolic pressure; HR = heart rate; dP/dt max = maximum rate of isovolumic contraction; dP/dt min = maximum rate of isovolumic relaxation; Tau = time constant of diastolic relaxation; Ea = effective arterial elastance; SW = stroke work; PVA = pressure volume area; SW/PVA = RV efficiency; Ees/Ea = ventriculoarterial coupling ratio.

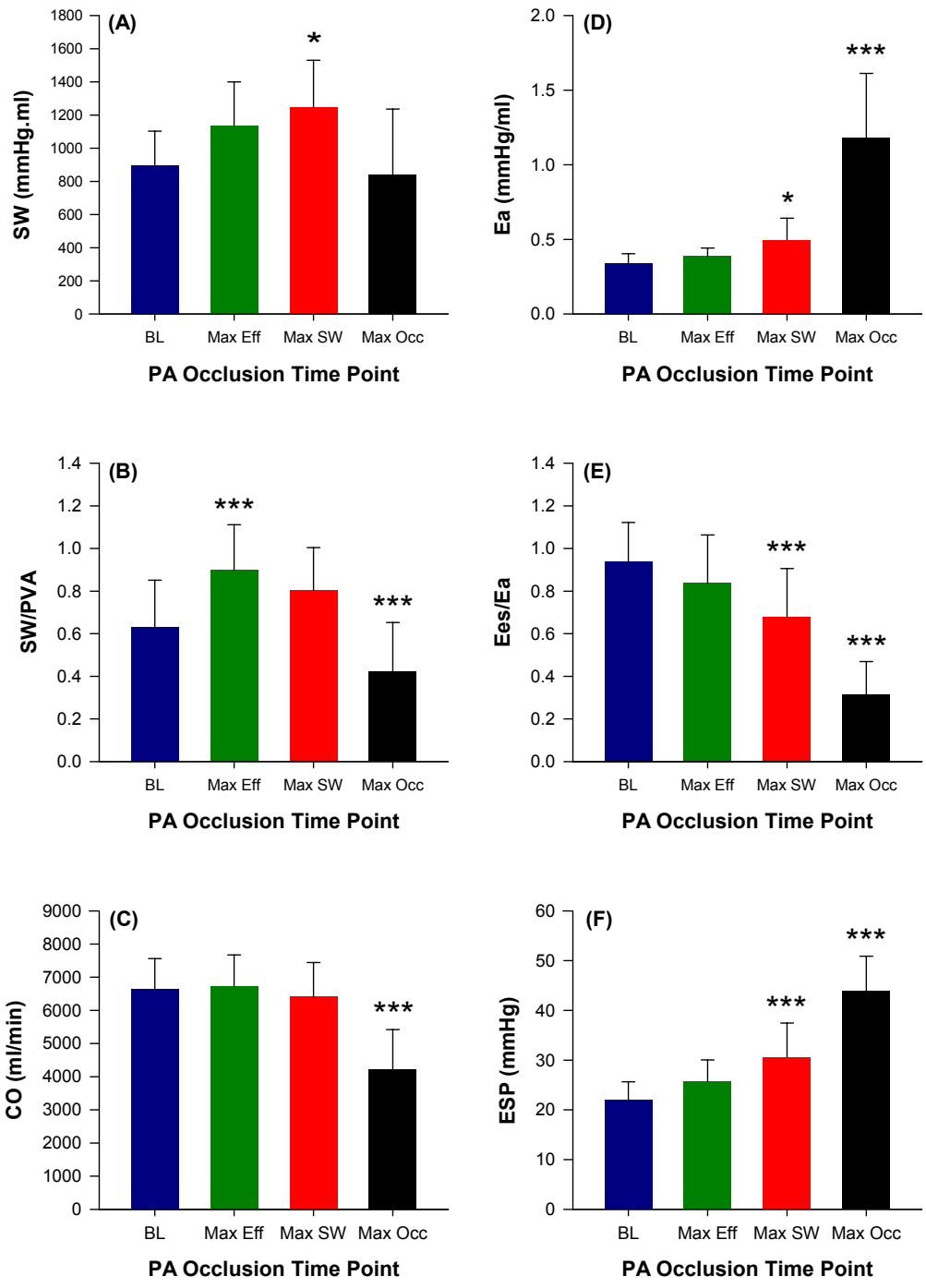

Figure 4-3 Animal model RV hemodynamic data for (A) SW; (B) CO; (C) ESV; (D) SW/PVA; (E) Ea; and (F) ESP at baseline (BL) and the PA occlusion time point for maximal efficiency (Max Eff), maximal SW (Max SW) and maximal PA occlusion (Max Occ). * $p < 0.05$; ** $p < 0.01$; *** $p < 0.001$.

4.3.3 Relations between Afterload Quantified by Ea and RV Function

Pooled data from 18 subjects (n=324) with mean regression lines and 95% confidence intervals are displayed in Figure 4-4 for the relation between afterload quantified by Ea and SW (A); and SW/PVA (B); and CO (C). The regression lines fitted to the data determined that maximal efficiency occurred at a lower afterload loading condition than at maximal SW. However, as the afterload increased further past this point, there was a decline in CO, since the RV fails to maintain sufficient output against the increasing loading conditions.

Figure 4-5 shows Ea at maximal SW vs. maximal efficiency (SW/PVA) determined from families of PV-loops recorded during each of the 18 subjects' PA Occlusions that increased RV afterload loading conditions. The majority of the data points fell above the line of identity, indicating a greater Ea was observed at maximal SW, when compared to Ea at maximal efficiency.

Relations between afterload quantified by Ea and other hemodynamic parameters of RV function (ESV, EDV, ESP, EDP, dP/dt max, dP/dt min, EF, SV, Tau) are presented in Appendix A.

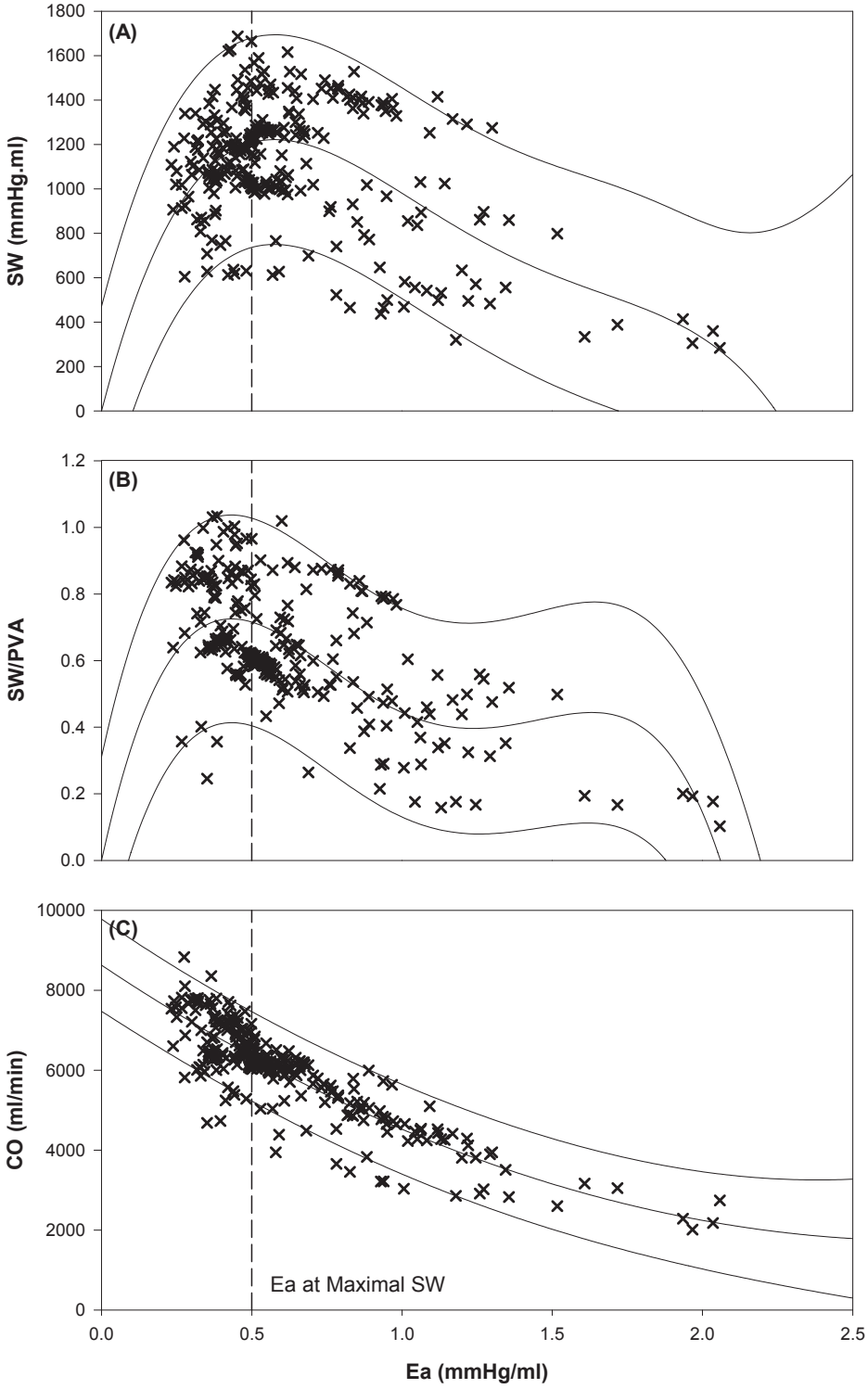

Figure 4-4 Animal model relation between afterload quantified by Ea and A) SW; B) SW/PVA; and C) CO. Pooled data from 18 hearts are shown (n=324). Mean regression lines with 95% prediction intervals are displayed.

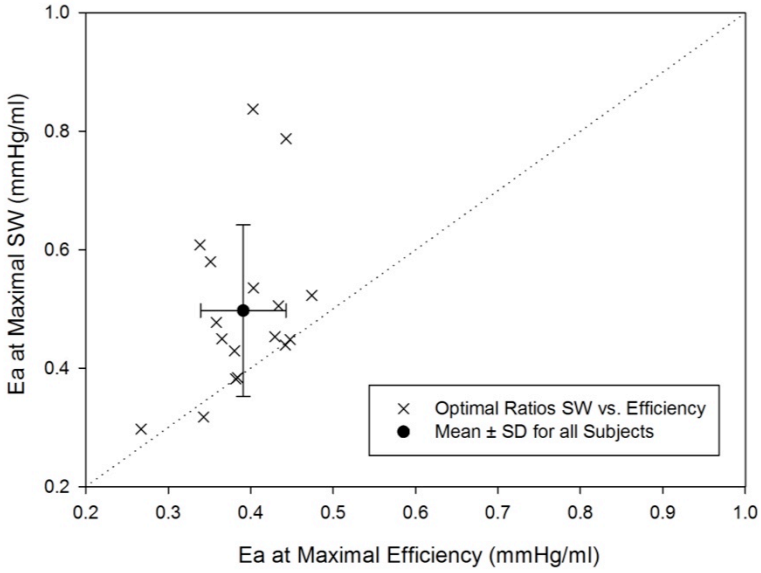

Figure 4-5 Optimum Ea for maximal SW vs. maximal efficiency determined from the 18 Porcine subjects. *Dotted line* – shows line of Identity.

4.3.4 Relations between Ventriculoarterial Coupling Quantified by Ees/Ea and RV Function

Pooled data from 18 subjects (n=324) with mean regression lines and 95% prediction intervals are shown in Figure 4-6 for the relation between the ventriculoarterial coupling ratio (Ees/Ea) and SW (A); and SW/PVA (B); and CO (C). The regression lines fitted to the data determined that maximal efficiency occurred at a higher coupling ratio than maximal SW. However, unlike the graphic representation of the relation between Ea and CO shown in Figure 4-4 where CO appears to decline with increasing afterload gradually. Figure 4-6 shows that CO remains fairly constant and is maintained as the coupling ratio decreases up to the point of maximal SW. However, beyond the point of maximal SW, as the coupling ratio continues to decrease the CO decreases. This would suggest that the RV fails to maintain sufficient output against increasing afterloads beyond the ventriculoarterial coupling ratio at maximal SW.

Figure 4-7 shows the ventriculoarterial coupling ratio (Ees/Ea) at maximal SW vs. maximal efficiency (SW/PVA) determined from families of PV-loops recorded during each of the 18 subjects' PA occlusions that increased RV afterload loading conditions. The majority of the data points fall below the line of identity, indicating a lower coupling ratio was observed at maximal SW, when compared to Ees/Ea at maximal efficiency.

Relations between ventriculoarterial coupling quantified by Ees/Ea and other hemodynamic parameters of RV function (ESV, EDV, ESP, EDP, dP/dt max, dP/dt min, EF, SV, Tau) are presented in Appendix B.

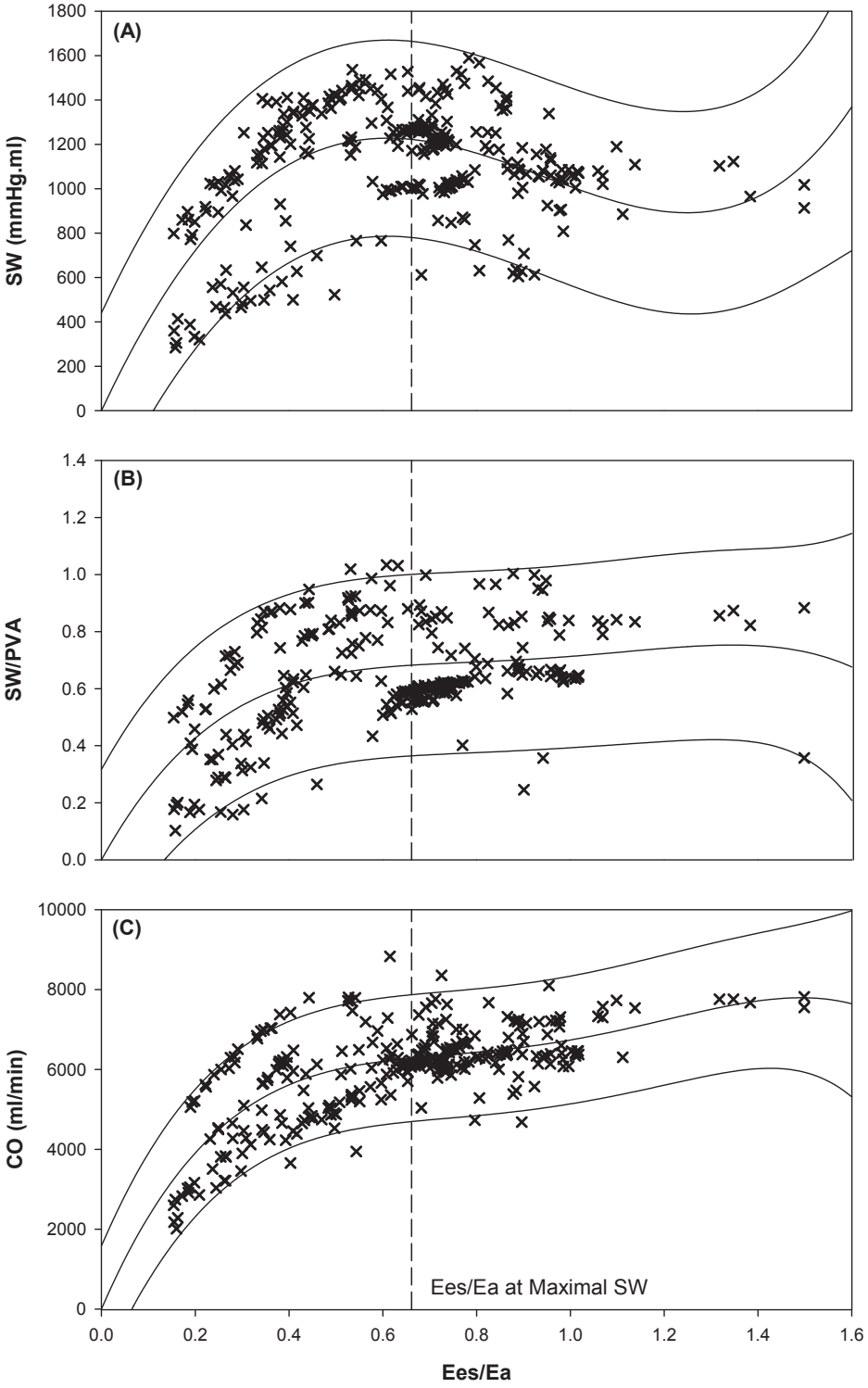

Figure 4-6 Relation between the ventriculoarterial coupling ratio (Ees/Ea) and A) SW; B) SW/PVA (SW/PVA); C) CO.

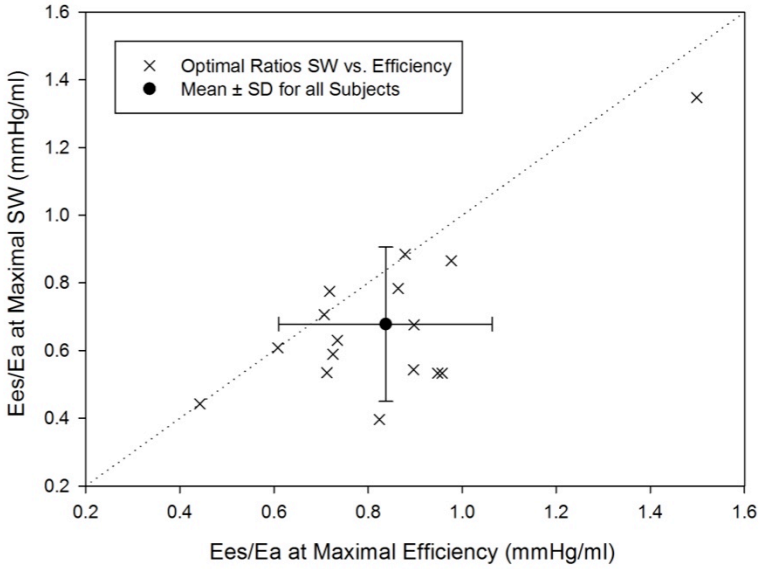

Figure 4-7 Optimum Ees/Ea coupling ratios for maximal SW vs. maximal efficiency determined from the 18 porcine subjects. *Dotted line* – shows line of Identity.

4.4 Discussion

This is the first study to use the conductance technique to determine the interaction between the RV and PA in a large animal model that can be used to define an Ees/Ea coupling threshold for maximal SW. The interaction between the RV and the PA determines the external work and metabolic efficiency of the ventricle. This data has shown that maximal SW occurred at an Ees/Ea coupling threshold of 0.68 ± 0.23 (Ea = 0.50 ± 0.14 mmHg/ml), beyond which RV dysfunction ensued. While maximal efficiency is important from the perspective of understanding ideal energy transfer conditions between RV work and oxygen consumption, the threshold of maximal SW is the determinant factor in RV failure. We have demonstrated acute RV adaptation in response to acute changes in afterload. There is an immediate response where the RV systolic pressure rises to maintain ejection. Then as the afterload continues to increase, there are only relatively small increases to EDP and EDV as the RV dilates and distends to accommodate the increasing systolic pressure required to attempt to facilitate ejection. As the systolic pressure rises beyond the threshold point of maximal SW, ESV increases and combined with the relatively small change in EDV results in a reduction in SV. This decrease in SV causes a decline in CO and SW, as the RV fails to maintain sufficient output against the increasing loading conditions. Therefore, in terms of efficiency and SW, as the afterload loading conditions increase from baseline, RV output is adequately maintained through the arbitrary point of maximal efficiency until the loading conditions reach a threshold point of maximal SW at an Ees/Ea = 0.68. Beyond this threshold of maximal SW, SW and CO may continue to offer sufficient output to meet demand at rest. However, if the afterload loading conditions are increased further (as is observed during modest exercise), there is insufficient RV energetic reserve and the RV will fail to meet demand. Quantifying afterload by Ea can be used as an indicator of RV failure; the Ea at maximal SW could determine disease severity and guide management.

We have established a threshold for RV-PA ventriculoarterial uncoupling in an animal model, beyond which, there is an insufficient energetic reserve to maintain adequate RV function. Theoretical models have predicted optimal mechanical coupling corresponded to an Ees/Ea = 1 (Sunagawa et al., 1984); with current literature suggesting in a healthy individual RV-PA ventriculoarterial coupling is between 1 to 2 (Naeije and Manes, 2014) and that the values for the LV and RV are comparable. While we demonstrate agreement with previous work at baseline, with slight uncoupling between the RV-PA at rest (Ees/Ea = 0.94 ± 0.18), our work has shown that maximal SW occurs at an Ees/Ea = 0.68 ± 0.23 and that uncoupling only occurred beyond this threshold as there was insufficient RV energetic reserve to maintain function. This finding is supported by previous work (Fourie et al., 1992) where authors suggested the RV uncoupled around an Ees/Ea = 0.6 mmHg/ml. One explanation for this apparent inefficient energy transfer between the RV and PA could be the complex pulmonary vascular structure. Whereas the LV is coupled with an elastic aorta and all energy expended during the pulsatile contraction is converted into flow energy due to the elastic recoil of the aorta (Yaginuma et al., 1985; Sasayama and Asanoi, 1991), the pulmonary artery has relatively short elastic proximal vessels which branch into the pulmonary trunk, so that 25-40% of the energy expended during the contraction of the RV is not converted into flow energy due to the restricted elastic recoil of the pulmonary vessels (Grignola et al., 2007; Saouti et al., 2010). This would explain the lower coupling ratio we observed.

Some limitations of this study must be recognized. First, the open-chested porcine model of RV-PA ventriculoarterial interaction has an open pericardium that reduces RV contractility. However, this remains the best physiological model of assessing the response of normal RV function to changes in afterload, as LV-RV interdependence is retained and others have used this model (Nicolosi et al., 1996; Kuehne et al., 2003; Missant et al., 2007; Ghuysen et al., 2008; Guihaire et al., 2015). Second, the acute load variations used to determine Ees and the relationship between different RV

hemodynamic parameters with Ees/Ea and Ea can be considered valid due to auto-regulation, termed the “Anrep Effect”; increasing afterload increases contractility and maintains CO, but it takes between 30 to 60 seconds for contractility to adapt in response to acute loading variations (von Anrep, 1912). Data were acquired for an adequate duration to detect these changes within the animal model. Third, while the conductance catheter is designed for orientation along the long-axis of the ventricle with the pigtail positioned in the apex of the heart, many researchers have presented work with the conductance catheter inserted through the LV and RV apex (Chaturvedi et al., 1998; Messer et al., 2016).

Finally, conductance derived PVA is only an approximation of myocardial efficiency. The correlation between PVA and myocardial efficiency excludes the energy consumption costs of excitation contraction coupling and basal metabolism (De Tombe et al., 1993). PVA is therefore an underestimate. De Tombe et al. (1993) have demonstrated that the Ea at maximal efficiency is closer to the Ea at maximal SW when calculated directly from MVO_2. However, the use of PVA derived from the same conductance catheterisation as used to determine SW, allows for a simplified approximation of myocardial efficiency, and a precise measure of maximal SW from the pressure volume relation derived from the Ea-SW relationship.

4.5 Summary

The research question for this chapter was to establish whether the in-vivo porcine model of RV Ventriculoarterial interaction developed in Chapter 3 could be used to determine the optimal coupling ratio at maximal efficiency and maximal SW. This work has shown that although maximal efficiency is important from a perspective of understanding ventriculoarterial coupling and the maximal RV work at minimal oxygen consumption, in RV failure, maximal SW derived from the pressure-volume relationship, is a key determinant of clinical and therapeutic outcomes. In terms of RV performance upon exercise (increased loading), if at rest, the RV is already pumping

against an afterload loading condition equal to or greater than that of maximal SW, as the PA afterload increases with exercise both SW and CO will fall. The RV will not be able to maintain an adequate output in the face of additional loading generated from exercise.

To investigate the clinical viability of these findings the first clinical study assessed how maximal SW and ventriculoarterial coupling ratio derived from the pressure-volume relationship may give insight into RV remodelling in two cohorts with pathological RV loading: in symptomatic (Chronic Thromboembolic Pulmonary Hypertension – CTEPH) and asymptomatic (Chronic Thromboembolic Disease - CTED) thromboembolic disease (elevated Ea – Chapter 5). The second clinical study investigated how ventricular interdependence affects RV contractility and the RV-PA ventriculoarterial coupling ratio following Transcatheter Aortic Valve Implantation (TAVI), which relieves the afterload of the LV by replacing the aortic valve using percutaneous therapy (changing Ees – Chapter 6).

5 Ventricular Remodelling in Patients with Chronic Thromboembolic Pulmonary Vascular Disease and Hypertension: Unlocking Pathology through Ventriculoarterial Interaction

The aim of this chapter was to determine if ventriculoarterial (Ees/Ea = 0.68) coupling ratio at maximal SW defined in Chapter 4 from the in-vivo porcine model of RV ventriculoarterial interaction could be translated to human physiology to better characterise patients' with symptomatic (Chronic Thromboembolic Pulmonary Hypertension) and asymptomatic (Chronic Thromboembolic Disease) thromboembolic obstruction.

5.1 Introduction

Chronic thromboembolic pulmonary hypertension (CTEPH) occurs when organized thrombi obstruct the pulmonary arteries (PA) increasing pulmonary vascular resistance (PVR) and mean PA pressure (mPAP) (Simonneau et al., 2013). There is a sub-group of patients who present with chronic thromboembolic disease (CTED), who have mPAP < 25 mmHg at rest, but who are nevertheless symptomatic and possibly deserving of treatment. Right ventricular (RV) dysfunction in these patients may limit pressure generation resulting in under-diagnosis. Invasive hemodynamic assessment by right heart catheterization is reportedly the gold standard diagnostic test and these data are the primary determinant of prognosis (Champion et al., 2009). However, it is pressure focused and patients with CTED and occult RV dysfunction that is contributory to their symptoms will again be overlooked (Castelain et al., 2001; Gan et al., 2007). The under-diagnosis of RV dysfunction in CTED and the limited understanding of its clinical course are significant unmet clinical needs. The concept of ventriculoarterial coupling and RV energetic reserve may offer novel insight in to the pathophysiology of CTED and CTEPH and more accurately define the disease state.

Pressure-Volume (PV)-loop methodology allows for RV-PA Ees/Ea coupling to be defined as the matching between RV contractility (End-systolic elastance - Ees) and

PA afterload (Effective arterial elastance – Ea) (Kelly et al., 1992). There has been an emerging trend of clinical studies performed using Ees/Ea coupling to detect changes in patients with different PH etiologies and disease severity. In the normal healthy RV McCabe et al. (2014) demonstrated normal values of Ea = 0.30 ± 0.10 mmHg/ml, Ees = 0.44 ± 0.20 mmHg/ml and Ees/Ea = 1.46 ± 0.30. In patients with a clinical diagnosis of CTED/CTEPH (McCabe et al., 2014), PH and associated systemic sclerosis (Tedford et al., 2013), and those with PH and without overt RV failure (Kuehne et al., 2004), it was demonstrated that Ees/Ea uncoupling was due to a disproportional increase in Ea and the inability to augment contractility (Ees). These observations suggest that in early stage PH, decreased Ees/Ea coupling is mainly reflected in increased afterload (Ea) and insufficient augmentation of RV contractility. However, in late stage PH, the continued progression of the disease state leads to the clinical development of RV failure and further impairs Ees/Ea coupling due to decreased contractility (Ees) (Kuehne et al., 2004). While there is potential for Ees/Ea coupling to be used as a marker of RV function and illustrate the transition from RV adaptation to RV maladaptation, it still remains unclear at what specific coupling ratio the RV becomes uncoupled to the PA. Previous animal model data suggests maximal stroke work (SW) was achieved at an $Ees/Ea_{max\ sw}$ = 0.6 mmHg/ml, and RV dysfunction ensued with any further increase in afterload. However, this study determined Ees from a PA occlusion that is now known to overestimate true Ees, and Ea was determined from mean RV pressures rather than the end-systolic pressure (ESP).

In health, the RV-PA is coupled to maintain optimal cardiac output but it is possible to determine the maximal SW in response to an acute artificial increase in afterload (Ea). The Ees/Ea coupling ratio at which this point is reached is termed $Ees/Ea_{max\ sw}$. Below the threshold for maximal SW there is RV energetic reserve, however, above this cut-off there is no energetic reserve and dysfunction will ensue (Burkhoff and Sagawa, 1986).

5.2 Methods

This work was carried out at Papworth Hospital NHS Foundation Trust (Papworth Everard, Cambridgeshire) under the Local Research Ethics Committee approval (REC number 12/EE/0085) as previously described in Section 2.2.4. As previously described in Section 2.2.5, Dr Stephen Hoole recruited the patients into the studies and the Consultant Interventional Cardiologist responsible for the care of the patient performed the interventional procedures.

5.2.1 Patient Population

Ten patients with a median age of 51 years (range 28 to 77) and a clinical diagnosis of CTEPH and ten patients with a median age of 64 years (range 28 to 73) and a clinical diagnosis of CTED were invited to participate. Patients were all in World Health Organization (WHO) Functional Class II/III. This is a means of classifying disease severity in PH: Class I has no symptom of PH at rest or exercise; Class II has no symptom of PH at rest but shortness of breath on exercise; Class III may not have symptoms at rest but activities greatly limited by shortness of breath; Class IV has symptoms at rest and severe symptoms with any activity. Exclusion criteria were a myocardial infarction in the preceding 12 weeks, previous permanent pacemaker implant or atrial fibrillation.

5.2.2 Catheterization

Routine Swan-Ganz catheterisation was performed via a 7-F sheath placed in the right femoral or jugular vein using lidocaine local anaesthetic. The catheter was advanced and positioned in the right atrium (right atrial pressures were measured), the RV and finally the PA (PA pressures were measured). An injection of cold saline (0.9% NaCl) was used to determine cardiac output (CO) by the standard thermodilution technique. This was repeated three times to determine an average measurement of CO. A 7-F, 8 electrode conductance catheter (Millar Instruments, Houston, Texas, USA) was then inserted through the venous sheath, advanced across the tricuspid valve and placed

along the long axis of the ventricle in to the RV apex under fluoroscopic guidance Figure 5-1.

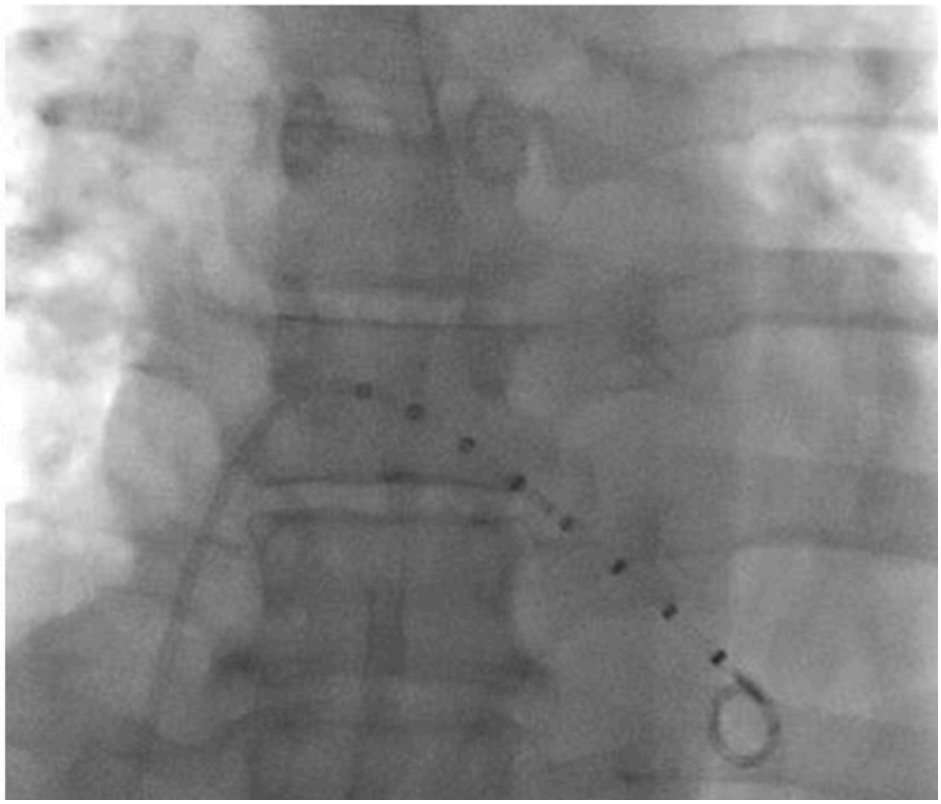

Figure 5-1 Conductance catheter positioned in the RV under fluoroscopic guidance

5.2.3 RV Functional Assessment

The conductance technique was used to measure the PV-loop relationship during ventilation suspension. Five steady-state PV-loops were recorded to generate load-dependent parameters of systolic and diastolic function. The conductance catheter data was analysed offline using LabChart software (LabChart 7.0, ADInstruments, New South Wales, Australia) as described in Chapter 2.

PV-loop morphology was used to determine maximal RV efficiency from the SW/Pressure volume area (PVA) relationship. Ventricular efficiency is defined as the ratio between SW and oxygen consumption (Burkhoff and Sagawa, 1986). PVA is a linear surrogate of myocardial oxygen consumption (Suga et al., 1980; Suga et al., 1983; Suga et al., 1984). PVA is the total mechanical work performed by the ventricle, calculated from the sum of the external stroke work (SW – determined from the area contained within the PV-loop) that propels the blood from the ventricle and mechanical potential energy (PE – the area bound by the ESPVR and EDPVR) stored in the ventricle at the end of each contraction (Figure 1) (Suga, 1979).

5.2.4 Statistical Analysis

Statistical significance was determined as described in Section 2.2.2.

5.2.5 Outcomes

The primary outcome was the characterisation of patients with chronic thromboembolic disease by ventriculoarterial (Ees/Ea = 0.68 ± 0.23) coupling ratio at maximal SW to identify ocult RV dysfunction.

5.3 Results

5.3.1 Demographics, Right Heart Catheterisation and RV Haemodynamic Data after Classification of Patients by mPAP

Demographic human data from 10 patients with CTEPH and 10 patients with CTED are shown in Table 5-1. We confirmed that the mPAP ($p<0.001$) and PVR ($p<0.001$) were normal in the CTED group and elevated in the CTEPH group. Typical PV-loop morphologies for the CTED and CTEPH patient groups are shown in Figure 5-2. While the mean pulmonary arterial pressures were normal in the CTED group, the CTED PV-loop morphology was abnormal when compared to a normal triangular shaped RV PV-loop. During systolic ejection there is a rise in RV pressures, as the ventricle has to work harder to eject the blood past the thromboembolic masses in the PA. This caused the CTED RV PV-Loop to resemble a typical LV PV-loop (McCabe et al., 2014; Redington et al., 1990). While HR ($p=0.560$) and Tau ($p=0.954$) remained constant, there was a significant increase in dP/dt max ($p=0.016$) and dP/dt min ($p<0.001$). This is explained by the load-dependency of these measurements and the significant rise in ESP ($p<0.001$) with EDP ($p=0.162$) remaining constant. Ea ($p=0.005$) was elevated in the CTEPH group and beyond the cut-off for maximal SW (0.50 ± 0.14 mmHg/ml) defined in Chapter 4 in the animal Model. This would indicate the patients with CTED would have some RV energetic reserve, however, those with CTEPH would have significant RV dysfunction and no capacity to increase contractility in the presence of increased afterload.

Table 5-1 Demographics, right heart catheterisation and RV hemodynamic data after classification of patients by mPAP at rest.

	mPAP ≤ 25 (n=10)	mPAP > 25 (n=10)	p-value
Demographics			
Age, years	55 ± 17	51 ± 14	0.564
Male Sex, N (%)	4 (40.0)	6 (60.0)	0.656
BMI, kg/m^2	31.2 ± 8.2	29.2 ± 4.4	0.880
6MWD, m	369 ± 79	377 ± 134	0.902
WHO Class II/III, N (%)	10 (100.0)	10 (100.0)	1.000
Right Heart Catheter			
mPAP, mmHg	18.8 ± 5.5	39.7 ± 7.1	<0.001
Systolic PAP, mmHg	30.7± 9.6	66.8 ± 16.4	<0.001
Diastolic PAP, mmHg	10.1 ± 4.8	24.1 ± 6.6	<0.001
mRAP, mmHg	5.8 ± 4.2	8.0 ± 3.5	0.109
PCWP, mmHg	8.3 ± 4.3	10.8 ± 4.9	0.244
RV EDP, mmHg	5.8 ± 3.5	10.1 ± 3.4	0.012
SvO_2,%	74.1 ± 4.2	71.5 ± 6.3	0.305
CO, L/min	5.3 ± 1.3	4.7 ± 1.0	0.249
CI, L/min/m^2	2.6 ± 0.3	2.4 ± 0.6	0.334
PVR, dyn/s/cm^5	163 ± 57	573 ± 220	<0.001
RV Hemodynamics			
Heart Rate, BPM	68 ± 10	71 ± 13	0.560
SW, mmHg.ml	1402 ± 500	2018 ± 732	0.041
CO, L/min	5.3 ± 1.4	4.9 ± 1.0	0.436
ESP, mmHg	34.2 ± 7.1	67.4 ± 16.6	<0.001
EDP, mmHg	10.3 ± 4.3	13.1 ± 4.4	0.162
ESV, ml	111.0 ± 44.4	85.2 ± 26.2	0.241
EDV, ml	149.8 ± 44.4	118.2 ± 37.7	0.104
SV, ml	78.7 ± 22.0	71.8 ± 26.3	0.532
EF, %	51.6 ± 8.3	55.5 ± 9.9	0.354
dP/dt max, mmHg/s	351 ± 76	502 ± 181	0.016
dP/dt min, mmHg/s	-326 ± 92	-618 ± 173	<0.001
Ea, mmHg/ml	0.47 ± 0.18	1.10 ± 0.52	0.005
Tau, ms	63.9 ± 17.3	64.3 ± 16.4	0.954
Ees/Ea	2.29 ± 1.68	0.72 ± 0.59	0.026

Values are mean ± S.D. or n (%).

BMI = body mass index; 6MWD = 6 minute walking distance; WHO Class = world health organisation classification; mPAP = mean pulmonary arterial pressure; mRAP = mean right atrial pressure; PCWP = pulmonary capillary wedge pressure; RV EDP = right ventricular end-diastolic pressure; SvO_2 = mixed venous oxygen saturations; CO = cardiac output; CI = cardiac index; PVR = pulmonary vascular resistance; SW = stroke work; ESP = end-systolic pressure; EDP = end-diastolic pressure; ESV = end-systolic volume; EDV = end-diastolic volume; SV = stroke volume; EF = ejection fraction; dP/dt max = maximum rate of isovolumic contraction; dP/dt min = maximum rate of isovolumic relaxation; Ea = effective arterial Elastance; Tau = time constant of diastolic relaxation.

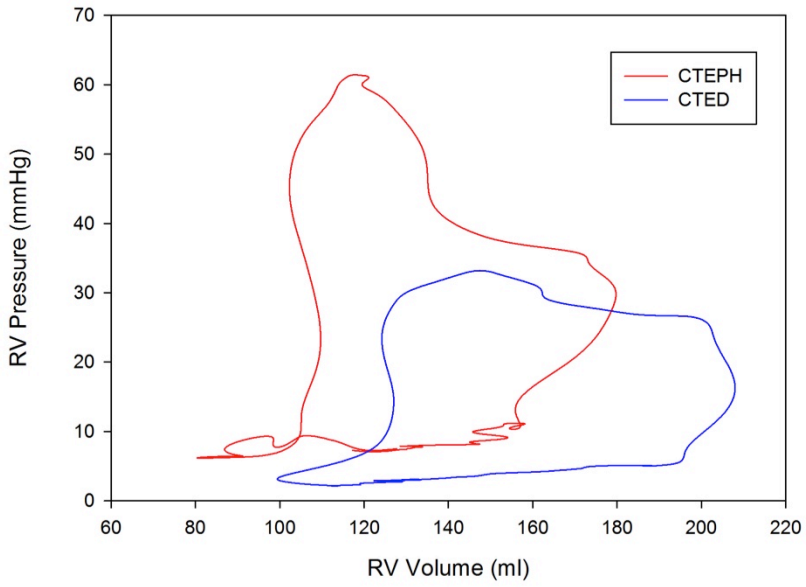

Figure 5-2 Typical RV PV-loop morphologies for patients with CTED (Blue) and CTEPH (Red)

5.3.2 Demographics, Right Heart Catheterisation and RV Haemodynamic Data after Classification of Patients with CTED or CTEPH by the Ees/Ea Coupling Ratio at the Threshold for Maximal SW Determined from the Animal Model.

After reclassifying patients according to the $Ees/Ea_{max\ sw}$ threshold established in the animal model (Table 5-2), we demonstrated that mPAP (p=0.006) and PVR (p=0.003) were normal in the Ees/Ea ≥ 0.68 group and elevated in the Ees/Ea < 0.68 group. There was a significant increase in HR (p=0.04) in the Ees/Ea < 0.68 group. While Tau (p=0.418) remained constant, there was a significant increase in dP/dt_{min} (p=0.003), again explained by the load-dependency of this measurement and the significant rise in ESP (p<0.001) whilst EDP (p=0.103) remained constant. Although SW (p=0.853) remained constant between the Ees/Ea subgroups, there was a significant reduction in CO (p=0.024), SV (p=0.006), ESV (p=0.034) and EDV (p=0.007) in the Ees/Ea < 0.68 group. The differences in heart rate and volumetric indices were not identified when patients were stratified by pressure.

Two patients with CTED were identified with an Ees/Ea < 0.68 indicating occult RV pathology (Figure 5-3) and three CTEPH patients still had RV contractile reserve (Ees/Ea ≥ 0.68). This equated to a reclassification of 25% of the entire cohort. The Ees/Ea coupling ratio for these three misclassified CTED patients was 0.35 and 0.45, even though they presented with normal mPAP (15 and 19 mmHg) and PVR (157 and 230 dyne/s/cm^5).

Table 5-2 Demographics, right heart catheterisation and RV hemodynamic data after classification of patients with CTED or CTEPH by the Ees/Ea coupling ratio at the threshold for maximal SW.

	Ees/Ea ≥ 0.68 (n=11)	Ees/Ea < 0.68 (n=9)	p-value
Demographics			
CTED, N (%)	8 (72.7)	2 (27.3)	0.072
CTEPH, N (%)	3 (22.2)	7 (77.7)	0.073
Age, years	55 ± 16	50 ± 16	0.516
Male Sex, N (%)	5 (45.4)	5 (55.6)	0.653
BMI, kg/m^2	30.9 ± 7.4	29.1 ± 4.9	0.804
6MWD, m	380 ± 81	364 ± 137	0.747
WHO Class (II/III)	11 (100.0)	9 (100.0)	1.000
Right Heart Catheter			
mPAP, mmHg	22.8 ± 8.0	37.1 ± 12.5	0.006
Systolic PAP, mmHg	38.8 ± 17.1	60.9 ± 23.5	0.026
Diastolic PAP, mmHg	12.4 ± 6.0	22.9 ± 9.1	0.006
mRAP, mmHg	7.1 ± 4.7	6.7 ± 3.0	0.817
PCWP, mmHg	10.8 ± 5.8	8.0 ± 2.2	0.144
RV EDP, mmHg	7.6 ± 4.5	8.3 ± 3.5	0.709
SvO_2,%	74.5 ± 4.7	71.0 ± 6.0	0.120
CO, L/min	5.3 ± 1.3	4.6 ± 1.0	0.217
CI, $L/min/m^2$	2.7 ± 0.3	2.3 ± 0.5	0.082
PVR, $dyne/s/cm^5$	181 ± 78	554 ± 250	0.003
RV Hemodynamics			
Heart Rate, BPM	65 ± 11	75 ± 10	0.04
SW, mmHg.ml	1683 ± 663	1743 ± 755	0.853
CO, L/min	5.6 ± 1.2	4.4 ± 0.8	0.024
ESP, mmHg	36.7 ± 11.6	68.1 ± 16.7	<0.001
EDP, mmHg	10.2 ± 3.8	13.5 ± 4.7	0.103
ESV, ml	114.0 ± 36.3	78.6 ± 31.4	0.034
EDV, ml	156.1 ± 35.5	107.0 ± 37.1	0.007
SV, ml	87.7 ± 22.1	60.1 ± 16.5	0.006
EF, %	53.3 ± 9.8	54.0 ± 8.8	0.875
dP/dt_{max}, mmHg/s	385 ± 114	475 ± 190	0.173
dP/dt_{min}, mmHg/s	-358 ± 136	-612 ± 183	0.003
Ea, mmHg/ml	0.42 ± 0.10	1.22 ± 0.43	<0.001
Tau, ms	67.1 ± 13.7	60.8 ± 19.2	0.418
Ees/Ea	2.38 ± 1.49	0.45 ± 0.14	<0.001

Values are mean ± S.D. or n (%).

CTED = chronic thromboembolic disease; CTEPH = chronic thromboembolic pulmonary hypertension; BMI = body mass index; 6MWD = 6 minute walking distance; WHO Class = world health organisation classification; mPAP = mean pulmonary arterial pressure; mRAP = mean right atrial pressure; PCWP = pulmonary capillary wedge pressure; RV EDP = right ventricular end-diastolic pressure; SvO_2 = mixed venous oxygen saturations; CO = cardiac output; CI = cardiac index; PVR = pulmonary vascular resistance; SW = stroke work; ESP = end-systolic pressure; EDP = end-diastolic pressure; ESV = end-systolic volume; EDV = end-diastolic volume; SV = stroke volume; EF = ejection fraction; dP/dt max = maximum rate of isovolumic contraction; dP/dt min = maximum rate of isovolumic relaxation; Ea = effective arterial Elastance; Tau = time constant of diastolic relaxation; Ees/Ea = Single-beat ventriculoarterial coupling ratio.

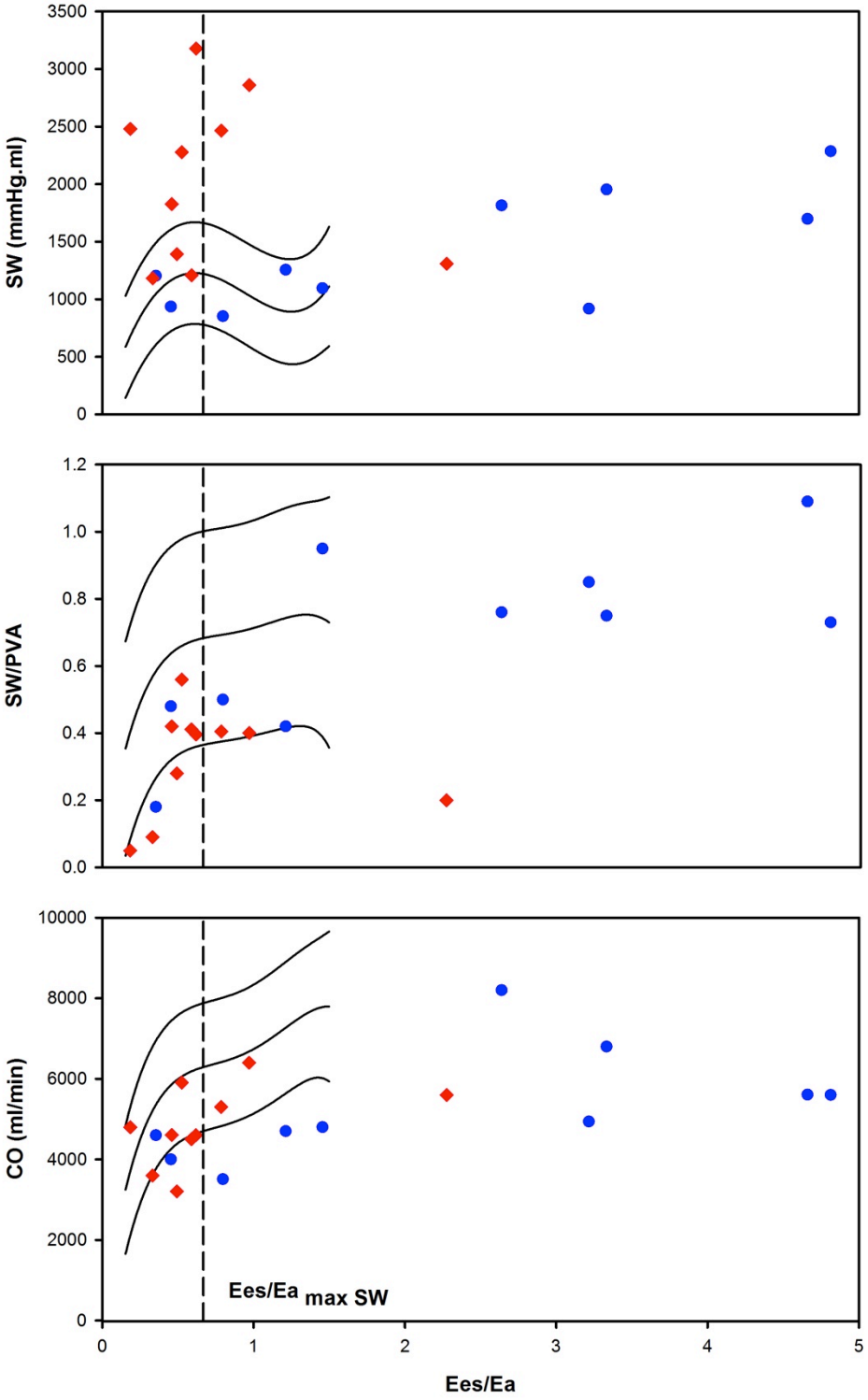

Figure 5-3 The individual data points for the patients with CTED or CTEPH overlaid on top of the mean regression lines determined from the animal model for the relation between ventriculoarterial coupling ratio (Ees/Ea) and A) SW; B) SW/PVA; and C) CO.

5.3.3 Demographics, Right Heart Catheterisation and RV Haemodynamic Data after Classification of Patients by Afterload as Quantified by Ea at the Threshold for Maximal SW Determined from the Animal Model.

After reclassifying the patients for Ea at the threshold for maximal SW established in the animal model (Table 5-3), we still demonstrated mPAP (p=0.022) and PVR (p=0.013) were normal in the Ea ≤ 0.5 mmHg/ml group and elevated in the Ea > 0.5 mmHg/ml group. While HR (p=0.224) and Tau (p=0.729) remained constant, there was a significant increase in dP/dtmin (p=0.014), again explained by the load-dependency of this measurement and the significant rise in ESP (p<0.001) with EDP (p=0.092) remaining constant. Although SW (p=0.903) remained constant between the Ea subgroups, there was a significant reduction in CO (p=0.004), SV (p=0.006), ESV (p=0.035) and EDV (p=0.010) in the Ea > 0.50 group.

Three patients with CTED were identified in the Ea > 0.50 mmHg/ml group indicating occult RV pathology (Figure 5-4) and two CTEPH patients still had RV energetic reserve (Ea ≤ 0.5 mmHg/ml). The three patients with CTED identified in the Ea > 0.5 group had normal mPAP (16.6 ± 2.1 mmHg) and PVR (178 ± 74 dyn/s/cm^5), but were identified to have an elevated afterload as determined by the conductance catheter Ea = 0.69 ± 0.18 mmHg/ml. Interestingly, of these patients, four were the same as those reclassified by the $Ees/Ea_{max\ sw}$ threshold established in the animal model (Figure 5-5).

Table 5-3 Demographics, right heart catheterisation and RV hemodynamic data after classification of patients with CTED or CTEPH by afterload as quantified by Ea at the threshold for maximal SW.

	Ea ≤ 0.50 (n=9)	Ea > 0.50 (n=11)	p-value
Demographics			
CTED, N (%)	7 (77.7)	3 (22.2)	0.073
CTEPH, N (%)	2 (27.3)	8 (72.7)	0.072
Age, years	54 ± 16	52 ± 15	0.777
Male Sex, N (%)	4 (44.4)	6 (54.5)	0.524
BMI, kg/m^2	31.8 ± 8.0	28.6 ± 4.4	0.285
6MWD, m	369 ± 79	377 ± 128	0.873
WHO Class (I/II/III/IV)	9 (100.0)	11 (100.0)	1.000
Right Heart Catheter			
mPAP, mmHg	22.4 ± 7.9	34.8 ± 12.9	0.022
Systolic PAP, mmHg	37.2 ± 16.2	58.2 ± 23.4	0.036
Diastolic PAP, mmHg	12.1 ± 6.5	21.2 ± 9.2	0.022
mRAP, mmHg	7.4 ± 5.1	8.2 ± 3.4	0.588
PCWP, mmHg	10.7 ± 6.5	8.6 ± 2.5	0.422
RV EDP, mmHg	7.7 ± 4.8	8.2 ± 3.4	0.783
SvO_2,%	74.7 ± 4.7	71.5 ± 5.5	0.100
CO, L/min	5.5 ± 1.3	4.6 ± 0.9	0.063
CI, $L/min/m^2$	2.8 ± 0.4	2.4 ± 0.5	0.081
PVR, $dyn/s/cm^5$	176 ± 70	490 ± 266	0.013
RV Hemodynamics			
Heart Rate, BPM	66 ± 10	73 ± 12	0.224
SW, mmHg.ml	1688 ± 622	1727 ± 766	0.903
CO, L/min	5.8 ± 1.1	4.4 ± 0.8	0.004
ESP, mmHg	34.9 ± 9.8	63.9 ± 18.8	<0.001
EDP, mmHg	9.8 ± 4.2	13.2 ± 4.3	0.092
ESV, ml	117.3 ± 39.4	82.4 ± 29.7	0.036
EDV, ml	160.1 ± 37.2	112.7 ± 36.4	0.010
SV, ml	89.8 ± 19.4	63.4 ± 21.0	0.006
EF, %	48.1 ± 15.9	49.1 ± 16.8	0.866
dP/dt max, mmHg/s	398 ± 122	446 ± 180	0.540
dP/dt min, mmHg/s	-355 ± 141	-569 ± 196	0.014
Ea, mmHg/ml	0.39 ± 0.07	1.11 ± 0.46	<0.001
Tau, ms	66.0 ± 15.1	63.0 ± 18.0	0.729

Values are mean ± S.D. or n (%).

CTED = chronic thromboembolic disease; CTEPH = chronic thromboembolic pulmonary hypertension; BMI = body mass index; 6MWD = 6 minute walking distance; WHO Class = world health organisation classification; mPAP = mean pulmonary arterial pressure; mRAP = mean right atrial pressure; PCWP = pulmonary capillary wedge pressure; RV EDP = right ventricular end-diastolic pressure; SvO_2 = mixed venous oxygen saturations; CO = cardiac output; CI = cardiac index; PVR = pulmonary vascular resistance; SW = stroke work; ESP = end-systolic pressure; EDP = end-diastolic pressure; ESV = end-systolic volume; EDV = end-diastolic volume; SV = stroke volume; EF = ejection fraction; dP/dt max = maximum rate of isovolumic contraction; dP/dt min = maximum rate of isovolumic relaxation; Ea = effective arterial Elastance; Tau = time constant of diastolic relaxation; Ees/Ea = Single-beat ventriculoarterial coupling ratio.

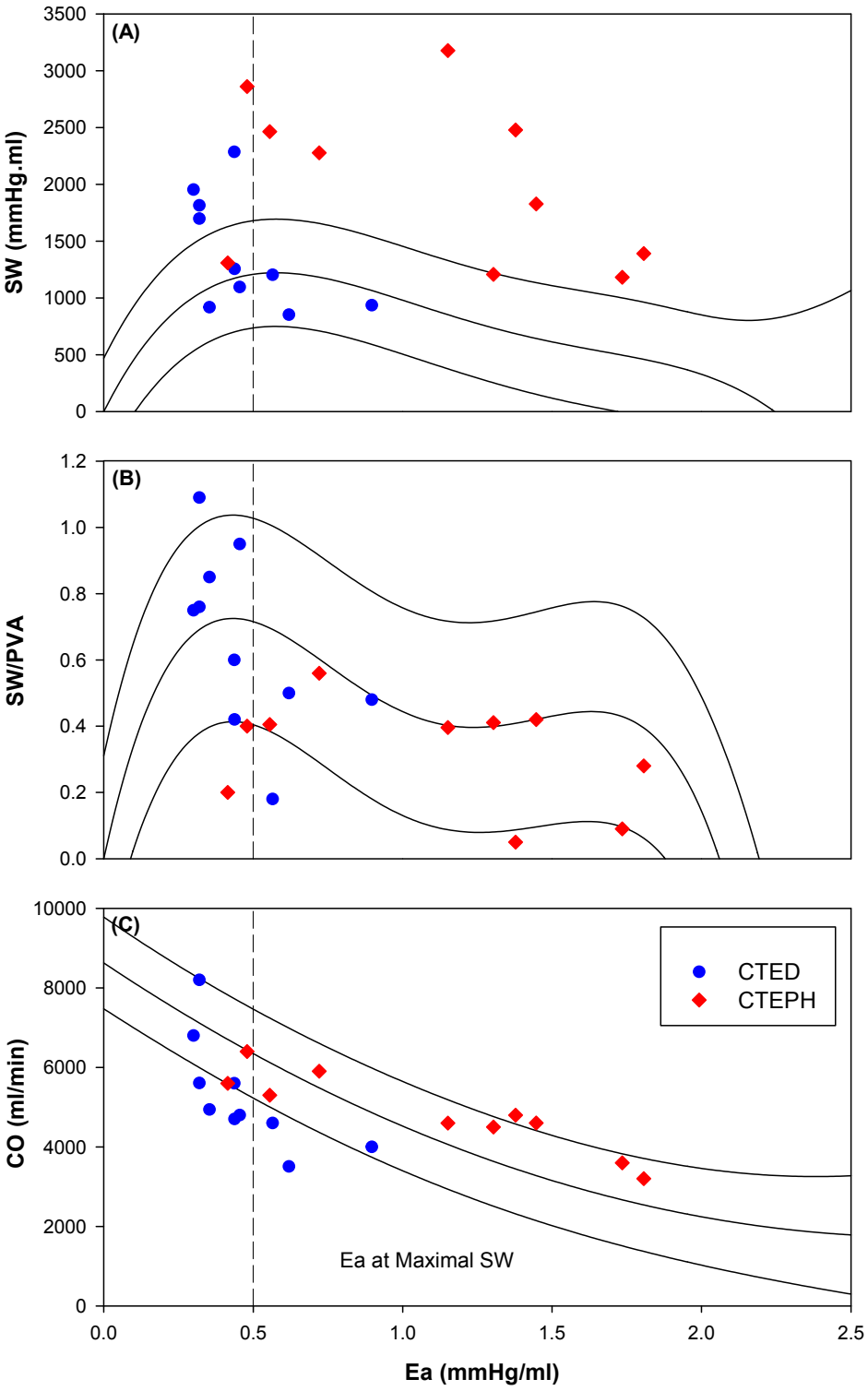

Figure 5-4 The individual data points for the patients with CTED or CTEPH overlaid on top of the mean regression lines determined from the animal model for the relation between afterload quantified by Ea and A) SW; B) SW/PVA; and C) CO.

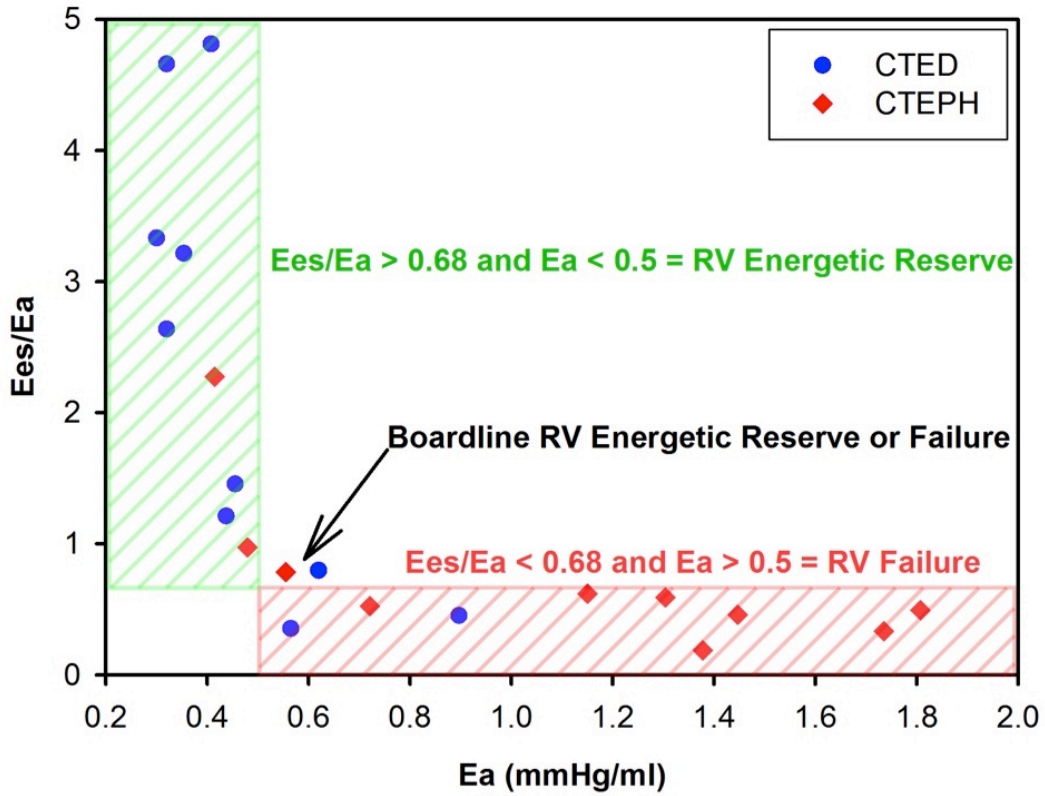

Figure 5-5 The individual data points for the patients with CTED or CTEPH to compare Ees/Ea with Ea. Patients with RV energetic reserve are highlighted in the green-hatched box (Ees/Ea ≥ 0.68 and Ea ≤ 0.5); patients with RV failure are highlighted in the red-hatched box (Ees/Ea < 0.68 and Ea < 0.5).

5.4 Discussion

This is the first study to use the conductance technique to determine the interaction between the RV and PA in a large animal model that can be used to define an Ees/Ea threshold for maximal SW and applied in a cohort of patients with CTED or CTEPH to help more accurately define RV pathophysiology. The interaction between the RV and the PA determines the external work and metabolic efficiency of the ventricle. Animal model data presented in Chapter 4 have shown that maximal SW occurred at an Ees/Ea coupling ratio threshold of 0.68 ± 0.23, beyond which RV dysfunction ensued. Redefining patients with CTED and CTEPH using this $Ees/Ea_{max\ sw}$ threshold, discovered three patients with CTEPH who had an Ees/Ea ≥ 0.68, demonstrating RV energetic reserve and two patients with CTED who had Ees/Ea < 0.68 confirming occult RV dysfunction that was not apparent on current gold-standard right heart catheterization. Any additional afterload increases in these three patients will inevitably result in RV compromise and a reduction in CO. These findings provide novel insight into RV energetics observed in CTED and CTEPH and potentially better identifies those at risk of deterioration. This may also offer a more sensitive assessment of response to treatment than standard right heart catheterization.

The natural history of CTED is poorly defined. This is the first study to use an animal model to define the Ees/Ea coupling ratio at maximal SW and apply this threshold to re-evaluate patients with CTED and CTEPH by assessing RV function. Previous studies have relied on single-beat estimation methodologies, to determine Ees from a real end-systolic point on the baseline PV-loop and a second theoretical point (Bellofiore and Chesler, 2013). This enables RV-PA ventriculoarterial coupling ratio adaption in response to increased loading conditions in PH to be observed. Our group has previously used this methodology to confirm that ventriculoarterial coupling is maintained in patients with CTED, through proportional increases to both Ees and Ea, whereas, in patients with CTEPH, Ea increases disproportionately and the RV uncoupled from the PA (McCabe et al., 2014). However, it remained unclear whether

the degree of uncoupling related to RV dysfunction and patient prognosis. Applying the Ees/Ea threshold from our animal model has now confirmed that although those patients with CTED retain RV energetic reserve, some do not, while most patients with CTEPH have significant RV dysfunction but a few still retain RV energetic reserve. After reclassification, those patients with Ees/Ea uncoupling suffer a reduced SV, and therefore, HR and ESP was significantly increased to maintain adequate CO at rest. Reclassification was made in 25% of our cohort which is clinically important. This inability to increase contractility in the presence of increased afterload has also been observed by Tedford et al. (2013) in a cohort of patients with systemic sclerosis. Patients with associated PH had elevated Ea but relatively smaller increases in Ees than those without PH, resulting in greater uncoupling.

However, simply using Ea may adequately define those that lack RV energetic reserve. The Ea threshold at maximal SW, also reclassified four out of the five patients that were identified using the Ees/Ea coupling ratio threshold. While Ea is normally interpreted as a measure of pulmonary vascular afterload, its dependency on both pressure and volume allows it to be interpreted as a load-independent surrogate measure of RV Function. Ea determines the pumping pressure that the RV has to generate to pump a unit volume of blood into the PA; an Ea> 1 indicates that the RV has to generate a pressure of >1-mmHg for every 1-ml ejected from the ventricle. Implicit in the definition of Ea, Ea can be elevated when ESP increases (as occurs with increasing afterload) but also when SV diminishes due to RV failure. Our measurements of Ea were made at rest but may also be useful to predict exercise-induced RV dysfunction. In a study of patients with PH and normal Ees/Ea coupling at rest who subsequently developed uncoupling during exercise and RV dysfunction, the resting Ea was >0.5 in all subjects, whereas in normal controls, who augmented RV function during exercise, the resting Ea was universally <0.5 (Spruijt et al., 2015). This appears to validate our derived Ea threshold in a separate PH population.

Some limitations of this study must be recognized. First, the clinical study population derives from a pool of selected individuals referred to a single tertiary centre for invasive hemodynamic investigation. The clinical management of this patient group allowed for one venous access site. Therefore, patients did not have biventricular conductance measurements performed and we cannot comment on the effect of ventricular interdependence on our findings. However, all the patients had confirmed normal LV function an echocardiography and normal capillary wedge pressures at right heart catheterization. It is unlikely that any LV systolic or diastolic impairment contributed to our findings of RV dysfunction. It was only possible to recruit ten patients into each of the CTED and CTEPH groups. Therefore, the study is underpowered and it is likely that more hemodynamic parameters would be statistically significant if we were able to recruit large group sizes.

Second, the single venous access site meant it was not possible perform an inferior vena cava (IVC) balloon occlusion to generate load-independent indices of contractility in the patients with CTED and CTEPH. Therefore, we used single beat methodology to determine the Ees/Ea coupling ratio. While this method has not been validated in the RV of patients with PH, it remains commonly used by others (Kuehne et al., 2004; McCabe et al., 2014; Herberg et al., 2013).

Finally, conductance derived PVA is only an approximation of myocardial efficiency. The correlation between PVA and myocardial efficiency excludes the energy consumption costs of excitation contraction coupling and basal metabolism (De Tombe et al., 1993). PVA is therefore an underestimate. De Tombe et al. (1993) demonstrated that the Ea at maximal efficiency is closer to the Ea at maximal SW when calculated directly from MVO_2. However, the use of PVA derived from the same conductance catheterisation as used to determine SW, allows for a simplified approximation of myocardial efficiency, and a precise measure of maximal SW from the pressure volume relation derived from the Ea-SW relationship.

5.5 Summary

The research question for this chapter was to determine if threshold for the Ees/Ea coupling ratio at maximal SW defined in Chapter 4 from the in-vivo porcine model of RV ventriculoarterial interaction could be translated to human physiology to better characterise patients' with symptomatic (Chronic Thromboembolic Pulmonary Hypertension) and asymptomatic (Chronic Thromboembolic Disease) thromboembolic obstruction. This work has shown that the threshold for Ees/Ea at maximal SW determined from the animal model in Chapter 4 has detected RV pathology at rest in patients with CTED and otherwise normal pulmonary hemodynamics, and demonstrated RV energetic reserve in some cases of CTEPH. Detailed ventriculoarterial coupling data may further risk stratify patients with CTED and CTEPH and usefully influence management.

6 Ventricular Remodelling Post Contralateral Transcatheter Aortic Valve Implantation (TAVI): A Ventricular Interdependence Paradox

The aim of this chapter was to determine whether right ventricular (RV) diastolic function improves following left ventricular (LV) afterload reduction following transfemoral (TF) Transcatheter Aortic Valve Implantation (TAVI) due to ventricular interdependence phenomena leading to changes in LV – RV interaction through septal wall reconfiguration. After unloading the LV, ventricular interdependence phenomena would be expected to cause a shift in the septal wall as the inter-ventricular haemodynamics reconfigure. This septal wall reconfiguration has the potential to improve the RV ventriculoarterial coupling (Ees/Ea) ratio, due to the ventricular interdependence phenomena unloading the RV and potentially causing improvements to systolic contractility (Ees).

6.1 Introduction

Over the last decade TF-TAVI has been established as a minimally invasive alternative treatment option to open heart surgery (Cribier et al., 2002) to repair severe aortic valve disease in patients considered unsuitable for surgery due to severe comorbidities (NICE, 2012). A severe comorbidity is a pre-existing cardiovascular risk factor such as hypertension (high blood pressure), chronic kidney dysfunction (loss of kidney function which may require dialysis), chronic obstructive pulmonary disorder (collective term for multiple lung diseases that cause difficulties with breathing due to narrowing or obstruction of the airways), diabetes (elevated blood sugar levels which is know to cause long-term cardiovascular and kidney failure), peripheral arterial disease (fatty deposits build up in the arteries affecting the blood flow around the body) and cancer. The Society of Thoracic Surgeons (STS) Score and European System for Cardiac Operative Risk Evaluation (EuroSCORE II) are used to assess the patients' comorbidities and evaluate their risk of mortality. The scores categorise the patients into groups of low (< 2), medium (2-5) and high (> 5) risk of mortality.

During the TAVI procedure, a balloon-mounted tissue valve is advanced along the patients' femoral artery under fluoroscopic guidance and aligned across the aortic valve. The balloon is inflated inside the prosthetic valve while the heart is rapid paced (RP) between 140 to 210 BPM. RP stabilises the aortic valve and holds the tissue valve in situ for deployment. A RP Test Capture (RPTC) is routinely performed to ensure adequate ablation of LV ejection prior to valve deployment. While TAVI has been shown to have immediate and long-term benefits to LV function (Muratori et al., 2015), data on RV function post TAVI is limited and somewhat confounding. Echocardiographic studies have shown both RV dysfunction (Ito et al., 2014) and no change in RV function (Kempny et al., 2012; Forsberg et al., 2011) following TAVI. Therefore, the mechanisms by which TAVI may influence RV systolic and diastolic performance remain unclear. Maintaining the healthy state of the RV appears to be important for TAVI success. Several parameters associated with poor TAVI outcome e.g. severe mitral regurgitation (Braunwald, 1969) or chronic lung disease (Burrows et al., 1972), also cause elevated pulmonary artery pressures and RV dysfunction.

The TF-TAVI patient group were selected since RV function could be assessed following ventricular remodelling after the stiffened aortic valve was replaced in the contralateral ventricle. An aortic stenosis causes enlargement to the LV chamber and hypotrophy. LV hypertrophy is the enlargement and thickening of the ventricular walls. Replacing the aortic valve will reduce the afterload on the LV and lead to septal wall reconfiguration. The reduction in afterload will cause the inter-ventricular LV pressure to decline and potentially allow the LV volume to decrease. This reduction in LV pressure and volume has the potential benefit of allowing the septal wall to reposition between the LV and RV chamber. The changes in RV chamber morphology will alter RV contractility (Ees) and should subsequently improve the RV ventriculoarterial coupling ratio (Ees/Ea). Therefore, this TF-TAVI cohort offers a clinical example of how altering Ees affects systolic and diastolic function in humans. This study was undertaken to use the conductance technique (Chapter 2) to assess RV function during

TF TAVI with the Edwards Lifesciences (Irvine, California, US) SAPIEN XT or SAPIEN 3 device (Figure 6-1).

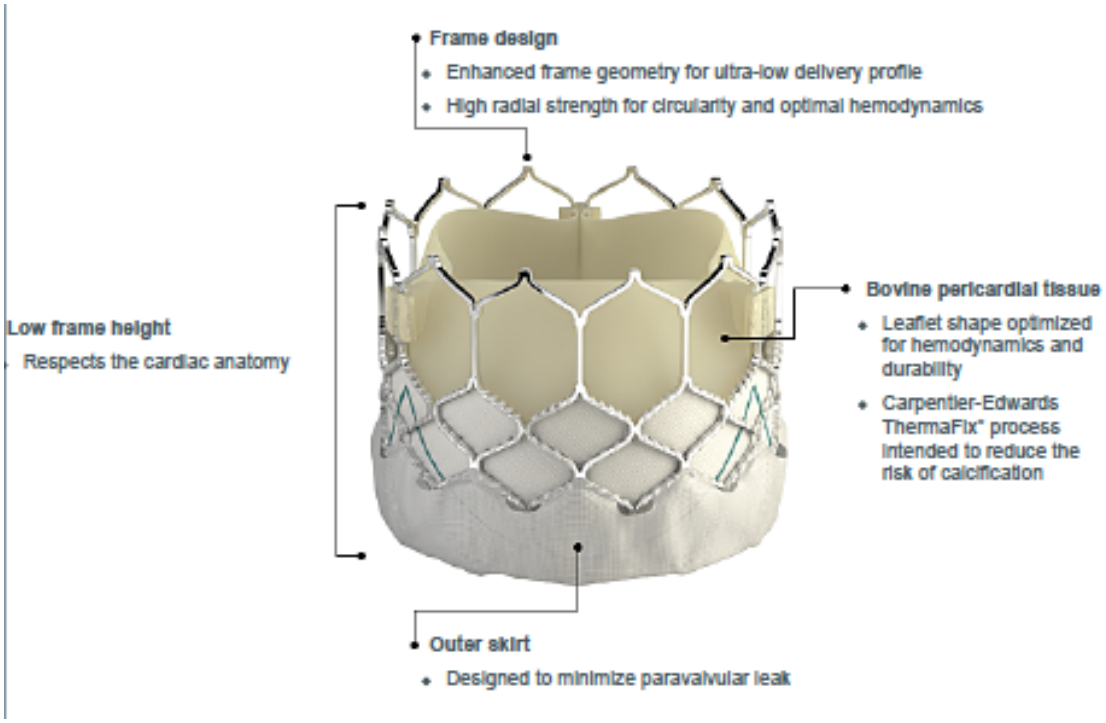

Figure 6-1 Edwards SAPIEN 3 transcatheter heart valve taken from http://www.edwards.com/eu/Products/TranscatheterValves/Pages/sapien3.aspx?WT.ac=S3campaignprod (accessed 30.01.2016)

6.2 Methods

This work was carried out at Papworth Hospital NHS Foundation Trust (Papworth Everard, Cambridgeshire) under the Local Research Ethics Committee approval (REC number 12/EE/0085) as previously described in Section 2.2.4. As previously described in Section 2.2.5, Dr Stephen Hoole recruited the patients into the studies, a Consultant Cardiologist performed the echocardiographic assessments, and the Consultant Interventional Cardiologist responsible for the care of the patient performed the interventional procedures.

6.2.1 Patient Population

Forty patients were screened for eligibility from the TF-TAVI waiting list and studied between June 2013 to February 2016. All patients had high-risk or inoperable aortic valve stenosis determined at a multi-disciplinary team meeting. Exclusion criteria included a myocardial infarction within the preceding 12 weeks, transapical TAVI, tricuspid stenosis, permanent pacemaker and atrial fibrillation. Nine were excluded due to: atrial fibrillation (3), refused consent (3), recruitment into another study (2) and permanent pacemaker (1). Thirty-one patients subsequently consented of whom 8 did not subsequently undergo RV assessment due to: logistical reasons (5), withdrawal of consent (1), occult mitral valve stenosis necessitating surgical replacement of aortic and mitral valves (1) and new-onset atrial fibrillation (1). Twenty-three patients with median age of years 75 (range 68 to 93) were studied under a general anaesthetic (GA sub-group: n = 13) or conscious sedation (CS sub-group: n = 10) protocol. One patient required emergency inotropic support immediately after valve deployment in the GA sub-group and was excluded from the final analysis.

6.2.2 Study Protocol

A schematic flow diagram of the study protocol is shown in Figure 6-2.

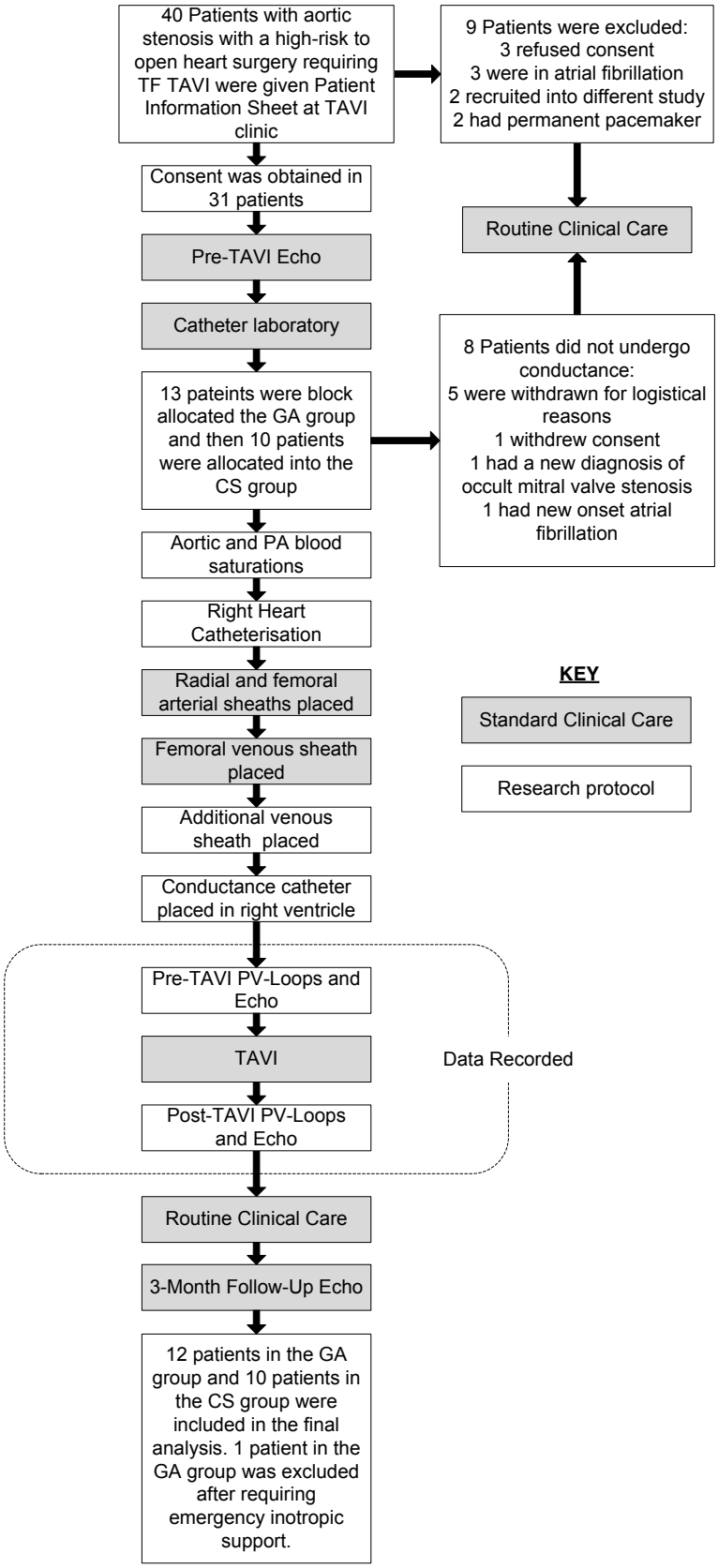

Figure 6-2 Flowchart illustrating the study protocol and timeline

6.2.3 Anaesthetic Protocol

In the GA sub-group, anaesthesia was induced with a bolus of propofol (0.5-1.5 mg/kg) and a remifentanil infusion (0.05-0.1 μg/kg/hr), and atracurium (0.5 mg/kg) were given. Endotracheal intubation was performed, and the patient ventilated with FIO_2 0.5 mixed with sevoflurane 0.8-1.0 MAC (minimum alveolar concentration), titrated to maintain 40-60 BIS (bispectral index). The bispectral index is a measure of the depth of anaesthesia, where 0 represents no anaesthesia and 100 represents a silent electrocardiograph. A BIS value between 40 to 60 indicates the appropriate depth of anaesthesia for a general anaesthetic. In the CS sub-group, a regional ilio-inguinal nerve block was performed using 40-60mL of 1% lidocaine to maintain access-site analgesia. Sedation was induced with a remifentanil infusion (0.05 μg/kg/hr). Flucloxacillin 1g and gentamicin 160mg for antibiotic prophylaxis and a bolus of heparin (70-100 U/Kg) was administered after 16-20F femoral arterial access in all patients. An activated coagulation time was maintained >250 s throughout the procedure. No hemodynamic-altering medication was administered during the study.

6.2.4 Pre-TAVI Cardiac Catheterization

A 7F sheath was placed in the jugular (GA sub-group) or femoral (CS sub-group) veins. A 6F multipurpose catheter was positioned in the pulmonary artery (PA) to measure mean pulmonary pressure and obtain mixed venous blood gas saturations for determination of indirect Fick cardiac output as described in Chapter 2. Right atrial pressure (RA) was also recorded. Blood was also sampled to measure blood resistivity. A 7F 8-Electrode conductance catheter (Millar Instruments, Houston, USA) was connected to an MPVS Ultra (Millar Instruments, Houston, USA) signal-conditioning unit in series with an ADInstruments PowerLab 16/30 Series (ADInstruments, New South Wales, Australia) sixteen-channel amplifier as described in Chapter 2. The conductance catheter was submerged in a bath of saline and the pressure transducer zeroed before introduction via the venous sheath and placement along the long axis of the RV under fluoroscopic guidance (Figure 6-3).

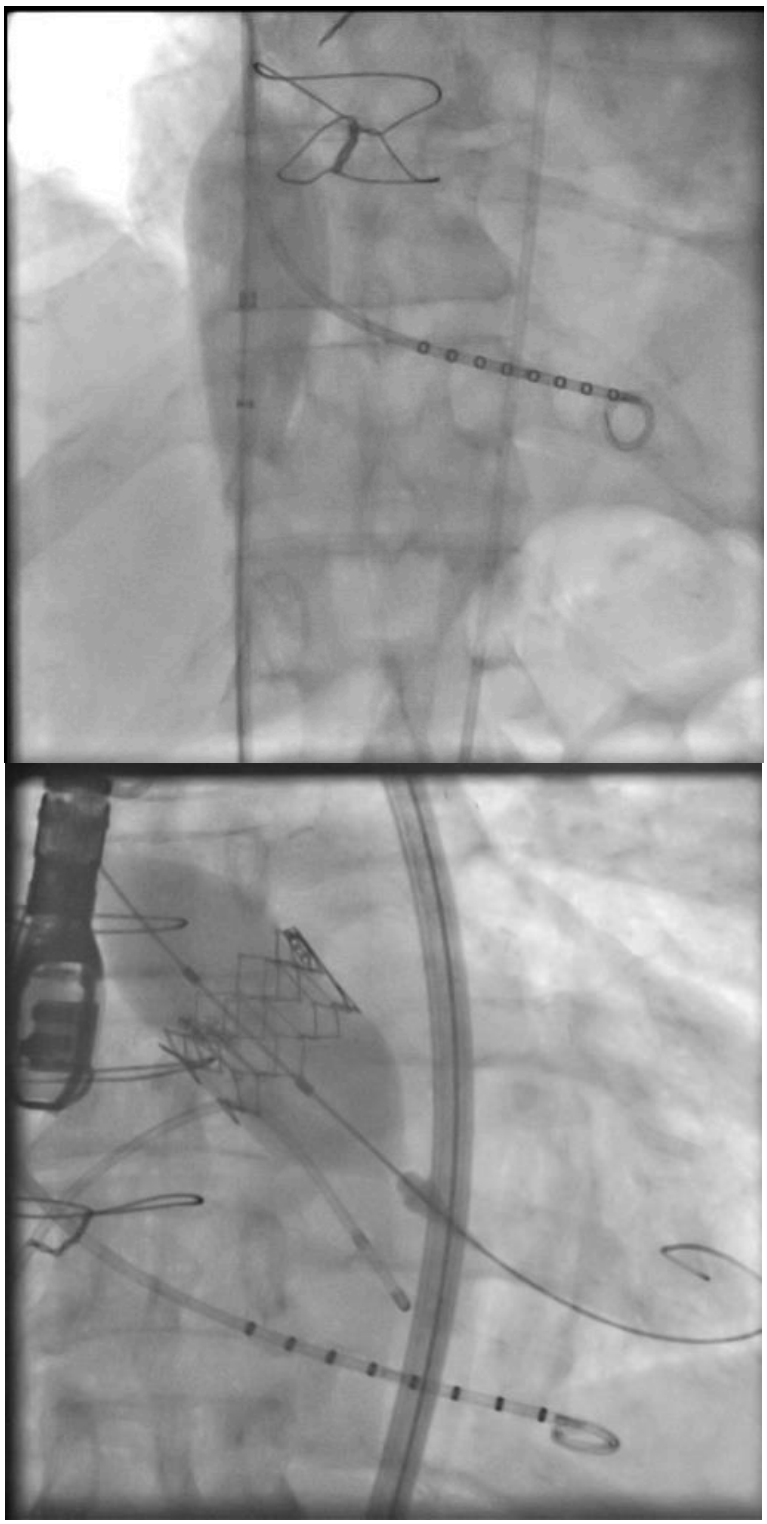

Figure 6-3 (Top) Fluoroscopic image of preload reduction by IVC balloon occlusion and RV PV-loop acquisition with a conductance catheter (Bottom) Fluoroscopic image of a conductance catheter located in the RV during SAPIEN XT valve deployment.

6.2.5 Pressure Volume Loop Data Acquisition

A 6F sheath placed in the right femoral vein for the temporary pacing wire was upsized to a 12F sheath to accommodate an Amplatzer 34mm Sizing Balloon II (St Jude Medical, St Paul, MN, USA) that was positioned in the inferior vena cava (IVC) at the mouth of the RA under fluoroscopic guidance. The conductance technique was used to measure the Pressure-Volume (PV)-loop relationship during ventilation suspension (GA Sub-Group) or breath hold in mid-expiration (CS Sub-Group) to provide a beat-to-beat assessment of RV function at steady state and pre-load reduction during IVC balloon occlusion for at least 5-cardiac cycles (Figure 6-3). PV-loop data was continuously recorded during the procedure including during RP Test Capture (RPTC). PV-loop recordings during pre-load reduction were repeated with a similar IVC balloon occlusion post-TAVI (Figure 6-3). Post-TAVI measurements were recorded a median time of 17 minutes (IQR 12 to 23) after valve replacement.

6.2.6 Echocardiographic Assessments

At an outpatients' clinic appointment transthoracic echocardiographic (TTE) parameters of aortic stenosis severity (peak gradient (mmHg), mean gradient (mmHg) and aortic valve area (cm^2) effective orifice area index (cm^2/m^2)), aortic annulus size (mm), LV function (ejection fraction (Good >50%; Moderate 30-49%; Poor <30%), stroke volume (mL)) and RV function (tricuspid annulus plane systolic excursion – TAPSE (cm), fractional area change – FAC (%) and tissue Doppler imaging – TDI S (cm/sec)) were recorded pre-operatively as described in Chapter 2. In the GA sub-group transesophageal (TEE) and in the CS sub-group TTE echocardiographic parameters of RV and LV function were repeated immediately prior to valve replacement, post-TAVI and again at 3-months (Figure 6-2). TEE was performed using an X7-2t transducer (Philips Healthcare, MA, USA) and an iE33 scanner (Philips Healthcare, MA, USA). TTE was performed using either an X3-1 or S5-1 transducer (Philips Healthcare, MA, USA) with an iE33 scanner (Philips Healthcare, MA, USA).

6.2.7 Rapid Pacing

After baseline echocardiographic and PV-loop during IVC balloon occlusion data acquisition, the sizing balloon was removed from the 12F venous sheath and replaced with a temporary pacing wire that was positioned at the RV apex. RPTC was performed at the operators' discretion aiming for a capture threshold of <1mV and suppression of LV ejection to a systolic BP < 40mmHg. The total number of RP beats was determined for RPTC and post-TAVI by multiplying pacing-rate by the pacing-duration.

6.2.8 TAVI implantation

After baseline echocardiographic and PV-loop data was collected the 6F femoral arterial sheath was then upsized to 18F to allow placement of the Edwards Lifesciences (Irvine, California, US) SAPIEN XT or III device. An Edwards SAPIEN XT or III Transcatheter Heart Valve (Edwards Lifesciences Irvine, California, US), appropriately sized to the aortic annulus, was inserted retrograde via an eSheath Expandable Introducer Sheath (Edwards Lifesciences, Irvine, California, USA) over an Amplatz Extra-stiff 0.035" guidewire. It was positioned under fluoroscopic and echocardiographic guidance across the stenosed valve using the Novaflex+ delivery system and deployed by balloon-expansion during RP determined by the operator. Once a satisfactory result had been confirmed by further imaging, the delivery system and the eSheath were removed using two Perclose Proglide suture-mediated closure devices (Abbott Vascular, Santa Clara, CA, USA), again using RP where necessary to lower systemic pressures and gain haemostasis. Finally, the temporary pacing wire was removed to enable venous access for the sizing balloon and final PV-loop data acquisition during IVC balloon occlusion. The remaining sheaths were then removed, the procedure completed and the patient recovered to the ward.

6.2.9 Offline RV Hemodynamic Measurements

The conductance catheter data was analysed offline using LabChart software (LabChart 7.0, ADInstruments, New South Wales, Australia) as described in Chapter 2. Five steady-state PV-loops were recorded pre-TAVI, post-RPTC and post-TAVI to generate load-dependant parameters of the systolic and diastolic function. A family of PV-loops were recorded during an IVC balloon occlusion pre-TAVI and post-TAVI generated load-independent parameters of RV systolic and diastolic function.

6.2.10 Statistical Analysis

Statistical significance was determined as described in Section 2.2.2.

6.3 Results

6.3.1 Patient Characteristics

Patient demographic data are shown in Table 1. One patient required emergency inotropic support immediately after valve deployment in the GA sub-group and was excluded from the final analysis. Twenty-two patients were included in the final conductance analysis. Although 2 patients in GA sub-group were categorised as low-risk by STS and EuroSCORE II scores, both are categorised as high-risk due to previous NHL mantle radiotherapy and one of these patients also had a porcelain aorta. The severity of the aortic stenosis assessment showed the patients met the TAVI clinical acceptability criteria of peak gradient ≥ 40 mmHg and/or an aortic valve area ≤ 1.0 cm^2. All patients had successful TAVI without complication, and there was zero 30-day mortality and only one death at 6-months follow-up.

Non-Hodgkin Lymphoma (NHL) mantle radiotherapy is used for the treatment of NHL. NHL is a type of blood cancer that develops in the lymphatic system, part of the immune system and damage the correct function of the white blood cells. Radiotherapy is normally used in combination with chemotherapy to treat the lymphoma cells. Porcelain aorta is the extensive calcification of the aorta or aortic arch and can be completely or near complete circumferential. Both pathologies increase cardiovascular risk factors and any patient presenting with either condition would automatically be rated as high-risk to any future cardiovascular procedure.

Table 6-1 Patient demographic data

	TAVI (n = 22)	GA Sub-Group (n=12)	CS Sub-Group (n=10)	P-value
Demographics				
Age, years	78 ± 8	78 ± 9	79 ± 8	0.895
Male sex, %	17 (77.3)	10 (83.3)	7 (70.0)	0.624
BMI, kg/m^2	26.6 ± 5.2	25.1 ± 3.9	28.4 ± 4.4	0.136
Active or ex-smoker	12 (54.5)	8 (66.7)	4 (40.0)	0.391
EuroSCORE II	6.0 ± 3.8	5.2 ± 3.3	7.1 ± 4.6	0.307
STS	3.4 ± 2.0	3.8 ± 2.4	3.1 ± 1.4	0.413
CCS (I/II/II)	18/3/1	10/1/1	8/2/0	0.500
NYHA Class (II/III/IV)	6/14/2	5/7/0	1/7/2	0.104
Hypertension	12 (54.5)	6 (50.0)	6 (60.0)	0.691
Diabetes mellitus	6 (27.2)	2 (16.7)	4 (40.0)	0.348
Previous MI	6 (27.2)	6 (50.0)	0 (0.0)	0.015
Previous PVD	5 (22.7)	2 (16.7)	3 (30.0)	0.624
Previous CABG	11 (50.0)	7 (58.3)	4 (40.0)	0.670
Previous BAV	8 (36.3)	6 (50.0)	2 (20.0)	0.204
Hb, g/L	122.7 ± 18.2	126.8 ± 22.0	116.7 ± 11.6	0.339
Cr, mg/dL	1.40 ± 0.49	1.43 ± 0.50	1.36 ± 0.50	0.488
Right Heart Catheter				
MRAP, mmHg	10.0 ± 5.8	9.2 ± 3.3	11.1 ± 7.9	0.715
MPAP, mmHg	24.4 ± 11.2	20.1 ± 4.4	29.5 ± 14.5	0.120
PA Sats,%	72.0 ± 7.2	76.9 ± 3.8	66.0 ± 5.4	<0.001
Ao Sats, %	96.8 ± 1.9	97.3 ± 1.5	96.1 ± 2.2	0.159
CO, L	5.3 ± 1.3	5.6 ± 1.5	4.8 ± 0.9	0.118
CI,	2.8 ± 0.7	3.0 ± 0.7	2.5 ± 0.5	0.059
SVI	41.3 ±	47.1 ± 13.1	34.1 ± 9.3	0.016
Severity of Aortic Stenosis				
Peak Gradient, mmHg	73.7 ± 28.0	71.3 ± 32.2	77.0 ± 22.5	0.655
Mean Gradient, mmHg	43.4 ± 17.4	41.8 ± 19.8	45.5 ± 14.3	0.637
AVA, cm^2	0.72 ± 0.13	0.69 ± 0.14	0.76 ± 0.12	0.250
EOA Index,	0.38 ± 0.07	0.37 ± 0.05	0.40 ± 0.08	0.348
Annulus size, mm	22.4 ± 2.5	22.5 ± 2.1	22.1 ± 3.1	0.728
LVH	16 (72.7)	8 (66.7)	8 (80.0)	0.646

Values are mean ± S.D. or n (%). P-values displayed for GA Sub-Group vs. CS Sub-Group.

BMI = body mass index; STS = society of thorasic surgeons risk score; CCS = Canadian cardiovascular society functional classification of angina; NYHA Class = ; MI

= myocardial infarction; PVD = peripheral vascular disease; CABG = coronary artery bypass graft; BAV = balloon aortic valvulaplasty; Hb = Haemoglobin; Cr = Creatinine; MRAP = mean right atrial pressure; MPAP = mean pulmonary arterial pressure; AVA = aortic valve area; EOA Index = effective orifice area Index; LVH = left ventricular hypotrophy.

6.3.2 Echocardiographic Assessment

Echocardiographic assessment performed in the catheter laboratory demonstrated that there was an immediate reduction in transaortic gradients after the prosthetic valve was implanted (Table 6-2). This reduction in transaortic gradients was preserved at the 3-month follow-up assessment. Although baseline RV echocardiographic function was normal (Table 6-2), 5 individual patients were identified with RV dysfunction at baseline (included within the 8 identified by RV haemodynamic assessment). There was no improvement in RV function following TAVI at 3-months.

Table 6-2 Echocardiographic data

	Pre-TAVI	Post-TAVI	3-Month Follow-Up	P value
Aortic Valve Area				
Peak Gradient, mmHg	73.7 ± 28.0	11.4 ± 3.6	21.0 ± 11.6	<0.001
Mean Gradient, mmHg	43.4 ± 17.4	5.4 ± 1.8	11.5 ± 6.2	<0.001
AVA, cm^2	0.72 ± 0.13	2.25 ± 0.55	1.83 ± 0.35	<0.001
EOA Index,	0.38 ± 0.07	1.18 0.26	0.98 ± 0.22	<0.001
EF, %	53.4 ± 13.4	-	55.3 ± 8.1	0.890
RV Function				
TAPSE, cm	1.94 ± 0.55	-	1.80 ± 0.61	0.387
TDIs, cm s^{-1}	10.5 ± 2.5	-	11.0 ± 2.9	0.288
FAC, %	47.4 ± 10.3	42.7 ± 9.8	47.2 ± 7.2	0.481
RV Function CS - Sub				
TAPSE, cm	2.25 ± 0.51	2.15 ± 0.50	1.84 ± 0.58	0.084
TDIs, cm s^{-1}	10.7 ± 2.7	10.8 ± 1.8	11.1 ± 2.1	0.815
FAC, %	42.2 ± 11.4	45.1 ± 8.8	44.2 ± 10.0	0.507

Values are mean ± S.D. Pre-TAVI vs. 3-Month Follow-Up p-values calculated using paired t-tests. Pre-TAVI vs. Post-TAVI vs. 3-Month Follow-Up p-values calculated using one-way repeated measures ANOVA.

AVA = aortic valve area; EOA Index = effective orifice area Index; EF = ejection fraction. TAPSE = tricuspid annular plane systolic excursion; TDIs = tissue Doppler imaging; FAC = fractional area change.

6.3.3 RV Hemodynamic Assessment

Baseline RV hemodynamic systolic (Ees/Ea = 1.1 ± 0.4 mmHg/ml) and diastolic (Tau = 58.0 ± 15.5 ms) (McCabe et al., 2014) function was normal. However, 8 patients were identified with evidence of RV diastolic dysfunction (Tau > 56.2 ± 6.7 ms) (McCabe et al., 2014). RPTC delivered a median number of 24 RP beats (IQR 19 to 37) at a mean rate of 198 ± 16 BPM, compared to a median number of 120 RP beats (IQR 87 to 205) accrued post-TAVI at a mean rate of 201 ± 18 BPM. RV diastolic dysfunction was evident after RPTC prior to valve implantation and stunning was apparent late after valve implantation at the time point of the post-TAVI measurements. Table 6-3 and Figure 6-4 shows that RPTC prior to valve implantation caused a reduction in diastolic function increasing Tau ($p = 0.003$) and EDP ($p < 0.001$). RV diastolic dysfunction persisted immediately after valve implantation (Tau: $p < 0.001$; EDP: $p < 0.001$). Load-independent indices of systolic contractility: Ees ($p = 0.020$) and PRSW ($p = 0.001$) both diminished post-TAVI. Since Ea remained constant ($p = 0.478$), this reduction in systolic contractility caused right ventriculoarterial (Ees/Ea) uncoupling ($p = 0.004$) indicating that the RV was failing. Although the gradient of EDPVR slope remained constant ($p = 0.693$), the upward and leftwards shift of the EDPVR slope suggested a reduction in ventricular compliance and increased diastolic dysfunction post-TAVI (Figure 6-5). We observed a significant increase in ESV following TAVI (Table 6-3), but the remaining indices of RV function remained unchanged after TAVI.

Table 6-3 RV hemodynamic data

	Pre-TAVI	Post-RPTC	Post-TAVI	P Value
Heart rate, beats/min	68 ± 13	69 ± 16	72 ± 17	0.350
Systolic BP, mmHg	133 ± 29	-	136 ± 25	0.936
Diastolic BP, mmHg	58 ± 14	-	60 ± 11	0.906
Mean BP, mmHg	80 ± 19	-	82 ± 15	0.957
ESP, mmHg	31.6 ± 15.5	42.6 ± 18.7	34.0 ± 15.2	<0.001
EDP, mmHg	8.5 ± 5.8	11.6 ± 6.1	10.7 ± 5.9	<0.001
ESV, ml	87.9 ± 31.4	98.6 ± 42.7	113.1 ± 39.7	0.007
EDV, ml	131.4 ± 40.4	142.8 ± 47.2	147.1 ± 43.1	0.173
SV, ml	81.9 ± 25.4	78.4 ± 29.8	87.8 ± 25.0	0.150
SW, mmHg.ml	1542 ± 529	1751 ± 798	1508 ± 502	0.278
CO, L/min	5.4 ± 1.3	5.1 ± 1.8	6.0 ± 1.6	0.187
EF, %	59.9 ± 13.8	54.1 ± 19.3	55.2 ± 13.3	0.244
dP/dt max, mmHg/s	460 ± 154	527 ± 169	436 ± 157	<0.001
dP/dt min, mmHg/s	-259 ± 119	-341 ± 144	-253 ± 124	0.028
Tau, ms	58.0 ± 15.5	72.3 ± 21.8	80.1 ± 24.4	<0.001
Ea, mmHg/ml	0.38 ± 0.15	-	0.40 ± 0.18	0.478
Ees, mmHg/ml	0.39 ± 0.19	-	0.28 ± 0.17	0.020
EDPVR, mmHg/ml	0.08 ± 0.06	-	0.08 ± 0.07	0.693
Ees/Ea	1.10 ± 0.40	-	0.80 ± 0.37	0.004
PRSW, mmHg/ml^3	21.0 ± 10.5	-	14.7 ± 8.4	0.001

Values are mean ± S.D. Pre-TAVI vs. Post-TAVI p-values calculated using paired t-tests. Pre-TAVI vs. Post-RPTC vs. Post-TAVI p-values calculated using one-way repeated measures ANOVA.

BP = Blood Pressure; RP = Rapid Pacing; ESP = end-systolic pressure; EDP = end-diastolic pressure; ESV = end-systolic volume; EDV = end-diastolic volume; SV = stroke volume; SW = stroke work; CO = cardiac output; EF = ejection fraction; dP/dt

min = maximum rate of isovolumic relaxation; dP/dt max = maximum rate of isovolumic contraction; Tau = time constant of diastolic relaxation; Ea = effective arterial Elastance; Ees = end-systolic Elastance; EDPVR = end-diastolic pressure volume relationship; Ees/Ea = ventriculoarterial coupling ratio; PRSW = preload recruitable stroke work.

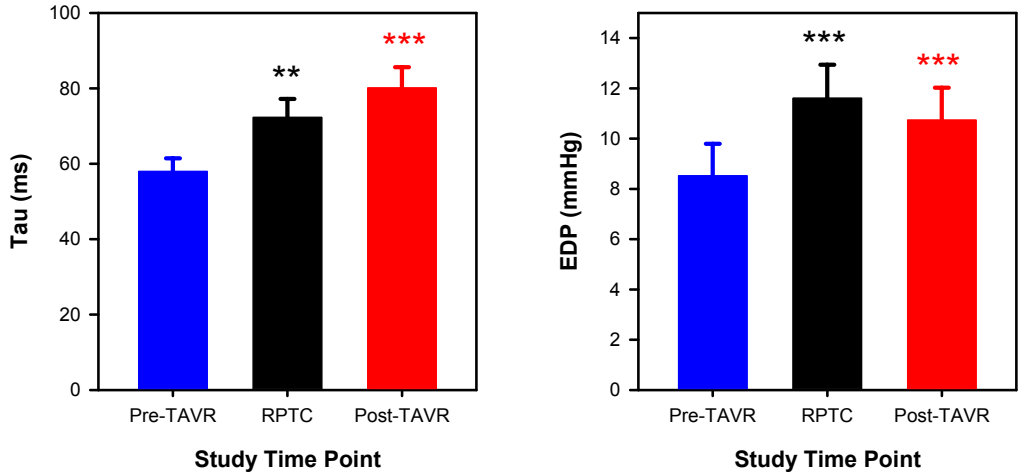

Figure 6-4 Comparisons of RV diastolic function (Left) Tau and (Right) EDP at baseline (Pre-TAVI – Blue) after rapid pacing test capture (RPTC – Black) and after valve deployment (Post-TAVI - Red). ** p < 0.01, *** p < 0.001.

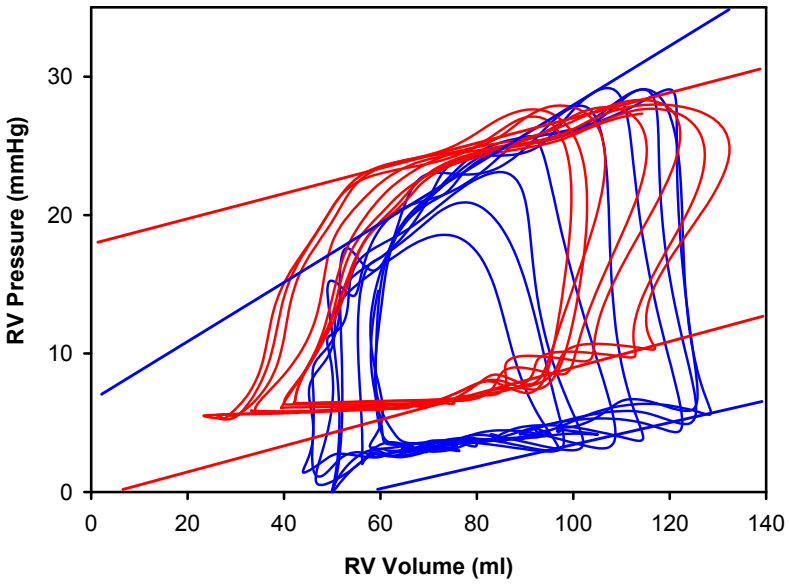

Figure 6-5 Families of RV PV-loops recorded at baseline (Pre-TAVI - Blue) and after valve deployment (Post-TAVI - Red) during preload reduction with IVC balloon occlusion to determine Ees and EDPVR

6.3.3.1 Comparisons between Early and Late Recovery

Comparisons of RV function during early recovery (+1 mins after valve deployment) with late recovery (median +17 mins after valve deployment) demonstrated persistent diastolic dysfunction (Figure 6-6: tau - early +50.8% vs. late +42.2%, $p = 0.86$; RVEDP - early +73.7% vs. late +32.4%, $p < 0.001$). However, systolic function reached supra-baseline levels at +1 minute into recovery that subsequently deteriorated at +15 mins post valve deployment (Figure 6-6: dP/dt max – early +40.4% vs. late – 6.4%, $p < 0.001$; SW – early +35.29% vs. -13.0%, $p < 0.001$). This observation is consistent with RV stunning.

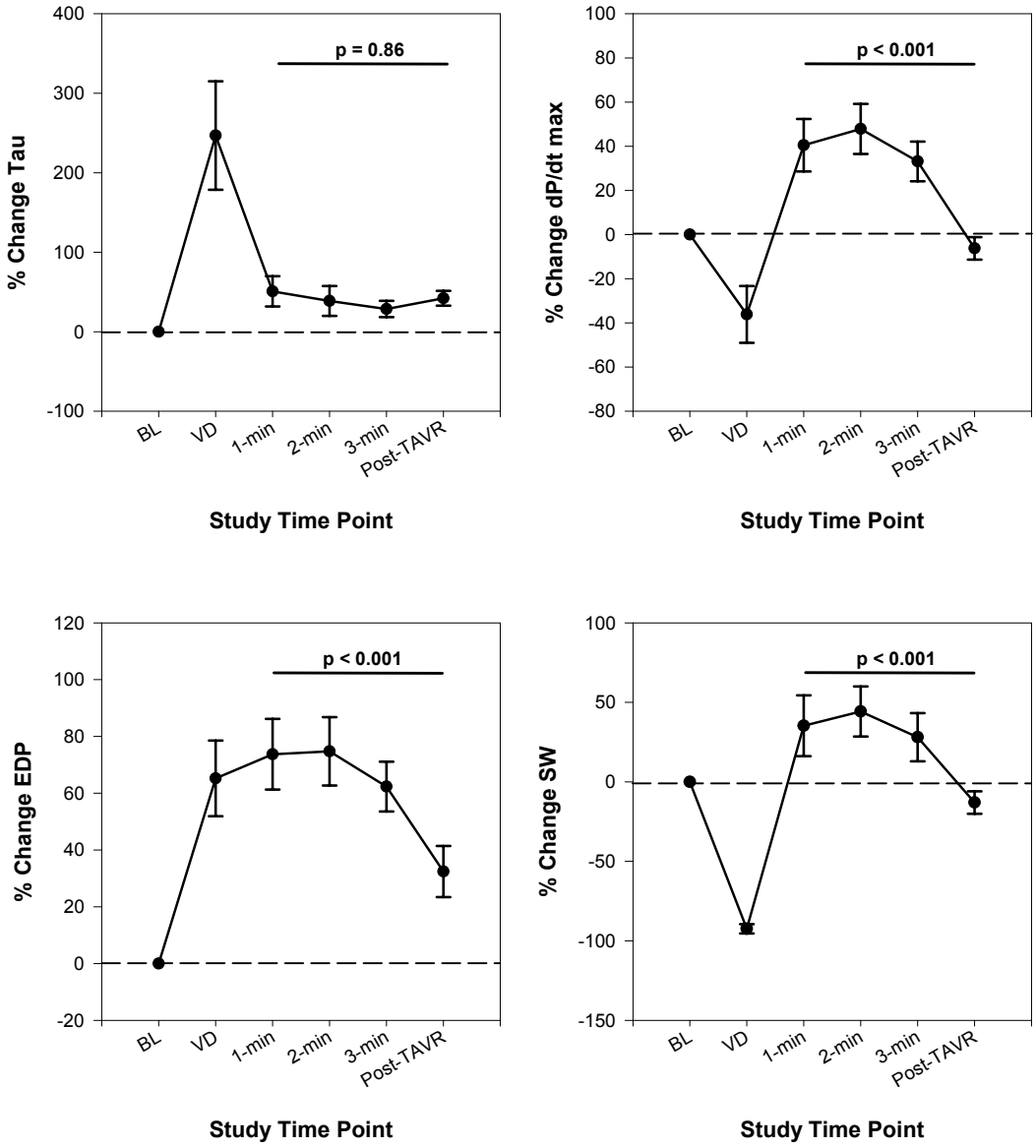

Figure 6-6 Comparisons of diastolic function (Top Left) Time constant of isovolumic relaxation – tau, (Bottom Left) end-diastolic pressure – EDP, and systolic function (Top Right) maximal rate of isovolumic contraction – dP/dt max, (Bottom Right) stoke work – SW, normalised to pre-TAVI values at baseline (pre-TAVI), during valve deployment (VD) at 1, 2, 3 mins post valve deployment and late (median 17 min: IQR 12 to 23) after valve deployment (post-TAVI). Mean ± SEM.

6.3.3.2 Comparisons between Anaesthetics Protocols and Pacing Burden

There were no significant differences in RV hemodynamic data between the GA and CS Sub-Groups (Figure 6-7). However, there was a significant two-fold increase in the number of RP paced beats delivered at the post-TAVI time point in GA Sub-Group compared to CS Sub-Group ($p < 0.001$). When comparing those with the highest pacing burden with the lowest, we were not able to determine a threshold below which RV dysfunction did not occur. The increase in RV diastolic dysfunction measured by Tau (Figure 6-8A) and EDP (Figure 6-8B) was immediately apparent after a minimal period of RP, and we did not observe any dose effect from greater pacing durations.

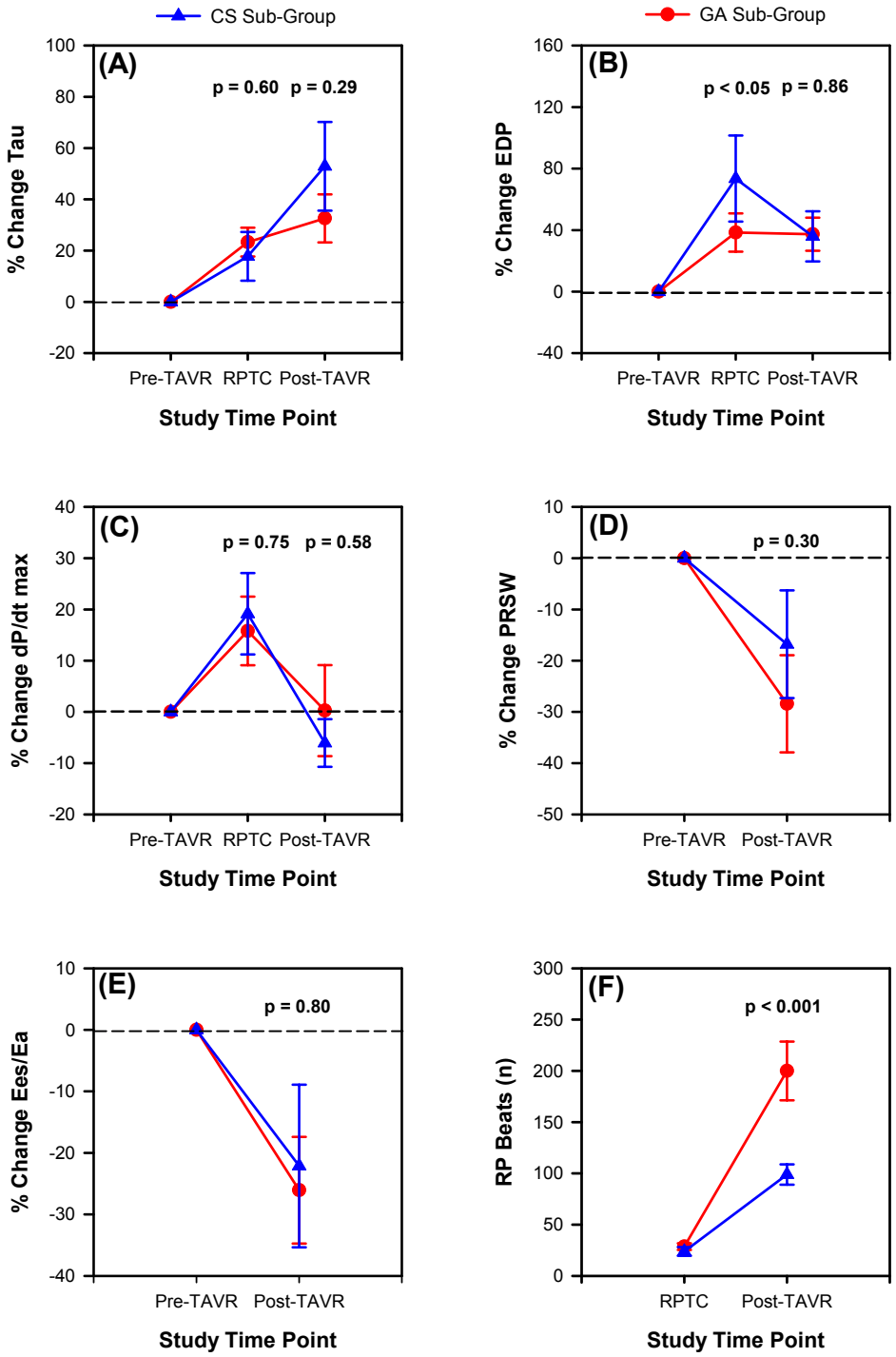

Figure 6-7 Comparisons between GA Sub-Group (blue) and CS Sub-Group (red) for: (A) Tau, (B) EDP, (C) dP/dt max, (D) PRSW, (E) Ees/Ea normalised to pre-TAVI values, and (F) number of RP beats after RPTC and Post-TAVI. Mean ± SEM.

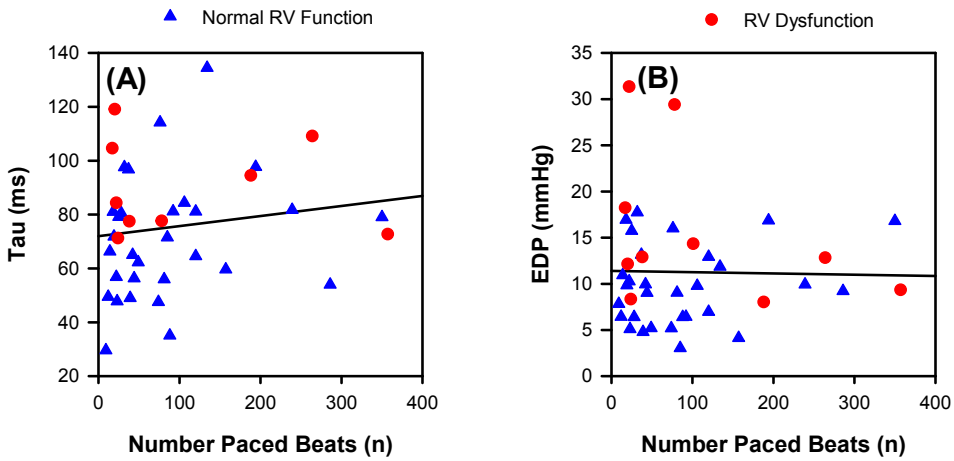

Figure 6-8 Comparisons of pacing burden and diastolic function for (A) Tau and (B) EDP displayed for those with baseline normal RV function (Blue) and RV dysfunction (Red).

6.3.3.3 Comparisons between Baseline RV Dysfunction and Pulmonary Hypertension

Those patients with pre-existing RV dysfunction identified by baseline echocardiographic assessment, were confirmed by hemodynamic assessment to have worse Tau ($p < 0.01$) and EDP ($p = 0.05$) at baseline (Figure 6-9A and B). RPTC caused RV dysfunction in those with or without RV dysfunction and the decline in RV function was not dramatically different between groups (Post RPTC ΔTau: +15.5 ± 3.0% vs. +22.5 ± 24.6%, $p = 0.516$; ΔEDP: +35.5 ± 27.3% vs. +59.1 ± 72.1%, $p = 0.773$). In those with RV dysfunction at baseline, Tau and to some extent EDP appeared to plateau maximally after TAVI whereas there was further decline in those with RV functional reserve (Post TAVI ΔTau: +17.5 ± 13.7 vs. +47.8 ± 44.7%, $p = 0.205$; ΔEDP: +19.8 ± 23.6 vs. +42.1 ± 45.0%, $p = 0.308$), so that by the end of the procedure, the degree of RV dysfunction measured by Tau was similarly impaired in both groups.

Patients with pre-existing pulmonary hypertension had an elevated EDP at baseline but there was no significant difference in response to RPTC identified between groups with or without PH (ΔTau: +23.6 ± 15.9% vs. +19.5 ± 25.3%, $p = 0.70$; ΔEDP: +35.1 ± 29.7% vs. +62.6 ± 76.5%, $p = 0.487$) (Figure 6-9C and D). However, in those patients with pulmonary hypertension, Tau continued to worsen post TAVI, whereas RV dysfunction numerically plateaued at a level that was less impaired in those with normal pulmonary pressures (ΔTau: +36.9 ± 26.3% vs. +17.9 ± 58.8%, $p = 0.420$; ΔEDP: +15.8 ± 27.7% vs. +47.3 ± 44.1%, $p = 0.102$).

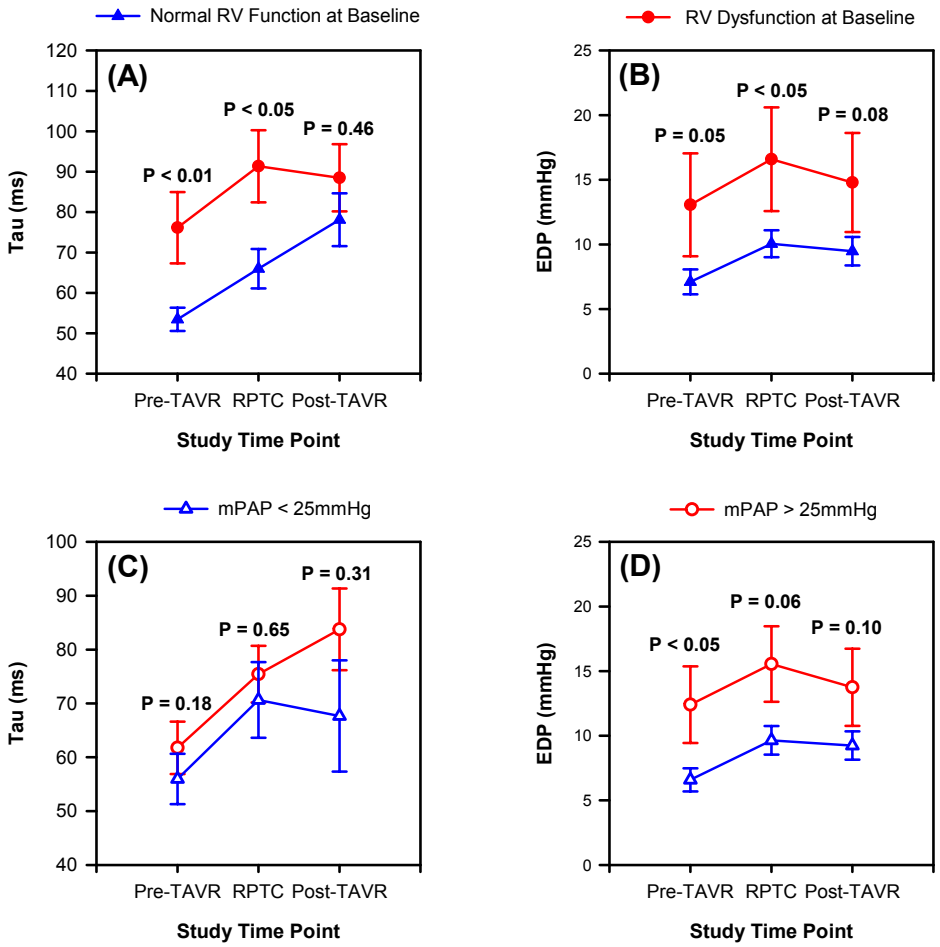

Figure 6-9 Comparison of the effect of RP on subgroups with pre-existing RV dysfunction and diastolic function (A) Tau, (B) EDP, at baseline (Pre-TAVI), after the pacing check (Post-RPTC) and late after the valve was deployed (Post-TAVI). Comparisons of pre-existing pulmonary hypertension and diastolic function (C) Tau, (D) EDP, at baseline (Pre-TAVI), after the pacing check (Post-RPTC) and late after the valve was deployed (Post-TAVI). P-values are displayed between groups.

6.4 Discussion

This is the first study to use the conductance technique to determine the effect of balloon-expandable TF TAVI implantation on right ventricular function in humans. We have established that RP during balloon-mounted TAVI implantation causes RV dysfunction that persists until at least the end of the procedure and was apparent and near-maximal after a relatively short period of RP required for RPTC. There was no echocardiographic improvement in RV function at 3-months post-TAVI, indicating that unloading the LV with TAVI did not transmit beneficial ventricular interdependence benefits to the RV. We postulate that the RV dysfunction is mediated by global ischemia precipitated by RP. We observed an early transient augmentation of RV systolic function due to reactive hyperemia to repay the oxygen debt after RP that dissipates to reveal RV dysfunction. Recovery to baseline was confirmed by echo at 3-months. These findings provide persuasive evidence of RV stunning in humans after TF TAVI and this may influence practice, particularly in patients with pre-existing pulmonary hypertension and RV failure.

Accurate assessment of RV function is important as it predicts 1-year mortality rates (Leon et al., 2010). Echo studies have provided inconsistent findings on the effect of TAVI on RV function, ranging from RV dysfunction (Ito et al., 2014) to improved RV function compared to SAVR (Forsberg et al., 2011). Conventional 2D echo assessment of RV function is challenging due to the complex geometry of the RV, and this may explain the discrepancies between studies (Lindman et al., 2015). More robust RV assessment using cardiac MR and 3D echo now report that RV function is maintained following SAVR (Crouch et al., 2015; Keyl et al., 2016) and that TAVI may lead to RV systolic dysfunction (Crouch et al., 2015). However, beat-by-beat, load independent assessment of RV function inter-operatively during TAVI can only be achieved by conductance catheter assessment. The mechanism of RV dysfunction observed following TAVI has not been elucidated.

The term myocardial stunning describes the phenomena of persistent contractile dysfunction after an ischemic insult, despite normal coronary flow in the absence of infarction that is completely reversible (Braunwald and Kloner, 1982; Bolli, 1990). This has been described in animal models of supply ischemia, which showed that LV stunning is proportional to the duration of the ischemic insult (Heyndrickx et al., 1975; Preuss et al., 1987). Exercise-induced demand ischemia has been shown to cause LV stunning in animals (Homans et al., 1991) and humans (Rinaldi et al., 1999; Barnes et al., 2002) as can RP-induced global supply and demand ventricular ischemia (Turer et al., 2011).

RP is required to transiently ablate LV contractility enabling optimal TAVI positioning and deployment without the premature expulsion of the balloon-mounted valve from inadvertent LV ejection. Great lengths are taken to ensure adequate LV suppression (confirmed by a systolic <40mmHg) and stable ventricular capture by the temporary pacing wire by sometimes repeated testing (RPTC). RP is also sometimes used to help gain haemostasis. However, valves are emerging that maintain flow through the prosthesis, can be repositioned and are introduced through smaller sheathes, perhaps negating the need for RP.

The RV appears to be exquisitely sensitive to the effects of RP. In this study, we have confirmed that even a short burst of RP required to assess RPCT was enough to cause near-maximal diastolic dysfunction. GA and CS sub-groups both had similar nadirs of RV dysfunction, despite the former having a two-fold greater number of RP beats delivered. In addition, those with preserved RV function and normal pulmonary pressures remained susceptible to significant RV dysfunction. Our data suggests there is no safe RP threshold – even a short burst of rapid pacing is deleterious to RV function. Although RP has previously been described as a safe and effective method to provide balloon stability for balloon aortic valvuloplasty (Daehnert et al., 2004), our data demonstrates that significant diastolic dysfunction is observed after as little as 24 RP

beats, equivalent to only 7 seconds of RP. We observed modest further worsening of RV dysfunction despite up to 5-fold more RP beats (median 120; IQR 87 to 205) required for the actual TAVI implantation. Attempting to mitigate the effects of RP on the RV by RP dose reduction in CS sub-group, did not improve matters.

We demonstrated a transient augmentation of RV systolic function immediately after the valve was deployed and the RP was switched off, although diastolic dysfunction persisted during this period. We believe this can be explained by reactive hyperaemia – an augmentation of coronary flow due to coronary vasodilatation to repay the oxygen debt (Heyndrickx et al., 1975). During hyperemia there is an increase in microvascular volume and myocytes adjacent to these vessels are stretched, opening stretch-activated calcium channels, causing calcium influx and an augmentation of calcium-dependent myofibrillar contractility, known as the Gregg effect (Gregg, 1963). We have previously described this in a model of LV supply ischemia (Hoole et al., 2010) and this hyperemic response masks stunning in the early phase of reperfusion (Stahl et al., 1986). Interestingly, diastolic dysfunction remains depressed during this period, and this may be due to a scaffold effect from distended coronary and collateral vessels during hyperemia acting on the thin walled RV that stiffens the ventricular cavity (Hoole et al., 2010). Alternatively, this may be explained by the sequence of the ischemic cascade -diastolic dysfunction is more profound as it occurs earlier.

There was an increase in absolute RV volumes following valve implantation explained by ventricular interdependence across the shared septum; LV afterload diminishes post-TAVI, reducing LV volume and enabling ventricular reconfiguration and RV volume expansion. However, this did not improve RV ventriculoarterial coupling. To the contrary, the simultaneous reduction in Ees and PRSW uncoupled the RV from the PA, reducing efficiency. The interdependence of the ventricular cavities due to the shared septum should result in biventricular effects (Saleh et al., 2006) and by unloading the

LV, RV functional improvement should follow (Santamore and Dell'Italia, 1998b), but this was not observed.

There are a number of limitations that need to be taken into account when interpreting the results of this study. First, although the conductance technique allowed the operator to determine the real-time load-independent beat-to-beat assessment of RV function, it was not ethically possible to perform a higher risk additional invasive procedure during the 3-month follow-up appointment. We were only able to measure load-dependant echocardiographic parameters of RV function, but these appeared to confirm that RV function returned to baseline – a pre-requisite of the definition of stunning.

Second, it is not possible to accurately assess RV echocardiographic function with TEE. Difficulties in the alignment of the Doppler beam with the tricuspid annulus can cause significant underestimation of TAPSE and RV TDIs. Therefore, we were not able to present RV data immediately following valve deployment in the GA sub-group. However, we were able to present consistent TTE data for the CS sub-group and have no reason to believe these findings are not valid for the GA sub-group.

Third, we did not confirm ischemia-induction by coronary sinus lactate sampling after RP, although this has been confirmed previously (Bagger et al., 1983). Nor were we able to assess coronary flow as this was impractical in an already complex human study. Again, the effect of RP on coronary flow and the subsequent reactive-hyperemia has been previously published (Hodgson and Mancini, 1985). The RV temporal dysfunction data post-TAVI are consistent with this being the most plausible mechanism.

Fourth, the use of volatile anaesthetics can depress ventricular function (Horan et al., 1977; Pagel et al., 1993) but can also be cardioprotective (Bland and Lowenstein, 1976), which could have influenced the degree of RV stunning observed. However, RV

stunning occurred to a comparable degree in the GA and CS subgroups, and we believe the anaesthetic protocol had minimal effect on RV dysfunction observed.

Fifth, this study population derives from a pool of patients who met the clinical acceptability criteria for TF TAVI. This patient group were high risk or inoperable and as a result of comorbidity had a degree of pulmonary hypertension (mPAP 24.4mmHg for the cohort) and possibly some pre-existing RV dysfunction. Despite this, patients acted as their own control and our observations rem Forsbergain valid.

Finally, we were not able to establish a dose-response to RP that would have strengthened our assertion that RP was the cause of RV stunning. However, the RV dysfunction occurred without an observable threshold; it was an all-or-nothing effect

6.5 Summary

The research question for this chapter was to determine whether right ventricular (RV) diastolic function improves following left ventricular (LV) afterload reduction following transfemoral (TF) Transcatheter Aortic Valve Implantation (TAVI) due to ventricular interdependence phenomena leading to changes in LV – RV interaction through septal wall reconfiguration. This work has demonstrated that although ventricular interdependence phenomena caused septal reconfiguration increasing RV volumes after valve deployment due to the reduction in LV afterload; RP-induced ischemia was found to cause RV stunning after valve deployment. RV systolic and diastolic dysfunction was apparent in the stunned ventricle late after the RP-induced ischemic insult. Therefore, rather than the hypothesised improvements in RV ventriculoarterial coupling and diastolic function, uncoupling and diastolic dysfunction was observed.

7 Conclusions and Future Work

In recent years, an increasing body of evidence has emerged postulating the role of ventriculoarterial uncoupling as a marker of RV adaptation and RV maladaptation, and how this may offer new insight into the pathophysiology of pulmonary hypertension. While the relationship between the pressure-volume relationship and ventriculoarterial coupling had been extensively described in the LV and used to determine optimal conditions for the efficient transfer to blood from the ventricle into the aorta, it remained unclear whether this relationship could be translated to the thinner walled RV that pumps at lower pressures against a more compliant pulmonary vascular system. The studies in this thesis were therefore undertaken to assess whether ventriculoarterial uncoupling due to pressure overload or sub-optimal contractility caused RV diastolic dysfunction. These studies comprised of the development of an in-vivo porcine model of RV ventriculoarterial coupling to define the optimal RV – PA ventriculoarterial coupling conditions. This animal model of RV-PA ventriculoarterial coupling was then translated in two clinical patient groups that have RV dysfunction: chronic RV afterload in patients with CTED and CTEPH, and assessing RV-LV ventricular interdependence through septal wall reconfiguration after TAVI.

7.1 Animal Model

An in-vivo animal model was developed to determine the PV-loop derived maximal SW-Ea and maximal SW-Ees/Ea relationships during acute increases to PA afterload. This work has shown that although maximal efficiency improves our understanding of ventriculoarterial coupling, in RV failure the maximal SW derived from the pressure-volume relationship, is a key determinant of clinical and therapeutic outcomes. In terms of RV performance upon exercise (increased loading), if at rest the RV is already pumping against an afterload loading condition equal to or greater than that of maximal SW, further increasing the PA afterload will cause SW and CO to fall. The RV will not be able to maintain an adequate output in the face of additional loading generated from

exercise. Unlike historical LV ventriculoarterial coupling data that demonstrated maximal SW occurred at a coupling ratio of 1.25 ± 0.16 (De Tombe et al., 1993), this work has suggested that in a healthy porcine RV maximal SW occurred at a coupling ratio of 0.68 ± 0.23. This work is the first to demonstrate that there is fundamental inefficiency (low coupling ratio) even in health, as the RV has to expend excess energy to pump blood against the inelastic PA.

7.2 RV Remodelling in Patients with Long Term Pressure Overload

The first clinical study examined how the in-vivo porcine model of RV ventriculoarterial interaction could be translated to human physiology to better characterise two cohorts of patients' with pathological chronic excess RV afterload. Although the natural history of CTED is poorly defined and it remains unclear whether patients with CTED deteriorate over time. This work has shown that the threshold for Ees/Ea at maximal SW determined from the animal model has detected RV pathology at rest in patients with CTED and otherwise normal pulmonary hemodynamics and demonstrated RV energetic reserve in some cases of CTEPH. Detailed ventriculoarterial coupling data may further risk stratify patients with CTED and CTEPH, and could usefully influence management.

7.3 RV Remodelling in Patients with Aortic Valve Stenosis

The second clinical study examined whether RV diastolic function improves following LV afterload reduction following TF-TAVI due to ventricular interdependence phenomena leading to changes in LV – RV interaction through septal wall reconfiguration. This work has demonstrated that although ventricular interdependence phenomena caused septal reconfiguration, increasing RV volumes after valve deployment due to the reduction in LV afterload. RP-induced ischemia caused overwhelming RV stunning after valve deployment. We established that RP during balloon-mounted TAVI implantation caused RV dysfunction that persists until at least the end of the procedure and was apparent and near-maximal after a relatively short

period of RP required for RPTC. We postulate that the RV dysfunction was mediated by global ischemia precipitated by RP; a presumed early hyperemic phase immediately after RP transiently augmented systolic RV function but both RV systolic and diastolic function were depressed once reactive hyperaemia had dissipated at +17 minutes. There was no echocardiographic improvement in RV function at 3-months post-TAVI, with RV function only recovering to baseline level. The potential ventricular interdependence benefits of unloading the LV after TAVI, has not manifested in an improvement in RV function, possibly due to this procedural factor. These findings have provided persuasive evidence of RV stunning in humans after TF TAVI and may give clinical insight in to why TAVI results are disappointing in those with pre-existing pulmonary hypertension and RV failure. Therefore, rather than the hypothesised improvements in RV ventriculoarterial coupling and diastolic function, uncoupling and diastolic dysfunction was observed. Changes to the valve deployment protocol avoiding RP may be required to prevent iatrogenic RV dysfunction and optimal TAVI results, particularly in patients with pre-existing right heart disease.

7.4 Conclusion Summary

In conclusion, the in-vivo animal model of RV ventriculoarterial coupling determined that maximal SW is a key determinant of clinical and therapeutic outcomes in RV failure. Beyond the threshold for maximal SW (Ees/Ea 0.68; Ea = 0.50 mmHg/ml) RV dysfunction occurs. This threshold for the RV Ees/Ea ratio at maximal SW was then used to detect occult RV dysfunction at rest in patients with CTED and otherwise normal pulmonary hemodynamics and demonstrated RV energetic reserve in some cases of CTEPH. Detailed ventriculoarterial coupling data may further risk stratify patients with CTED and CTEPH and usefully influence management. While global LV function was shown to improve in patients undergoing TAVI, ventricular interdependence improvements in RV contractility were overwhelmed by RP-induced RV ischemic dysfunction and stunning. Nevertheless, we were able to demonstrate

that a reduction in RV Ees led to a reduction in the RV Ees/Ea ratio and further deterioration of RV diastolic dysfunction.

7.5 Future Work

There are a number of avenues which need exploring further to build on the conclusions drawn from this work. While this work demonstrated that Ea could be a clinical relevant descriptor for classifying patients with PH, it is not feasible to interrogate every patient with the conductance catheter. However, it may be possible to validate a surrogate measure of Ea from the standard right heart catheterisation. If this is found to be reliable and accurate it could help identify those patients who have RV pathology at rest, but otherwise present with normal pulmonary haemodynamics.

The findings from the TAVI have provided persuasive evidence of RV stunning in humans after TF TAVI and may give clinical insight in to why TAVI results are disappointing in those with pre-existing pulmonary hypertension and RV failure. Many avenues need exploring further to minimise the effects of RP on RV stunning during TAVI. Is it possible to deploy the Edwards device using a balloon that does not require RP and allows continued blood flow? Is it possible to use a device that does not require RP? There is also further work required to better understand how and why the process of RP causes RV stunning. Is abnormal septal function detected after performing a TEE at baseline, following RP test capture and again after device implantation? Finally, by performing an ECG at the same time points it would be possible to determine if the RV stunning is mediated by elongation of the QRS complex.

8 References

Baan, J., Jong, T. T., Kerkhof, P. L., Moene, R. J., Van Dijk, A. D., Van Der Velde, E. T. & Koops, J. 1981. Continuous stroke volume and cardiac output from intra-ventricular dimensions obtained with impedance catheter. *Cardiovascular Research,* 15, pp.328-34.

Baan, J., Van Der Velde, E. T., De Bruin, H. G., Smeenk, G. J., Koops, J., Van Dijk, A. D., Temmerman, D., Senden, J. & Buis, B. 1984. Continuous measurement of left ventricular volume in animals and humans by conductance catheter. *Circulation,* 70, pp.812-23.

Babu-Narayan, S. V., Goktekin, O., Moon, J. C., Broberg, C. S., Pantely, G. A., Pennell, D. J., Gatzoulis, M. A. & Kilner, P. J. 2005. Late gadolinium enhancement cardiovascular magnetic resonance of the systemic right ventricle in adults with previous atrial redirection surgery for transposition of the great arteries. *Circulation,* 111, pp.2091-8.

Bachman, T. N., Bursic, J. J., Simon, M. A. & Champion, H. C. 2013. A Novel Acquisition Technique to Utilize Swan-Ganz Catheter data as a Surrogate for High-fidelity Micromanometry within the Right Ventricle and Pulmonary Circuit. *Cardiovascular Engineering and Technology,* 4, pp.183-191.

Bagger, J. P., Nielsen, T. T. & Henningsen, P. 1983. Increased coronary sinus lactate concentration during pacing induced angina pectoris after clinical improvement by glyceryl trinitrate. *British Heart Journal,* 50, pp.483-90.

Barnes, E., Dutka, D. P., Khan, M., Camici, P. G. & Hall, R. J. 2002. Effect of repeated episodes of reversible myocardial ischemia on myocardial blood flow and function in humans. *American Journal of Physiology: Heart and Circulatory Physiology,* 282, pp.H1603-8.

Baumgartner, H., Hung, J., Bermejo, J., Chambers, J. B., Evangelista, A., Griffin, B. P., Iung, B., Otto, C. M., Pellikka, P. A., Quinones, M. & Eae/Ase 2009. Echocardiographic assessment of valve stenosis: EAE/ASE recommendations for clinical practice. *European Journal of Echocardiography,* 10, pp.1-25.

Bellofiore, A. & Chesler, N. C. 2013. Methods for Measuring Right Ventricular Function and Hemodynamic Coupling with the Pulmonary Vasculature. *Annuals of Biomedical Engineering*.

Bernheim, P. L. 1910. L'asystolie veneuse dans l'hypertrophie du coeur gauche par stenote concomitante du ventricule droit. . *Reviews in Medicine,* 39, pp.785.

Bishop, A., White, P., Groves, P., Chaturvedi, R., Brookes, C., Redington, A. & Oldershaw, P. 1997. Right ventricular dysfunction during coronary artery occlusion: pressure-volume analysis using conductance catheters during coronary angioplasty. *Heart,* 78, pp.480-7.

Bland, J. H. & Lowenstein, E. 1976. Halothane-induced decrease in experimental myocardial ischemia in the non-failing canine heart. *Anesthesiology,* 45, pp.287-93.

Bland, J. M. & Altman, D. G. 1986. Statistical methods for assessing agreement between two methods of clinical measurement. *Lancet,* 1, pp.307-10.

Bolli, R. 1990. Mechanism of myocardial "stunning". *Circulation,* 82, pp.723-38.

Braunwald, E. 1969. Mitral regurgitation: physiologic, clinical and surgical considerations. *The New England Journal of Medicine,* 281, pp.425-33.

Braunwald, E. & Kloner, R. A. 1982. The stunned myocardium: prolonged, postischemic ventricular dysfunction. *Circulation,* 66, pp.1146-9.

Brimioulle, S., Wauthy, P., Ewalenko, P., Rondelet, B., Vermeulen, F., Kerbaul, F. & Naeije, R. 2003. Single-beat estimation of right ventricular end-systolic pressure-

volume relationship. *American Journal of Physiology Heart Circulation Physiology,* 284, pp.H1625-30.

Brookes, C. I., White, P. A., Bishop, A. J., Oldershaw, P. J., Redington, A. N. & Moat, N. E. 1998. Validation of a new intraoperative technique to evaluate load-independent indices of right ventricular performance in patients undergoing cardiac operations. *Journal of Thoracic Cardiovascular Surgery,* 116, pp.468-76.

Burkhoff, D. & Sagawa, K. 1986. Ventricular efficiency predicted by an analytical model. *American Journal of Physiology,* 250, pp.R1021-7.

Burrows, B., Kettel, L. J., Niden, A. H., Rabinowitz, M. & Diener, C. F. 1972. Patterns of cardiovascular dysfunction in chronic obstructive lung disease. *The New England Journal of Medicine,* 286, pp.912-8.

Caso, P., Galderisi, M., Cicala, S., Cioppa, C., D'andrea, A., Lagioia, G., Liccardo, B., Martiniello, A. R. & Mininni, N. 2001. Association between myocardial right ventricular relaxation time and pulmonary arterial pressure in chronic obstructive lung disease: analysis by pulsed Doppler tissue imaging. *Journal of the American Society of Echocardiography,* 14, pp.970-7.

Castelain, V., Herve, P., Lecarpentier, Y., Duroux, P., Simonneau, G. & Chemla, D. 2001. Pulmonary artery pulse pressure and wave reflection in chronic pulmonary thromboembolism and primary pulmonary hypertension. *Journay of the American College of Cardiology,* 37, pp.1085-92.

Chakko, S., De Marchena, E., Kessler, K. M., Materson, B. J. & Myerburg, R. J. 1990. Right ventricular diastolic function in systemic hypertension. *American Journal of Cardiology,* 65, pp.1117-20.

Champion, H. C., Michelakis, E. D. & Hassoun, P. M. 2009. Comprehensive invasive and noninvasive approach to the right ventricle-pulmonary circulation unit: state of the art and clinical and research implications. *Circulation,* 120, pp.992-1007.

Chaturvedi, R. R., Lincoln, C., Gothard, J. W., Scallan, M. H., White, P. A., Redington, A. N. & Shore, D. F. 1998. Left ventricular dysfunction after open repair of simple congenital heart defects in infants and children: quantitation with the use of a conductance catheter immediately after bypass. *Journal of Thoracic Cardiovascular Surgery,* 115, pp.77-83.

Chen, C. H., Nakayama, M., Nevo, E., Fetics, B. J., Maughan, W. L. & Kass, D. A. 1998. Coupled systolic-ventricular and vascular stiffening with age: implications for pressure regulation and cardiac reserve in the elderly. *Journal of the American College of Cardiology,* 32, pp.1221-7.

Chin, K. M. & Coghlan, G. 2012. Characterizing the right ventricle: advancing our knowledge. *American Journal of Cardiology,* 110, pp.3S-8S.

Chin, K. M., Kingman, M., De Lemos, J. A., Warner, J. J., Reimold, S., Peshock, R. & Torres, F. 2008. Changes in right ventricular structure and function assessed using cardiac magnetic resonance imaging in bosentan-treated patients with pulmonary arterial hypertension. *American Journal of Cardiology,* 101, pp.1669-72.

Cicala, S., Galderisi, M., Caso, P., Petrocelli, A., D'errico, A., De Divitiis, O. & Calabro, R. 2002. Right ventricular diastolic dysfunction in arterial systemic hypertension: analysis by pulsed tissue Doppler. *European Journal of Echocardiography,* 3, pp.135-42.

Coffman, J. D. & Gregg, D. E. 1960. Reactive hyperemia characteristics of the myocardium. *American Journal of Physiology,* 199, pp.1143-9.

Colah, S., Freed, D. H., Mundt, P., Germscheid, S., White, P., Ali, A., Tian, G., Large, S. & Falter, F. 2012. Ex vivo perfusion of the swine heart as a method for pre-transplant assessment. *Perfusion,* 27, pp.408-13.

Comtor, J. H., Jr. 1982. Harvey's 1651 perfusion of the pulmonary circulation of man. *Circulation,* 65, pp.1-3.

Cortigiani, L., Rigo, F., Sicari, R., Gherardi, S., Bovenzi, F. & Picano, E. 2009. Prognostic correlates of combined coronary flow reserve assessment on left anterior descending and right coronary artery in patients with negative stress echocardiography by wall motion criteria. *Heart,* 95, pp.1423-8.

Cribier, A., Eltchaninoff, H., Bash, A., Borenstein, N., Tron, C., Bauer, F., Derumeaux, G., Anselme, F., Laborde, F. & Leon, M. B. 2002. Percutaneous transcatheter implantation of an aortic valve prosthesis for calcific aortic stenosis: first human case description. *Circulation,* 106, pp.3006-8.

Crouch, G., Bennetts, J., Sinhal, A., Tully, P. J., Leong, D. P., Bradbrook, C., Penhall, A. L., De Pasquale, C. G., Chakrabarty, A., Baker, R. A. & Selvanayagam, J. B. 2015. Early effects of transcatheter aortic valve implantation and aortic valve replacement on myocardial function and aortic valve hemodynamics: insights from cardiovascular magnetic resonance imaging. *Journal of Thoracic Cardiovascular Surgery,* 149, pp.462-70.

Currie, P. J., Seward, J. B., Reeder, G. S., Vlietstra, R. E., Bresnahan, D. R., Bresnahan, J. F., Smith, H. C., Hagler, D. J. & Tajik, A. J. 1985. Continuous-wave Doppler echocardiographic assessment of severity of calcific aortic stenosis: a simultaneous Doppler-catheter correlative study in 100 adult patients. *Circulation,* 71, pp.1162-9.

Daehnert, I., Rotzsch, C., Wiener, M. & Schneider, P. 2004. Rapid right ventricular pacing is an alternative to adenosine in catheter interventional procedures for congenital heart disease. *Heart,* 90, pp.1047-50.

Danton, M. H., Greil, G. F., Byrne, J. G., Hsin, M., Cohn, L. & Maier, S. E. 2003. Right ventricular volume measurement by conductance catheter. *American Journal of Physiology: Heart Circculation Physiology,* 285, pp.H1774-85.

Davlouros, P. A., Niwa, K., Webb, G. & Gatzoulis, M. A. 2006. The right ventricle in congenital heart disease. *Heart,* 92 Suppl 1, pp.i27-38.

De Bruyne, B., Bartunek, J., Sys, S. U., Pijls, N. H., Heyndrickx, G. R. & Wijns, W. 1996. Simultaneous coronary pressure and flow velocity measurements in humans. Feasibility, reproducibility, and hemodynamic dependence of coronary flow velocity reserve, hyperemic flow versus pressure slope index, and fractional flow reserve. *Circulation,* 94, pp.1842-9.

De Rosa, R., Piccolo, R., Cassese, S., Petretta, A., D'andrea, C., D'anna, C., Piscione, F. & Chiariello, M. 2011. Coronary flow reserve evaluation: basics, techniques and clinical applications. *Minerva Cardioangiol,* 59, pp.569-80.

De Tombe, P. P., Jones, S., Burkhoff, D., Hunter, W. C. & Kass, D. A. 1993. Ventricular stroke work and efficiency both remain nearly optimal despite altered vascular loading. *Amerian Journal of Physiology,* 264, pp.H1817-24.

Dell'italia, L. J. 1991. The right ventricle: anatomy, physiology, and clinical importance. *Current Problems in Cardiology,* 16, pp.653-720.

Dourvas, I. N., Parharidis, G. E., Efthimiadis, G. K., Karvounis, H. I., Gemitzis, K. D., Styliadis, I. H., Karoulas, T. N. & Louridas, G. E. 2004. Right ventricular diastolic function in patients with chronic aortic regurgitation. *American Journal of Cardiology,* 93, pp.115-7.

Efthimiadis, G. K., Parharidis, G. E., Gemitzis, K. D., Nouskas, I. G., Karvounis, H. I., Styliadis, I. K. & Louridas, G. E. 1999. Doppler echocardiographic evaluation of right ventricular diastolic function in isolated valvular aortic stenosis. *Journal of Heart Valve Disease,* 8, pp.261-9.

Efthimiadis, G. K., Parharidis, G. E., Karvounis, H. I., Gemitzis, K. D., Styliadis, I. H. & Louridas, G. E. 2002. Doppler echocardiographic evaluation of right ventricular diastolic function in hypertrophic cardiomyopathy. *European Journal of Echocardiography,* 3, pp.143-8.

Faber, M. J., Dalinghaus, M., Lankhuizen, I. M., Steendijk, P., Hop, W. C., Schoemaker, R. G., Duncker, D. J., Lamers, J. M. & Helbing, W. A. 2006. Right and left ventricular function after chronic pulmonary artery banding in rats assessed with biventricular pressure-volume loops. *American Journal of Physiology: Heart Circulation Physiology,* 291, pp.H1580-6.

Florea, V. G., Florea, N. D., Sharma, R., Coats, A. J., Gibson, D. G., Hodson, M. E. & Henein, M. Y. 2000. Right ventricular dysfunction in adult severe cystic fibrosis. *Chest,* 118, pp.1063-8.

Folse, R. & Braunwald, E. 1962. Determination of fraction of left ventricular volume ejected per beat and of ventricular end-diastolic and residual volumes. Experimental and clinical observations with a precordial dilution technic. *Circulation,* 25, pp.674-85.

Forsberg, L. M., Tamas, E., Vanky, F., Nielsen, N. E., Engvall, J. & Nylander, E. 2011. Left and right ventricular function in aortic stenosis patients 8 weeks post-transcatheter aortic valve implantation or surgical aortic valve replacement. *European Journal of Echocardiography,* 12, pp.603-11.

Fourie, P. R., Coetzee, A. R. & Bolliger, C. T. 1992. Pulmonary artery compliance: its role in right ventricular-arterial coupling. *Cardiovascular Research,* 26, pp.839-44.

Galderisi, M., Cicala, S., Caso, P., De Simone, L., D'errico, A., Petrocelli, A. & De Divitiis, O. 2002. Coronary flow reserve and myocardial diastolic dysfunction in arterial hypertension. *American Journal of Cardiology,* 90, pp.860-4.

Galderisi, M., Cicala, S., De Simone, L., Caso, P., Petrocelli, A., Pietropaolo, L., Celentano, A., Mininni, N. & De Divitiis, O. 2001. Impact of myocardial diastolic dysfunction on coronary flow reserve in hypertensive patients with left ventricular hypertrophy. *Italian Heart Journal,* 2, pp.677-84.

Galderisi, M. & D'errico, A. 2008. Beta-blockers and coronary flow reserve: the importance of a vasodilatory action. *Drugs,* 68, pp.579-90.

Galderisi, M., De Simone, G., D'errico, A., Sidiropulos, M., Viceconti, R., Chinali, M., Mondillo, S. & De Divitiis, O. 2008. Independent association of coronary flow reserve with left ventricular relaxation and filling pressure in arterial hypertension. *Ameriacn Journal of Hypertension,* 21, pp.1040-6.

Gan, C. T., Holverda, S., Marcus, J. T., Paulus, W. J., Marques, K. M., Bronzwaer, J. G., Twisk, J. W., Boonstra, A., Postmus, P. E. & Vonk-Noordegraaf, A. 2007. Right ventricular diastolic dysfunction and the acute effects of sildenafil in pulmonary hypertension patients. *Chest,* 132, pp.11-7.

Geddes, L. A. & Baker, L. E. 1967. The specific resistance of biological material--a compendium of data for the biomedical engineer and physiologist. *Medical Biological Engineering,* 5, pp.271-93.

Ghuysen, A., Lambermont, B., Kolh, P., Tchana-Sato, V., Magis, D., Gerard, P., Mommens, V., Janssen, N., Desaive, T. & D'orio, V. 2008. Alteration of right ventricular-pulmonary vascular coupling in a porcine model of progressive pressure overloading. *Shock,* 29, pp.197-204.

Goor, D. A. & Lillehei, C. W. 1975. *Congenital malformations of the heart : embryology, anatomy, and operative considerations,* New York ; London, Grune & Stratton.

Grant, B. J. & Paradowski, L. J. 1987. Characterization of pulmonary arterial input impedance with lumped parameter models. *American Journal of Physiology,* 252, pp.H585-93.

Gregg, D. E. 1963. Effect of Coronary Perfusion Pressure or Coronary Flow on Oxygen Usage of the Myocardium. *Circulation Research,* 13, pp.497-500.

Grignola, J. C., Gines, F., Bia, D. & Armentano, R. 2007. Improved right ventricular-vascular coupling during active pulmonary hypertension. *International Journal of Cardiology,* 115, pp.171-82.

Guazzi, M., Castelvecchio, S., Bandera, F. & Menicanti, L. 2012. Right ventricular pulmonary hypertension. *Current Heart Failure Reports,* 9, pp.303-8.

Guihaire, J., Haddad, F., Noly, P. E., Boulate, D., Decante, B., Dartevelle, P., Humbert, M., Verhoye, J. P., Mercier, O. & Fadel, E. 2015. Right ventricular reserve in a piglet model of chronic pulmonary hypertension. *European Respiratory Journal,* 45, pp.709-17.

Habib, G. B. & Zoghbi, W. A. 1992. Doppler assessment of right ventricular filling dynamics in systemic hypertension: comparison with left ventricular filling. *American Heart Journal,* 124, pp.1313-20.

Hadjiloizou, N., Davies, J. E., Malik, I. S., Aguado-Sierra, J., Willson, K., Foale, R. A., Parker, K. H., Hughes, A. D., Francis, D. P. & Mayet, J. 2008. Differences in cardiac microcirculatory wave patterns between the proximal left mainstem and proximal right coronary artery. *American Journal of Physiology: Heart Circulation Physiology,* 295, pp.H1198-H1205.

Henderson, Y. P., A.L. 1914. The relative systolic discharges of the right and left ventricles and their bearing on pulmonary congestion and depletion. *Heart,* 4, pp.217-226.

Herberg, U., Gatzweiler, E., Breuer, T. & Breuer, J. 2013. Ventricular pressure-volume loops obtained by 3D real-time echocardiography and mini pressure wire-a feasibility study. *Clinical Research in Cardiology,* 102, pp.427-38.

Heyndrickx, G. R., Millard, R. W., Mcritchie, R. J., Maroko, P. R. & Vatner, S. F. 1975. Regional myocardial functional and electrophysiological alterations after brief coronary artery occlusion in conscious dogs. *Journal of Clinical Investigation,* 56, pp.978-85.

Ho, S. Y. & Nihoyannopoulos, P. 2006. Anatomy, echocardiography, and normal right ventricular dimensions. *Heart,* 92 Suppl 1, pp.i2-13.

Hodgson, J. M. & Mancini, G. B. 1985. Relation between graded, subcritical impairments of coronary flow reserve and regional myocardial dysfunction induced by atrial pacing in dogs. *Journal of the American College of Cardiology,* 5, pp.1116-24.

Homans, D. C., Laxson, D. D., Sublett, E., Pavek, T. & Crampton, M. 1991. Effect of exercise intensity and duration on regional function during and after exercise-induced ischemia. *Circulation,* 83, pp.2029-37.

Homik, L. A., Bshouty, Z., Light, R. B. & Younes, M. 1988. Effect of alveolar hypoxia on pulmonary fluid filtration in in situ dog lungs. *Journal of Applied Physiolgy* 65, pp.46-52.

Hoole, S. P., Heck, P. M., White, P. A., Read, P. A., Khan, S. N., West, N. E., O'sullivan, M. & Dutka, D. P. 2010. Stunning and cumulative left ventricular dysfunction occurs late after coronary balloon occlusion in humans insights from simultaneous coronary and left ventricular hemodynamic assessment. *Journal of the American College of Cardiology: Cardiovascular Interventions,* 3, pp.412-8.

Horan, B. F., Prys-Roberts, C., Roberts, J. G., Bennett, M. J. & Foex, P. 1977. Haemodynamic responses to isoflurane anaesthesia and hypovolaemia in the dog, and their modification by propranolol. *British Journal of Anaesthesia,* 49, pp.1179-87.

Ito, S., Pislaru, S. V., Nkomo, V. T., Oh, J. K., Greason, K. L., Mathew, V., Holmes, D. R., Rihal, C. S. & Suri, R. M. 2014. Abstract 15719: Right Ventricular Dysfunction After Transcatheter Aortic Valve Replacement (TAVR). *Circulation,* 130, pp.A15719.

Jurcut, R., Giusca, S., La Gerche, A., Vasile, S., Ginghina, C. & Voigt, J. U. 2010. The echocardiographic assessment of the right ventricle: what to do in 2010? *European Journal of Echocardiography,* 11, pp.81-96.

Kalkan, G. Y., Gur, M., Sahin, D. Y., Baykan, A. O., Elbasan, Z., Kuloglu, O., Kivrak, A., Turkoglu, C., Arik, O. Z. & Cayli, M. 2013. Coronary Flow Reserve and Myocardial Performance Index in Newly Diagnosed Diabetic Patients. *Echocardiography*.

Kass, D. A., Midei, M., Graves, W., Brinker, J. A. & Maughan, W. L. 1988. Use of a conductance (volume) catheter and transient inferior vena caval occlusion for rapid determination of pressure-volume relationships in man. *Catheterization and Cardiovascular Diagnosis,* 15, pp.192-202.

Kass, D. A., Yamazaki, T., Burkhoff, D., Maughan, W. L. & Sagawa, K. 1986. Determination of left ventricular end-systolic pressure-volume relationships by the conductance (volume) catheter technique. *Circulation,* 73, pp.586-95.

Kaul, S., Tei, C., Hopkins, J. M. & Shah, P. M. 1984. Assessment of right ventricular function using two-dimensional echocardiography. *American Heart Journal,* 107, pp.526-31.

Kawaguchi, M., Hay, I., Fetics, B. & Kass, D. A. 2003. Combined ventricular systolic and arterial stiffening in patients with heart failure and preserved ejection fraction: implications for systolic and diastolic reserve limitations. *Circulation,* 107, pp.714-20.

Kelly, R. P., Ting, C. T., Yang, T. M., Liu, C. P., Maughan, W. L., Chang, M. S. & Kass, D. A. 1992. Effective arterial elastance as index of arterial vascular load in humans. *Circulation,* 86, pp.513-21.

Kempny, A., Diller, G. P., Kaleschke, G., Orwat, S., Funke, A., Schmidt, R., Kerckhoff, G., Ghezelbash, F., Rukosujew, A., Reinecke, H., Scheld, H. H. & Baumgartner, H. 2012. Impact of transcatheter aortic valve implantation or surgical aortic valve replacement on right ventricular function. *Heart,* 98, pp.1299-1304.

Keyl, C., Schneider, J., Beyersdorf, F., Ruile, P., Siepe, M., Pioch, K., Schneider, R. & Jander, N. 2016. Right ventricular function after aortic valve replacement: a pilot study comparing surgical and transcatheter procedures using 3D echocardiography. *European Journal of Cardiothoracic Surgery,* 49, pp.966-71.

Kilner, P. J. 2011. The role of cardiovascular magnetic resonance in adults with congenital heart disease. *Progress in Cardiovascular Diseases,* 54, pp.295-304.

Kilner, P. J., Geva, T., Kaemmerer, H., Trindade, P. T., Schwitter, J. & Webb, G. D. 2010. Recommendations for cardiovascular magnetic resonance in adults with congenital heart disease from the respective working groups of the European Society of Cardiology. *European Heart Journal,* 31, pp.794-805.

Kitahori, K., He, H., Kawata, M., Cowan, D. B., Friehs, I., Del Nido, P. J. & Mcgowan, F. X., Jr. 2009. Development of left ventricular diastolic dysfunction with preservation of ejection fraction during progression of infant right ventricular hypertrophy. *Circulation Heart Faililure,* 2, pp.599-607.

Kolb, T. M. & Hassoun, P. M. 2012. Right ventricular dysfunction in chronic lung disease. *Cardiology Clinics,* 30, pp.243-56.

Kornet, L., Schreuder, J. J., Van Der Velde, E. T., Baan, J. & Jansen, J. R. 2000. A new approach to determine parallel conductance for left ventricular volume measurements. *Cardiovascular Research,* 48, pp.455-63.

Kuehne, T., Saeed, M., Gleason, K., Turner, D., Teitel, D., Higgins, C. B. & Moore, P. 2003. Effects of pulmonary insufficiency on biventricular function in the developing heart of growing swine. *Circulation,* 108, pp.2007-13.

Kuehne, T., Yilmaz, S., Meinus, C., Moore, P., Saeed, M., Weber, O., Higgins, C. B., Blank, T., Elsaesser, E., Schnackenburg, B., Ewert, P., Lange, P. E. & Nagel, E. 2004. Magnetic resonance imaging-guided transcatheter implantation of a prosthetic valve in aortic valve position: Feasibility study in swine. *Journal of the American College of Cardiology,* 44, pp.2247-9.

Lai, W. W., Gauvreau, K., Rivera, E. S., Saleeb, S., Powell, A. J. & Geva, T. 2008. Accuracy of guideline recommendations for two-dimensional quantification of the right ventricle by echocardiography. *International Journal of Cardiovascular Imaging,* 24, pp.691-8.

Lambermont, B., Kolh, P., Detry, O., Gerard, P., Marcelle, R. & D'orio, V. 1999. Analysis of endotoxin effects on the intact pulmonary circulation. *Cardiovascular Research,* 41, pp.275-81.

Langendorff, O. 1895. Untersuchungen am überlebenden Säugethierherzen. *Pflügers Arch,* 61, pp.291–332.

Leibundgut, G., Rohner, A., Grize, L., Bernheim, A., Kessel-Schaefer, A., Bremerich, J., Zellweger, M., Buser, P. & Handke, M. 2010. Dynamic assessment of right ventricular volumes and function by real-time three-dimensional echocardiography: a comparison study with magnetic resonance imaging in 100 adult patients. *Journal of the American Society of Echocardiography,* 23, pp.116-26.

Leite-Moreira, A. F., Correia-Pinto, J. & Gillebert, T. C. 1999. Afterload induced changes in myocardial relaxation: a mechanism for diastolic dysfunction. *Cardiovascular Research,* 43, pp.344-53.

Leon, M. B., Smith, C. R., Mack, M., Miller, D. C., Moses, J. W., Svensson, L. G., Tuzcu, E. M., Webb, J. G., Fontana, G. P., Makkar, R. R., Brown, D. L., Block, P. C., Guyton, R. A., Pichard, A. D., Bavaria, J. E., Herrmann, H. C., Douglas, P. S., Petersen, J. L., Akin, J. J., Anderson, W. N., Wang, D., Pocock, S. & Investigators, P. T. 2010. Transcatheter aortic-valve implantation for aortic stenosis in patients who cannot undergo surgery. *New England Journal of Medicine,* 363, pp.1597-607.

Lindman, B. R., Maniar, H. S., Jaber, W. A., Lerakis, S., Mack, M. J., Suri, R. M., Thourani, V. H., Babaliaros, V., Kereiakes, D. J., Whisenant, B., Miller, D. C., Tuzcu, E. M., Svensson, L. G., Xu, K., Doshi, D., Leon, M. B. & Zajarias, A. 2015. Effect of tricuspid regurgitation and the right heart on survival after transcatheter aortic valve replacement: insights from the Placement of Aortic Transcatheter Valves II inoperable cohort. *Circulation Cardiovascular Interventions,* 8.

Mancini, G. B., Mcgillem, M. J., Deboe, S. F. & Gallagher, K. P. 1989. The diastolic hyperemic flow versus pressure relation. A new index of coronary stenosis severity and flow reserve. *Circulation,* 80, pp.941-50.

Marcus, M. L., Wilson, R. F. & White, C. W. 1987. Methods of measurement of myocardial blood flow in patients: a critical review. *Circulation,* 76, pp.245-53.

Marquardt, D. W. 1963. An Algorithm for Least-Squares Estimation of Nonlinear Parameters. *Journal of the Society for Industrial and Applied Mathematics,* 11, pp.431-441.

Matsubara, H., Takaki, M., Yasuhara, S., Araki, J. & Suga, H. 1995. Logistic time constant of isovolumic relaxation pressure-time curve in the canine left ventricle. Better alternative to exponential time constant. *Circulation,* 92, pp.2318-26.

Mccabe, C., White, P. A., Hoole, S. P., Axell, R. G., Priest, A. N., Gopalan, D., Taboada, D., Mackenzie Ross, R., Morrell, N. W., Shapiro, L. M. & Pepke-Zaba, J. 2014. Right ventricular dysfunction in chronic thromboembolic obstruction of the pulmonary artery: a pressure-volume study using the conductance catheter. *Journal Applied Physiology,* 116, pp.355-63.

Mckay, R. G., Spears, J. R., Aroesty, J. M., Baim, D. S., Royal, H. D., Heller, G. V., Lincoln, W., Salo, R. W., Braunwald, E. & Grossman, W. 1984. Instantaneous measurement of left and right ventricular stroke volume and pressure-volume relationships with an impedance catheter. *Circulation,* 69, pp.703-10.

Messer, S. J., Axell, R. G., Colah, S., White, P. A., Ryan, M., Page, A. A., Parizkova, B., Valchanov, K., White, C. W., Freed, D. H., Ashley, E., Dunning, J., Goddard, M., Parameshwar, J., Watson, C. J., Krieg, T., Ali, A., Tsui, S. & Large, S. R. 2016. Functional assessment and transplantation of the donor heart following circulatory death. *The Journal of Heart and Lung Transplantation,* 35, pp.1443-1452.

Missant, C., Rex, S., Segers, P. & Wouters, P. F. 2007. Levosimendan improves right ventriculovascular coupling in a porcine model of right ventricular dysfunction. *Critical Care Medicine,* 35, pp.707-15.

Moon, M. R., Deanda, A., Castro, L. J., Daughters, G. T., 2nd, Ingels, N. B., Jr. & Miller, D. C. 1997. Effects of mechanical left ventricular support on right ventricular diastolic function. *Journal of Heart and Lung Transplant,* 16, pp.398-407.

Morcos, P., Vick, G. W., 3rd, Sahn, D. J., Jerosch-Herold, M., Shurman, A. & Sheehan, F. H. 2009. Correlation of right ventricular ejection fraction and tricuspid annular plane systolic excursion in tetralogy of Fallot by magnetic resonance imaging. *Int J Cardiovasc Imaging,* 25, pp.263-70.

Morimont, P., Lambermont, B., Ghuysen, A., Gerard, P., Kolh, P., Lancellotti, P., Tchana-Sato, V., Desaive, T. & D'orio, V. 2008. Effective arterial elastance as an index

of pulmonary vascular load. *American Journal of Physiology: Heart and Circulatory Physiology,* 294, pp.H2736-42.

Muratori, M., Fusini, L., Tamborini, G., Gripari, P., Delgado, V., Marsan, N. A., Ghulam Ali, S., Barbier, P., Bartorelli, A. L., Alamanni, F. & Pepi, M. 2015. Sustained favourable haemodynamics 1 year after TAVI: improvement in NYHA functional class related to improvement of left ventricular diastolic function. *European Heart Journal: Cardiovascular Imaging*.

Naeije, R. & Manes, A. 2014. The right ventricle in pulmonary arterial hypertension. *European Respiratory Review,* 23, pp.476-87.

Nicolosi, A. C., Hettrick, D. A. & Warltier, D. C. 1996. Assessment of right ventricular function in swine using sonomicrometry and conductance. *The Annals of Thoracic Surgery,* 61, pp.1381-7; discussion 1387-8.

Niemann, P. S., Pinho, L., Balbach, T., Galuschky, C., Blankenhagen, M., Silberbach, M., Broberg, C., Jerosch-Herold, M. & Sahn, D. J. 2007. Anatomically oriented right ventricular volume measurements with dynamic three-dimensional echocardiography validated by 3-Tesla magnetic resonance imaging. *Journal of the American College of Cardiology,* 50, pp.1668-76.

Pagel, P. S., Kampine, J. P., Schmeling, W. T. & Warltier, D. C. 1993. Reversal of volatile anesthetic-induced depression of myocardial contractility by extracellular calcium also enhances left ventricular diastolic function. *Anesthesiology,* 78, pp.141-54.

Pignatelli, R. H., Mcmahon, C. J., Chung, T. & Vick, G. W., 3rd 2003. Role of echocardiography versus MRI for the diagnosis of congenital heart disease. *Current Opinion in Cardiology,* 18, pp.357-65.

Preuss, K. C., Gross, G. J., Brooks, H. L. & Warltier, D. C. 1987. Time course of recovery of "stunned" myocardium following variable periods of ischemia in conscious and anesthetized dogs. *American Heart Journal,* 114, pp.696-703.

Raff, G. L. & Glantz, S. A. 1981. Volume loading slows left ventricular isovolumic relaxation rate. Evidence of load-dependent relaxation in the intact dog heart. *Circulation Research,* 48, pp.813-24.

Ramanathan, T. & Skinner, H. 2005. Coronary blood flow. *Continuing Education in Anaesthesia, Critical Care & Pain,* 5, pp.61-64.

Read, P. A., Hoole, S. P., White, P. A., Khan, F. Z., O'sullivan, M., West, N. E. & Dutka, D. P. 2011. A pilot study to assess whether glucagon-like peptide-1 protects the heart from ischemic dysfunction and attenuates stunning after coronary balloon occlusion in humans. *Circulation Cardiovascular Intervention,* 4, pp.266-72.

Redington, A. N., Rigby, M. L., Shinebourne, E. A. & Oldershaw, P. J. 1990. Changes in the pressure-volume relation of the right ventricle when its loading conditions are modified. *British Heart Journal,* 63, pp.45-9.

Reiter, G., Reiter, U., Kovacs, G., Kainz, B., Schmidt, K., Maier, R., Olschewski, H. & Rienmueller, R. 2008. Magnetic resonance-derived 3-dimensional blood flow patterns in the main pulmonary artery as a marker of pulmonary hypertension and a measure of elevated mean pulmonary arterial pressure. *Circulation Cardiovascular Imaging,* 1, pp.23-30.

Rickham, P. P. 1964. Human Experimentation. Code of Ethics of the World Medical Association. Declaration of Helsinki. *British Medical Journal,* 2, pp.177.

Riggs, T. W. 1993. Abnormal right ventricular filling in patients with dilated cardiomyopathy. *Pediatric Cardiology,* 14, pp.1-4.

Rigo, F. 2005. Coronary flow reserve in stress-echo lab. From pathophysiologic toy to diagnostic tool. *Cardiovasc Ultrasound,* 3, pp.8.

Rigo, F., Ciampi, Q., Ossena, G., Grolla, E., Picano, E. & Sicari, R. 2011. Prognostic value of left and right coronary flow reserve assessment in nonischemic dilated cardiomyopathy by transthoracic Doppler echocardiography. *Journal of Cardiac Failure,* 17, pp.39-46.

Rinaldi, C. A., Masani, N. D., Linka, A. Z. & Hall, R. J. 1999. Effect of repetitive episodes of exercise induced myocardial ischaemia on left ventricular function in patients with chronic stable angina: evidence for cumulative stunning or ischaemic preconditioning? *Heart,* 81, pp.404-11.

Ryan, T., Petrovic, O., Dillon, J. C., Feigenbaum, H., Conley, M. J. & Armstrong, W. F. 1985. An echocardiographic index for separation of right ventricular volume and pressure overload. *Journal of the American College of Cardiology,* 5, pp.918-27.

Saleh, S., Liakopoulos, O. J. & Buckberg, G. D. 2006. The septal motor of biventricular function. *European Journal of Cardiothoracic Surgery,* 29 Suppl 1, pp.S126-38.

Salo, R. W. 1989. The theoretical basis of a computational model for the determination of volume by impedance. *Automedica,* 11, pp.299-310.

Salo, R. W., Wallner, T. G. & Pederson, B. D. 1986. Measurement of ventricular volume by intracardiac impedance: theoretical and empirical approaches. *IEEE Transitions Biomedical Engineering,* 33, pp.189-95.

Samyn, M. M. 2004. A review of the complementary information available with cardiac magnetic resonance imaging and multi-slice computed tomography (CT) during the study of congenital heart disease. *International Journal Cardiovascular Imaging,* 20, pp.569-78.

Santamore, W. P. & Dell'italia, L. J. 1998a. Ventricular interdependence: significant left ventricular contributions to right ventricular systolic function. *Progress in Cardiovascular Diseases,* 40, pp.289-308.

Santamore, W. P. & Dell'italia, L. J. 1998b. Ventricular interdependence: significant left ventricular contributions to right ventricular systolic function. *Prog Cardiovasc Dis,* 40, pp.289-308.

Saouti, N., Westerhof, N., Helderman, F., Marcus, J. T., Boonstra, A., Postmus, P. E. & Vonk-Noordegraaf, A. 2010. Right ventricular oscillatory power is a constant fraction of total power irrespective of pulmonary artery pressure. *American Journal of Respiratory Critical Care Medecine,* 182, pp.1315-20.

Sasayama, S. & Asanoi, H. 1991. Coupling between the heart and arterial system in heart failure. *American Journal of Medicine,* 90, pp.14S-18S.

Schwarz, E. R. & Dashti, R. 2010. The clinical quandary of left and right ventricular diastolic dysfunction and diastolic heart failure. *Cardiovascular Journal of Africa,* 21, pp.212-20.

Sheehan, F. H., Ge, S., Vick, G. W., 3rd, Urnes, K., Kerwin, W. S., Bolson, E. L., Chung, T., Kovalchin, J. P., Sahn, D. J., Jerosch-Herold, M. & Stolpen, A. H. 2008. Three-dimensional shape analysis of right ventricular remodeling in repaired tetralogy of Fallot. *American Journal of Cardiology,* 101, pp.107-13.

Simonneau, G., Gatzoulis, M. A., Adatia, I., Celermajer, D., Denton, C., Ghofrani, A., Gomez Sanchez, M. A., Krishna Kumar, R., Landzberg, M., Machado, R. F., Olschewski, H., Robbins, I. M. & Souza, R. 2013. Updated clinical classification of pulmonary hypertension. *Journal of the American College of Cardiology,* 62, pp.D34-41.

Spruijt, O. A., De Man, F. S., Groepenhoff, H., Oosterveer, F., Westerhof, N., Vonk-Noordegraaf, A. & Bogaard, H. J. 2015. The effects of exercise on right ventricular contractility and right ventricular-arterial coupling in pulmonary hypertension. *American Journal of Respiratory and Critical Care Medicine,* 191, pp.1050-7.

Stahl, L. D., Aversano, T. R. & Becker, L. C. 1986. Selective enhancement of function of stunned myocardium by increased flow. *Circulation,* 74, pp.843-51.

Starr, J., Jeffers, W. A. & Meade, R. H. 1943. The absence of consipcuous increments of venous pressure after severe damage to the RV of the dog, with discussion of the relation between clinical congestive heart failure and heart disease. *American Heart Journal,* 65, pp.1-3.

Steendijk, P., Van Der Velde, E. T. & Baan, J. 1992. Single and dual excitation of the conductance-volume catheter analysed in a spheroidal mathematical model of the canine left ventricle. *European Heart Journal,* 13 Suppl E, pp.28-34.

Strauer, B. E., Motz, W., Vogt, M. & Schwartzkopff, B. 1997. Evidence for reduced coronary flow reserve in patients with insulin-dependent diabetes. A possible cause for diabetic heart disease in man. *Experiemntal and Clinical Endocrinol Diabetes,* 105, pp.15-20.

Suga, H. 1979. Total mechanical energy of a ventricle model and cardiac oxygen consumption. *American Journal of Physiology,* 236, pp.H498-505.

Suga, H., Hayashi, T., Shirahata, M. & Ninomiya, I. 1980. Critical evaluation of left ventricular systolic pressure volume areas as predictor of oxygen consumption rate. *Japanese Journal of Physiology,* 30, pp.907-19.

Suga, H., Hisano, R., Goto, Y., Yamada, O. & Igarashi, Y. 1983. Effect of positive inotropic agents on the relation between oxygen consumption and systolic pressure volume area in canine left ventricle. *Circulation Research,* 53, pp.306-18.

Suga, H., Yamada, O., Goto, Y., Igarashi, Y. & Ishiguri, H. 1984. Constant mechanical efficiency of contractile machinery of canine left ventricle under different loading and inotropic conditions. *Japanese Journal of Physiology,* 34, pp.679-98.

Sunagawa, K., Maughan, W. L., Burkhoff, D. & Sagawa, K. 1983. Left ventricular interaction with arterial load studied in isolated canine ventricle. *American Journal of Physiology,* 245, pp.H773-80.

Sunagawa, K., Maughan, W. L. & Sagawa, K. 1985. Optimal arterial resistance for the maximal stroke work studied in isolated canine left ventricle. *Circulation Research,* 56, pp.586-95.

Sunagawa, K., Sagawa, K. & Maughan, W. L. 1984. Ventricular interaction with the loading system. *Annals of Biomedical Engineering,* 12, pp.163-89.

Sunagawa, K., Sagawa, K. & Maughan, W. L. 1987. Ventricular interaction with the vascular system. *In:* YIN, F. C. P. (ed.) *Ventricular / Vascular Interaction.* New York: Springer.

Sunagawa, K., Yamada, A., Senda, Y., Kikuchi, Y., Nakamura, M., Shibahara, T. & Nose, Y. 1980. Estimation of the hydromotive source pressure from ejecting beats of the left ventricle. *IEEE Transactions on Biomedical Engineering,* 27, pp.299-305.

Tabima, D. M., Hacker, T. A. & Chesler, N. C. 2010. Measuring right ventricular function in the normal and hypertensive mouse hearts using admittance-derived pressure-volume loops. *American Journal Physiolsiology - Heart and Circulation Physiology,* 299, pp.H2069-75.

Tedford, R. J., Mudd, J. O., Girgis, R. E., Mathai, S. C., Zaiman, A. L., Housten-Harris, T., Boyce, D., Kelemen, B. W., Bacher, A. C., Shah, A. A., Hummers, L. K., Wigley, F. M., Russell, S. D., Saggar, R., Saggar, R., Maughan, W. L., Hassoun, P. M. & Kass, D.

A. 2013. Right Ventricular Dysfunction in Systemic Sclerosis–Associated Pulmonary Arterial Hypertension. *Circulation: Heart Failure,* 6, pp.953-963.

Teragaki, M., Yanagi, S., Toda, I., Sakamoto, K., Hirota, K., Takeuchi, K. & Yoshikawa, J. 2003. Coronary flow reserve correlates left ventricular diastolic dysfunction in patients with dilated cardiomyopathy. *Catheterization and Cardiovascular Interventions,* 58, pp.43-50.

Torrent-Guasp, F., Ballester, M., Buckberg, G. D., Carreras, F., Flotats, A., Carrio, I., Ferreira, A., Samuels, L. E. & Narula, J. 2001. Spatial orientation of the ventricular muscle band: physiologic contribution and surgical implications. *Journal of Thoracic and Cardiovascular Surgery,* 122, pp.389-92.

Turer, A. T., Addo, T. A., Martin, J. L., Sabatine, M. S., Lewis, G. D., Gerszten, R. E., Keeley, E. C., Cigarroa, J. E., Lange, R. A., Hillis, L. D. & De Lemos, J. A. 2011. Myocardial ischemia induced by rapid atrial pacing causes troponin T release detectable by a highly sensitive assay: insights from a coronary sinus sampling study. *Journal of the American College of Cardiology,* 57, pp.2398-405.

Van Herck, P. L., Vrints, C. J. & Carlier, S. G. 2005. Coronary circulation and interventional cardiology. *Annuls of Biomedical Engineering,* 33, pp.1735-42.

Van Wolferen, S. A., Marcus, J. T., Boonstra, A., Marques, K. M., Bronzwaer, J. G., Spreeuwenberg, M. D., Postmus, P. E. & Vonk-Noordegraaf, A. 2007. Prognostic value of right ventricular mass, volume, and function in idiopathic pulmonary arterial hypertension. *European Heart Journal,* 28, pp.1250-7.

Vogel, M., Gutberlet, M., Dittrich, S., Hosten, N. & Lange, P. E. 1997. Comparison of transthoracic three dimensional echocardiography with magnetic resonance imaging in the assessment of right ventricular volume and mass. *Heart,* 78, pp.127-30.

Von Anrep, G. 1912. On the part played by the suprarenals in the normal vascular reaction of the body. *Journal of Physiology,* 48, pp.465.

Warnes, C. A. 2009. Adult congenital heart disease importance of the right ventricle. *Journal of the American College of Cardiology,* 54, pp.1903-10.

Wauthy, P., Pagnamenta, A., Vassalli, F., Naeije, R. & Brimioulle, S. 2004. Right ventricular adaptation to pulmonary hypertension: an interspecies comparison. *American Journal of Physiology: Heart Circulation Physiology,* 286, pp.H1441-7.

Weiss, J. L., Frederiksen, J. W. & Weisfeldt, M. L. 1976. Hemodynamic determinants of the time-course of fall in canine left ventricular pressure. *Journal Clinical Investigation,* 58, pp.751-60.

Westerhof, N., Boer, C., Lamberts, R. R. & Sipkema, P. 2006. Cross-talk between cardiac muscle and coronary vasculature. *Physiological Reviews,* 86, pp.1263-308.

White, P. A., Bishop, A. J., Conroy, B., Oldershaw, P. J. & Redington, A. N. 1995. The determination of volume of right ventricular casts using a conductance catheter. *Eurpean Heart Journal,* 16, pp.1425-9.

Wilkins, M. R., Paul, G. A., Strange, J. W., Tunariu, N., Gin-Sing, W., Banya, W. A., Westwood, M. A., Stefanidis, A., Ng, L. L., Pennell, D. J., Mohiaddin, R. H., Nihoyannopoulos, P. & Gibbs, J. S. 2005. Sildenafil versus Endothelin Receptor Antagonist for Pulmonary Hypertension (SERAPH) study. *American Journal of Respiratory and Critical Care Medicine,* 171, pp.1292-7.

Winter, M. M., Bernink, F. J., Groenink, M., Bouma, B. J., Van Dijk, A. P., Helbing, W. A., Tijssen, J. G. & Mulder, B. J. 2008. Evaluating the systemic right ventricle by CMR: the importance of consistent and reproducible delineation of the cavity. *Journal of Cardiovascular Magnetic Resonance,* 10, pp.40.

World Medical, A. 2013. World Medical Association Declaration of Helsinki: ethical principles for medical research involving human subjects. *Journal of the Americal Medical Association,* 310, pp.2191-4.

Yaginuma, T., Noda, T., Tsuchiya, M., Takazawa, K., Tanaka, H., Kotoda, K. & Hosoda, S. 1985. Interaction of left ventricular contraction and aortic input impedance in experimental and clinical studies. *Japanese Circulation Journal,* 49, pp.206-14.

Zeng, W. J., Sun, Y. J., Xiong, C. M., Gu, Q. & He, J. G. 2011. Prognostic value of echocardiographic right/left ventricular end-diastolic diameter ratio in idiopathic pulmonary arterial hypertension. *Chinese Medical Journal* 124, pp.1672-7.

Zimbarra Cabrita, I., Ruisanchez, C., Grapsa, J., Dawson, D., North, B., Pinto, F. J., Gibbs, J. S. & Nihoyannopoulos, P. 2013. Validation of the isovolumetric relaxation time for the estimation of pulmonary systolic arterial blood pressure in chronic pulmonary hypertension. *European Heart Journal: Cardiovascular Imaging,* 14, pp.51-5.

Zipes, D. P. & Braunwald, E. H. D. 2005. *Braunwald's heart disease : a textbook of cardiovascular medicine,* Philadelphia ; Oxford, Elsevier Saunders.

9 Appendices

9.1 Appendix A – Relations between Afterload Quantified by Ea and RV Function

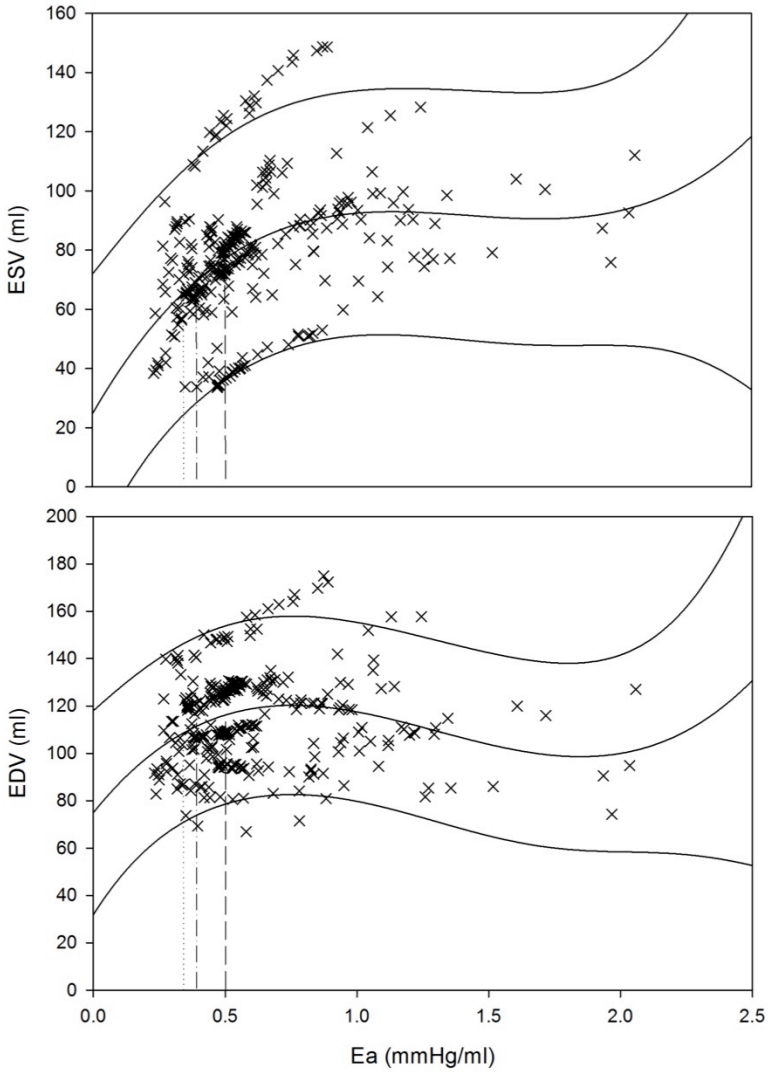

Figure 9-1 (Top) Relation between afterload quantified by effective arterial elastance (Ea) and end-systolic volume; (Bottom) and end-diastolic volume.

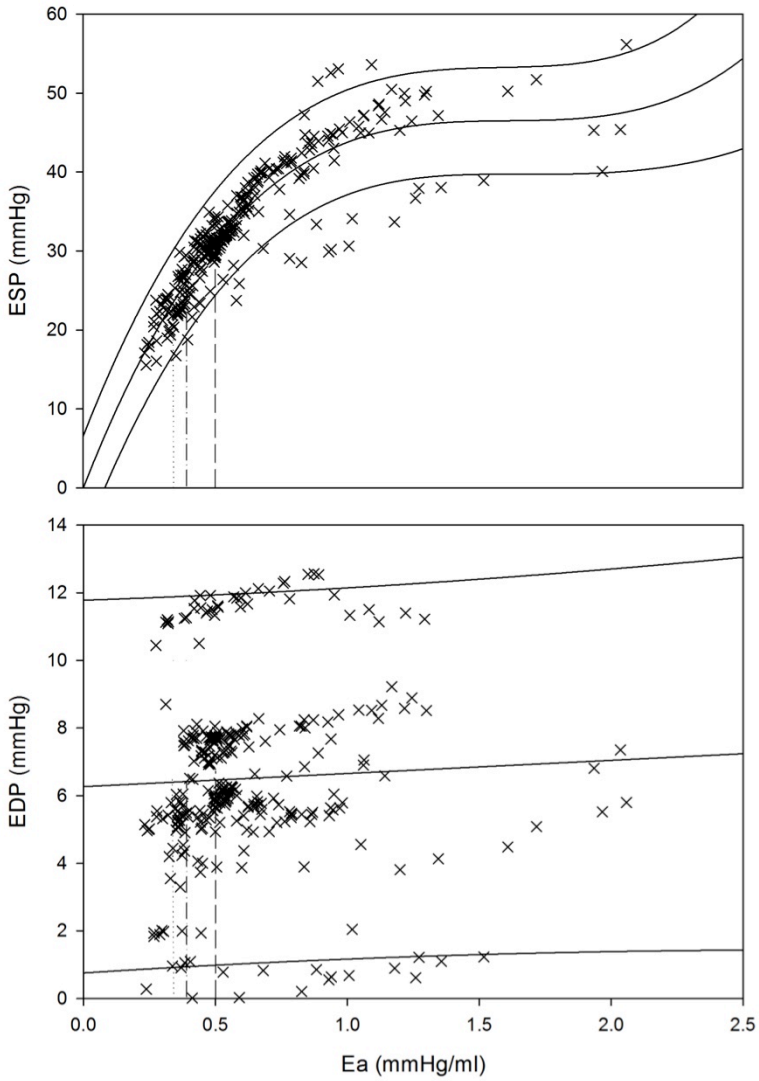

Figure 9-2 (Top) Relation between afterload quantified by effective arterial elastance (Ea) and end-systolic pressure; (Bottom) and end-diastolic pressure.

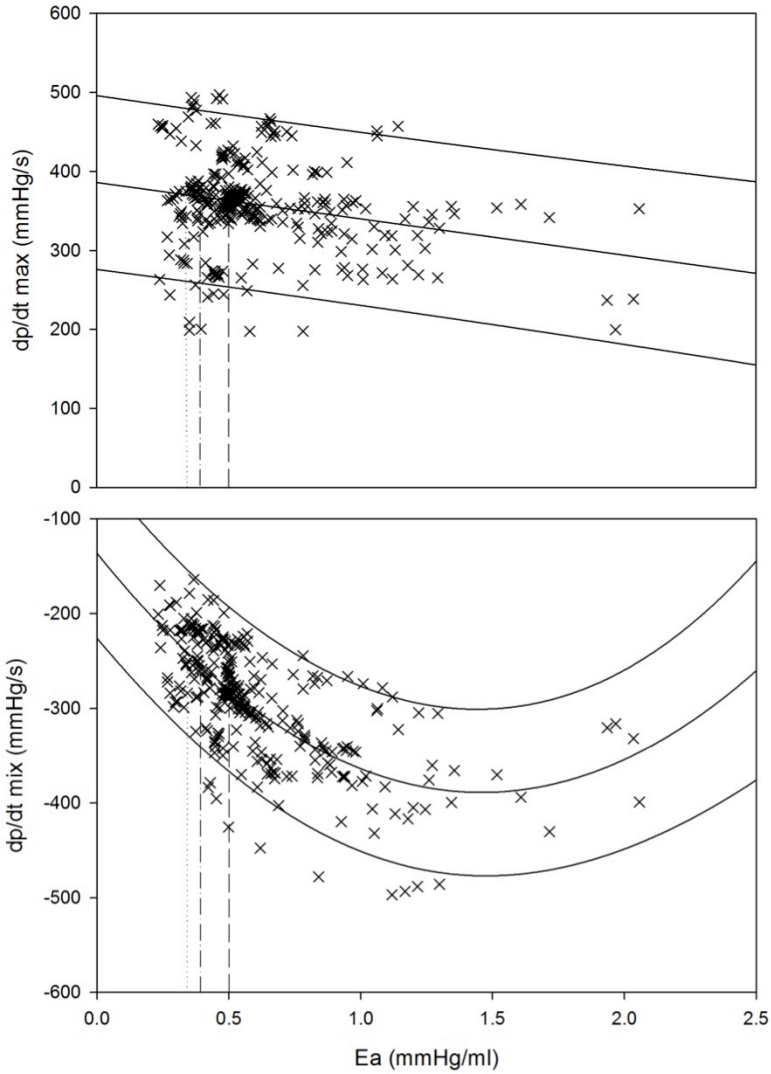

Figure 9-3 (Top) Relation between afterload quantified by effective arterial elastance (Ea) and maximum rate of isovolumic contraction; (Bottom) and maximum rate of isovolumic relaxation.

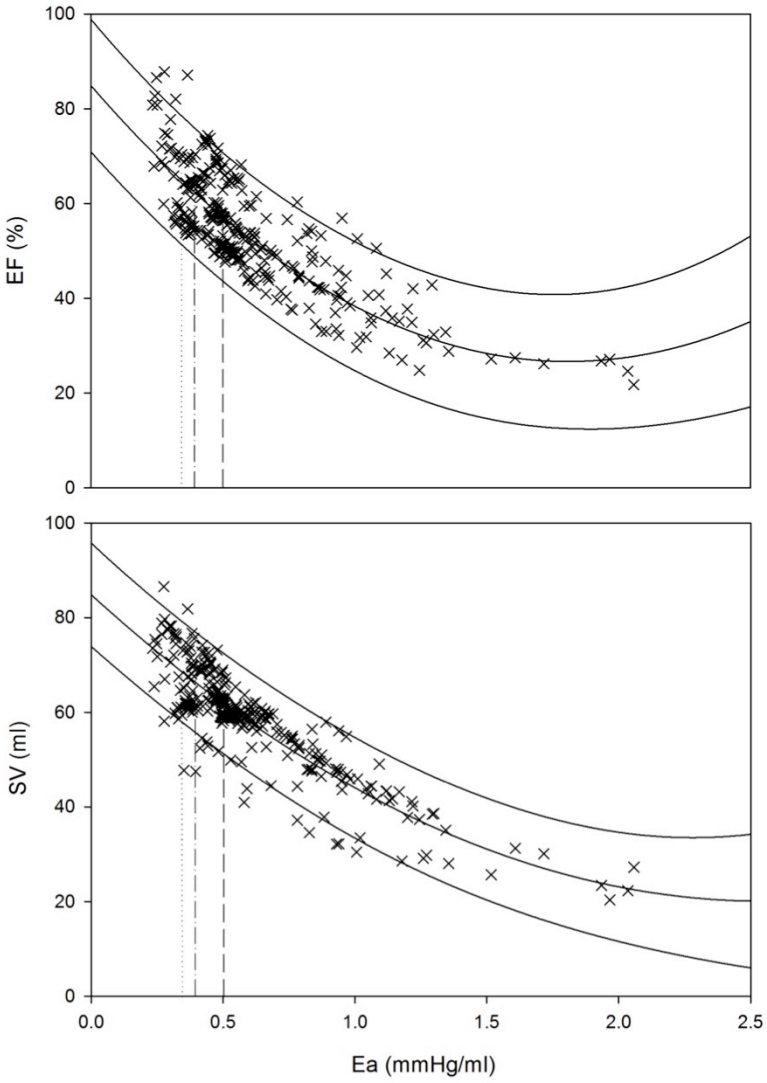

Figure 9-4 (Top) Relation between afterload quantified by effective arterial elastance (Ea) and ejection fraction; (Bottom) and stroke volume.

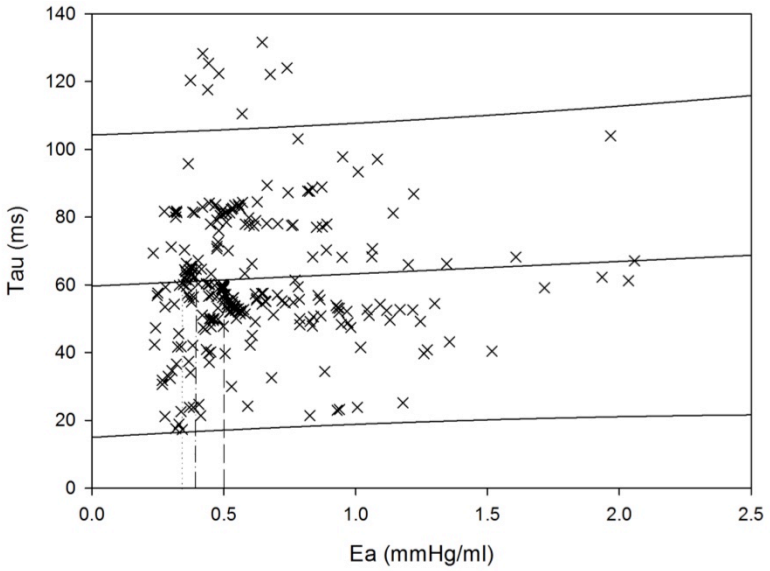

Figure 9-5 Relation between afterload quantified by effective arterial elastance (Ea) and the time constant of diastolic relaxation (Tau).

9.2 Appendix B – Relations between Ventriculoarterial Coupling Quantified by Ees/Ea and RV Function

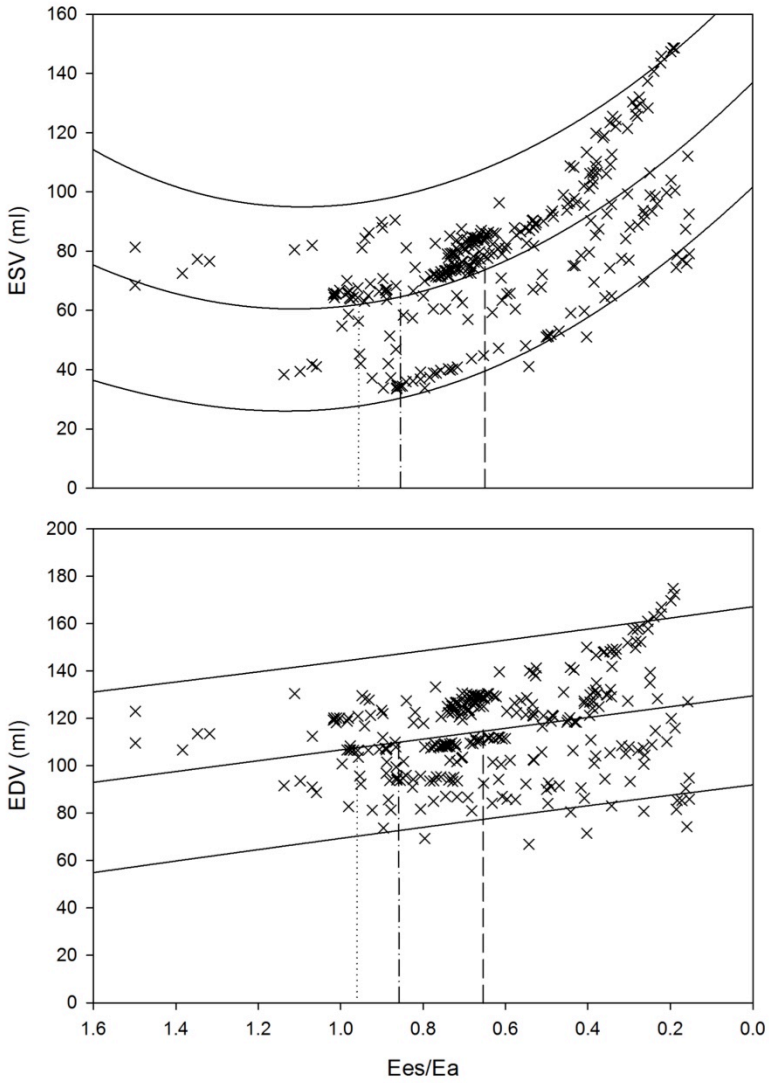

Figure 9-6 (Top) Relation between the ventriculoarterial coupling ratio (Ees/Ea) and end-systolic volume; (Bottom) and end-diastolic volume.

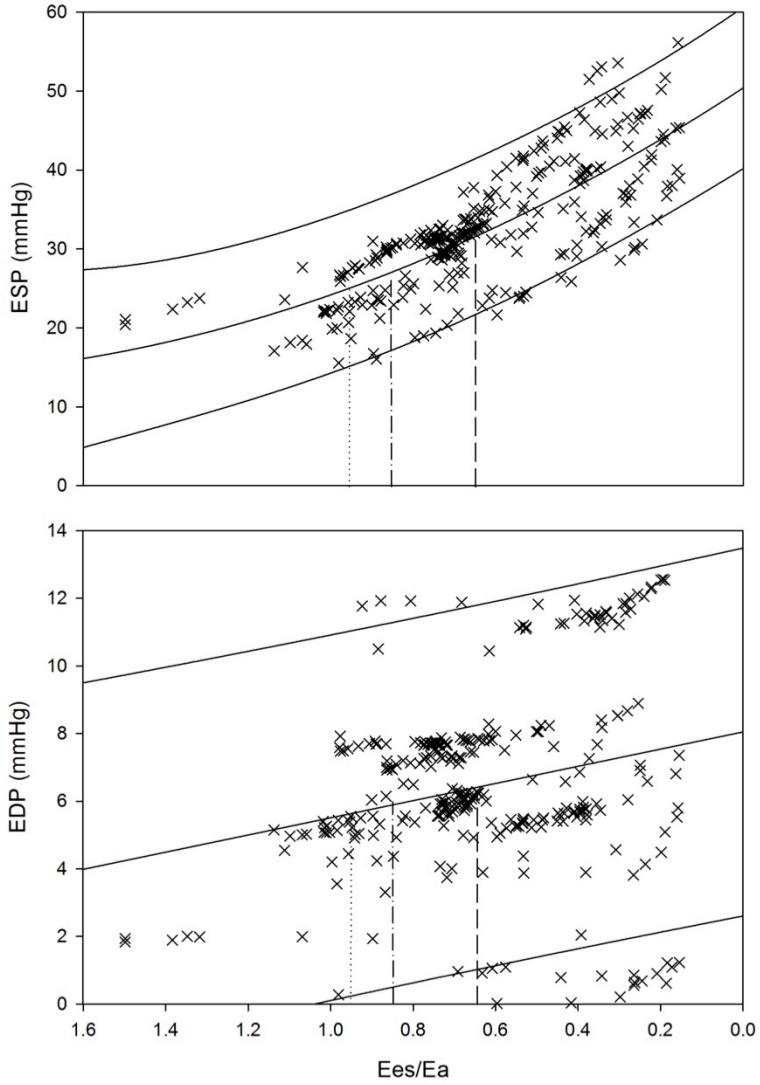

Figure 9-7 (Top) Relation between the ventriculoarterial coupling ratio (Ees/Ea) and end-systolic pressure; (Bottom) and end-diastolic pressure.

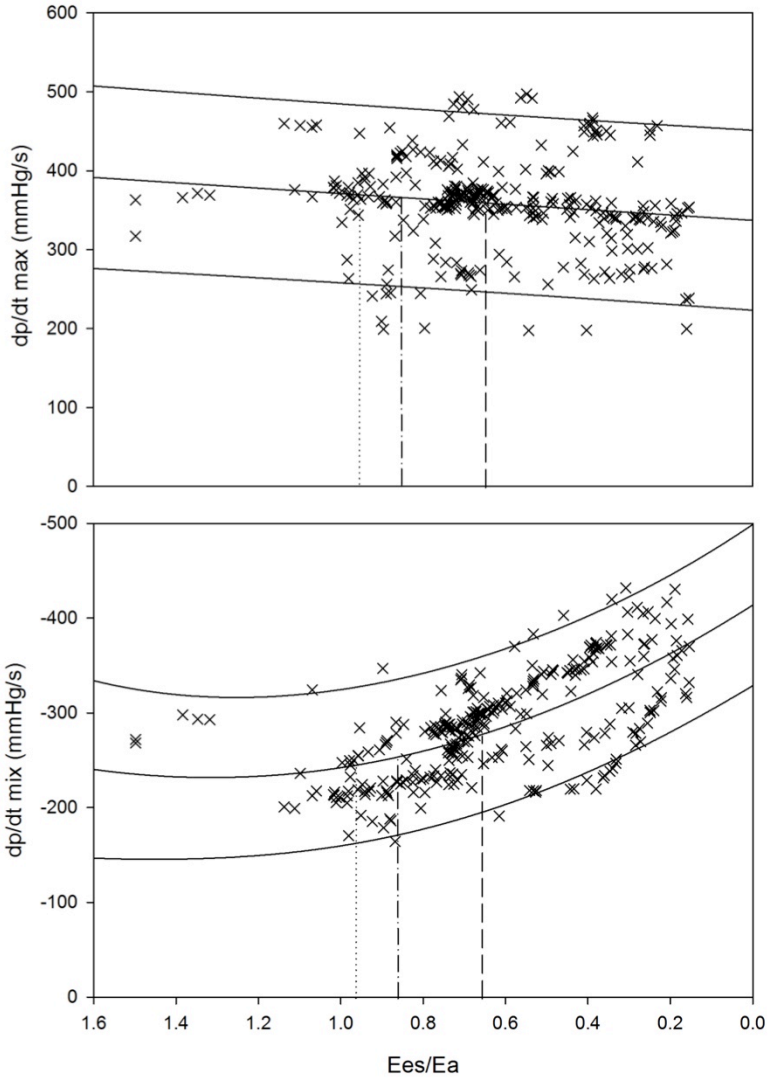

Figure 9-8 (Top) Relation between the ventriculoarterial coupling ratio (Ees/Ea) and maximum rate of isovolumic contraction; (Bottom) and maximum rate of isovolumic relaxation.

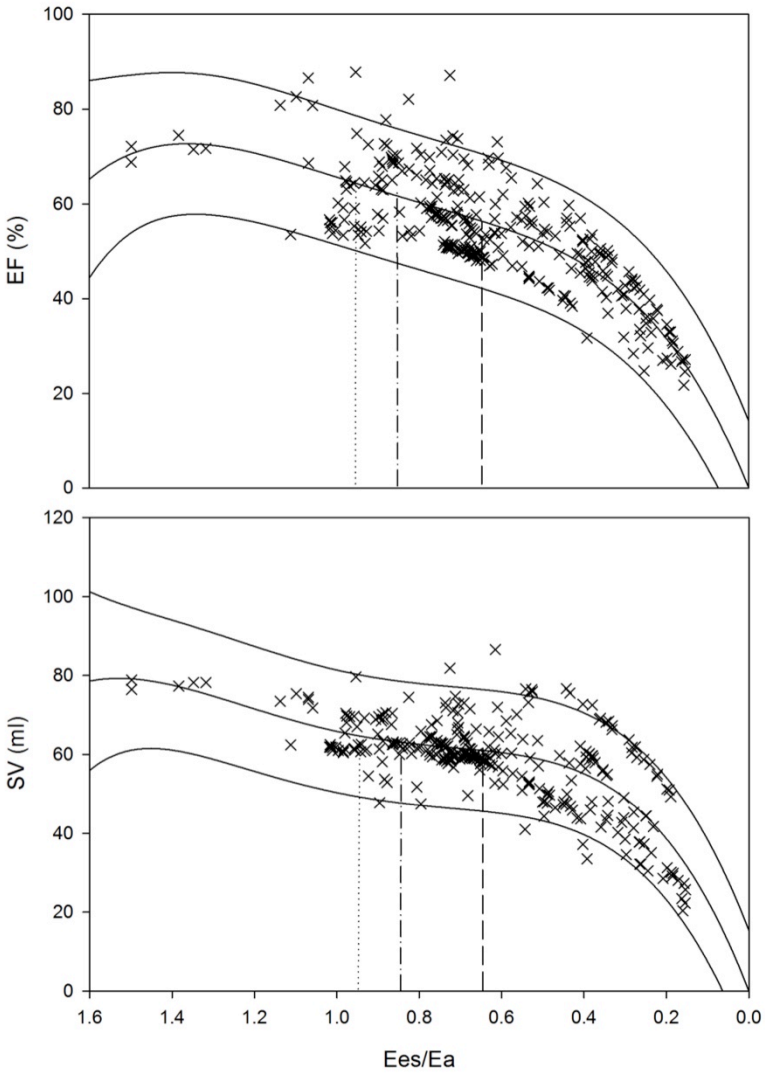

Figure 9-9 (Top) Relation between the ventriculoarterial coupling ratio (Ees/Ea) and ejection fraction; (Bottom) and stroke volume.

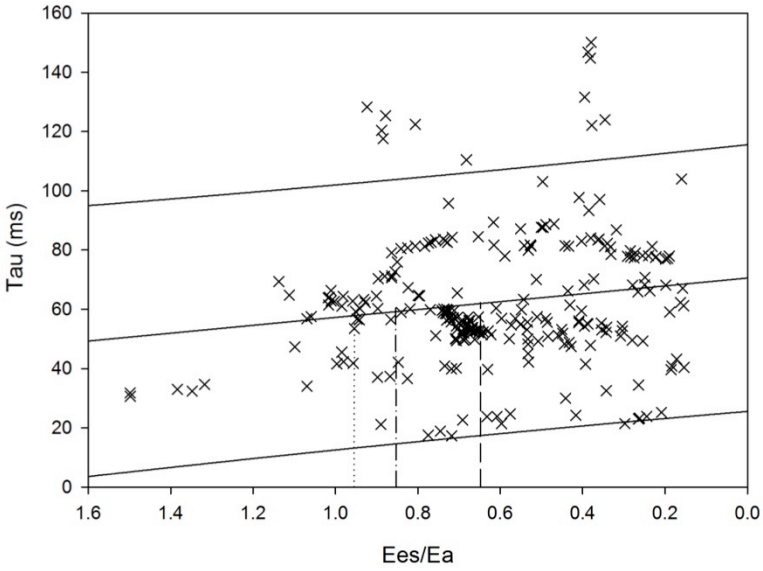

Figure 9-10 Relation between the ventriculoarterial coupling ratio (Ees/Ea) and the time constant of diastolic relaxation.

9.3 Appendix C - Bibliography of Published Work

9.3.1 Published Work described in this Thesis

The following peer reviewed scientific papers and abstracts have formed the basis of this thesis and are described in detail in Chapters 1 – 8.

Axell, R.G., White, P.A., Giblett, J.P., Williams, L., Rana, B.S., Klein, A., Hampton-Till, J., O'Sullivan, M., Braganza, D., Davies, W.R., West, N.E.J., Dutka, D.P., Densem, C.G., Hoole, S.P. 2017. Stunning and right ventricular function is induced by coronary balloon occlusion and rapid pacing in humans: Insights from right ventricular conductance catheter studies. Journal of the American Heart Association, 6 (6), pp.e005820.

Axell, R.G., Messer, S., White, P.A., McCabe, C., Priest, A., Statopoulou, T., Maja, D., Viscasillas, J., Hinchy, E.C., Hampton-Till, J., Alibhai, H.I., Morrell, N., Pepke-Zaba, J.,Large, S.R., Hoole, S.P. Ventriculo-Arterial Coupling Detects Occult RV Dysfunction in Chronic Thromboembolic Pulmonary Vascular Disease. Physiological Reports, 5 (7), pp.e13227.

Axell, R.G., White, P.A., Giblett, J.P., Williams, L., Rana, B.S., Klein, A., Hampton-Till, J., O'Sullivan, M., Davies, W.R., Densem, C.G., Hoole, S.P. 2017. Rapid Pacing Induced Right Ventricular Dysfunction is Evident after Balloon-Expandable Transfemoral Aortic Valve Replacement. Journal of the American College of Cardiology, 69 (7), pp.903-904.

Axell, R.G., White, P.A., Rana, B.S., Klein, A., O'Sullivan, M., Densem, C.G., Hoole, S.P. 2016. Conductance catheter derived right ventricular diastolic dysfunction is evident after rapid pacing test capture prior to transcatheter aortic valve replacement. Journal of the American College of Cardiology, 67 (13_S), pp.119-119. **Moderated**

poster presentation. American College of Cardiology Scientific Sessions. Chicago, US.

Axell, R.G., Messer, S., White, P.A., McCabe, C., Large, S., Pepke-Zaba, J., Hoole, S.P. 2016. Conductance catheter derived right ventricular SW-Ea relationship can detect RV dysfunction in CTED. Journal of the American College of Cardiology, 67 (13_S), pp.2058-2058. **Moderated poster presentation**. American College of Cardiology Scientific Sessions. Chicago, US.

Axell, R.G., Hoole, S.P., Hampton-Till, J., White, P.A. 2015. RV diastolic dysfunction: time to re-evaluate its importance in heart failure. Heart Failure Reviews, 20, pp.363-373.

Axell, R.G., White, P.A., Rana, B.S., Klein, A., O'Sullivan, M., Shapiro, L., Densem, C.G., Hoole, S.P., 2015. Conductance catheter derived right ventricular dysfunction is evident after balloon expandable transcutaneous aortic valve replacement in humans. Journal of the American College of Cardiology, 65 (10_S). **Moderated poster presentation**. American College of Cardiology Scientific Sessions, San Diego, US.

McCabe, C., White, P., Hoole, S., **Axell, R**., Priest, A., Goplan, D., Taboada, D., Mackenzie-Ross, R., Morrell, N., Shapiro, L., Pepke-Zaba, J. 2014. Right Ventricular Dysfunction in Chronic Thromboembolic Obstruction of the Pulmonary Artery. Journal of Applied Physiology, 116 (4), pp.355 -363.

9.3.2 Published Work not described in this Thesis

The following peer reviewed papers and abstracts, although not described in this thesis, have been written and presented during this PhD.

Giblett, J.P., **Axell, R.G**., White, P.A., Clarke, S.J., McCormick, L., Read, P.A., Reinhold, J., Brown, A.J., O'Sullivan, M, West, N.E.J., Dutka, D.P., Hoole, S.P. 2016. TCT-214 GLP-1 cardioprotection against ischemic dysfunction in humans is not mediated by a mitochondrial KATP dependent pathway in left ventricular conductance catheter studies. Journal of the American College of Cardiology, 68 (18_S), pp.B87-B87. **Moderated poster presentation**. Cardiovascular Research Foundation Transcatheter Cardiovascular Therapeutics, Washington DC, US.

Giblett, J.P., **Axell, R.G**., White, P.A., Clarke, S.J., McCormick, L., Read, P.A., Reinhold, J., Brown, A.J., O'Sullivan, M, West, N.E.J., Dutka, D.P., Hoole, S.P. 2016. Glucagon-like peptide-1 derived cardioprotection does not utilize a KATP-channel dependent pathway: mechanistic insights from human supply and demand ischemia studies. Cardiovascular Diabetology, 15 (1), pp.99.

Messer, S.J., **Axell, R.G.**, Colah, S., White, P.A., Ryan, M., Page, A., Parizkova, B., Valchanov, K., White, C., Freed, D.H., Ashley, E., Dunning, J., Goddard, M., Parameshwar, J., Watson, C.J., Kreig, T., Ali, A., Tsui, S., Large, S.R. 2016. Functional assessment and transplantation of the donor heart following circulatory death. The Journal of Heart and Lung Transplant, 35 (12), pp.1443-1452.

Messer, S., **Axell, R.**, Colah, S., White, P., Page, A., Parizkova, B., Valchanov, K., Dunning, J., Parameshwar, J., Ali, A., Tsui, S., Large, S. 2016. Functional assessment of the donor heart following circulatory death and clinical transplantation. The Journal of Heart and Lung Transplant, 35 (4), pp.S79-80. **Oral presentation**. International Society for Heart and Lung Transplantation Scientific Sessions. Washington DC, US.

Axell, R.G., Messer, S.J., White, P., Colah, S., Page, A.A., Parizkova, B., Valchonov, K., Dunning, J., Goddard, M., Parameshwar, J., Ali, A., Tsui, S., Large, S.R. 2016. Using the conductance catheter to define functional acceptability criteria for the first clinical DCD heart transplant programme. **Oral presentation**. European Society for Heart and Lung Transplantation Conference. Wengen, Switzerland.

Messer, M. **Axell, R**. White, P. Roman, M. Colah, S. Ali, A. Large, S. 2015. (22) – Functional assessment of the DCD heart within the donor and ex-vivo. The Journal of Heart and Lung Transplant, 34(4), pp.S17. **Oral presentation**. International Society for Heart and Lung Transplantation Scientific Sessions. Nice, France.

Messer, M. Lannon, J. Wong, E. Hopkinson, C. Fielding, S. **Axell, R**. Ali, A. Tsui, S. Large, S. 2015. (754) – The potential of transplanting hearts from donation after circulatory determined death (DCD) donors within the United Kingdom. The Journal of Heart and Lung Transplant, 34(4), pp.S275. **Moderated poster presentation**. International Society for Heart and Lung Transplantation Scientific Sessions. Nice, France.

Messer, M. **Axell, R**. White, P. Roman, M. Colah, S. Tritton, T. Whitehouse, A. Bermudez, O. Goddard, M. Tsui, S. Ali, A. Large, S. 2015. (761) – Restoring function to the DCD human heart using ECMO followed by transportation and functional assessment on the TransMedics Organ Care System. The Journal of Heart and Lung Transplant, 34(4), pp.S278. **Moderated poster presentation**. International Society for Heart and Lung Transplantation Scientific Sessions. Nice, France.

Tan, S.C.Y., Hampton-Till, J., White, P.A., **Axell, R.G**., Harris, S. 2015. The acute affects of selective site right ventricular pacing on left and right ventricular hemodynamic function in a normal heart population. Journal of the American College of Cardiology, 65 (10_S). **Moderated poster presentation**. American College of Cardiology Scientific Sessions. San Diego, US.

McCormick, L.M., Hoole, S.P., White, P.A., Read, P.A. **Axell, R.G**., Clarke, S.J., O'Sullivan, M., West, N.E.J., Dutka, D.P. 2015. Pre-treatment with glucagon-like peptide-1 protects against ischemic left ventricular dysfunction and stunning without a detected difference in myocardial substrate utilization. JACC: Cardiovascular Interventions, 8(2), pp.292-301.

Lawrence, E.M., Tang, S.Y.W., Barrett, T., Koo, B., Goldman, D.A., Warren, A.Y., **Axell, R.G**., Doble, A., Gallagher, F.A., Gnanapragasam, V.J., Kastner, C., Sala, E. 2014. Prostate cancer: Performance characteristics of combined T2W and DW-MRI scoring in the setting of template transperineal re-biopsy using MR-TRUS fusion. European Radiology, 24 (7), pp.1497-1505.

Axell, R., Gillett, A., Pasupathy, D., Chudleigh, T., Brockelsby, J., White, P., Lees C. 2014. The accuracy of nuchal translucency measurement depends on the equipment used and its calibration. Journal of Ultrasound in Obstetrics and Gynecology, 44(11). pp.31-37.

McCabe, C., White, P., **Axell, R**., Shapiro, L., Pepke-Zaba, J. 2013. S48 Inefficient ventriculo-arterial coupling contributed to reduced exercise capacity in pulmonary hypertension. Thorax, 68 (S3), pp.A26-A27. **Oral presentation**. British Thoracic Society Winter Meeting 2013, London, UK.

McCormick, L.M., Hoole, S.P., White, P.A., **Axell, R.G**., Clarke, S.J., O'Sullivan, M., West, N.E.J., Dutka, D.P. 2013. Pre-treatment with glucagon-like peptide-1 protects against supply ischemic left ventricular dysfunction-insights from conductance catheter assessment during elective PCI. Circulation, 128 (S22), pA17497. **Moderated poster presentation**. American Heart Association Scientific Sessions, Texas, US.

McCormick, L.M., Hoole, S.P., White, P.A., Read, P.A. **Axell, R.G**., Clarke, S.J., O'Sullivan, M., West, N.E.J., Dutka, D.P. 2013. TCT-318 Cardioprotection with

Glucagon-like Peptide-1 (GLP-1) may occur independent of coronary collaterals and metabolic substrate utilisation. Journal of the American College of Cardiology, 62 (18_S1), ppB101-B102. **Moderated poster presentation**. American College of Cardiology. Cardiovascular Research Foundation Transcatheter Cardiovascular Therapeutics, San Francisco, US.

9.3.3 Book Chapters

The following book chapters, although not described in this thesis, have been written during this PhD.

Axell, R.G.. (2014). Chapter 12 Clinical Measurement. In: Taktak, A.F.G. Ganney, P. Hegarty, F. Long, D. and White, P. Clinical Engineering: A Handbook for Clinical and Biomedical Engineers. Oxford: Academic Press Inc. pp.211-218.

Axell, R.G.. (2014). Chapter 13 Cardiology. In: Taktak, A.F.G. Ganney, P. Hegarty, F. Long, D. and White, P. Clinical Engineering: A Handbook for Clinical and Biomedical Engineers. Oxford: Academic Press Inc. pp.219-228.

White, P.A. and **Axell, R.G**.. (2014). Chapter 14 Pressure and Flow. In: Taktak, A.F.G. Ganney, P. Hegarty, F. Long, D. and White, P. Clinical Engineering: A Handbook for Clinical and Biomedical Engineers. Oxford: Academic Press Inc. pp.229-234.